The fabrication and modification of capillary polymer monoliths for the separation of small ions

For the award of Doctor of Philosophy

Áine Moyna

Student no: 57126046
School of Chemical Sciences

Under the supervision of:

Prof. Brett Paull
&
Dr. Damian Connolly

Table of Contents

Chapter 3.0:

Modification of capillary polymer monoliths using photo-grafted chains of [2(methacryloyloxy)ethyl] trimethylammonium chloride (META) for the separation of anions

Chapter 4.0:

Separation of cations using a capillary polymer monolith functionalised with 3-sulfopropyl methacrylate

Chapter 5.0:

Separation of selected transition metals by chelation ion chromatography using acetyl-iminodiacetic acid modified polymer monoliths

Chapter 6.0:

Modification of capillary polymer monoliths with iminodiacetic acid using poly(glycidyl methacrylate) for the separation of metal cations by high performance chelation ion chromatography

.

I hereby certify that this material, which I now submit for assessment on the programme of study leading to the award of Doctor of Philosophy is entirely my own work, that I have exercised reasonable care to ensure that the work is original and does not to the best of my knowledge breach any law of copyright, and has not been taken from the work of others save to the extent that such work has been cited and acknowledged within the text of my work.

Signed:_____ Date:_____

Candidate ID No:_____

List of Publications

1) Á. Moyna, D. Connolly, E. Nesterenko, P. N. Nesterenko, B. Paull.
Separation of selected transition metals by chelation ion chromatography using acetyl-iminodiacetic acid modified capillary polymer monoliths.
Journal of Chromatography A 1249 (2012) 155-163.

2) Á. Moyna, D. Connolly, E. Nesterenko, P. N. Nesterenko, B. Paull.
Iminodiacetic acid functionalised organopolymer monolithis: Application to the separation of metal cations by capillary high performance chelation ion chromatography.
Accepted to Analytical and Bioanalytical Chemistry August 2012.

List of Oral Presentations

1) Marine and Environmental Sensing Technology Hub (MESTECH) Workshop: Gaps and opportunities. Dublin City University, March 2011.
Title: Capillary Chelation Ion Chromatography: Transition and heavy metal analysis using iminodiacetic acid modified polymer monoliths.
Authors: Áine Moyna, Damian Connolly, Ekaterina Nesterenko and Brett Paull.

2) Conference - Pittcon Conference and Expo, Atlanta, USA, March 2011.
Title - Capillary chelation ion chromatography using monolithic chelating ion exchangers
Authors: Brett Paull, Áine Moyna, Ekaterina Nesterenko.

3) Analytical Research Forum, Loughborough, UK, July 2010
Title: Development of a Capillary Chelation Ion Chromatography System for application to transition metal analysis
Authors: Áine Moyna, Damian Connolly, Sinead Currivan and Brett Paull.

4) 21st International Ion Chromatography Symposium, Malahide, Dublin, Sept 09.
Title: Grafted methacrylate monoliths for ion chromatographic separations of inorganic anions and cations.
Authors: Damian Connolly, Áine Moyna, Brett Paull.

5) UNCSR 10 year anniversary symposium, Dublin City University, Dublin. Nov 2009.
Title: Development of a Capillary Chelation Ion Chromatography System for the separation of small ions.
Authors: Áine Moyna, Damian Connolly, Mirek Macka and Brett Paull.

List of Poster Presentations

1) HPLC 2011, Budapest, Hungary, July 2011.
Poster title: Capillary chelation ion chromatography: Transition and heavy metal analysis using iminodiacetic acid modified polymer monoliths
Áine Moyna, Damian Connolly, Ekaterina Nesterenko and Brett Paull.
Poster short listed in top 26 out of approximately 800 posters.

2) Marine and Environmental Sensing Technology Hub (MESTECH) Workshop: Gaps and opportunities. Dublin City University, March 2011.
Poster title: Transition and heavy metal analysis using iminodiacetic acid modified polymer monoliths
Áine Moyna, Damian Connolly, Ekaterina Nesterenko and Brett Paull.

3) Conference on Analytical Science Ireland (CASi), Dublin City University, Feb 2011.
Poster title: Capillary Chelation Ion Chromatography: Transition and heavy metal analysis using iminodiacetic acid modified polymer monoliths.
Áine Moyna, Damian Connolly, Ekaterina Nesterenko and Brett Paull.

4) UNSCR Symposium, DCU, Dublin, Sept 2010.
Poster title: Development of a Capillary Chelation Ion Chromatography System for Application within Environmental Monitoring/Transition metal analysis
Áine Moyna, Damian Connolly, Sinead Currivan, Mirek Macka and Brett Paull.

5) International Ion Chromatography Symposium, Cincinnati, OH, USA, Sept 2010.
Poster title: Development of a Capillary Chelation Ion Chromatography System for Application within Environmental Monitoring/Transition metal analysis
Áine Moyna, Damian Connolly, Sinead Currivan, Mirek Macka and Brett Paull.

6) International Symposium of Chromatography 2010, Valencia, Sept 2010.
Poster title: Development of a Capillary Chelation Ion Chromatography System for Application within Environmental Monitoring/Transition metal analysis
Áine Moyna, Damian Connolly, Sinead Currivan, Mirek Macka and Brett Paull.

7) HPLC 2010, Boston, USA, June 2010
Poster title: Development of a Capillary Chelation Ion Chromatography System for Application within Environmental Monitoring/Transition metal analysis
Áine Moyna, Damian Connolly, Sinead Currivan, Mirek Macka and Brett Paull.

8) Beaufort Marine Sensing Research Awards Workshop, DCU, Dublin, Feb 2010.
Poster title: Development of a capillary liquid chromatography system for application in environmental monitoring.
Áine Moyna, Damian Connolly, Sinead Currivan, Mirek Macka and Brett Paull.

9) 21st International Ion Chromatography Symposium, Malahide, Dublin, Sept 09.
Poster title: Development of a capillary ion chromatography system for the separation of inorganic anions on a methacrylate based polymer monolith grafted with [2(methacryloyloxy)ethyl] trimethylammonium chloride.
Áine Moyna, Damian Connolly, Eoin Gillespie, Leon Barron, Mirek Macka & Brett Paull.

10) Euroanalysis 2009, Innsbruck, Austria, Sept 09.
Poster title: Development of a capillary ion chromatography system for the separation of small ions.
Áine Moyna, Damian Connolly, Eoin Gillespie, Leon Barron, Mirek Macka & Brett Paull.

11) Analytical Research Forum 2009, Kent, UK, July 09.
Poster title: Development of a capillary ion chromatography system for the separation of inorganic anions on a methacrylate based polymer monolith grafted with [2(methacryloyloxy)ethyl] trimethylammonium chloride.
Áine Moyna, Damian Connolly, Eoin Gillespie, Leon Barron, Mirek Macka & Brett Paull.

List of Figures

Figure 1.8: Separations of anions obtained by placing the detector at various positions along the column. The effective column length is 4.5 cm for the bottom chromatogram, 8.5 cm for the middle chromatogram and 12.5 cm for the top chromatogram. Chromatographic conditions: Eluent: 0.5 m*M* phthalate, flow-rate: 1 µL/min and injection volume: 50 nL.

Figure 1.9: Separation of anions using a silica particle packed column (100 mm x 350 µm I.D.) modified with BSA. Separation conditions: eluent: (A) 3 m*M* aspartic acid, (B) 0.05 m*M* sulfuric acid, (C) 0.15 m*M* tartaric acid, Flow-rate: 5.6 µL/min, injection volume: 0.2 µL, peaks: (1) iodate, (2) bromide, (3) nitrate, (4) iodide, (5) thiocyanate.

Figure 1.10: Separation of cations using a 100 x 0.32 mm I.D. TSKgel IC-anion SW, silica particle packed column (modified with dextran sulfate). Separation conditions: Eluent: 6 m*M* copper sulfate, flow-rate: 4.2 µL/min, injection volume: 0.2 µL, detection: indirect UV detection at 210 nm.

Figure 1.11: Flowpath of the eluent through a particulate packed column (A) and a monolith column (B).

Figure 1.12: Comparison of Van Deemter plots for a 3 µm particle packed column and a monolithic column.

Figure 1.13: Chemical structures of methacrylate monomers and cross linkers. used in the polymerisation of polymer monoliths. (a) glycidyl methacrylate (GMA), (b) butyl methacrylate (BuMA), (c) lauryl methacrylate (LMA), (d) hydroxylethyl methacrylate (HeMA) and (e) ethylene dimethacrylate (EDMA).

Figure 1.14: SEM images of BuMA-co-EDMA polymer monoliths using (A) 1-decanol as the porogen and (B) using a mixture consisting of 1-decanol and cyclohexanol.

Figure 1.15: Separation of selected cations using a sulphonated polymer monolith. Separation conditions: Eluent: 10 mM copper sulphate, flow-rate: (A) 3 µL/min, (B) 6

µL/min, (C) 9 µL/min, (D) 12 µL/min and (E) 15 µL/min, detection: indirect UV at 210 nm, injection volume: 0.2 µL.

Figure 1.16: Separation of selected cations using a GMA-co-EDMA polymer monolith modified with a mixture of PEI and DMA. Separation conditions: Eluent: potassium phthalate, detection: UV detection at 254 nm.

Figure 1.17: Separation of (1) iodate, (2) bromate, (3) nitrite, (4) bromide and (5) nitrate using a GMA-co-EDMA polymer monolith functionalised with quaternary ammonium functionalities. Eluent: 10 m*M* $NaClO_4$, injection volume: 10 nL, detection: UV at 210 nm, column dimensions: 100 µm x 750 mm.

Figure 1.18: Separation of 6 common anions using a GMA-*co*-EDMA polymer monolith modified with grafted polymer chains of META. Eluent: 2 m*M* sodium benzoate, flow rate: 1 µL/min., detection: on-column C^4D detection, injection volume: 50 nL, peaks: (1) 0.7 mg/L fluoride, (2) 3 mg/L chlorite, (3) 3 mg/L, bromate, (4) 0.7 mg/L chloride, (5) 0.7 mg/L nitrite, (6) 3 mg/L bromide.

Figure 1.19: Separation of common anions using an AS18 latex functionalised polymer monolith. Separation conditions: eluent: 1 m*M* KOH, flow-rate: 18 µL/min, detection: non-suppressed conductivity detection, peaks: (1) iodate, (2) bromate, (3) nitrite, (4) bromide and peak (5) nitrate.

Figure 1.20: Separation of 5 anions using an AS18 latex functionalised polymer monolith. Separation conditions: Eluent: 0.5 - 5 m*M* KOH, flow-rate: 18 µL/min, detection: suppressed conductivity detection, peaks: (1) iodate, (2) bromate, (3) nitrite, (4) bromide and (5) nitrate.

Figure 1.21: Separation of 7 anions using a AS18 latex nano-particle modified GMA-*co*-EDMA polymer monolith. Separation conditions: Eluent: NaOH gradient, flow-rate: 3.2 µL/min, detection: UV detection at 220 nm, Peaks: (1) iodate, (2) bromate, (3) nitrite, (4) bromide, (5) nitrate, (6) iodide and (7) benzenesulfonate.

Figure 1.22: Separation of selected anions using a lysine modified silica monolith. Separation conditions: Eluent: 50 m*M* phosphate buffer, detection: UV detection at 214 nm and flow-rate: 4.9 mL/min.

Figure 1.23: Separation of common anions using a CTAC modified silica monolith (100 µm x 200 mm I.D.). Eluent: 50 m*M* NaCl and 0.1 m*M* CTAC, flow-rate: 11.1 µL/min, detection: UV detection at 210 nm.

Figure 1.24: Separation of anion standards using a DDAB modified capillary silica monolith (top chromatogram) and determination of bromide in seawater (bottom chromatogram). Separation conditions: Eluent: 500 m*M* NaCl, flow-rate: 2.1 µL/min, detection: UV detection at 210 nm and injection volume: 20 nL.

Figure 1.25: Separation of common anions using a DDMAU coated silica capillary monolith. Separation conditions: eluent: 0.5 m*M* phthalate, flow-rate: 0.3 µL/min, detection: on-column C^4D.

Figure 1.26: Scanning C^4D profile where (a) depicts void regions, (b) depict the areas where the monolith frits are situated and (c) is the area that contains the packing material.

Figure 1.27: C^4D scan of an unmodified monolith, a scan after the first surfactant coating and a scan after the second surfactant coating.

Figure 1.28: Separation of transition metals on a bare silica monolith using an eluent consisting of 80 % acetonitrile and 10.3 m*M* ammonium acetate buffer at pH 4.6. Analysis was carried out using flow-rates of 1 mL/min, 3 mL/min and 5 mL/min.

Figure 1.29: Pre-concentration and separation of metals in coastal seawater samples (b). A blank sample (a) showed small concentrations of Zn(II) and Cu(II), possibly due to leaching from the eluent pump.

Figure 1.30: (a) Separation of Mg(II) and Ca(II) in a saline eyewash sample overlaid with a spiked 200 µg/L sample. (b): separation of Mg(II) and Ca(II) in 0.5 *M* KCl

overlaid with a spiked 300 µg/L sample, column used: IDA bonded silica (250 x 4.0 mm I.D).

Figure 1.31: Overlay of separations of Mg(II) and Ca(II) in 1 *M* KCl solutions at various flow-rates using the IDA immobilised monolith column. The eluent used in the analysis was a HNO_3 eluent (pH adjusted to 4.85). Peaks: (1) 10 ppm Mg(II) and (2) 10 ppm Ca(II). Detection used was UV-Vis at 570 nm after PCR with o-CPC.

Figure 1.32: Overlay of chromatograms obtained for various transition and heavy metals using the lysine bonded silica monolith. Separation conditions: Eleunt: 3 m*M* KCl pH 4.5, flow-rate: 2 mL/min, detection: UV-Vis detection at 495 nm following reaction with PAR.

Figure 1.33: (left) Schematic demonstrating the chelating monolith solid phase extraction module prepared in a syringe tip. (right) Dimensions of syringe tip filter. Reproduced from

Figure 1.34: Separation of alkaline earth metals using an IDA bonded silica particulate column using (a) 0.1 *M* KNO_3, (b) 0.2 *M* KNO_3, (c) 0.3 *M* KNO_3, (d) 0.5 *M* KNO_3, (e) 1.0 *M* KNO_3 and (f) 1.5 *M* KNO_3 eluents.

Figure 1.35: (left): Van't hoff plots of alkali metals, alkaline earth metals and amines showing changes in selectivity as the temperature is increased. (right): Separation of selected alkaline earth metals and BuA carried out at 27 ^{o}C (top) and 46 ^{o}C (bottom) demonstrating the benefits of the use of temperature to alter separation selectivity

Figure 1.36: (left): Van't Hoff plots for alkaline earth metals, transition and heavy metals cations obtained by increasing the temperature from 25 ^{o}C to 55 ^{o}C. (right): Separation of selected alkaline earth metals, transition and heavy metals using optimised temperature conditions (50 ^{o}C). The eluent used was 0.2 *M* KCl and 0.9 m*M* nitric acid.

Figure 2.1: The in-house constructed capIC system incorporating a high pressure analytical pump, a 20 nL injector valve, the poly(META) functionalised anion exchange polymer monolith and on-column C^4D detection.

Figure 2.2: Fluidic set-up for dual detection HPCIC.

Figure 2.3 (a) Kapton flexible heating tape used in the manufacture of the capillary column heater (dimensions: 2.5 cm x 10 cm) and (b): Kapton heater wrapped in insulating tape and aluminum foil, encasing the cation exchange polymer monolith. The column was placed in the centre of the heater with 2 MicroTight unions positioned at each end.

Figure 2.4: (a) Placement of the flexible heating tape inside a stainless steel tube and (b): In-house constructed capillary column heater demonstrating off-column C^4D detection. Temperature monitoring was carried out using a thermocouple wire.

Figure 2.5: Photo-grafting of poly(META) on the surface of the polymer monolith.

Figure 2.6: Photo-grafting of poly(SPM) on the surface of the polymer monolith.

Figure 2.7: Immobilisation of IDA on the VAL grafted polymer monolith.

Figure 2.8: Immobilisation of AIDA on the poly(GMA) photo-grafted polymer monolith

Figure 3.1: (a) Separation of 6 anions on poly(META) polymer monolith using the two-step functionalising procedure and (b) separation of the same anion mix using the poly(META) functionalised polymer monolith using the one step procedure. Figure 2.2 (b) reproduced from [103]. Chromatographic conditions: effective column length: 100 mm x 100 µm (a) and 110 mm x 100 µm (b), eluent: 2 m*M* sodium benzoate, injection volume: 50 nL, detection: on-column C^4D, flow-rate: 1 µL/min. Peak (1) 0.7 mg/L fluoride, (2) 3 mg/L chlorite, (3) 3 mg/L bromate, (4) 0.7 mg/L chloride, (5) 0.7 mg/L nitrite and (6) 3 mg/L bromide.

Figure 3.2: Overlaid chromatograms of separations of the 5 anions using the META functionalised polymer monolith obtained by varying the eluent concentration where (a) 2 mM sodium benzoate, (b) 1.4 mM sodium benzoate, (c) 1 mM sodium benzoate and (d) 0.6 mM sodium benzoate. Chromatographic conditions: as in Figure 3.1.

Peaks: (1) 0.7 mg/L fluoride, (2) 3 mg/L chlorite, (3) 3 mg/L bromate, (4) 0.7 mg/L chloride, (5) 0.7 mg/L nitrite.

Figure 3.3: Plots of log *k* versus log[benzoate] demonstrating that the mode of separation was anion exchange using the META functionalised polymer monolith. (1) nitrite, (2) chloride, (3) bromate, (4) chlorite and (5) fluoride.

Figure 3.4: Separation of 5 anions using an in-house constructed capIC system. Chromatographic conditions: Column dimensions: 100 mm x 100 µm, eluent: 2 m*M* sodium benzoate, injection volume: 20 nL, flow rate: 1.3 µL/min and detection: on-column C^4D detection. Peak: (1) 0.7 mg/L fluoride, (2) 3 mg/L chlorite, (3) 3 mg/L bromate, (4) 0.7 mg/L chloride, (5) 0.7 mg/L nitrite.

Figure 3.5: Overlay of chromatograms obtained using the poly(META) polymer monolith. Chromatographic conditions: as in Figure 2.5. Peaks: (a) 10 ppm formate, (b) 10 ppm bromate and (c) 10 ppm chloride. Also included in Figure 3.5 is the chromatogram obtained for a blank injection (green trace).

Figure 3.6: Overlay of chromatograms obtained using the META functionalised polymer monolith. Chromatographic conditions: as in Figure 2.6, peak (a) 100 ppm chlorite, (b) 10 ppm chloride and (c) 100 ppm chlorate. Also included in Figure 3.6 is the chromatogram obtained for a blank injection (green trace).

Figure 3.7: Overlay of chromatograms obtained using the META functionalised polymer monolith. Peak (a) = 10 ppm acetate and peak (b) = 10 ppm formate. Also included in Figure 3.7 is the chromatogram obtained for a blank injection (black trace).

Figure 4.1: Separation of 100 ppm Mg(II), 100 ppm Ca(II) and 100 ppm Ba(II) using the in-house constructed capIC system. Chromatographic conditions: column: BuMA-*co*-EDMA functionalised with SPM (100 µm I.D x 90 mm), eluent: 1 m*M* copper sulpfate, flow-rate: 1 µL/min, injection volume: 20 nL, detection: indirect UV at 210 nm.

Figure 4.2: Plot of temperature versus voltage applied to the heating tape showed a linear correlation between 25 – 80 ^{o}C.

Figure 4.3: Separation of Ca(II), Mg(II) and Ba(II) at 27 ^{o}C (a) and 62 ^{o}C (b). All chromatographic conditions as in Figure 4.1.

Figure 4.4: Van't Hoff plots where ◊ = Ba(II), ◊= Ca(II) and ◊ = Mg(II). Data obtained from individual injections of each alkaline earth metal at various temperatures.

Figure 4.5: Plot of temperature versus backpressure showing linear correlation (R^2 = 0.99). Measurements obtained using the capIC system with the backpressure noted as the temperature of the column heater was increased.

Figure 5.1: Plots of - log [HNO_3] versus log *k* for the 6 metals studied where ♦ = Co(II), ♦ = Mn(II), ♦ = Ni(II), ♦ = Zn(II), ♦ = Cd(II) and ♦ = Cu(II). Chromatographic conditions: Eluent: 0.2 – 0.4 m*M* nitric acid, all other conditions as in Table 5.1.

Figure 5.2: (a) Separation of 5 ppm Mn(II), 10 ppm Cd(II) and 10 ppm Cu(II) using C^4D detection. Chromatographic conditions: Column: VAL15a, eluent: 0.2 m*M* nitric acid, flow-rate: 1 µL/min, column length: 250 mm x 100 µm I.D., injection volume: 20 nL. (b): Same separation using simultaneous post column reaction and UV-Vis detection. Chromatographic conditions: Eluent: 0.2 m*M* nitric acid, PCR: 0.15 m*M* PAR in 0.5 *M* ammonia, pH = 10.4, PCR flow-rate: 1µL/min, all other conditions as in Table 5.1.

Figure 5.3: Overlay of chromatograms obtained for the separation of 5 ppm Mn(II), 10ppm Cd(II) and 10ppm Cu(II) using VAL15b and VAL15c. Chromatographic conditions: Eluent: 0.2 mM HNO_3, all other conditions as in Table 4.2.

Figure 5.4: Calibration plot of applied voltage (V) versus temperature (^{o}C) for the capillary column heater.

Figure 5.5: Overlay of chromatograms showing the effect of temperature on retention where (a) = 54 ^{o}C, (b) = 43 ^{o}C, (c) = 34 ^{o}C and (d) = 24 ^{o}C. Chromatographic conditions: column length: 230 mm x 100 µm I.D., eluent: 0.1 m*M* nitric acid, all other conditions as in Table 5.1.

Figure 5.6: Van't Hoff plots constructed for Mn(II) (◊), Cd(II) (□) and Cu(II) (Δ) demonstrating that for Cu(II) and Cd(II), the sorption process exhibited exothermic behaviour and for Mn(II) the sorption process exhibited endothermic behaviour.

Figure 5.7: (a) Scanning C^4D profiles obtained using a 1 m*M* ethanolamine buffer pH = 9.8 for VAL20 where (■) is the scan of the un-modified polymer monolith and (■) is the scan following modification with IDA. (b): Scanning C^4D profiles where (●) VAL15, (■) VAL20, (▲) VAL25 and (♦) VAL30.

Figure 5.8: Chelation ion chromatography system set-up incorporating on-column C^4D and UV-Vis detection.

Figure 5.9: Separation of transition/heavy metals utilising simultaneous on-column C^4D detection (a) and UV-Vis detection at 500 nm following reaction of the eluted metals with PAR (b). Chromatographic conditions: Eluent: 0.2 mM nitric acid, Eluent flow-rate: 1 µL/min, PCR flow-rate: 1 µL/min, PCR: 0.4 mM PAR in 0.1 M ammonia, pH 10.7. Peak (1) 0.5 ppm Mn(II), (2) 1 ppm Cd(II) and (3) = 1ppm Cu(II). A 10 pt moving average was applied to the chromatograms (using Microsoft excel) obtained using UV-Vis detection.

Figure 5.10: Overlay of chromatograms obtained for the separations of 0.5 ppm Mn(II), 1 ppm Cd(II) and 1 ppm Cu(II) by varying the effective column length where (a) = 9 cm, (b) = 8.5 cm, (c) = 8 cm, (d) = 7.5 and (e) = 7 cm. Chromatographic conditions: Column: VAL30, eluent: 0.2 m*M* nitric acid, all other conditions as in Table 4.1.

Figure 6.1: (a) Overlay of scanning C^4D profiles obtained for GMA15 (♦), GMA20 (♦), GMA25 (♦), GMA30 (♦) and GMA35 (♦). (b): Scanning C^4D profile obtained for

GMA30 where (♦) is the profile of the un-modified polymer monolith and (♦) is the profile obtained after modification with IDA. All scans were carried out using a 1 m*M* ethanolamine buffer (pH 9.8) at a flow-rate of 1 µL/min.

Figure 6.2: Differences in corrected conductive response obtained during the C^4D scanning of the poly(VAL) IDA-modified polymer monoliths and GMA-IDA polymer monoliths.

Figure 6.3: Order of elution of the four metal cations using monolith VAL25 (♦) and GMA25 (♦) showing the changes in selectivity

Figure 6.4: (a) Overlay of a separation of 5 ppm Mn(II), 10 ppm Cd(II) and 10ppm Zn(II) using GMA15 and GMA20. (b) Separation of 5 ppm Mn(II), 10ppm Cd(II) and 10ppm Zn(II) using GMA25 overlaid with a 10 ppm Co(II) standard. Chromatographic conditions: Eluent: 0.1 m*M* HNO_3, flow-rate: 1 µL/min, injection volume: 100 nL, detection: on-column C^4D, effective column length: 14 cm

Figure 6.5: (a) Overlay of separations of 5 ppm Mn(II), 10 ppm Co(II), 10 ppm Cd(II) and 10 ppm Zn(II) using GMA30 and GMA35. (b) Overlay of separations of the metals standards carried out using GMA30. Chromatographic conditions: Eluent: 0.2 m*M* nitric acid. All chromatographic conditions as in Figure 6.4.

Figure 6.6: Overlay of separations of 5 ppm Mn(II), 10 ppm Co(II), 10 ppm Cd(II) and Zn(II) using 4 GMA30 monoliths. Chromatographic conditions: As in Figure 6.4.

Figure 6.7: (left) Separation of 1 ppm Mg(II) and 5 ppm Ca(II) overlaid with 5 ppm Ba(II) using GMA30. (right) Separation of 0.5 ppm Mg(II), 1 ppm Ca(II) and 5 ppm Ba(II). Chromatographic conditions: Eluent: 0.2 m*M* HNO_3, effective column length: 250 mm (GMA30) and 190 mm (GMA35). All other conditions as in Figure 6.4.

Figure 6.8: Linearity plots for Mg(II) and Ca(II) using GMA35 of concentration (mg/L) of Mg(II) and Ca(II) versus detector response (mV)

Figure 6.9: Overlay of chromatograms obtained for (a) blank sample (0.2 m*M* nitric acid), (b) 0.8 ppm Ca(II) and 0.25 ppm Mg(II) standard and (c) 100 fold dilution of the bottled water sample. Chromatographic conditions: Eluent: 0.2 m*M* nitric acid. All other conditions as in Figure 6.4.

Figure 6.10: Separation of 5 ppm Mg(II), 5 ppm Mn(II), 10 ppm Co(II), Cd(II) and Zn(II) using GMA30. Chromatographic conditions: Eluent: 0.2 mM nitric acid, effective column length: 250 mm. All other conditions as in Figure 6.4.

Figure 6.11: Overlay of 10 fold dilution of spiked pseudo seawater sample (a), 10 ppm Co(II), Cd(II) and Zn(II) standard solution (b) and un-spiked pseudo seawater (c). Chromatographic conditions: Column: GMA30, effective column length: 100 mm, eluent: 0.2 m*M* HNO_3. All other conditions as in Table 6.4.

Figure 6.12: Void peaks for injections of spiked pseudo seawater (black), un-spiked pseudo seawater (blue) and 10 ppm Co(II), Cd(II) and Zn(II) (red). The high ionic strength of the samples resulted in a maximum conductivity at 2500 mV. The void peaks contained high concentrations of Mg(II) and Ca(II) which were unretained.

Figure 6.13: Metal analysis of seawater samples from (I) Quays beach, Co. Clare and (II) Ringsend, Co. Dublin where (a) is unspiked seawater sample, (b) 10 ppm Co(II), Cd(II) and Zn(II) standards (b) and spiked seawater (c). Chromatographic conditions: Eluent: 0.2 m*M* HNO_3, column: GMA30, effective column length: 100 mm. All other conditions as in Figure 5.4.

Figure 6.14: Un-spiked tap water (a), 10 ppm Co(II), Cd(II) and Zn(II) standards (b) and tap water sample spiked with 10 ppm Co(II), Cd(II) and Zn(II) (c). Chromatographic conditions as in Figure 5.4.

Figure 6.15: Overlay of chromatograms of Co(II), Cd(II) and Zn(II) obtained over a 12 hour period. Chromatograms offset for clarity. All other chromatographic conditions as in Figure 5.4.

Figure A1.1: Backpressure profile obtained for HEMA-co-EDMA polymer monoliths with 40 % monomer (◊), 30 % monomer (◊), 20 % monomer (◊), 15 % monomer (◊) and 10 % monomer (◊). Measurements carried out using methanol and flow-rate increased from 0.5 – 8 µL/min.

Figure A1.2: SEM images obtained for monolith mixers: (a) 5 % monomer, (b) 10 % monomer, (c,d) 15 % monomer, (e) 20 % monomer, (f) 30 % monomer and (g,h) 40 % monomer.

Figure A1.3: Micro-fluidic nano-mixer chip showing the low (red) and high (blue) configuration.

Figure A1.4: Plot of wavelength (nm) versus peak height (V) showing that the optimum wavelength was between 565 nm and 570 nm. Separation conditions: Injection volume: 20 nL, Eluent: 5 m*M* nitric acid, PCR: 4 m*M* o-CPC, 10 m*M* boric acid pH adjusted to 9.8 with 250 m*M* NaOH, flow-rate: 1 µL/min (eluent and PCR).

Figure A1.5: Mg(II) peaks obtained on the FIA system using (a) the nano-mixer, (b) 15 % monomer monolith, 3.5 cm in length, (c) 20 % monolith mixer, 3.5 cm in length and (d) 3.5 cm of empty FSC.

Figure A1.6: Mg(II) peaks obtained using the FIA system with (a) the micro-fluidic nano-mixer, (b) the 15 % monolith mixer, 3.5 cm in length and (c) open tubular FSC, 3.5 cm in length. Injection volume: 20 nL, Eluent: 5 m*M* nitric acid, PCR: 4 m*M* o-CPC, 10 m*M* boric acid pH adjusted to 9.8 with 250 m*M* NaOH., flow-rate: 1 µL/min (eluent and PCR).

Figure A1.7: Injections of 500 ppm Mg(II) on the flow injection system using the optimised conditions. Chromatographic conditions: PCR mixer: Low dead volume T-piece, all other conditions as in Figure A1.6.

List of Tables

Table 4.3: Linear regression data from van't Hoff plots.

Table 5.1: Chromatographic performance data for transition and heavy metals obtained by varying eluent pH. Chromatographic conditions: Eluent: 0.2 m*M* – 0.4 m*M* nitric acid, column: VAL15a (250 mm x 100 µm I.D), injection volume: 20 nL, detection: on-column C^4D, flow-rate: 1 µL/min.

Table 5.2: Chromatographic performance data showing the direct comparison of on-column C^4D detection with UV-Vis detection for the separation of 5 ppm Mn(II), 10 ppm Cd(II) and 10 ppm Cu(II). Chromatographic conditions: Eluent: 0.2 m*M* HNO_3, all other chromatographic conditions as in Table 5.1.

Table 5.3: Chromatographic performance data obtained from the separations of 5 ppm Mn(II), 10 ppm Cd(II) and 10ppm Cu(II). Chromatographic conditions: Eluent: 0.2 m*M* nitric acid, all other conditions as in Table 5.1.

Table 5.4: Chromatographic performance obtained for the separation of Mn(II), Cd(II) and Cu(II) with increasing column temperature. Chromatographic conditions: Column: VAL15b, eluent: 0.1 mM HNO_3, effective column length: 230 mm x 100 µm I.D., all other conditions as in Table 5.1.

Table 5.5: Linear regression data from van't Hoff plots.

Table 5.6: Comparison of heats of adsorption (ΔH) on various analytical columns

Table 5.7: Chromatographic performance data for 6 metals using IDA modified polymer monoliths with increasing complexation capacity. Chromatographic conditions: eluent: 0.1 m*M* nitric acid, metal concentrations: 1 mg/L, all other conditions as in Table 5.1.

Table 5.8: Chromatographic performance data for the comparison of IDA polymer monoliths with varying degrees of complexation capacity using on-column C^4D and UV-Vis detection.

Table 6.1: Retention factor values for transition and heavy metals using poly(GMA) IDA-modified polymer monoliths with increasing complexation capacity. Chromatographic conditions: effective column length: 140 mm, detection: on-column C^4D and flow-rate: 1 µL/min.

Table 6.2: Comparison of *k* values for metal cations studied using poly(GMA) IDA-modified polymer monoliths and poly(VAL) IDA-modified polymer monoliths. Eluents used: VAL15, VAL 20 and VAL25: 0.1 m*M* HNO_3 and VAL30: 0.2 m*M* HNO_3

Table 6.3: Comparison of efficiency of poly(GMA) IDA-modified polymer monoliths and poly(VAL) IDA-modified polymer monoliths with other IDA functionalised columns.

Table 6.4: Chromatographic performance data obtained for the separation of Mn(II), Cd(II) and Zn(II) using GMA15, GMA20 and GMA25 and separations of Mn(II), Co(II), Cd(II) and Zn(II) using GMA30 and GMA35.

Table 6.5: Chromatographic performance data for alkaline earth metals using various GMA-IDA monoliths. Chromatographic conditions: Eluent: as specified in table, metals standard concentration: 5 ppm. All other condition as in Figure 6.4.

Table A1.1: % composition of monomer, cross-linker, porogen and initiator used in the preparation of the six polymer monolith mixers.

Table A1.2: Chromatographic performance data comparing mixing efficiency of monoliths of varying monomer concentration and varying lengths with a commercially available micro-fluidic nano-mixer.

Table A1.3: Peak areas (V.s) (n=6 injections) using the micro-fluidic nano-mixer, 15 % monolith mixer, open tubular fused silica capillary and low dead volume T-piece.

Acknowledgements

First and foremost, I would like to thank my supervisors Proff. Brett Paull and Dr. Damian Connolly for all your advice and encouragement throughout my years in DCU. It has been a tough journey and your guidance was greatly appreciated. Special thanks to Dr. Ekaterina Nesterenko for her assistance with the chelation work.

I would like to thank the Beaufort Marine Institute Awards and the Irish Separation Science Cluster for allowing me the opportunity to carry out this work.

To my lab colleagues, Nicola, Paddy, Sinead, Ugis, Gillian, Dave, Ali, Lily and Sara, I thank you for keeping me sane.

Special thanks to Dr. Leon Barron and Dr. Eoin Gillespie for your friendship and assistance during your time spent in DCU. You were both sorely missed when you left.

Thank you to my family, especially my mum and dad, for all the encouragement and financial assistance over the last few years. Without you, I wouldn't be the person I am today and I thank you dearly.

Finally, to my two handsome nephews Shane (4 years) and Pauric (1 year) and my beautiful niece Sorcha (9 months), who all made an appearance during my PhD and to whom I dedicate this thesis. Special thanks to Shane for showing me that 'just because' is not a valid answer to any question asked in life and for all the hours spent Nina and the Neurons. My science knowledge has been vastly improved thanks to Nina.

To all I have forgotten or omitted, I thank you too.

For Shane, Pauric and Sorcha

A child can ask questions that a wise man cannot answer
(Author unknown)

Abstract

The fabrication and modification of polymer monoliths, in capillary formats, for the separation of small ions is presented. The separation of small ions using polymer monoliths has limitations and this work aims to investigate increasing the ion exchange capacity using photo-grafting techniques. Chapter 1.0 includes a comprehensive review on the use of capillary ion chromatography including advancements made in capillary instrumentation, stationary phases and detection devices. This chapter also includes the various methods of modifying stationary phase with ionogenic functionalities suitable for use in capillary ion chromatography.

Chapter 2.0 shows the modification of polymer monoliths with quaternary ammonium ions, namely poly([2(methacryloyloxy)ethyl] trimethylammonium chloride) with immobilisation of the ion exchange functionalities taking place using photo-grafting techniques. In this work, the method of functionalisation of the polymer monolith was compared to a previously published polymer monolith bearing the same ion exchange functionalities. Chapter 2.0 also includes the separation of anions using a portable in-house assembled capillary ion chromatography system.

In Chapter 3.0, the photo-grafting of poly(3-sulfopropyl methacrylate) on a polymer monolith for the separation of cations is presented. The effect of temperature on the retention of Mg(II), Ca(II) and Ba(II) was carried out using an in-house constructed capillary column heater which was easily incorporated into the ion chromatography system. This chapter also introduces post-column reaction chemistry which involves the reaction of the eluted metals with a suitable reagent in a post-column mixer and detection of the coloured complex formed. In this work, the use of polymer monoliths as post-column mixers was investigated. Monoliths prepared with increasing pore size were incorporated into a flow injection analysis system and their suitability as post-column mixers was determined and compared to a commercially available post-column mixer.

Chapters 4.0 and 5.0 deal with the immobilisation of chelating ligands on a polymer monolith to produce a capillary chelating ion exchanger. Two methods of immobilisation of the chelating ligand were identified and compared. Scanning

capacitively coupled contactless conductivity detection was used to characterise the chelating stationary phases. Chapter 5.0 includes the use of a novel bimodal detector set-up i.e. on-column C^4D was used in conjugation with UV-Vis detection following the reaction of the eluted metals with a post-column reagent. Chapter 4.0 shows applications of the capillary chelating ion exchangers including the determination of Ca(II) and Mg(II) in bottled water samples and also the separation of metal cations in a spiked sea-water samples.

Chapter 1.0:

Literature Review

1.0 Background

Research carried out to date on the separation of small ions by ion chromatography using polymer based monolithic columns has proven to be less effective when compared to their silica based counterparts. This is mainly due to the reduced surface area exhibited by the polymer monolithic columns, therefore reducing the surface area available for modification with the desired functional groups. This literature review aims to dicuss the methods currently available for the separation of small ions using surface modified monolithic columns and improvements that have been made over the years. A number of methods have been reported for the surface modification of polymer and silica monoliths which will be discussed throughout the text. One method that has received little attention is the use of photo-grafting techniques to introduce functional groups onto the surface of the monolith and this thesis aims to further investigate this method of surface modification of polymer monoliths for use in the separation of anions and cations using capillary ion chromatography (CIC).

This thesis also aims to investigate the fabrication of chelating polymer monoliths through the photografting of chelating ligands onto the surface of the polymer monoliths, which has currently received no attention. The production of capillary chelating polymer monoliths demonstrates a novel, previously unpublished method for the separation of metal cations. The advantages of capillary chromatography is also descussed in detail throughout the text.

1.1 Introduction to ion chromatography

Since its development by Small *et al.* in 1975 [1], ion chromatography (IC) has become a widely used analytical technique for the separation of charged species. Separation in IC relies on the exchange equilibrium of the analyte ions in solution between the stationary phase and the eluent. As the eluent flows through the separation column, the eluent ions compete with the analyte ions for the ion exchange sites on the stationary phase thus displacing them. Electroneutrality must be retained at all times, therefore one monovalent eluent ion displaces one monovalent analyte ion [2]. Equation 1.1 demonstrates the replacement of an eluent ion with an analyte ion during the retention process. Retention depends on the affinity of the analyte ions

for the ion exchange sites. If the analyte ions have a high affinity for the ion exchange sites, they will be retained on the column longer than analyte ions that have a low affinity.

$$Res^+ E^- + A^- = Res^+A^- + E \qquad \text{Equation 1.1}$$

where Res^+ denotes the ion exchange resin, E^- denotes the eluent ions and A^- denotes the analyte ions.

Ion exchangers can be classified as strong or weak anion exchangers or strong or weak cation exchangers. Strong ion exchangers retain their charge over the entire pH range whereas weak ion exchangers are ionised over a narrow pH range. An example of a strong anion exchanger was demonstrated by Krata *et al.* [3], who used an AS14 column packed with 9 µm beads and surface functionalised with quaternary ammonium groups for the separation of anions. The authors separated 8 organic and inorganic anions using an eluent consisting of 1 m*M* $NaHCO_3$ and 3.2 m*M* Na_2CO_3. Separation occured in < 8.5 minutes with fluoride well resolved from the system peak. Weak anion exchangers are formed through the addition of a primary amine on the stationary phase matrix, however ion exchangers prepared this way have the disadvantage in that the eluent must be sufficiently acidic to give adequate anion exchange to obtain suitable retention [2]. The addition of sulfonate groups can produce strong cation exchangers such as the IonPac CS10 supplied by the Dionex Corporation. As mentioned previously, strong cation exchangers remain ionised over the entire pH range, whereas cation exchangers employing carboxyl groups, forming weak cation exchangers, are protonated at pH values of < 4 and lose their ion exchange capacity. Kadner *et al.* [4] separated sodium, lithium, ammonium and potassium using the IonPac CS10 (sulfonated) separation column and a 22 m*M* sulphuric acid eluent. All 4 ions were separated in a run-time of 15 minutes using a flow-rate of 1 mL/min and suppressed conductivity detection. The same authors also separated sodium, lithium, ammonium and potassium using an IonPac CS12A (carboxylic and phosphonic groups) separation column with a run-time of 6 minutes using an eluent consisting of 11 m*M* sulfuric acid. Separation of Mg(II), Sr(II) and Ca(II) was also possible, with a total run-time for all seven ions of < 12 minutes. The

separation of the alkaline earth metals using the IonPac CS10 separation yielded long run-times (> 20 minutes).

IC is now considered a mature technique for the separation of ionic species. Developments in stationary phase technology, instrumentation and detection modes ensure that it is a routinely used technique. A number of reviews have appeared in the literature with regard to ion chromatography including its conception and early development [5, 6] developments in ion chromatography [7-9], stationary phases in ion chromatography [10-14] and applications [15-17]. An number of text books on the topic of IC are also available [2, 18, 19].

1.2 Capillary ion chromatography

Interest in the use of capillary ion chromatography (capIC) has grown in recent years due to the advances made in stationary phase technology, particularly in the field of capillary monoliths and the use of capacitively coupled contactless conductivity detection (C^4D) detection [20]. Capillary columns are considered to have an internal diameter (I.D.) of 50 - 500 µm [21] as opposed to standard bore columns, which have an average I.D. of 4 mm.

There are a number of advantages in using capIC, which have been summarised in a review by Kuban and Dasgupta [20], such as improved sensitivity in comparison to a standard bore column, when the same mass of analyte was injected on both columns. Figure 1.1 shows a separation of common cations separated on a capillary column (0.4 mm I.D.), a microbore column (2 mm I.D.) and a standard bore column (4 mm I.D.). All columns were packed with the same packing material (CS12A) and contained surface carboxylic and phosphonic functionalities. In all cases, the injection volume was 0.4 µL. Flow-rates used were 10 µL/min for the capillary column (A) and 1 mL/min for the standard bore column (C).

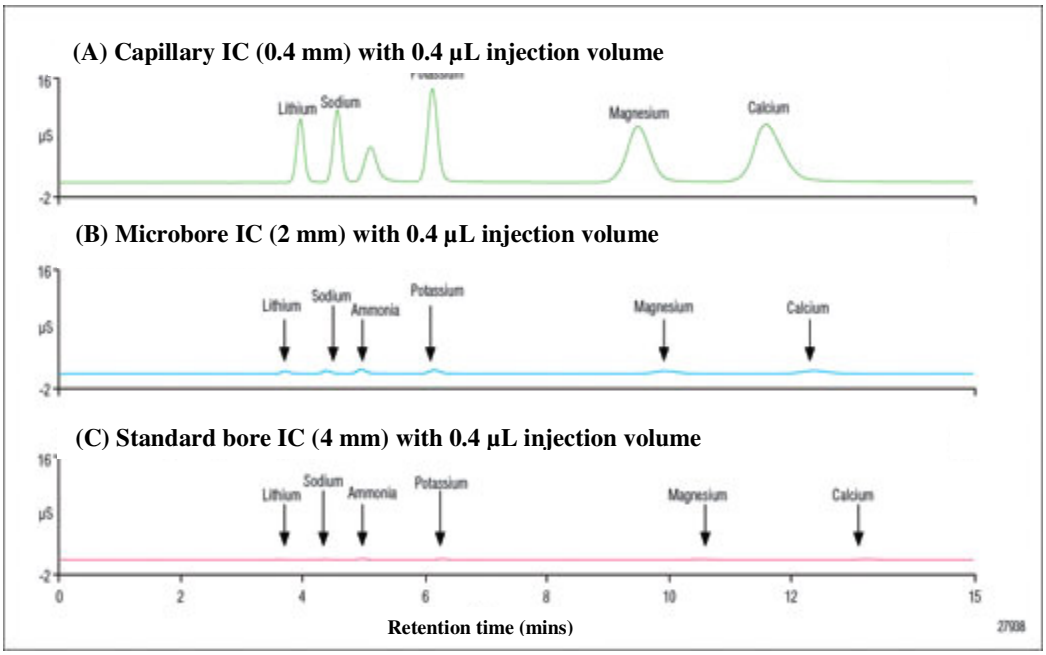

Figure 1.1: Comparison of detector sensitivity for the separation of cations using a capillary column (A), a microbore column (B) and a standard bore column (C). All columns are packed with the same packing material. An injection volume of 0.4 µL was used in all cases. Reproduced from [22].

As can be seen from this plot, a 100 fold decrease in the flow-rate from standard bore to capillary, resulted in a 100 fold increase in the analyte concentration passing through the conductivity detector for the capillary scale separation, resulting in an increase in the detector sensitivity when the capillary column was used [22]. Other advantages of capIC include low eluent consumption, therefore low waste generated. Due to the low eluent consumption, the system can be left continuously running and is therefore always ready to use. The low eluent consumption ensures that capIC is suitable for incorporation in microfluidic platforms and field deployable devices. CapIC is ideal for low sample injection which is important if only a small amount of sample is available [20]. The use of low flow-rates ensure that it compatible with sensitive detection techniques, such as mass spectrometry, as a flow splitter is not required prior to the analytes reaching the detector. The disadvantages of capIC include the requirement of the use of specialised equipment, such as analytical pumps capable of pumping at low µL/min or nL/min flow-rates. Extra-column volume also becomes an issue in capIC and the use of specialised fittings are required.

1.2.1 Commercially available capIC system

As mentioned previously, the internal diameter of capillary columns is < 500 µm and as such, the volume of each component (such as the injector valve and the detector cell) also need to be minimised. The Dionex Corporation recently launched the first commercially available capIC system (ICS 5000) consisting of a capillary pump capable of accurately pumping at flow-rates of 0.001–3 mL/min, an eluent generator capable of suppling hydroxide or methanesulfonic acid eluents which are commonly used in suppressed IC, an IC 'cube', which houses the injector valve, eluent generator degasser, the capillary column and capillary electrolytic suppressor. The 'cube' also allows for temperature controlled chromatography to be carried out. Detection on the capIC system is carried out using capillary conductivity with a 0.02 µL flow cell volume (as opposed to the standard flow cell which has a volume of 0.7 µL) [23].

1.2.2 In-house constructed capIC systems

Prior to the release of the capIC system by the Dionex Corporation, research groups investigated the use of novel in-house constructed capIC systems. In 1997, Sjogren *et al.* [24] constructed a capIC system incorporating a pump, an electrodialytic NaOH generator, an capillary particle packed separation column, a chemically regenerated suppressor and a protype capillary conductivity detector cell. The capillary particle packed column (500 mm x 180 µm I.D.) was packed with AS11 particles (containing quaternary ammonium functionalities) and was applied to the separation of 19 anions using a gradient elution profile (Figure 1.2).

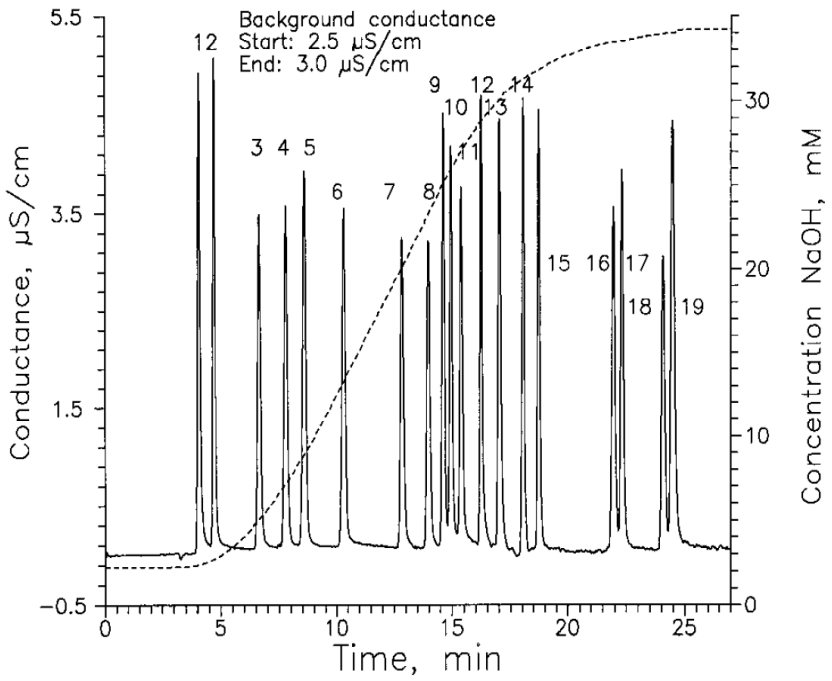

Figure 1.2: Separation of 19 anions using an in-house constructed capIC system using suppressed conductivity detection. Eluent: NaOH (gradient elution), injection volume: 100 nL, flow-rate: 2 µL/min, peaks (1) fluoride, (2) formate, (3) monochloroacetate, (4) bromate, (5) chloride, (6) nitrite, (7) trifluoroacetate, (8) dichloroacetate, (9) bromide, (10) nitrate, (11) chlorate, (12)selenite, (13) tartrate, (14) sulfate, (15) selenate, (16) phthalate, (17) phosphate, (18) arsenate, (19) citrate. Reproduced from [24].

Following on from the work in [24], the same research group produced a portable capIC system which incorporated a syringe pump, an electodialytic NaOH generator, a 100 nL injector valve, a packed capillary column made from fused silica capillary (500 mm x 180 µm I.D.), chemical suppressor and conductivity detection [25]. The capillary column was packed with AS11 particles (13 µm diameter with attached quaternary ammonium ions). A frit was prepared at the outlet of the capillary column by packing small pieces of glass wool into a 0.3 mm I.D PTFE tubing and pushing this into the the end of the fused silica capillary separation column. No entrance frit was used, which allowed trimming of the head of the column as the packing material became compressed over time. This system also incorporated a trap column packed with Chelex 100, a chelating metal resin to remove metal impurites, which was

situated prior to the separation column. The dimensions of the entire system were 28 x 43 x 15 cm with an overall weight of 10 kg. The use of the electrodialytic NaOH generator allowed for the gradient elution of 15 anions as shown in Figure 1.3.

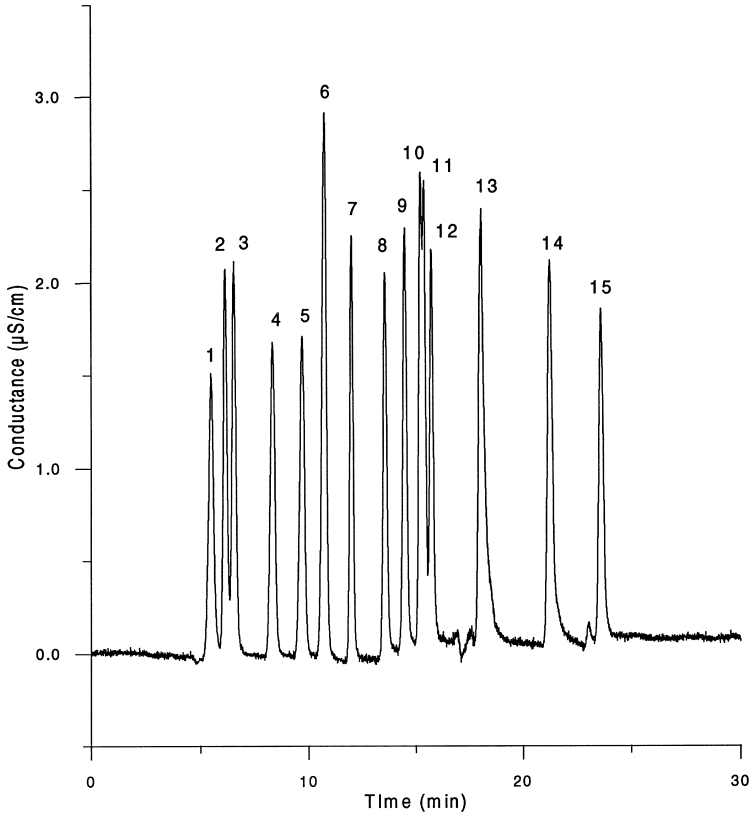

Figure 1.3: Separation of 15 anions using a capillary packed capillary column (500 mm x 180 µm) using a portable in-house constructed capIC system. Separation conditions; Eluent: linear gradient from 2 m*M* to 38 m*M* NaOH from 5 to 17 minutes, injection volume: 100 nL, flow-rate: 1.5 µL/min, peaks: (1) acetate, (2) formate, (3) methanesulfonate, (4) monochloroacetate, (5) bromate, (6) chloride, (7) nitrite, (8) trifluoroacetate, (9) dichloroacetate, (10) bromide, (11) nitrate, (12) chlorate, (13) sulfate, (14) phthalate, (15) chromate. Reproduced from [25].

1.3 Detection in IC

1.3.1 Conductivity detection

Conductivity detection is considered a universal detector in ion chromatography as all ions are electrically conducting. Conductivity detectors consist of a conductivity cell which houses two electrodes and are in constant contact with the eluent. Conductivity detection can be subdivided under two main headings, non-suppressed ion chromatography and suppressed ion chromatography.

1.3.1.1 Non-suppressed ion chromatography

In liquid chromatography, the eluent provides the greatest flexibility with regards to affecting the retention of ions [2]. The choice of eluent used in a particular separation must be compatible with the mode of detection employed in the system. In the case of non-suppressed conductivity detection, the eluent chosen should exhibit a low background conductance. The main advances made in non-suppressed IC were due to the use of ion exchange resins with low capacity. The capacity of a resin is a measure of the number of functional groups per unit weight of resin and is normally expressed as milliequivalents of exchangable ions per gram of resin or milliequivalents per millilitre of resin [18]. Ion exchange resins of lower capacity require a lower concentration of eluent to elute the sample from the column and an eluent with a low ionic concentration has a low conductivity. The most common eluents used in non-suppressed IC for the separation of anions are salts of carboxylic acids such as sodium or potassium salts of benzoic acids [26, 27] or phthalates [28, 29]. The main advantage of using non-suppressed conductivity detection is the simplicity in instrument set-up as extra hardware is not required. Extra hardware can lead to band broadening (as a suppressor is placed between the separation column and the detection device) increasing the overall dead volume of the system.

1.3.1.2 Suppressed ion chromatography.

In suppressed IC, a suppressor is placed between the separation column and the detection device and its function is to reduce the background conductivity of the

eluent prior to it reaching the conductivity detector, which in turn results in increased detector signal of the analyte. The background conductivity using a NaOH eluent for example, results in high background conductivity if un-suppressed, as the eluent in fully ionised and therefore highly conducting. NaOH can be suppressed by exchanging the Na^+ ions with H^+ ions to produce water, resulting in an eluent (which also contains the sample analyte) with a lower conductivity passing out of the suppressor into the conductivity detector which increases the sample analyte signal, as shown in Figure 1.4.

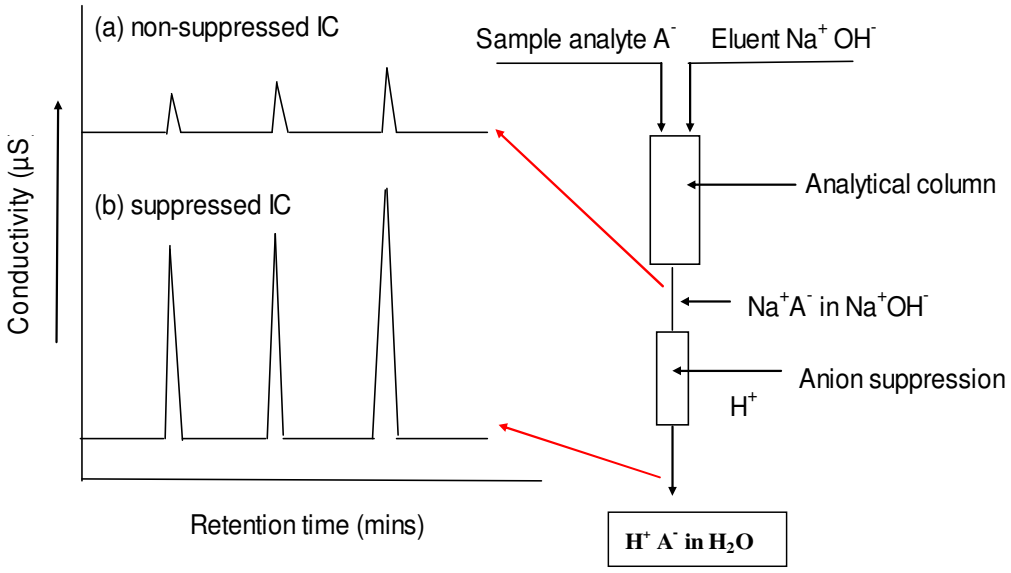

Figure 1.4: Increase in the conductivity signal of the analyte ion following the suppression of the NaOH eluent. Adapted from [31].

Examples of eluents used in suppressed IC include hydroxide [30], sodium hydrogen carbonate and sodium carbonate [3] and methanesulfonic acid [31, 32]. Examples of suppressors include packed bed suppressors, hollow fibre membrane suppressors and micro-membrane suppressors, a description on how they function has been documented in a review on suppressors by Haddad *et al.* [34]. Electrolytic suppressors are also available. Figure 1.5 shows a capillary electrolytic eluent suppressor (anion), available as part of the capIC system (ICS 5000) recently released by the Dionex Corporation. The design of the suppressor minimises dead volume, which is important as the suppressor is placed between the separation column and the detector. The suppressor consists of an ion exchange resin chamber (which also contains a coiled

membrane through which the eluent flows), with anode and cathode electrodes situated on each side, separated by membranes. The ion exchange resin contains an ion of opposite charge to that of the eluent ion. A current is applied to one electrode, forcing the regenerant ions into the ion exchange chamber via an electric field. Here, the regenerant ions exchange with the eluent ions through the coiled membrane where they are transferred from the ion exchange chamber into the second electrode chamber where they are removed. The suppressed eluent then passes through the conductivity detector [35].

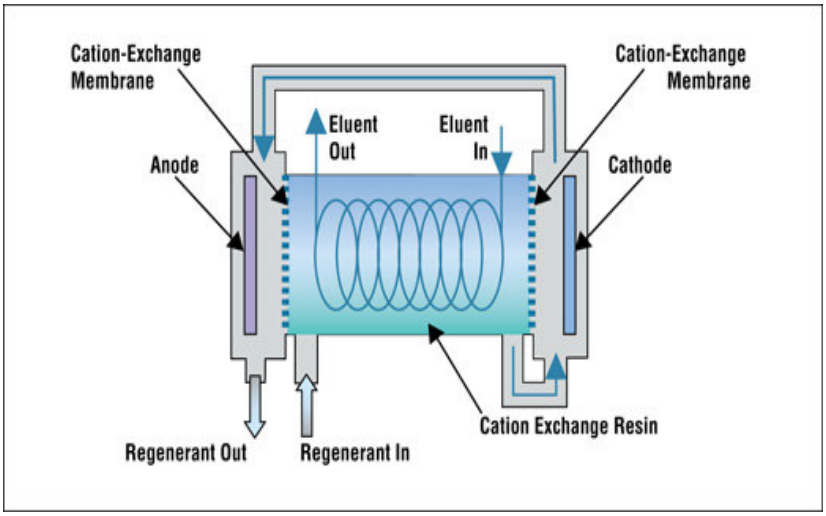

Figue 1.5: Capillary eluent suppressor (ACES^{TM} 300) available as part of the ICS 5000 capillary IC system. Reproduced from [35].

Standard bore conductivity flow-cells have internal volumes of 0.7 µL (Dionex) or 0.6 µL (Waters). Ion chromatography systems that are capable of analysis at capillary scale are generally equipped with UV detectors with a detector flow-cell volume of 0.02 µL. The use of conductivity detection at capillary scale has been possible through the use of capacitively coupled contactless conductivity detection (C^4D).

1.3.2 Capacitively coupled contactless conductivity detection.

Capacitively coupled contactless conductivity detection (C^4D) was first applied in capillary electrophoresis in 1998 [36] and has since being used in ion chromatography [37] and microfluidic platforms [38]. A number of reviews on the use of C^4D have appeared in the literature [39-41]. One of the main advantages of C^4D is that the arrangement of the ring electrodes around the fused silica capillary, as shown in Figure 1.6, means that this form of detection is contactless, therefore eliminating fouling of the electrodes. Other advantages includes the elimination of excess connective tubing, as the detector cell is placed on-column. This reduction in tubing reduces the effects of band broadening. The use of C^4D detection is also easily incorporated into an ion chromatography system as well as the low cost associated with the detection device.

C^4D detection is based on two ring electrodes (as shown in Figure 1.6) that are placed side by side which surround a capillary column, with the gap between the two electrodes (I) defining the detection volume (generally 2 mm, internal volume 16 nL). An AC voltage is applied to the first electrode and is picked up by the second electrode where it is amplified.

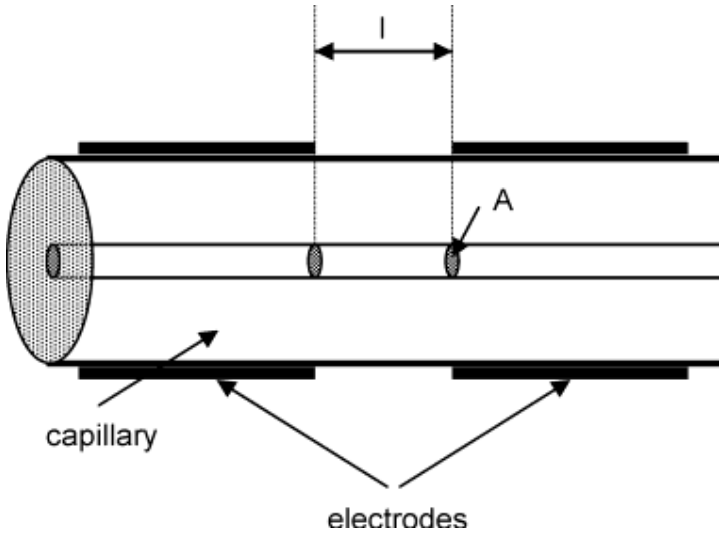

Figure 1.6: Two ring electrode encasing the separation column showing the cell area (A) and the distance between the two electrodes (I). Reproduced from [42].

As each electrode forms a capacitor with the solution inside the capillary, the conductivity of the liquid flow measured between the two electrodes can be determined [43]. As the analyte enters the detection gap, a reduction in resistance occurs and therefore an increase in conductivity.

In 2002, Kuban *et al.* [44] showed the effect of the electrode length and the distance between the two electrodes on the separation of selected cations using capillary electrophoresis. While varying the electrode length from 0.5 – 3.0 cm had no significant effect on column efficiency, a clear difference was noted when the detection gap was increased. Figure 1.7 (left) shows the effect of increasing the detection gap on the theoretical plates for the selected cations while (right) shows the differences in peak height obtained for the same cation separation when the detection gap was varied from 0.6 mm (A) to 5.1 mm (B). A peak efficiency of ~ 60,000 N/m was obtained for Mn(II) when the detection gap was 5.1 mm which increased to ~ 270,000 N/m when the detection gap was reduced to 0.6 mm.

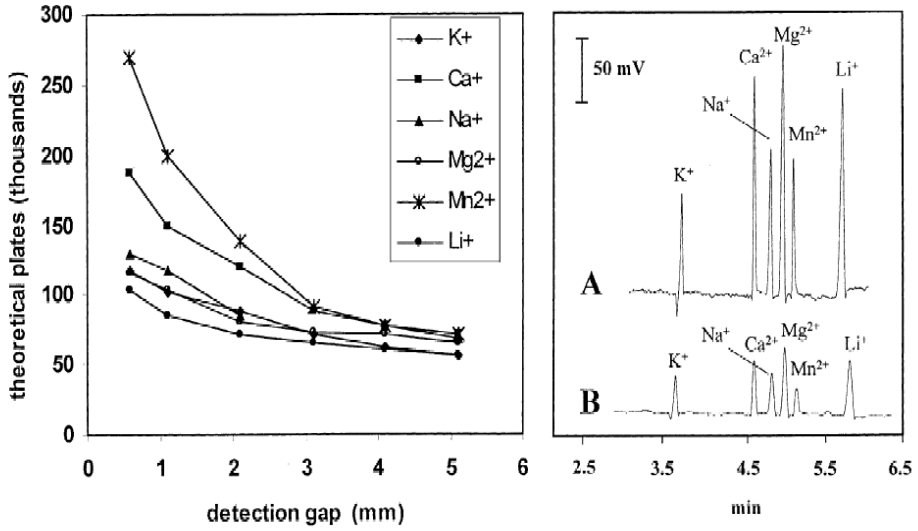

Figure 1.7: (left) Effect of detection gap on the efficiency of selected cations. (right) variation in peak height with a detection gap of 0.6 mm (A) and 5.1 mm (B). Reproduced from [44].

As mentioned above, the use of on-column C^4D detection eliminates extra-volume connective tubing associated with conventional conductivity detectors, as the detector head is placed on-column. The use of on-column C^4D is possible using columns with

an outer diameter (O.D.) of 375 µm, however, this does not mean that the use of C^4D detection is restricted to capillary columns. In 2004, Kubán *et al.* [43] used a Metrosep cation 1-2 column (125 x 4 mm I.D.) for the separation of lithium, sodium and potassium using non-suppressed C^4D detection. As the outer diameter of the separation column was > 375 µm, the authors used fused silica capillary, connected to the end of the separation column which facilitated the use of off-column C^4D detection. Off-column C^4D detection was compared to a conventional conductivity detector. The separations were carried out using a 1 m*M* tartaric acid eluent and a flow-rate of 1 mL/min. Using the same system set-up, the authors also obtained a separation of fluoride, chloride and nitrate using a Super-Sep anion exchange column (100 x 4.6 mm I.D.) with a 2.5 m*M* phthalic acid eluent. In this case, a flow-rate of 1.5 mL/min was used and an injection volume of 50 µL. The authors compared the LOD values obtained using both form of conductivity detection and found that the results were comparable. An LOD of 2.9 µg/L was obtained for lithium using off-column C^4D and an LOD of 3.4 µg/L was obtained for the same cation using conventional conductivity detection. Using the same anion exchange column, the authors carried out the same work using suppressed conductivity detection. Using a linear KOH gradient, the authors improved greatly on the LOD values for fluoride, chloride and nitrate using suppressed off-column conductivity detection. When non-suppressed C^4D detection was employed, an LOD value of 160 µg/L was obtained. With suppressed C^4D detection, an LOD of 1.5 µg/L was calculated.

In 2008, Gillespie *et al.* [26] fabricated a C^4D detector cell suitable for standard LC (1.6 mm O.D.). The authors used 2 copper electrodes, 2 mm in length wrapped around a length of teflon tubing. The electrodes were positioned 2 mm apart. A Faraday shield was used to surround the excitation electrode to prevent the capacitive coupling between the electrodes. The length of Teflon tubing encased by the electrodes was used to house the separation column. Following optimisation of the detector conditions, separations of nitrite and nitrate were carried out using on-column C^4D detection and a commercially available conductivity detector with similar dimensions. An eluent consisting of 2.5 m*M* sodium benzoate at a flow-rate of 20 µL/min was used. LOD values of 3.2 and 1.8 µg/L were obtained for nitrate and nitrite using C^4D detection and 5.2 and 2.0 µg/L using the commercially available detector.

Due to the capabilities of placing the detector cell on-column, the ability to place the detector cell at various positions along the column, thus affecting the effective column length, can be exploited. Ó Ríordáin *et al.* [37] demonstrated the use of on-column C^4D detection using a C_{18} silica monolith (150 mm x 0.1 mm I.D.) coated with N-dodecyl-N,N-(dimethylammonio)undecanoate (DDMAU) for the separation of anions in drinking water samples. Figure 1.8 shows chromatograms obtained when the detector was placed at various positions along the column.

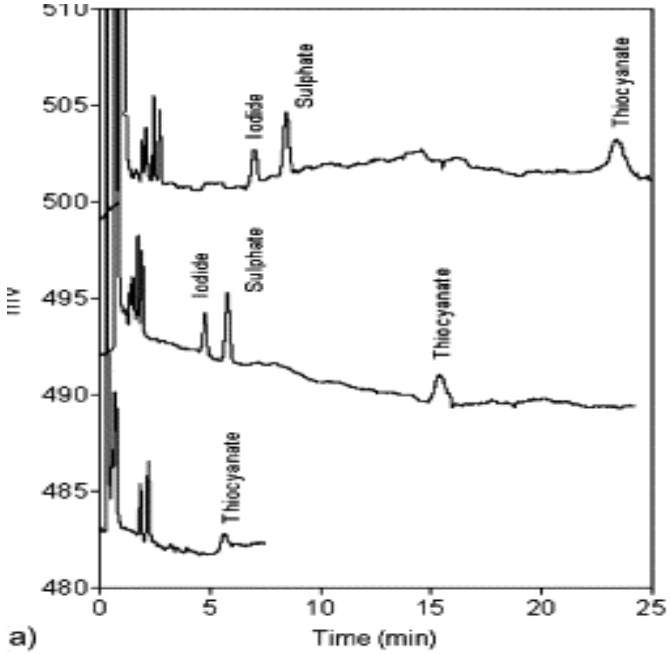

Figure 1.8: Separations of anions obtained by placing the detector at various positions along the column. The effective column length is 4.5 cm for the bottom chromatogram, 8.5 cm for the middle chromatogram and 12.5 cm for the top chromatogram. Chromatographic conditions: Eluent: 0.5 m*M* phthalate, flow-rate: 1 µL/min and injection volume: 50 nL. Reproduced from [36].

Ó Ríordáin's work demonstrated the ability to move the detector along the capillary to optimise separation efficiency and reduce the overall run-time of the separation. Due to the mobile nature of the C^4D detector cell, chromatographic performance with regards to resolution, efficiency and separation run-time can be optimised by varying the effective column length in a non-destructive manner when the columns are in

fused silica capillary formats. To vary the effective column length using conventional conductivity detection, cutting of the capillary column is required.

Due to the mobile nature of the C^4D detector cell, researchers began to investigate the information to be gained by scanning the entire length of the column and recording the conductive response at each pre-defined location [45]. The use of scanning C^4D techniques will be discussed in more detail in Section 1.6.4.

1.3.3 UV detection

UV detection is the most common form of detection used in high performance liquid chromatography, however within IC, UV detection is a selective detector and will only respond to certain ions [46]. A range of anions, such as nitrate, nitrite, bromide, chloride, iodide, iodate and phosphate are UV absorbing anions and can be detected using UV detection with a wavelength between 190 nm and 220 nm [2]. O'Ríordáin used UV detection at 214 nm for the detection of nitrate, nitrite, bromide, iodide and thiocyanate [47]. In this work, the author coated a Chromolith Performance C_{18} silica monolith with the surfactant dodecyldimethylamino acetic acid. The resultant ion exchange monolithic column was applied to the separation of the above mentioned anions using a 150 m*M* KCl eluent. The eluent also contained 0.2 m*M* dodecyldimethylamino acetic acid. Positive peaks were obtained as the molar absorptivity of the analyte anion exceeded that of the eluent ions, known as direct UV detection. In 2006, Li *et al.* [48] coated a Cromolith Flash RP-18e silica monolithic column with the surfactant cetylpyridinium chloride and used the resultant modified monolith for the separation of acetate, nitrate, bromide, tungstate, chromate and nitrite using UV detection at 210 nm. An eluent consisting of 20 m*M* sodium chloride was used at a flow-rate of 3 mL/min. Using a 20 µL injection volume, detection limits ranging from 1 – 19 µg/L were obtained. Using a 1.5 mmol/L phthalate eluent, the authors successfully separated the same group of 6 anions using UV detection at 279 nm. Negative peaks were obtained, as the molar absorptivity of the eluent was higher than the anions, known as indirect UV detection. In this case, detection limits of 100 - 500 µg/L were obtained demonstrating a loss in sensitivity using indirect UV detection. In 2004, Ueki *et al.* [49] prepared a polymer monolith with attached sulphonate groups. The authors separated ammonium, sodium, potassium, magnesium

and calcium using a 10 m*M* copper sulfate eluent with indirect UV detection at 210 nm. A flow-rate of 3 µL/min was used and an injection volume of 0.2 µL. More recently, Connolly *et al.* [45] modified the surface of a polymer monolith (120 mm x 100 µm I.D.) with 3-sulfopropylmethacrylate (SPM) to which the authors used for the separation of potassium, magnesium calcium and barium. An eluent consisting of 0.5 m*M* copper sulfate was used at a flow-rate of 1 µL/min using indirect UV detection at 210 nm. The injection volume was 50 nL.

Typically, UV detectors employed in standard systems have a flow cell volume of about 10 µL. Dionex have introduced the Ultimate 3000 variable wavelength detectors for use with capillary IC systems. The flow cells available for this detector include 3 nL, 45 nL and 180 nL, all with 10 mm optical pathlengths.

To improve sensitivity in IC, the use of post column reaction (PCR) detection is common practice. PCR requires the use of a reagent that can form coloured complexes with ions with a wavelength of maximum absorptivity well differentiated from that of the free reagent. Bromate can be determined using UV-Vis detection by reacting the bromate, as it elutes from the column, with a post column reagent *o*-dianisidine (ODA). This results in a complex that can be determined at 352 nm with detection limits in the sub-µg/L range [50]. UV-Visible detection with PCR is commonly used for the determination of metals using chelation ion chromatography [51]. The most commonly used PCR reagents are complexing dyes and there are a number of reagents available for post column chemistry such as 4-(2-pyridylazo) resorcinol (PAR) [52] and 2-(5-bromo-2-pyridylazo)-5-diethylaminophenol (5-Br-PADAP) [53] which are generally used for the determination of transition metals, *o*-cresolphthalein complexone (*o*-CPC) which has been demonstrated for the determination of alkaline earth metals forming stable purple complexes [54] and chrome azurol S (CAS) which has been used as a post column reagent for Be(II) [55]. PCR requires the use of a mixing coil to allow sufficient mixing of the analytes, as they are eluted from the column with the PCR reagent. Careful selection of the mixer is required as increases in the connecting tubing between the injector and detector can result in an increase in band broadening [51]. Open tubular eg. PEEK tubing is commonly employed as mixers in PCR chemistry and is normally coiled so as to aid mixing [51]. While PCR chemistry can improve sensitivity and selectivity, the

method does possess some disadvantages, such as the cost associated with a second pump, increased complexity in the system due to the incorportation of a PCR mixer, the deleterious effects on band broadening due to the requirements of the mixer and an increase in baseline noise.

1.4 Stationary phases in capIC

CapIC particulate packed columns are packed with the same packing material that is used for standard bore columns. A frit is placed at one end and the column packed under high pressure. Some of the earlier work in the field of capIC was carried out using modified packed silica columns. In 1996, Takeuchi *et al.* [56] packed a capillary column with silica particles (5 µm diameter) modified with bovine serum albumin (BSA). Using an eluent consisting of 1 m*M* sodium iodide and 0.3 m*M* tartaric acid, the authors separated chloride, bromide and nitrate in tap water samples. Following on from this, Zein *et al.* [57] used the same column for the separation of a range of anions (Figure 1.9) using various acidic eluents. Applications of the capillary packed column included anion analysis of saliva in smokers and non-smokers [57].

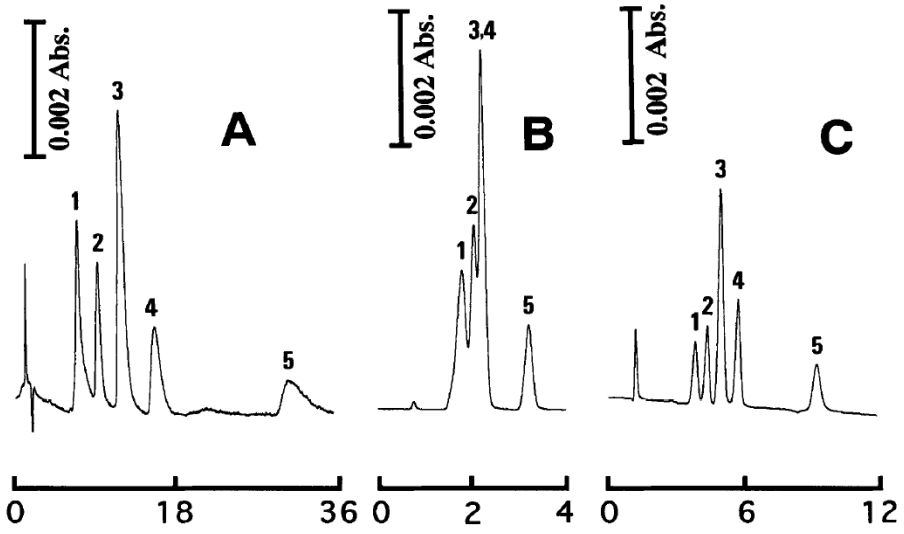

Figure 1.9: Separation of anions using a silica particle packed column (100 mm x 350 µm I.D.) modified with BSA. Separation conditions: eluent: (A) 3 m*M* aspartic acid, (B) 0.05 m*M* sulfuric acid, (C) 0.15 m*M* tartaric acid, Flow-rate: 5.6 µL/min, injection volume: 0.2 µL, peaks: (1) iodate, (2) bromide, (3) nitrate, (4) iodide, (5) thiocyanate. Reproduced from [57].

Takeuchi *et al*. [58] packed a capillary column with TKSgel IC Anion SW particles (silica based) and modified the surface with dextran sulfate. The resultant column was used for the separations of cations using a copper sulfate eluent as shown in Figure 1.10.

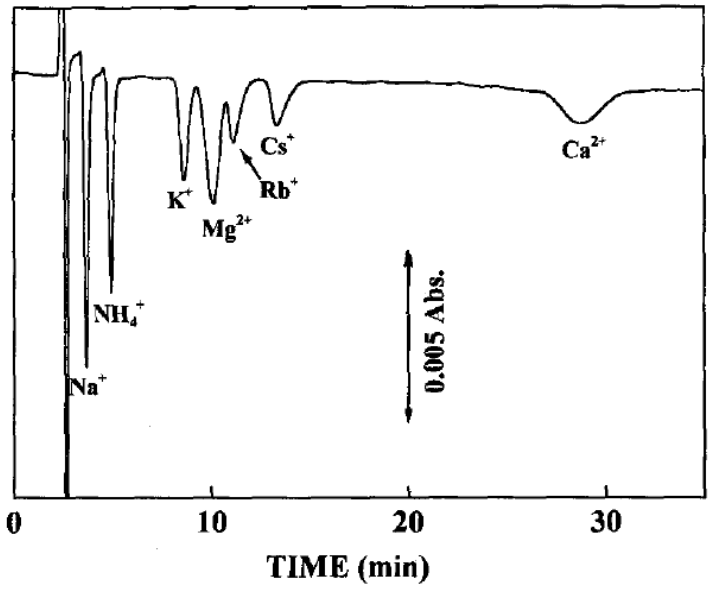

Figure 1.10: Separation of cations using a 100 x 0.32 mm I.D. TSKgel IC-anion SW, silica particle packed column (modified with dextran sulfate). Separation conditions: Eluent: 6 m*M* copper sulfate, flow-rate: 4.2 µL/min, injection volume: 0.2 µL, detection: indirect UV detection at 210 nm. Reproduced from [58]

Other commercially available particle packed (silica) capillary columns include the Jupiter range available from Phenomenex, which are packed with 3 - 15 µm silica particles. The silica particles are available with C18, C5 and C4 bonded phases. These columns are available in 300 or 500 µm I.D. formats and are used for the separations of proteins and peptides [59]. The same company also supply the Luna range which are packed with 3 - 15 µm silica particles, which are also available in 300 - 500 µm I.D. formats. These columns are also packed with C18, C5 or C4 bonded phases and are recommended for the separation of hydrophobic compounds. A cation exchange capillary column is also available as part of the Luna range. Attached benzene sulfonic acid bonded phases with a bead diameter of 5 or 10 µm are available in capillary formats (300 – 500 µm I.D.), with a surface area of 400 m^2/g [60].

Phenomenex also supply Onyx silica monolithic columns. The column dimensions are 150 mm x 100 µm I.D. and are currently available in C8 or C18 form. The ability to modify reversed phase stationary phases with surfactants (in the case of silica based stationary phases) has been studied. For example, O'Ríordáin *et al.* [37] modified an Onyx silica monolithic column (C_{18}) described above with N-dodecyl-N,N-(dimethylammonio)undecanoate (DDMAU), an amphoteric surfactant. The authors used the DDMAU modified silica monolith for the separation of inorganic anions using a 0.5 m*M* phthalate eluent. Average column efficiencies of ~ 35,000 N/m were obtained for the anions studied. Detection was carried out using on-column C^4D detection uisng a flow-rate of 0.3 µL/min.

Thermo also supply packed silica capillary columns in 320 µm I.D. formats. These columns are packed with silica particles with 1.9 µm particle size. The use of columns packed with smaller particles (< 2 µm) can improve separation efficiency. However, one of the biggest drawbacks of using smaller particles is the higher back-pressure that is generated. Because of this high pressure, heat is generated inside the column. The heat power generated per column volume increases with decreasing particle size [61]. The heat generated results in axial heating (from one end of the column to the other) and radial heating (from the centre of the column to the column wall). Temperature increases in the axial direction and decreases in the radial direction. These axial and radial gradients contribute to band broadening. A band of analyte will move faster in the core region of the column than at the column wall, as the core region is hotter and the mass transfer will increase. The viscosity of the eluent is higher near the wall of the column than at the centre, which will also contribute to band broadening. This in turn results in a loss of column efficiency. This temperature gradient will be significantly lessened with the use of capillary particle packed columns, as the heat has less distance to travel (from the centre of the column to the capillary wall) or with the use of monolithic columns as the backpressure exhibited by monolithic columns is lower than that of particulate packed columns.

The use of polymer packed capillary columns for the separations of anions has also been demonstrated [24, 25]. In recent years, Dionex have released standard bore analytical column materials in capillary format with internal diameters of < 0.4 mm. The AS18 capillary column (150 mm x 400 µm) is packed with 7.5 µm diameter

beads with attached quaternary ammonium functionalities and has a capacity of 1.71 μeq. This column has been applied to the separation of 11 inorganic anions, organic acids and oxyhalides using a 23 m*M* KOH eluent and suppressed conductivity detection. Using a 10 μL/min flow-rate, separation of the 11 analytes occurred in < 15 minutes [62]. The AS19 capillary column (250 mm x 400 μm), packed with particles of the same size and functional groups as the AS18, was applied to the separation of 22 anions using a KOH eluent gradient and a flow-rate of 10 μL/min [63] Separation of the 22 anions occurred in < 50 minutes at a temperature of 30 ^{o}C. In this case, the column capacity was 2.5 μeq.

Capillary cation exchange columns are also available from Dionex such as the CS16, packed with 5 μm particles with grafted carboxylic acid functionalities. This column (250 mm x 400 μm), was applied to the separation of lithium, sodium, ammonium, potassium, magnesium and calcium using a 30 m*M* methanesulfonic acid eluent and a 10 μL/min flow-rate [64]. The analysis was carried out at 40 ^{o}C with baseline resolution of all analytes occurring in < 18 minutes. This column had a capacity of 80 μeq. Finally, CS12A capillary columns packed with 8 μm or 5 μm particles with grafted carboxylic acid and phosphonic acid functionalities are also available. Using a 20 m*M* methanesulfonic acid eluent, separations of lithium, sodium, ammonium, potassium, magnessium and calcium are possible in < 10 minutes at a flow-rate of 12 μL/min. Increasing the flow-rate results in the separation of all 6 cations in < 7 minutes. The capacity of this column was 28 μeq [65].

The packing of particles into capillaries is a difficult task and the use of monoliths has received significant attention in capLC due to their ease of manufacture, as the monolith is polymerised within the capillary walls. A decrease in column efficiency is usually observed at higher flow-rates using particulate packed columns, as separation is based on diffusive mass transfer of the sample analytes into the pores of the particle. Also at higher flowrates, particle based columns exhibit higher back-pressures [66].

Van Deemter (equation 1.2) summarised the column effects that contribute to plate height and thus band broadening.

$$H = A + \frac{B}{u} + Cu \qquad \text{Equation 1.2}$$

where A = eddy diffusion, B = longitudunal diffusion, C = mass transfer of the analyte between the eluent and the stationary phase and u = linear velocity of the eluent.

Nguyen *et al.* [67] showed the effect of reducing the particle size on the C-term of the Van Deemter equation. By decreasing the particle size from 10 µm to 1.7 µm, the authors noted improvements in the plate height resulting in a flatter C-term from the constructed Van Deemter plots. However, a disadvantage of using smaller particles is the increase in the back-pressure generated [67]. Another method of exploiting the flatter C-term from the Van Deemter equation is through the use of monolithic columns [68].

1.5 Monoliths

1.5.1 Introduction

In the last number of years, monoliths have become increasingly popular in chromatographic separations. This is evident in the number of reviews published on the topic [69-76]. The introduction of monoliths marked significant increases in the use of capLC. Silica and polymer monoliths have been applied to a wide range of analyte separations such as oligonucleotides [77-79], proteins and peptides [80-82] and carbohydrates [83], however, this section will focus on the use of capillary polymer and silica monoliths for the separation of small anions and cations.

A monolith is a single piece of porous material that is formed of interconnecting flow-through channels from one end of the capillary to the other. Monoliths have a number of advantages over particle packed columns. One of the main problems associated with particle packed columns is the void volumes that exist between the particles.

Even the best packed columns contain 35 – 40 % void volume in addition to the internal porosity of the beads [84]. This leads to band broadening and decreases the efficiency [85]. As monoliths are a single piece of porous material, the effect of band broadening due to voids between particles is eliminated. A second advantage of monoliths over particle based columns is that in particle based columns, the analyte penetrates into the inner pores of the porous particle and this slows down the speed of the separation [85]. The mass transfer of the analyte between the eluent and the stationary phase should be fast and frequent [72]. Separation in particulate columns depends upon diffusive mass transfer and this is slow and unfavourable for large molecules. In monoliths, the eluent is forced to flow through the pores of the monolith and this enhances the mass transfer rate [86]. This also ensures that there is constant interaction between the eluent and the stationary phase which results in increased mass transfer, even when high flow rates are used. Figure 1.11 shows the flowpath of the eluent through a particulate packed column (a) and a monolith column (b).

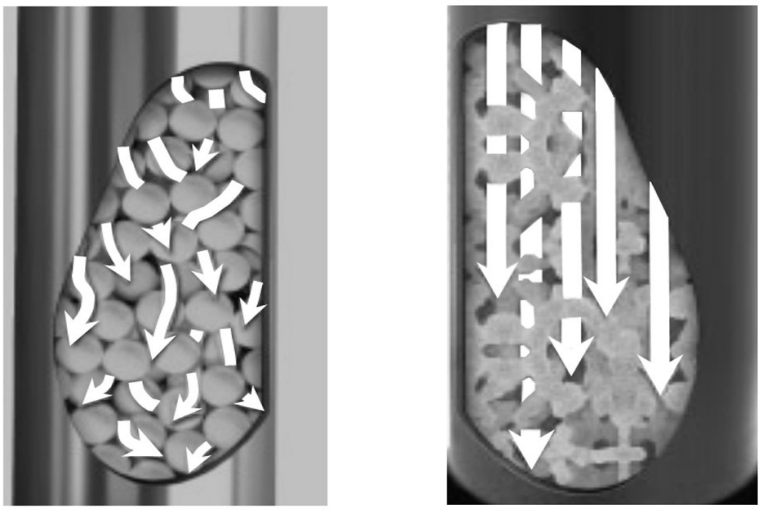

Figure 1.11: Flowpath of the eluent through a particulate packed column (A) and a monolith column (B). Reproduced from [87].

Figure 1.12 shows a comparison of Van Deemter plots obtained using a particle packed column (Kingsorb C18, 30 cm x 4.6 mm I.D, particle size of 3 µm) and a Chromolith monolithic stationary phase (50 mm x 4.6 mm I.D.) [66]. As can be seen

from this plot, a flatter C-term was obtained using the monolithic stationary phase, allowing the use of faster flow-rates, without any significant loss in column efficiency

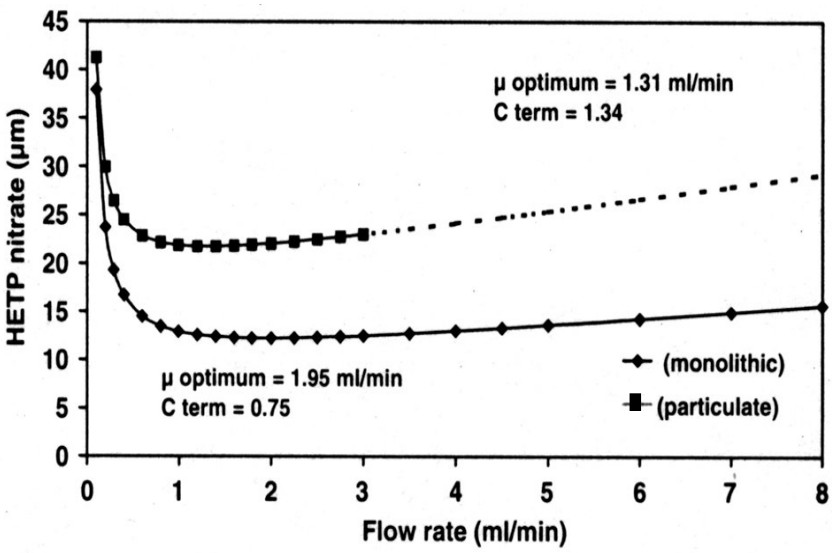

Figure 1.12: Comparison of Van Deemter plots for a 3 µm particle packed column and a monolithic column. Reproduced from [66].

The high column permeability associated with monoliths allows the use of longer columns, resulting in highly efficient separations [88]. Other advantages of monoliths include the fact that frits are not required to hold the monolith in place, as the monolith is covalently bonded to the walls of the capillary. As well as keeping the monolith in place, the attachment of the monolith to the capillary wall (the capillary column in pretreated to allow the covalent attachment of the monolith to the capillary wall) also prevents the eluent from flowing down the sides of the monolith, ensuring that the eluent and therefore the sample analytes are forced to percolate through the monolith bed [84]. Finally, the surface of the monolith can be modified with a wide range of surface functionalities (particularly in the case of polymer monoliths) and have become particularly useful in the field of ion chromatography for the determination of small anions and cations.

It is well known that silica monoliths are more efficient in the separations of small ions than polymer monoliths due to the increased surface area exhibited by the silica monoliths. This is due to the mesoporous structures available on the surface of the silica monoliths [87]. Silica monoliths generally have a porosity greater than 80 %

and a surface area of about 300 m^2/g [66]. While the use of silica monoliths are useful for the separation of small ions, they are not as efficient in the separation of large molecules, such as proteins. The opposite can be said for polymer monoliths. Due to the absence of mesopore structures on the polymer monolith surface, mass transfer is enhanced for the separation of large molecules [80-82].

One of the major drawbacks in the use of silica monoliths in ion chromatography is the limited pH range in which they can be operated (pH 2.0 – 8.0). Polymer monoliths are stable over the entire pH range, whereas at pH values greater than 8, silica dissolves, leading to poor efficiency, poor reproducibility and high back pressures [87, 89]. As well as being stable over the entire pH range, polymer monoliths are also more resistant to high temperatures. At pH < 2, the silylether bond on the silica monolith is hydrolysed which can lead to a loss of the bonded ligand.

1.5.2 Polymer monoliths

1.5.2.1 Fabrication

For the fabrication of methacrylate polymer monoliths, the polymerisation mixture consists of a monomer, cross linker, porogens and a free radical initiator [88]. The monomer used will determine the polarity of the final monolith, pore formation depends on the type of porogen and concentration of cross linker used and the choice of initiator depends on the mode of polymerisation. Polymerisation starts when the mixture is heated (using thermal polymerisation) [49] or initiated using UV (using photopolymerisation) [90] to create free radicals. Another less common method of polymerisation includes polymerisation via γ-irradiation [85, 91].

As the polymerisation proceeds, polymer chains form that will not be dissolved and will precipitate as nuclei in the reaction medium, as their solubility in the porogen decreases. Polymerisation continues to take place both within the nuclei and in the surrounding mixture. The concentration of monomer within the swollen nuclei is higher than the surrounding mixture and the nuclei continue to swell. As the nuclei become bigger, they begin to form clusters. These clusters continue to grow and

eventually form an interconnected matrix with neighbouring clusters. Structural rigidity is secured through extensive cross linking to form a porous polymer monolith.

Photopolymerisation has a number of advantages over thermal polymerisation, such as faster polymerisation times and the ability to place the monolith in pre-defined sections by masking of other areas, which is useful for the incorporation of monoliths into microfluidic channels. A recent study comparing the polymerisation of a GMA-*co*-EDMA polymer monolith (100 µm I.D fused silica capillary) using thermal polymerisation and photopolymerisation has been carried out by by Bruchet *et al.* [92]. The authors used the same polymerisation mixture as Ueki *et al.* [81] and the only difference in the preparation of the polymer monoliths was the mode of polymerisation used. Ueki *et al.* [49] used thermal polymerisation during the fabrication of the polymer monolith (60 ^{o}C x 24 hours), whereas Bruchet *et al.* [92] used photopolymerisation (30 minutes irradiation time). In all cases, AIBN was used as the initiator. Scanning electron microscopy (SEM) images obtained by Bruchet *et al.* [92] showed globules of 1 µm diameter, while SEM analysis carried out by Ueki *et al.* [49] showed polymer globules of 2 – 5 µm diameter demonstrating that although the same polymerisation mixture was used in both sets of work, the mode of polymerisation used during the fabrication of the polymer monolith will have an overall effect on pore diameter.

1.5.2.2 Monomers and cross linkers.

Figure 1.13 shows the chemical structure of common monomers used in the polymerisation of methacrylate monoliths. The most widely used monomers for the production of methacrylate monoliths is glycidyl methacrylate (GMA). This is mainly due to the presence of reactive epoxy groups that facilities surface modification [93]. Other monomers used in the polymerisation of polymer monoliths include butyl methacrylate (BuMA), which incorporates hydrophobic functionalities into the final monolith structure and hydroxyethyl methacrylate (HeMA), which forms a hydrophilic stationary phase. Ethylene dimethacrylate (EDMA) is a commonly used cross linking monomer in the formation of methacrylate monoliths. High % content of cross linking monomers, results in more highly cross-linked polymers formed in the early stages of polymerisation, which leads to a decrease in the average pore size

[68]. Viklund *et al.* [89] prepared GMA-*co*-EDMA monoliths with varying concentrations of the cross linker, EDMA. The authors noted a decrease in the diameter of the flow-through pores as the concentration of the cross linker was increased.

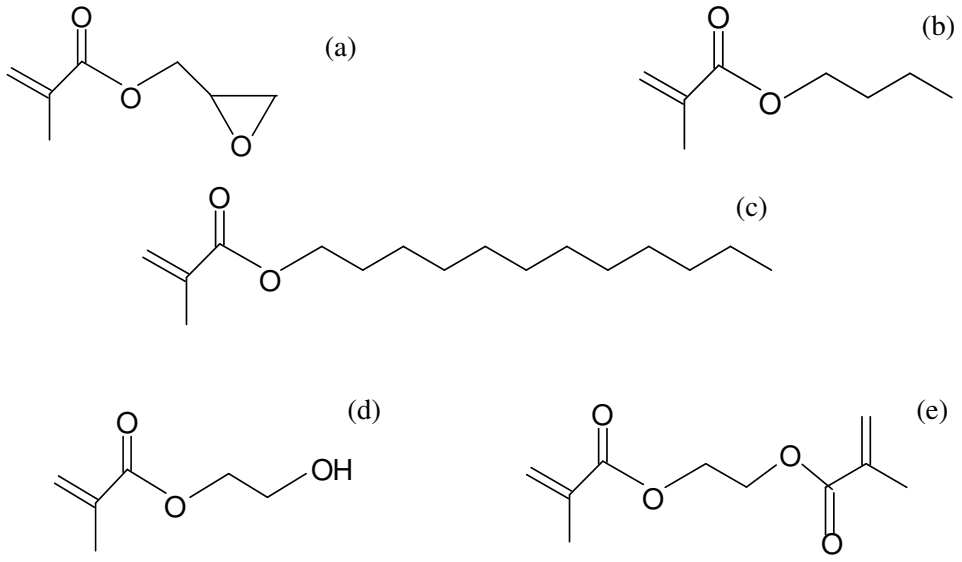

Figure 1.13: Chemical structures of methacrylate monomers and cross linkers. used in the polymerisation of polymer monoliths. (a) glycidyl methacrylate (GMA), (b) butyl methacrylate (BuMA), (c) lauryl methacrylate (LMA), (d) hydroxylethyl methacrylate (HeMA) and (e) ethylene dimethacrylate (EDMA).

Styrene based polymer monoliths with divinylbenzene as a crosslinker prepared in capillary formats have also been reported in the literature which have been applied to the separation of small molecules such as antibiotics and thyroid hormones [94] and alkylbenzenes [95, 96].

1.5.2.3 Porogens

The porogens are considered the most important factor in relation to pore size control. Porogens can be described as being 'good' or 'bad' solvents for the polymer. If the porogen is considered a good solvent for the polymer, phase separation (nucleation) occurs later resulting in an increased number of nuclei before all the monomers are

exhausted. This results in the formation of a large number of swollen nuclei, which coalesce forming smaller pores. If the porogen is a 'bad' solvent, phase separation occurs early in the polymerisation system which lead to the formation of a limited number of nuclei and larger pores are formed [85].

In 2004, Lee *et al.* [90] showed the effect of porogen composition on the formation of the pores. A BuMA-*co*-EDMA monolith was prepared using 1-decanol as the porogen and a second BuMA-*co*-EDMA monolith was prepared using a porogenic mixture consisting of 1-decanol and cyclohexanol. Figure 1.14 shows the SEM images obtained for both monoliths showing that although the overall concentration of the porogens was the same in both monoliths (60 %), differences in the pore sizes were noted. Figure 1.14 (A) shows the SEM image obtained when 1-decanol was used solely as the porogen and Figure 1.14 (B) shows the SEM image obtained when cyclohexanol was added to the porogen mixture. The monolith using 1-decanol as the porogen exhibited smaller pores in comparison to the monolith in which cyclohexanol was used as the porogen.

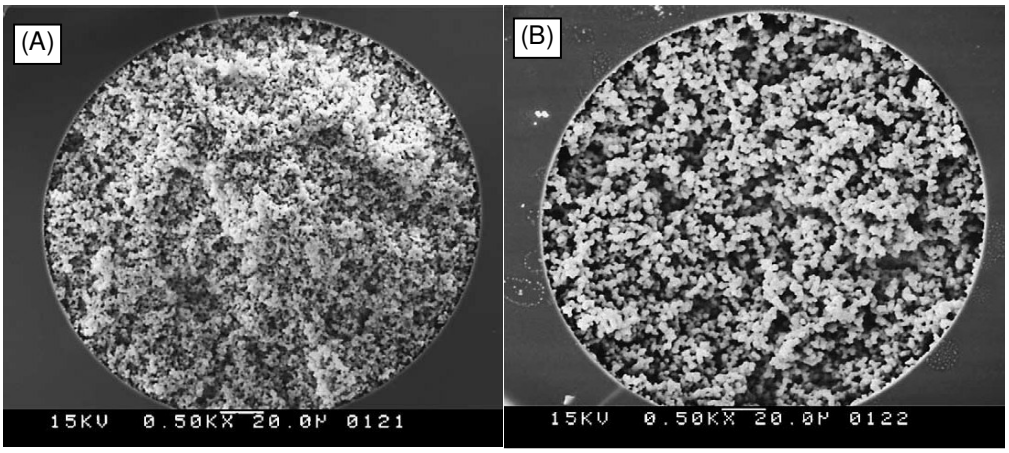

Figure 1.14: SEM images of BuMA-co-EDMA polymer monoliths using (A) 1-decanol as the porogen and (B) using a mixture consisting of 1-decanol and cyclohexanol. Reproduced from [90].

1.5.2.4 Temperature of polymerisation

The temperature at which polymerisation takes place has an effect on the pore size formed. Generally the higher the temperature, the smaller the pores [79]. The iniatiator used in the polymerisation mixture decomposes at a certain temperature, which results in the formation of free radicals. Higher temperatures leads to the formation of a large number of free radicals. The free radicals, in turn, lead to the formation of nuclei and globules. As the concentration of the monomers remains the same for each polymerisation regardless of the temperature, the rate of nuclei formation results in a large number of swollen nuclei and as the swollen nuclei coalesce, smaller pores are formed. The effect of temperature on the size of the pores formed was demonstrated by Viklund *et al.* [89]. GMA-*co*-EDMA monoliths, using a porogenic solution consisting of dodecanol and cyclohexanol, were prepared at different polymerisation temperatures. This work showed that at a temperature of 55 ^{o}C, the formation of free radicals was slow and large pores (1,010 nm average pore diameter) were formed. At higher temperatures of 70 ^{o}C, the formation of free radicals was faster, resulting in the formation of smaller pores (120 nm average pore diameter). The specific surface was 17 m^2/g when the polymerisation was allowed to proceed at 55 ^{o}C and 43.2 m^2/g at 70 ^{o}C. This shows an increase in the surface area of the polymer monolith due to the use of a higher polymerisation temperature.

1.5.3 Controlling the surface chemistry of polymer monoliths

1.5.3.1 Co-polymerisation of polymer monomers with desired functionalities.

In order to render a monolith suitable for ion exchange chromatography, ionic groups on the pore surface are required. The first method is carried out by the preparation of monoliths by the direct co-polymerisation of monomers with desired functionalities. A monomer with ionisable groups will result in a final monolith having ionisable groups [73]. Gu *et al.* [97] prepared a 160 mm x 75 µm polymer monolith using a polymerisation mixture consisting of 2,2-dimethoxy-2-phenylacetophenone (DMPA), 2-acrylamido-2-methyl-1-propanesulfonic acid (AMPS) and poly(ethyleneglycol) diacrylate (PEGDA) dissolved in a porogenic mixture containing water, methanol and ethyl ether. The final monolith afforded sulfonate groups due to the presence of

AMPS in the polymerisation mixture and was used for the analysis of peptides. Li *et al.* [98] prepared a polymer monolith via copolymerization of 2-(acryloyloxy)ethyl trimethylammonium chloride and polyethylene glycol diacrylate (PEGDA). The resultant monolith, with quaternary amine anion exchanger groups was applied to the separation of proteins.

There are a number of advantages to using this approach. There are a wide range of monomers with ionisable sites available for polymerisation. As the functional groups are incorporated into the monolith during the polymerisation step no further modification is required. However this method does have the drawback that a large number of the functional groups become embedded inside the polymer matrix and cannot be used as ion exchange sites. Changing the monomer type or concentration in a polymerisation mixture requires re-optimising of the polymerisation conditions, which can be a time consuming task [79].

1.5.3.2 Addition of functional groups on the surface of the monolith

To date, only a small number of research groups have studied the retention of small ions using capillary polymer monoliths modified with ion exchange functionalities. Ueki *et al.* [49] prepared a GMA-*co*-EDMA polymer monolith in 250 µm I.D fused silica capillary formats. The surface of the monolith was subsequently reacted with Na_2SO_3 at 70 ^oC allowing the attachment of sulfonated groups through ring opening of the epoxy groups. In this work, the authors demonstrated the ability to increase the ion exchange capacity of the polymer monolith by varying the conditions used during sulfonation (such as reaction time, concentration of Na_2SO_3 and solution pH). Increasing the reaction time from 1 hour to 12 hours resulted in a increase in the ion exchange capacity of the polymer monolith from 19 µequiv/mL to 92 µequiv/mL respectively. The ion exchange capacity was further increased (300 µequiv/mL) when the solution pH was increased from pH 6 to more alkaline pH conditions (pH 11). As expected, an increase in the ion exchange capacity resulted in an increased retention of all metal cations studied. The separation was carried out using a 10 m*M* copper sulphate eluent and a flow-rate of 3 µL/minute as shown in Figure 1.15. Detection was carried out using indirect UV detection at 210 nm. Average peak efficiencies of 20,000 N/m were obtained.

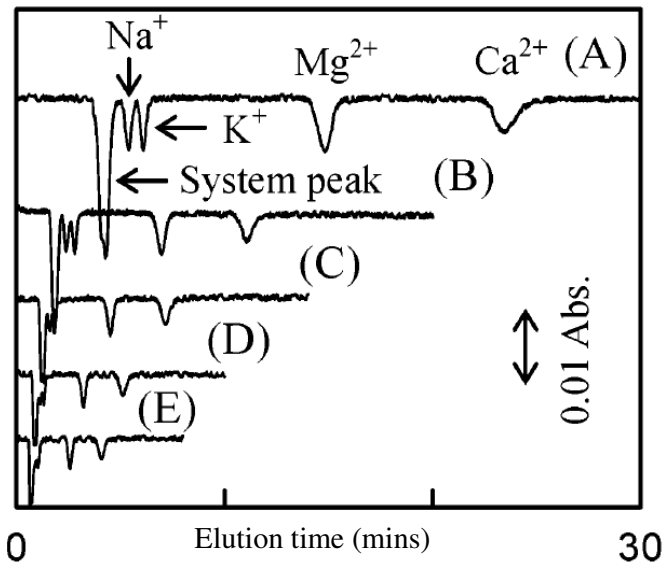

Figure 1.15: Separation of selected cations using a sulphonated polymer monolith. Separation conditions: Eluent: 10 mM copper sulphate, flow-rate: (A) 3 µL/min, (B) 6 µL/min, (C) 9 µL/min, (D) 12 µL/min and (E) 15 µL/min, detection: indirect UV at 210 nm, injection volume: 0.2 µL. Reproduced from [49].

In 2007, Kanatyeva *et al.* [99] prepared a GMA-*co*-EDMA monolith and functionalised the surface using three different methods, the first involved modification with polyethylenimine (PEI), the second involved modification with dimethylamine (DMA) and the third monolith was modified with a mixture of PEI and DMA (1:1). The authors noted that the monoliths modified with PEI demonstrated the lowest retention and selectivity for selected anions, while the monolith modified with DMA yielded long retention times and low efficiency. The monoliths modified with the mixture of PEI and DMA gave optimum results in terms of selectivity and retention time. The anions used in this study were fluoride, chloride, nitrate, nitrite and bromide and the separation can be seen in Figure 1.16. Although inproved separation was obtained using the polymer monolith prepared using a mixture of PEI and DMA, a run-time of 80 minutes was required to separate all six anions.

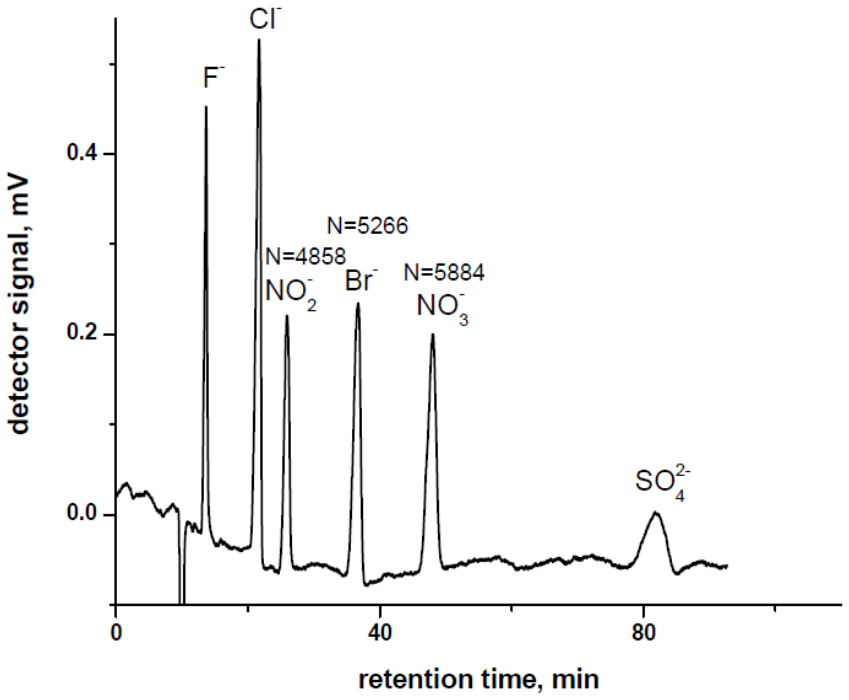

Figure 1.16: Separation of selected cations using a GMA-co-EDMA polymer monolith modified with a mixture of PEI and DMA. Separation conditions: Eluent: potassium phthalate, detection: UV detection at 254 nm. Reproduced from [99].

In 2011, Bruchet *et al.* [92] prepared a GMA-*co*-EDMA monolith in 100 µm fused silica capillary. The surface of the monolith was modified by flushing a solution of triethylamine (TEA) in 50:50 v/v ethanol/water through the polymer monolith for 4 hours at 85 ^{o}C at 1 µL/min. The final monolith modified with quaternary ammonium functionalities was applied to the separation of iodate, bromate, nitrite, bromide and nitrate as shown in Figure 1.17. The ion exchange capacity was measured using break through experiments and found to be 8 nequiv/cm. Calculated efficiencies of 75,000 N/m for nitrate, bromate and nitrite were obtained using a sodium perchlorate eluent at a flow-rate of 100 nL/min. At 700 nL/min peak efficiencies of ~ 18,000 N/m were reported.

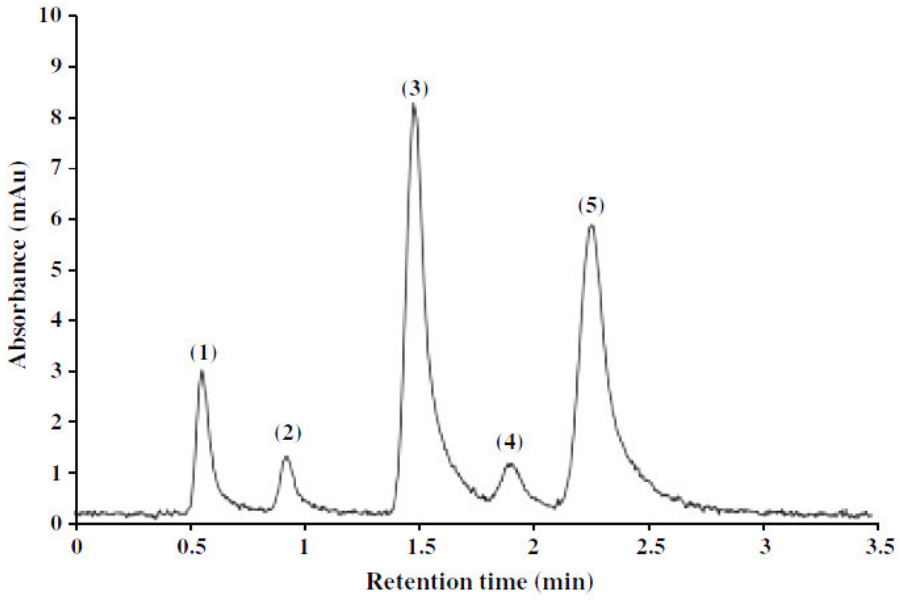

Figure 1.17: Separation of (1) iodate, (2) bromate, (3) nitrite, (4) bromide and (5) nitrate using a GMA-co-EDMA polymer monolith functionalised with quaternary ammonium functionalities. Eluent: 10 m*M* $NaClO_4$, injection volume: 10 nL, detection: UV at 210 nm, column dimensions: 100 µm x 750 mm. Reproduced from [92].

1.5.3.3 Photo-grafting

To avoid re-optimising of the polymerisation conditions a second method has been studied. The second method involves the fabrication of a generic monolith followed by modification of the surface chemistry of the monolith (post polymerisation) via photo-grafting methods. This method has the advantage in that all the grafted functionalities are available on the surface of the monolith. Other advantages of using this method include that fact that grafted functionalities can be precisely placed on different sections of the monolith by masking off other sections prior to the application of UV energy [100], or the ability to functionalise different sections of the monolith with different surface chemistries [101].

Research has also been carried out on the photografting of functionalities onto the surface of a polymer monolith structure. As mentioned previously, the separation of

small ions on polymer monoliths is challenging, due to the reduction in the surface area in comparison to silica based monoliths. This reduction in the surface area in polymer monoliths results in a limited number of reactive sites available on the surface of the monolith, resulting in limited access for the incorporation of ion exchange functionalities. One method to increase the number of available sites is the growth of highly branched polymer chains from each reactive site on the monolith surface.

In 1999, Rånby [101] demonstrated the surface photografting (on a low density polyethylene film) of a polymer (acrylic acid) in the presence of the free radical initiator, benzophenone using UV energy. In 2003, Rohr *et al.* [102] applied this benzophenone initiated surface polymerisation chemistry to BuMA-*co*-EDMA polymer monoliths, where the authors modified the surface of the monoliths with a solution of 2-acrylamido-2-methyl-1-propanesulfonic acid (AMPS) in the presence of benzophenone. Following the application of UV energy, benzophenone is immobilised onto the monolith surface through hydrogen abstraction resulting in the formation of free radicals on the surface of the polymer monolith, which then initiates propagation reactions leading to grafting from the surface of the monolith. As the polymer chains also contain abstractable hydrogens, the chains continue to grow forming a highly branched polymer structure from each reactive site on the surface of the polymer monolith. The subsequent monolith was applied to the separation of peptides.

To date, the use of surface grafting techniques to increase the capacity of the final functional groups on polymer monoliths for the separations of small ions has received little attention. Connolly *et al.* [103] introduced poly[2(methacryloyloxy)ethyl] trimethylammonium chloride poly(META) onto the surface of a GMA-*co*-EDMA polymer monolith in 100 µm UV transparent fused silica capillary using UV irradiation to produce a strong anion exchanger. This was carried out by flushing META in a solution of t-butanol/water in the presence of the free radical initiator benzophenone through the monolith followed by irradiation with UV energy. The resultant poly(META) monolith was applied to the separation of six common inorganic anions as shown in Figure 1.18, using a 2 m*M* benzoate eluent which facilitated the use of on-column C^4D detection. The authors separated six common

anions in a run-time of 13 minutes and reported efficiencies of 15,000 N/m for fluoride at 1 µL/min and 29,500 N/m using a flow rate of 100 nL/min with a 50 nL injection volume. The authors also reported excellent retention for fluoride with a retention factor (*k*) of 2.5.

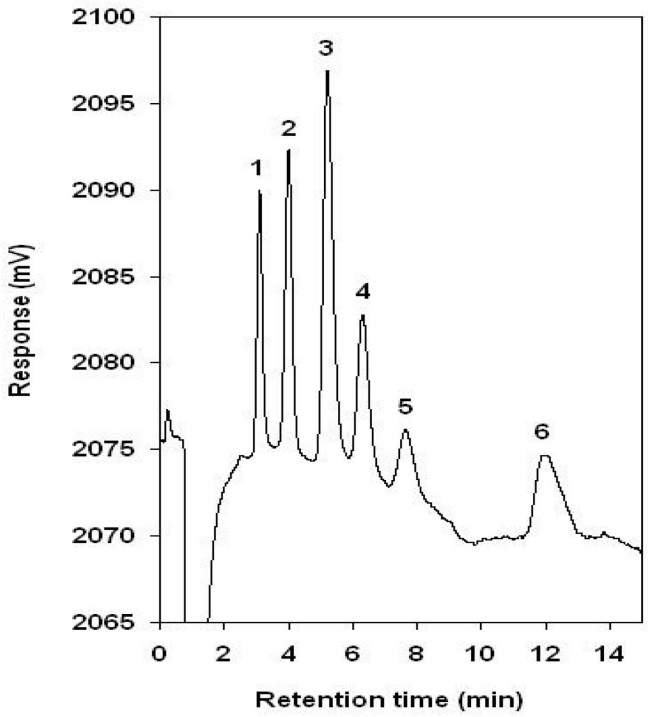

Figure 1.18: Separation of 6 common anions using a GMA-*co*-EDMA polymer monolith modified with grafted polymer chains of META. Eluent: 2 m*M* sodium benzoate, flow rate: 1 µL/min., detection: on-column C^4D detection, injection volume: 50 nL, peaks: (1) 0.7 mg/L fluoride, (2) 3 mg/L chlorite, (3) 3 mg/L, bromate, (4) 0.7 mg/L chloride, (5) 0.7 mg/L nitrite, (6) 3 mg/L bromide. Reproduced from [103].

1.5.3.4 Latex coated polymer monoliths

Another method that has appeared in the literature for the surface functionalisation of polymer monoliths is the covalent attachement of latex particles. In 2004, Hilder *et al.* [83] prepared a BuMA-*co*-EDMA-*co*-AMPS polymer monolith using a porogenic system consisting of 1-propanol, 1,4-butanediol and water ensuring sulfonated functionalities were available due to the AMPS used in the initial polymerisation

mixture. This was followed by the attachment of quaternary amine functionalised latex particles (60 nm diameter) via electrostatic interactions. The authors found an increase in the surface area of the monolith from 35 to 47 m^2/g following the attachment of the latex nanoparticles. This monolith was applied to the separation of carbohydrates.

Following on from this, Zakaria *et al.* [104] fabricated a BuMA-*co*-EDMA polymer monolith and attached AS18 particles. The latex nano-particles were 65 nm in diameter with quaternary ammonium functionalities. Using a KOH eluent with suppressed conductivity detection, a peak efficiency of 5,400 N/m was obtained for iodate. Figure 1.19 shows the separation of iodate, bromate, nitrite, bromide and nitrate using indirect non-suppressed conductivity detection (the conductivity of the eluent was higher than that of the anions and as the anions pass through the conductivity detector, a decrease in conductivity was observed).

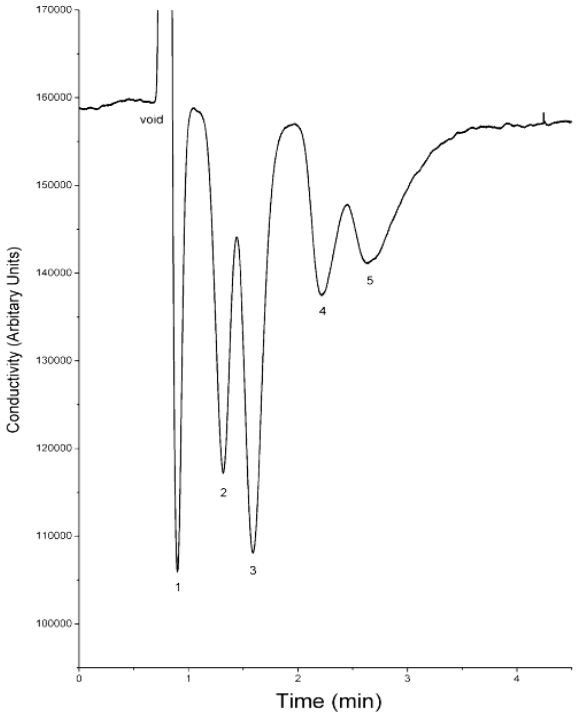

Figure 1.19: Separation of common anions using an AS18 latex functionalised polymer monolith. Separation conditions: eluent: 1 m*M* KOH, flow-rate: 18 µL/min,

detection: non-suppressed conductivity detection, peaks: (1) iodate, (2) bromate, (3) nitrite, (4) bromide and peak (5) nitrate. Reproduced from [104].

From Figure 1.19, baseline resolution was not achieved. Due to the high background conductivity of the KOH eluent, the sensitivity of indirect conductivity was poor, therefore the authors incorporated a hollow fibre suppressor after the separation column. Figure 1.20 shows the separation of the same five anion mixture, obtained using suppressed conductivity detection. This separation was carried out using varying concentrations of KOH eluents. In Figure 1.23, the eluent used was 1 mM KOH and baseline resolution was not achieved. Using the same 1mM KOH eluent with suppressed conductivity (Figure 1.20) resulted in the baseline separation of the five anions.

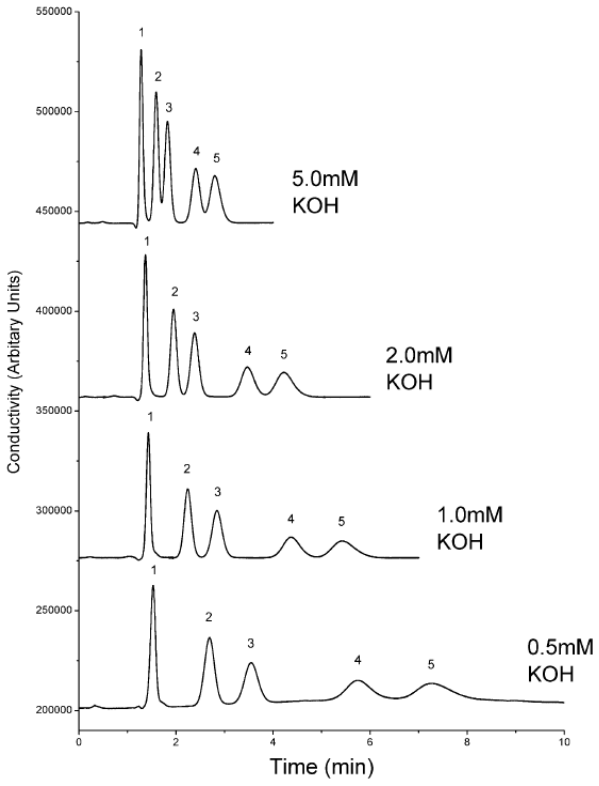

Figure 1.20: Separation of 5 anions using an AS18 latex functionalised polymer monolith. Separation conditions: Eluent: 0.5 - 5 m*M* KOH, flow-rate: 18 µL/min, detection: suppressed conductivity detection, peaks: (1) iodate, (2) bromate, (3) nitrite, (4) bromide and (5) nitrate. Reproduced from [104].

Hutchinson *et al.* [105] prepared a PS-DVB polymer monolith using 1-decanol and toluene as the porogens. The authors sulfonated a PS-DVB monoliths using two different reaction methods namely (1) by reaction with sulfuric acid and silver sulfate at 95 ^{o}C and (2) through reaction with a 50 % (v/v) solution of chlorosulfonic acid and dichloromethane followed by the attachment of AS18 latex nano-particles. Polymer monoliths with 8 % DVB resulted in a sulfonated monolith with a capacity that was two times higher than a polymer ion exchanger prepared by the same group using co-polymerisation with AMPS as described above [104]. However, due to the low concentration of the cross linker used in the polymerisation of the polymer monolith, the use of this column as a chromatographic support was not feasible. A PS-DVB monolith with 20 % cross linker was also prepared and sulfonated. Although a 10 % increase in capacity was obtained relative to the BuMA-*co*-EDMA-*co*-AMPS monolith described above [104], the separation of anions was not improved upon and the authors concluded that the direct sulfonation of PS-DVB monoliths was not practical.

In the same body of work, Hutchinson *et al.* [105] prepared three GMA-*co*-EDMA polymer monoliths (250 µm I.D.), the surface of which were sulfonated using three different methods. The first method involved flushing a solution of 4-hydroxybenzenesulfonic acid and triethylamine dissolved in acetonitrile, followed by coating with AS18 latex nano-particles (quaternary ammonium functionalities). The second method used involved flushing a solution of thiobenzoic and triethylamine dissolved in acetonitrile. The generated thiol groups were oxidised using tert-butylhydoperoxide and following a washing step, the monolith was coated with AS18 latex nano-particles. Finally, Hutchinson *et al.* [105] also prepared a GMA-*co*-EDMA polymer monolith and sulfonation was carried out using a solution of sodium sulfate followed by attachment of AS18 latex nano-particles. The GMA-*co*-EDMA polymer monolith prepared using the first method yielded an ion exchange capacity of 15 nequiv/cm, method 2 had an ion exchange capacity of 6.9 nequiv/cm and method 3 had an ion exchange capacity of 12.6 nequiv/cm. The modified polymer monoliths were applied to the separation of iodate, bromate, nitrite, bromide, nitrate, iodide and benzenesulfonate using a sodium perchlorate eluent with UV detection. Although the GMA-*co*-EDMA polymer monolith sulfonated using method one yielded the highest ion exchange capacity, significant peak tailing was observed for benzesulfonate and

baseline resolution of all anions was not achieved. The polymer monolith prepared using method two yielded the lowest ion exchange capacity of the three monoliths prepared. In this case, the authors concluded that the low ion exchange capacity may have resulted in the in the retention of the anions due to hydrophobic interactions of the anions with the monolith surface rather than the latex nano-particles. Using the third method of sulfonation, the authors obtained improved peak shape and efficiency, particularly for the later eluting peaks. The increased ion exchange capacity also allowed the elution of the anions using a NaOH gradient up to 100 m*M*. Previous work carried out by the same authors [104], only allowed a gradient elution profile up to a concentration of 5 m*M* NaOH. Therefore an improvement in the ion exchange capacity resulted in enhanced suitability of the latex coated polymer monolith in ion exchange chromatography. Figure 1.21 shows a separation of 7 anions using an NaOH gradient elution (1 mM NaOH initial concentration ramped up to 100 mM NaOH at 10 minutes).

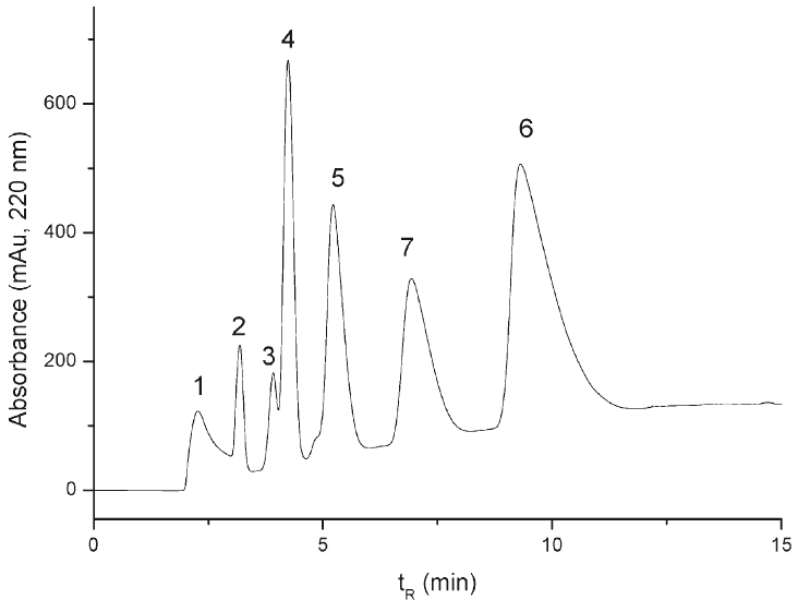

Figure 1.21: Separation of 7 anions using a AS18 latex nano-particle modified GMA-*co*-EDMA polymer monolith. Separation conditions: Eluent: NaOH gradient, flow-rate: 3.2 µL/min, detection: UV detection at 220 nm, Peaks: (1) iodate, (2) bromate, (3) nitrite, (4) bromide, (5) nitrate, (6) iodide and (7) benzenesulfonate. Reproduced from [105].

1.5.4 Silica monoliths

1.5.4.1 Fabrication of silica monoliths

As with polymer monoliths, silica monoliths can be fabricated in a mould such a column, capillary or in the channel of microfludic channels. Silica monoliths are prepared by a sol gel process [106]. This process consists of hydrolyzing a silane compound, such as tert alkoxysilanes, in the presence of a porogen, such as poly ethylene glycol (PEG). This is a polycondensation reaction i.e. a chemical condensation that leads to the formation of a polymer by the linking together of the molecules of a monomer. During polycondensation, the viscosity of the solution increases. The polymer becomes insoluble and precipitates, either as particles or as a monolithic mass with large pores. Urea is added to the polymerisation mixture to maintain an alkaline pH, as the basic pH helps the mesopore structures to form. The silica monolith is subjected to higher temperatures (120 ^{o}C) which allows mesopore formation through hydrolysis of the urea resulting in the formation of ammonia. Following the drying step, the monolith is then heat treated at 330 ^{o}C for 25 hours.

1.5.4.2 Silica monoliths for the separation of small ions

As with polymer monoliths, the surface of silica monoliths can be modified to introduce ion exchange functionalities. In 2005, Sugrue *et al.* [107] modified a commercially available bare silica monolith (100 mm x 4.6 mm) with lysine to produce a stationary phase with zwitterionic characteristics. This was carried out by activating the surface of the silica monolith with hot water in a column water bath at 60 ^{o}C for 4 hours. Modification of the monolith with lysine took place by recycling a solution of γ-glycidoxypropyltrimethoxysilane, lysine and water. The resultant monolith was applied to the separation of nitrite, bromide, bromate, nitrate, iodide and thiocyanate using a phosphate buffered eluent as seen in Figure 1.22. Peak efficiencies ranged from 41,000 N/m for iodate to 55,900 N/m for thiocyanate using a 10 m*M* phosphate buffer (pH 3.0) and a flow-rate of 2 mL/min.

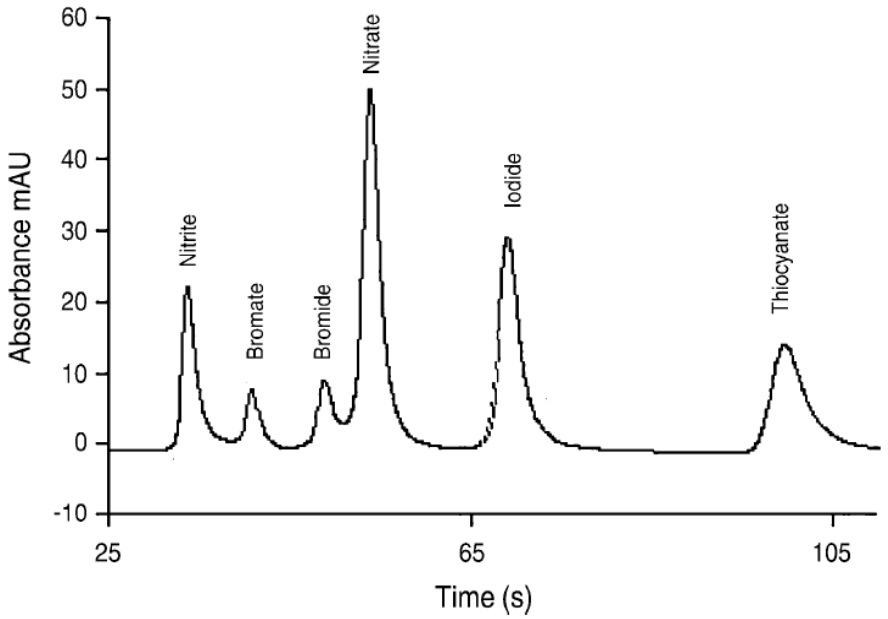

Figure 1.22: Separation of selected anions using a lysine modified silica monolith. Separation conditions: Eluent: 50 m*M* phosphate buffer, detection: UV detection at 214 nm and flow-rate: 4.9 mL/min. Reproduced from [107].

The main applications in the use of silica monoliths for the separation of small ions has been carried out using surfactant modified monoliths.

1.5.4.3 Surfactant coating

The use of surfactants is an inexpensive way of rendering a reversed phase column suitable for ion exchange chromatography. Long chain carboxybetaine surfactants such as DDMAU and (*N*-dodecyl *N*,*N*-dimethylammonio)butyrate (DDMAB) have been used to modify standard bore packed particulate columns and silica monoliths for the separation of small anions. While this has been well documented in the literature [108, 109], a number of research groups have also investigated the use of capillary silica monoliths surface modified with surfactants and applied to the separation of small ions.

Using a cetyltrimethylammonium (CTAC) coated silica monolith, Suzuki *et al.* [110] separated five anions (iodate, bromate, nitrite, bromide and nitrate) in less than 1

minute (Figure 1.23) with a 50 m*M* sodium eluent (and 0.1 mM CTAC) at a flow-rate of 11.1 µL/min. The authors noted a decrease in the retention of nitrate over time with an eluent containing no CTAC and found that the stability of the anion retention could be stabilised through the addition of CTAC to the eluent. The relative standard deviation (% RSD) was < 0.61 % for six successive injections of the standard mix. The CTAC coated silica monolith was applied to the determination of bromide in seawater with results showing that the high ionic strength from the salt anions in the seawater did not affect the retention time of bromide.

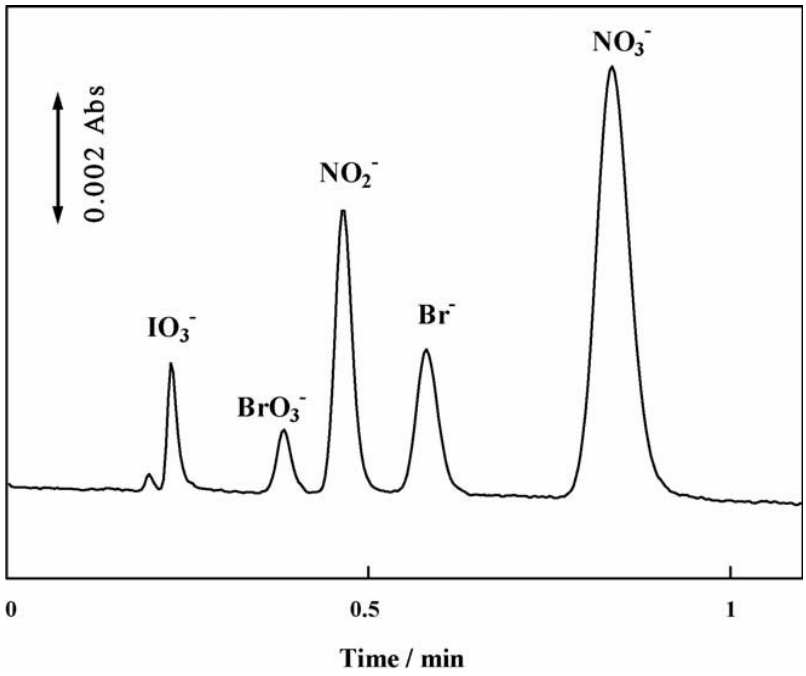

Figure 1.23: Separation of common anions using a CTAC modified silica monolith (100 µm x 200 mm I.D.). Eluent: 50 m*M* NaCl and 0.1 m*M* CTAC, flow-rate: 11.1 µL/min, detection: UV detection at 210 nm. Reproduced from [110].

Following on from this, Suzuki *et al.* [111] coated a silica monolith with dilauryldimethylammonium bromide (DDAB) and applied the modified monolith to the separation of the same five anions (Figure 1.24) and found that the retention time of the 5 anions were almost double those obtained using the CTAC coated silica monolith. In this work, the authors concluded that the silica monolith coated with DDAB was more stable than that coated with CTAC. The DDAB coated silica

monolith was also applied to the determination of bromide in seawater and as before, the retention time of the bromide standard was the same as the retention time of the bromide in the seawater sample.

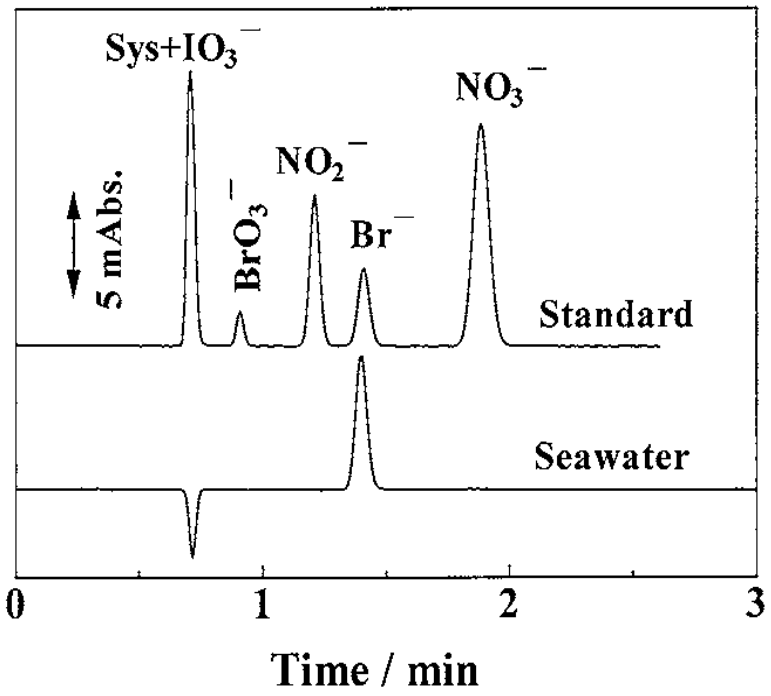

Figure 1.24: Separation of anion standards using a DDAB modified capillary silica monolith (top chromatogram) and determination of bromide in seawater (bottom chromatogram). Separation conditions: Eluent: 500 m*M* NaCl, flow-rate: 2.1 µL/min, detection: UV detection at 210 nm and injection volume: 20 nL. Reproduced from [111].

In 2007, Ó'Ríordáin *et al.* [37] coated an Onyx C_{18} capillary silica monolith with *N*-dodecyl-*N*,*N*-(dimethylammonio)undecanoate (DDMAU). This modified silica column was used for the separation of iodate, bromate, nitrite, bromide, nitrate, iodide, sulphate, thiocyanate and perchlorate using a 0.5 m*M* phthalate eluent as shown in Figure 1.25. On-column C^4D was used as the mode of detection with all 9 anions separated in a run-time of 30 minutes (effective column length was 8 cm). Average peak efficiencies of 35,000 N/m were reported. Retention factor data was also obtained for a range of other anions.

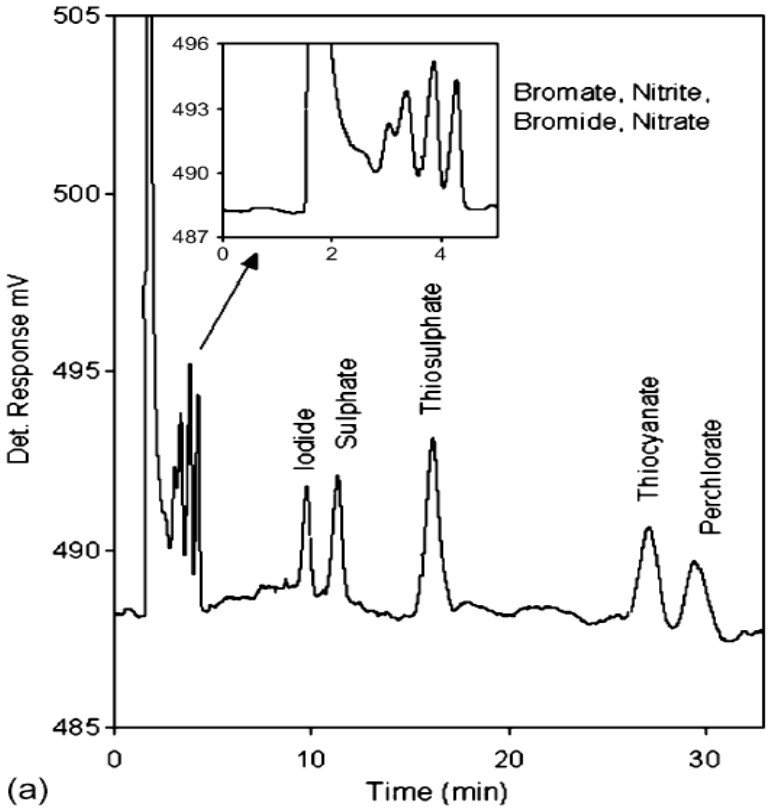

Figure 1.25: Separation of common anions using a DDMAU coated silica capillary monolith. Separation conditions: eluent: 0.5 m*M* phthalate, flow-rate: 0.3 µL/min, detection: on-column C^4D. Reproduced from [37].

Gillespie *et al.* [112] carried out the separation of Mg(II), Ca(II), Sr(II) and Ba(II) using a sodium dioctyl sulfosuccinate (DOSS) coated capillary silica monolith (150 mm x 100 µm I.D.). This monolith was applied to the determination of Mg(II), Ca(II), Sr(II) and Ba(II) using a 0.5 m*M* ethylenediamine eluent (pH 4.5) and on-column C^4D detection. The flow-rate used was 1 µL/min with a 10 nL injection volume. Absolute detection limits (of the 10 nL injection) were in the picogram range (from 1.0 pgram for Mg(II) to 9.0 pgram for Ba(II)). A peak efficiency of 48,400 N/m was obtained for Sr(II) and 46,900 N/m for Ba(II). The DOSS coated silica monolith was used for the determination of alkaline earth metals in bottled and tap water samples.

1.6 Characterisation of monolithic stationary phases.

A number of methods have been used to characterise the pore morphology of monolithic stationary including scanning electron microscopy [90], mercury intrusion porosimetry [113, 114], inverse size exclusion chromatography [113, 115] and scanning C^4D.

1.6.1 Scanning C^4D

The applications of scanning C^4D within capillary chromatography have been highlighted in a recent review by Connolly *et al.* [45]. These applications include the evaluation of packing homogeneity of particulate packed columns, evaluation of structural homogeneity of monolithic rods and the ability to determine axial homogeneity of grafted functional groups on the surface of monoliths. In 2007, Connolly *et al.* [116] demonstrated the visualisation of discrete bands of charged functional groups photo-grafted onto a monolithic column using C^4D. By scanning the length of the column, zones grafted with 2-acrylamido-2-methyl-1-propanesulfonic acid (AMPS) could be detected. This was followed up by Gillepsie *et al*. [100] who functionalised increasing concentration of AMPs along the monolith by varying the amount of UV energy applied. By scanning the length of the column in mm increments, the authors were able to obtain an increase in detector response (mV) on the sections of the monolith that was functionilised with AMPs. An increase in detector response was obtained with an increase in applied UV energy.

As mentioned in Section 1.4, the packing of particles in capillary column formats is a difficult task. Poorly packed columns can lead to band broadening and poor column efficiency [117]. In 2009, Connolly *et al.* [118] used scanning C^4D techniques for the characterisation and visualisation of packing homogeneity in capillary packed columns. In this work, the authors packed two 100 µm I.D fused silica capillary monoliths with Dionex OmniPac PAX-100, 8.5 µm diameter particles, prepared as a slurry in acetonitrile. Following the placement of a monolithic frit at one end of the column, the slurry was pumped into the capillary at 0.1 mL/min. Following the packing of the capillary column, a monolithic frit was fabricated at the other end of the capillary, ensuring that the packing material was kept inside the capillary column.

The packed capillary column was scanned using scanning C^4D techniques. The capillary column was scanned in predefined increments and the conductive response noted. The resultant plot of on-column detector position versus the conductive response can be seen in Figure 1.26. From this plot, differences in the conductive response were noted. Void volumes (denoted as (a) in Figure 1.26) were present and can be seen at the head of the column. A void area was also noted at the end of the column between the packing material and the monolithic frit. Area (c) in Figure 1.26 was the scanning C^4D profile obtained during the scan of the packing material in the capillary column. A change in the conductive response can be seen between 10 mm and 15 mm in comparison to the conductive response obtained during the scan of the column from 15 mm to 35 mm demonstrating a deviation in the axial homogeneity of the packing material. This work demonstrated the simplicity of visualising the axial homogeneity of stationary phase packings in capillary column formats.

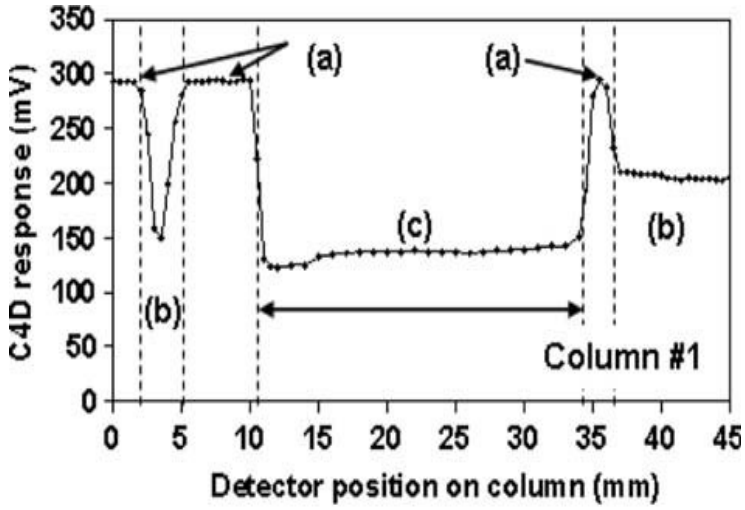

Figure 1.26: Scanning C^4D profile where (a) depicts void regions, (b) depict the areas where the monolith frits are situated and (c) is the area that contains the packing material. Reproduced from [118].

Section 1.5.4.3 discusses the use of surfactant coated silica monolith in IC. One of the main disadvantages of using surfactant coated monoliths is that the coating tends to bleed off the column, thus affecting retention time precision. Methods to overcome this problem include, re-coating the column at regular intervals, adding the surfactant to the eluent, known as dynamic coating [119] or to include a pre-column, coated with

the surfactant, before the separation column [120]. Another drawback of using surfactant coating is the non-uniform coverage of the surfactant on the stationary phase. In capillary columns, the use of scanning C^4D has been used to determine the homogeneity of the coverage of the surfactant on the stationary phase.

In 2006 Gillespie *et al.* [121] coated a 150 mm x 0.1 mm I.D silica capillary column with sodium dioctyl sulfosuccinate (DOSS). The authors used scanning C^4D to characterise surfactant coatings on monolithic columns for application to capillary ion chromatography. The longitudinal homogeneity and temporal stability of the coating was investigated. A capillary column was coated with DOSS surfactant in the forward direction (i.e. from one end of the capillary column to the other). Using C^4D, the column was scanned and the detector response noted. From Figure 1.27 below, it can be seen that the detector response after the first coating indicated an uneven coverage of the surfactant. The column was re-coated in the reverse direction and the scan repeated. The second coating gave a more uniform coverage than the first coating. Although the surfactant coverage was improved after the second coating, this plot shows the uneven coverage of the surfactant along the length of the DOSS coated monolith.

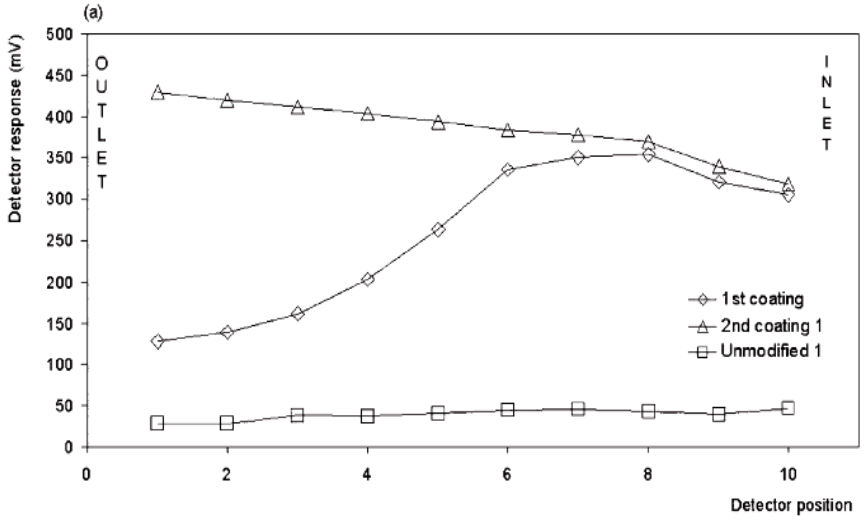

Figure 1.27: C^4D scan of an unmodified monolith, a scan after the first surfactant coating and a scan after the second surfactant coating. Reproduced from [121].

The work described so far in this literature review has focused on the used of capillary columns (particulate and monolithic) for the separation of anions and cations. In the following sections, this review will focus on the separation of metal cations by ion chromatography and also introduce high performance chelation ion chromatography.

1.7 High performance chelation ion chromatography (HPCIC)

1.7.1 The separation of metal cations using monolithic columns

The use of monoliths (in standard bore formats) for the determination of metal cations by ion chromatography has been studied. Xu *et al.* [122] modified an ODS silica monolith (100 mm x 4.6 cm) with lithium dodecylsulfate. The resultant cation exchanger was used for the separation of Na^+, NH_4^+, K^+ and H^+ using a 60 m*M* LiCl eluent and conductivity detection. The column was appled to the determination of metal cations in acid rain samples. Connolly *et al.* [123] modified a commercially available silica monolith with the surfactant DOSS and used the resultant column was used for the separation of Cu(II), Mg(II), Ca(II), Sr(II) and Ba(II). Sugrue *et al.* [124] separated transition earth metals and transition metals on a porous silica monolith using solvent enhanced ion chromatography. In this case, weak ion exchange interactions are responsible for retention of the metal cations and these interactions become stronger when high concentrations of organic solvents are used within the eluent. The authors successfully separated a range of selected transition metals, as shown in Figure 1.28 using an eluent consisting of 80 % acetonitrile and 10.3 m*M* ammonium acetate buffer at pH 4.6.

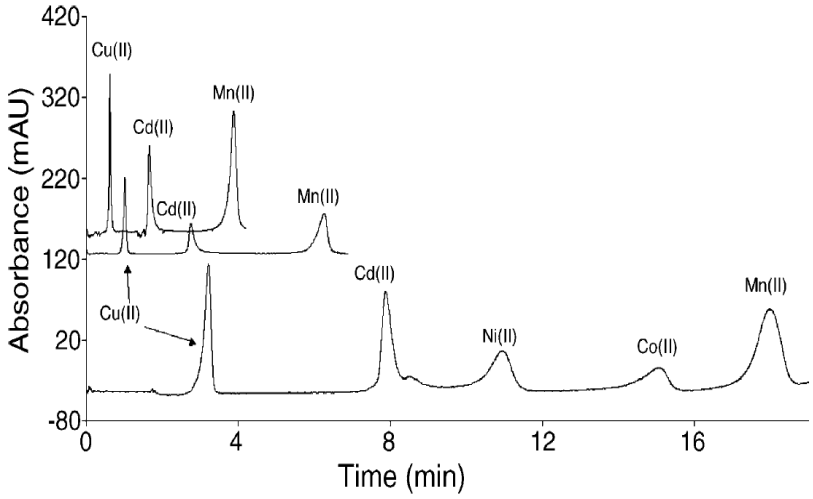

Figure 1.28: Separation of transition metals on a bare silica monolith using an eluent consisting of 80 % acetonitrile and 10.3 m*M* ammonium acetate buffer at pH 4.6. Analysis was carried out using flow-rates of 1 mL/min, 3 mL/min and 5 mL/min. Reproduced from [124].

The examples of metal cation separations in Section 1.7.1 were all carried out using monolithic columns. An alternative method for the separation of metal cations is through the use of high performance chelation ion chromatography (HPCIC). To date, the only work carried out using HPCIC where the separations were carried out using monolithic columns has been performed by Sugrue *et al.* [125, 126], therefore the research reviewed will include various stationary phases with immobilised chelating ligands.

1.7.2 Introduction to HPCIC

Retention in HPCIC is based on the formation of ion exchange interactions in conjugation with the formation of a coordinate bond. It differs from ion exchange chromatography in that a new bond is formed and separation is dependent on the stability of metal complex formation and subsequent dissociation [51]. Advances in stationary phases with immobilised chelating ligands have allowed for the direct determination of trace metals in complex sample matrices using HPCIC. There are a number of requirements for the use of chelating ligands in HPCIC including mechanical stability to withstand periods of applied pressure and hydrolytic stability,

to withstand changes in the pH of the eluent employed in the analysis [51]. Acidic eluents are normally used in HPCIC, as the acidic environment prevents the hydrolysis of the metals of interest, therefore the chelating substrate must be structurally stable to withstand such acidic conditions. The stability of the chelating substrate should also be stable at high temperatures. Increases in temperature have been shown to improve selectivity and efficiency in HPCIC (see Section 1.7.5.3). As separation in HPCIC is based on the formation of surface complexes between metal ions and an immobilised ligand, ideally for efficient separations, there should be fast kinetics of complexation. Chelating ligands that form relativiely weak stability constants have been shown to deliver the most efficient separations of metals cations, as low stability constants result in faster dissociation of the immobilised chelating ligand. Finally, the homogeneous distribution of the chelating ligands along the entire length of the column is important as chelate formation providing 1:1 metal-ligand interactions are desirable, as this allows for faster association/dissociation kinetics.

Aminopolycarboxylates are often employed as chelating ligands in HPCIC. The most common aminopolycarboxylate used is iminodiacetic acid (IDA). IDA is commonly used in HPCIC, as the complexes formed between the metal cation and the IDA ligand are relatively weak, therefore strong eluents are not required for their elution. Large stability constants of metals with chelating ligands can cause broad peaks [127]. The use of IDA as a chelating ligand bound to a silica substrate has been shown to be useful for the separations of alkaline earth metals [128-131] and transition and heavy metals [132-133]. Other chelating ligands used include 8-hydroxyquinoline [134] dye coated columns [135-137] and aminomethylphosponic acid [127].

The determination of trace metals in high concentration saline samples suffer from interferences from high salt concentrations, which swamp the ion exchange sites if ion exchange chromatography is used. A preconcentration step may be required prior to the separation of the metal cations. In HPCIC, the alkali metals form weak coordinate bonds with the chelating ligand, therefore reducing the interference from these salts and allowing the determination of trace metals in high salt sample matrices. In 1994, Paull *et al.* [136] used a dye (xylenol orange) impregnated silica particle column for the pre-concentration and separation of metals in coastal seawater samples (Figure

1.29). Xylenol orange contained carboxylic acid groups, allowing for the formation of complexes with sample metals.

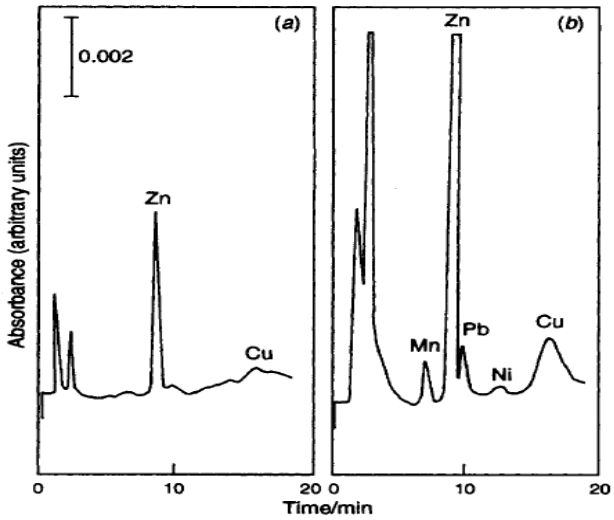

Figure 1.29: Pre-concentration and separation of metals in coastal seawater samples (b). A blank sample (a) showed small concentrations of Zn(II) and Cu(II), possibly due to leaching from the eluent pump. Reproduced from [136].

In 2001, Bashir *et al.* [130] used an IDA bonded silica column for the determination of trace alkaline earth metals in brines. Samples analysed included a 0.9 % eyewash saline solution and 0.5 *M* KCl solutions for the determination of Mg(II) and Ca(II). Through the use of optimised eluent conditions, the authors successfully separated µg/L levels of Mg(II) and Ca(II) in high ionic strength samples without the presence of large matrix peaks as shown in Figure 1.30.

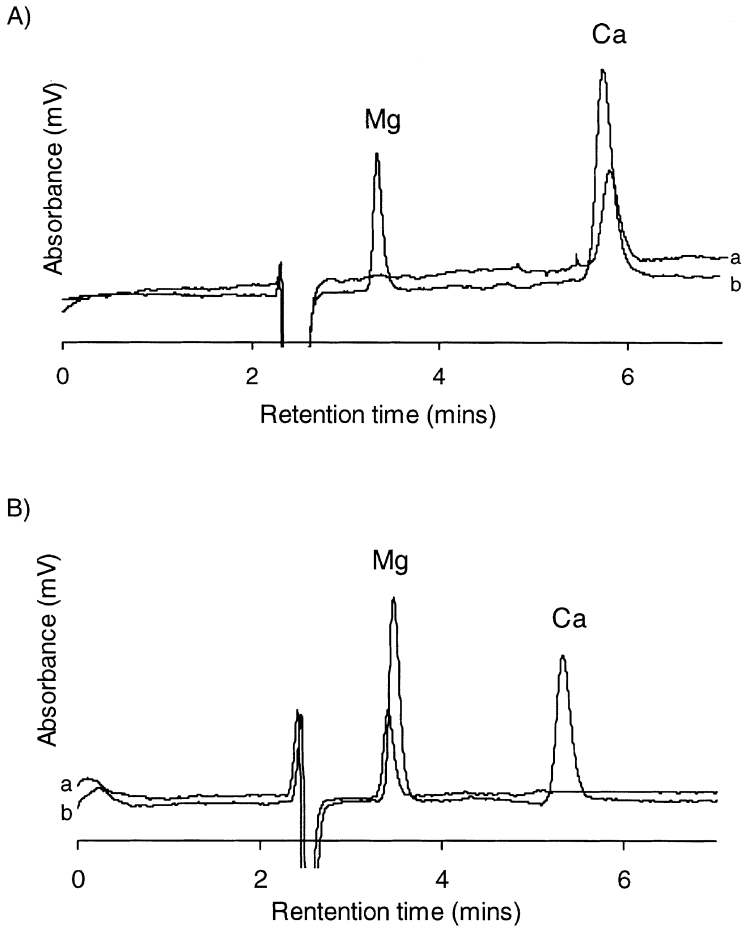

Figure 1.30: (a) Separation of Mg(II) and Ca(II) in a saline eyewash sample overlaid with a spiked 200 µg/L sample. (b): separation of Mg(II) and Ca(II) in 0.5 *M* KCl overlaid with a spiked 300 µg/L sample, column used: IDA bonded silica (250 x 4.0 mm I.D). Reproduced from [130].

1.7.3 Monoliths in HPCIC

The use of monolithic stationary phases with immobilised chelating ligands for the direct separation of metal cations has received little attention over the years, particularly in the case of polymeric monoliths, where no reports have appeared in the literature. Sugrue *et al.* [125] first reported the use of a silica monolithic column for the separation of alkaline earth metals in high ionic strength matrices. The authors modified a commercially available 100 mm x 4.6 mm I.D. bare silica monolith with IDA. Briefly, the surface of the silica was first activated by washing the monolith with distilled water at 60 ^{o}C in a thermostated water bath. Modification of the monolith with IDA took place by recycling a mixture of γ-

glycidoxypropyltrimethoxysilane, IDA and water through the column at 70 ^{o}C for 4 hours. Finally, the column was washed with 0.01 *M* nitric acid followed by the eluent, resulting in a chelating ion exchanger with covalently bonded IDA functionalities.

The authors successfully separated Mg(II) and Ca(II) in a 1 *M* KCl brine solution using flow rates of 1.0, 2.0 and 3.5 mL/min using *o*-cresolphthalein complexone (*o*-CPC) as a post column reagent and UV-Vis detection at 572 nm. As can be seen in Figure 1.31, no system peak was observed for K^+ showing the excellent selectivity demonstrated by *o*-CPC for the separation the of alkaline earth metals. At flow-rates of 3.5 mL/min, separation occurred in < 1 minute demonstrating a novel IDA silica modified monolith for the fast separation of alkaline earth metals in high ionic strength samples.

Following on from this work, Sugrue *et al.* [126] carried out a more comprehensive study, using the same IDA bound silica monolith, for the separations of alkaline earth and transition metals. The IDA immobilised silica monolith column (100 mm x 4.6 mm I.D.) was also compared to an IDA bound silica particulate column (250 mm x 4.0 mm I.D.). Using either a 2 m*M* HNO_3 or a 2 m*M* methanesulfonic acid (MSA) eluent, the authors obtained elution orders of Mg(II) < Sr(II) = Ca(II) < Ba(II), with the MSA eluent. Baseline resolution of Ca(II) and Sr(II) was not achieved using either the IDA-monolith or the IDA-silica particulate column.

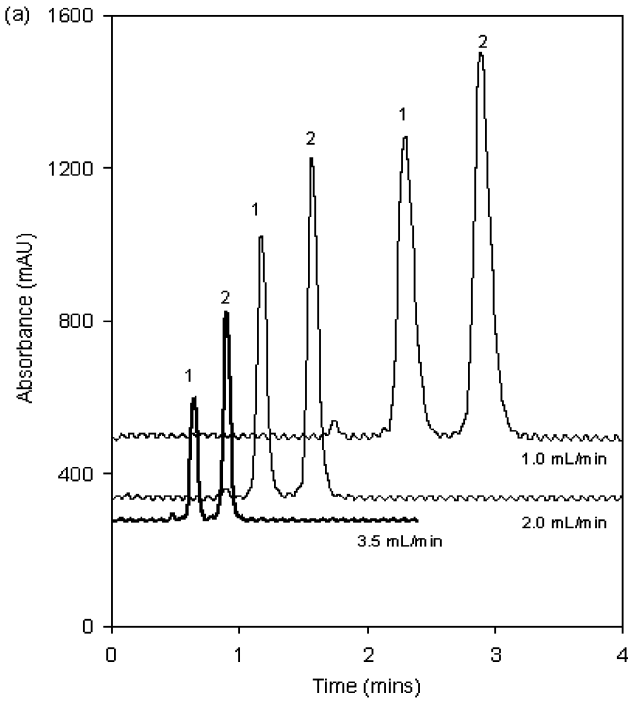

Figure 1.31: Overlay of separations of Mg(II) and Ca(II) in 1 *M* KCl solutions at various flow-rates using the IDA immobilised monolith column. The eluent used in the analysis was a HNO_3 eluent (pH adjusted to 4.85). Peaks: (1) 10 ppm Mg(II) and (2) 10 ppm Ca(II). Detection used was UV-Vis at 570 nm after PCR with o-CPC. Reproduced from [126].

Separations of transition and heavy metals, namely Mn(II), Cd(II), Zn(II) and Pb(II) with 0.2 *M* KCl eluents (pH 2 – 2.5) were carried out using the IDA immobilised silica monolith and the IDA-silica particle column and both stationary phases compared. It was found that the eluent with the higher pH, resulted in complete retention of the later eluting metal Pb(II) using the particulate packed column. However, using the same separation conditions with the monolithic column, Pb(II) eluted after 15 minutes. The capacity of both columns were measured and the capacity of the IDA monolith column was lower than that exhibited by the particulate packed column, thus demonstrating an advantage in the use of lower capacity columns for the elution of the more strongly retained metals in the same run as Mn(II) and Cd(II) using isocratic elution conditions.

As mentioned previously, Sugrue *et al.* [107] modified a commercially available silica monolith (100 mm x 4.6 mm) with lysine to produce a stationary phase with zwitterionic characteristics. As well as studying the retention of common anions, the authors also studied the retention of alkali, alkaline earth, transition and heavy metals. While the retention of the alkali and alkaline earth metals was due to ion exchange, the retention of the transition and heavy metals was a result of metal complex formation. Figure 1.32 shows an overlay of transition and heavy metals using the lysine bonded silica monolith.

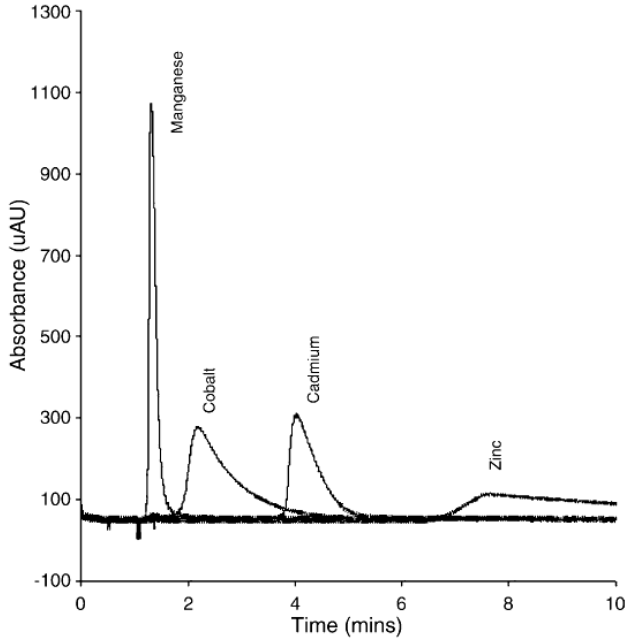

Figure 1.32: Overlay of chromatograms obtained for various transition and heavy metals using the lysine bonded silica monolith. Separation conditions: Eleunt: 3 m*M* KCl pH 4.5, flow-rate: 2 mL/min, detection: UV-Vis detection at 495 nm following reaction with PAR. Reproduced from [107].

Rahmi *et al.* [139] reported the use of GMA-*co*-EDMA monoliths modified with IDA, fabricated in commercially available syringe filter tips (Figure 1.33), for the solid phase micro-extraction of 29 transition/heavy metals and rare earth elements prior to their determination by ICP-MS. A polymerisation mixture consisting of GMA, EDMA and a porogenic system consisting of either cyclohexanol/toluene or 1-proponol/1,4-butanediol/water was used. In all cases the initiator was AIBN. Following de-oxygenation of the polymerisation mixture, an aliquot was drawn into a

predefined space in the tip of the syringe and sealed. The syringe was placed in a water bath for thermal polymerisation. Following washing of the syringe tip, IDA was immobilised onto the surface of the monolith by reacting with an IDA solution consisting of IDA and NaCl in a ratio of 5:1 in 2 *M* Na_2CO_3 and the pH adjusted to the required pH. The chelating syringe monolith tips were tested by measuring the % recoveries of various transition and heavy metals in two river water certified reference materials. Recoveries of > 80 % were obtained for all metals tested.

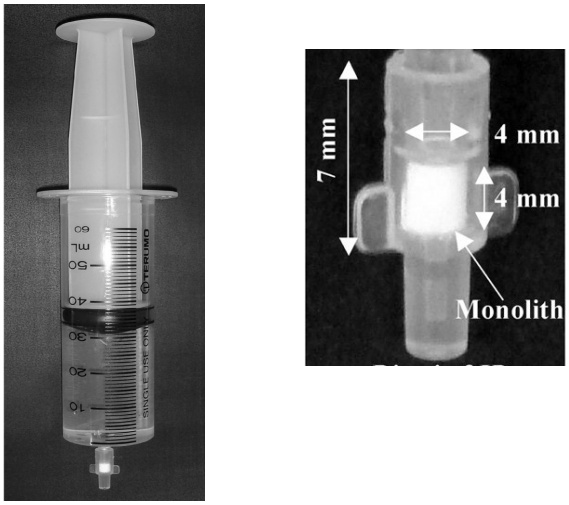

Figure 1.33: (left) Schematic demonstrating the chelating monolith solid phase extraction module prepared in a syringe tip. (right) Dimensions of syringe tip filter. Reproduced from [139].

1.7.4 Polymer monoliths with immobilised chelating ligands for immobilised metal affinity chromatography (IMAC).

The uses of capillary polymer monoliths with immobilised chelating ligands have been reported in the literature. However, these monoliths have only been used in the IMAC form for the separations of proteins. No reports have appeared in the literature using capillary polymer monoliths for the direct separation of transition and heavy metals. Luo *et al*. [80] immobilised IDA groups onto a GMA-*co*-EDMA monolith via the ring opening reaction of the epoxy groups on the surface of the monolith. The resultant IDA immobilised polymer monolith was loaded with Cu(II), Ni(II) or Zn(II) resulting in an IMAC separation column which was used for the determination of

proteins in egg white samples. In 2004, Chuang *et al.* [138] prepared a PS-DVB polymer monolith with IDA functionalities, followed by the addition of Cu(II) for the IMAC separations of amino acids and oligopeptides. A polymerisation mixture consisting of 4-vinylbenzyl chloride, diethyl iminodiacetate and pyridine was prepared, followed by the addition of DVB, toluene, n-proponol and AIBN. The polymerisation mixture was filled into previously silanised fused silica capillary (75 µm I.D.) followed by thermal polymerisation at 70 ^{o}C for 24 hours. Following washing of the polymer monolith to remove any unreacted polymerisation mixture, hydrolysis of the functionalised diethyl iminodiacetate was required prior to the loading of the column with Cu(II).

1.7.5 Factors effecting retention in HPCIC

1.7.5.1 Eluent pH

As the pH of the eluent controls the dissociation/protonation of the immobilised chelating ligand, it is the most important parameter effecting retention in HPCIC. Decreasing the eluent pH results in a decrease in retention of all metal cations, as a decrease in the eluent pH induces protonation of the immobilised chelating ligand on the surface of the stationary phase. This results in a reduced number of charged functional groups, therefore leading to a reduction in retention. As most of the chelating ligands used in HPCIC contain weak acidic or basic groups such as IDA, the conditional stability constants formed between the metal ion and the immobilised chelating will also depend on the pH of the eluent [140]. Conditional stability constants decrease with decreasing pH, therefore to obtain narrow peaks and short retention times, eluents with pH values between 1–3 are commonly used. Plots of log k versus – log [eluent] should be linear with slopes equal to the number of protons replaced by each metal coordinated to the chelating ligand immobilised on the stationary phase surface [51].

Bashir *et al.* [141] showed the effects of eluent pH on the separation of alkaline earth and transition and heavy metals using weak nitric acid eluents and an itaconic acid cation exchange column. Itaconic acid contains two carboxylic acid groups and the authors noted that the selectivity exhibited by this stationary phase was similar to that

shown on other dicarboxylated stationary phases such as IDA. Stationary phase selectivity was found to be Li < Na < NH_4 < K < Cs < Mg(II) < Ca(II) < Sr(II) < Mn(II) < Ba(II) < Cd(II) < Zn(II) < Co(II) << Pb(II) << Cu(II) using a weak nitric acid eluent. The elution order obtained by Bashir et al. [141] of Mg(II) < Ca(II) < Sr(II) < Ba(II) corresponds to known stability constants for IDA-alkaline earth metals complexes [51]. Using nitric acid eluent varying in concentration from 0.6 – 2 m*M,* the authors successfully separated Mg(II), Ca(II), Mn(II), Cd(II), Zn(II) and Co(II), however the run times were excessive (30 minutes) and peak shape was poor. Pb(II) and Cu(II) were completely retained under these conditions. Plots of log *k* versus log [HNO_3] were linear and slopes ranging from -1.8 for Mn(II) to -1.98 for Cu(II). As mentioned previously, the slopes should be equal to the number of protons replaced by each metal coordinated to the chelating ligand immobilised on the stationary phase surface and in this case of this work, the slopes should be 2. The acid concentration of the eluent was increased, however this resulted in the co-elution of the early eluting metals Mg(II), Ca(II) and Mn(II). Finally, the authors applied an ionic strength gradient to the separation using 20 m*M* KCl increased up to 1 *M* KCl and successfully obtained a separation of Mg(II), Ca(II), Mn(II), Cd(II), Zn(II), Co(II) and Pb(II) in under 20 minutes, however Cu(II) was still retained.

Sugrue *et al.* [126] also showed the effect of eluent pH on the selectivity of the alkaline earth metals using an IDA modified silica monolithic column. Using a $NaNO_3$ eluent, the pH was varied from 4.7 – 6.7 with results showing that an increase in the eluent pH resulted in an increase in the retention of all metals studied. The authors also noted that the selectivity, under the conditions studied, was different to that obtained by other cation exchangers, such as those employing sulfonated functionalities. The change in selectivity obtained by the IDA modified silica monolith was due to the suppression of the ion exchange interactions through the use of electrolytes in the eluent.

Barron *et al.* [52] demonstrated the effect of eluent concentration on the retention of metal ions using a Dionex ProPac IMAC-10 polyIDA polymer resin. The author found that by increasing the eluent concentration from 0.25 – 15 m*M* nitric acid, therefore decreasing the eluent pH resulted in a decrease in the retention of all metals studied. Plots of log *k* versus –log [HNO_3] were linear and parallel for all the metal

cations showing that the selectivity did not change with a change in the eluent pH. Optimum selectivity of Mn(II), Fe(II), Co(II), Cd(II) and Zn(II) was obtained using a 0.25 m*M* nitric acid eluent, however, at this eluent pH, Pb(II) and Cu(II) were strongly retained and the authors were unable to separate all seven metal cations isocratically.

1.7.5.2 Ionic strength

To ensure that chelation is the dominant separation mechanism, electrostatic interactions must be suppressed. This can be carried by the addition of electrolytes, such as salts of the alkali metals, to the eluent. The addition of these salts to the eluent produces a shield of counter ions around the negatively charged moieties on the chelating ligand, therefore preventing electrostatic interactions with the metal cations. The addition of electrolytes to the eluent to suppress ion exchange interactions to make chelation the dominant separation mechanism has been reported in the literature and has been illustrated by Bashir *et al.* [130]. Using an IDA bonded silica column, the authors studied the effect on selectivity of alkaline earth metals using high ionic strength eluents. Fig 1.34(a) shows a separation of the alkaline earth metals using a 0.1 *M* KNO_3 eluent (for all eluents the pH was kept constant at 4.2 using dilute HNO_3). An elution order of Mg(II) < Sr(II) < Ca(II) < Ba(II) was obtained showing that using the 0.1 *M* KNO_3 eluent, separation occurred due to a combination of ion exchange and chelation. Using a 0.2 *M* KNO_3 eluent, the selectivity of Ba(II) and Ca(II) was reversed as shown in (b). Examination of (c) - (f) show that the retention of Ba(II) is mainly due to ion exchange as Ba(II), which was the last eluting peak using a 0.1 *M* KNO_3 eluent, became the first eluting peak when their ionic strength was increased to 1.5 *M* KNO_3. This demonstrates that the use of high ionic strength eluents resulted in suppression of ion exchange interactions, thus resulting in a decrease in the retention ability of Ba(II) when chelation was the dominant separation mechanism. The authors also concluded that the retention of Ca(II), eluting as the last peak when eluent concentrations > 0.2 *M* KNO_3 were used, showed that retention of Ca(II) was possibly due to complexation, rather than simple ion exchange.

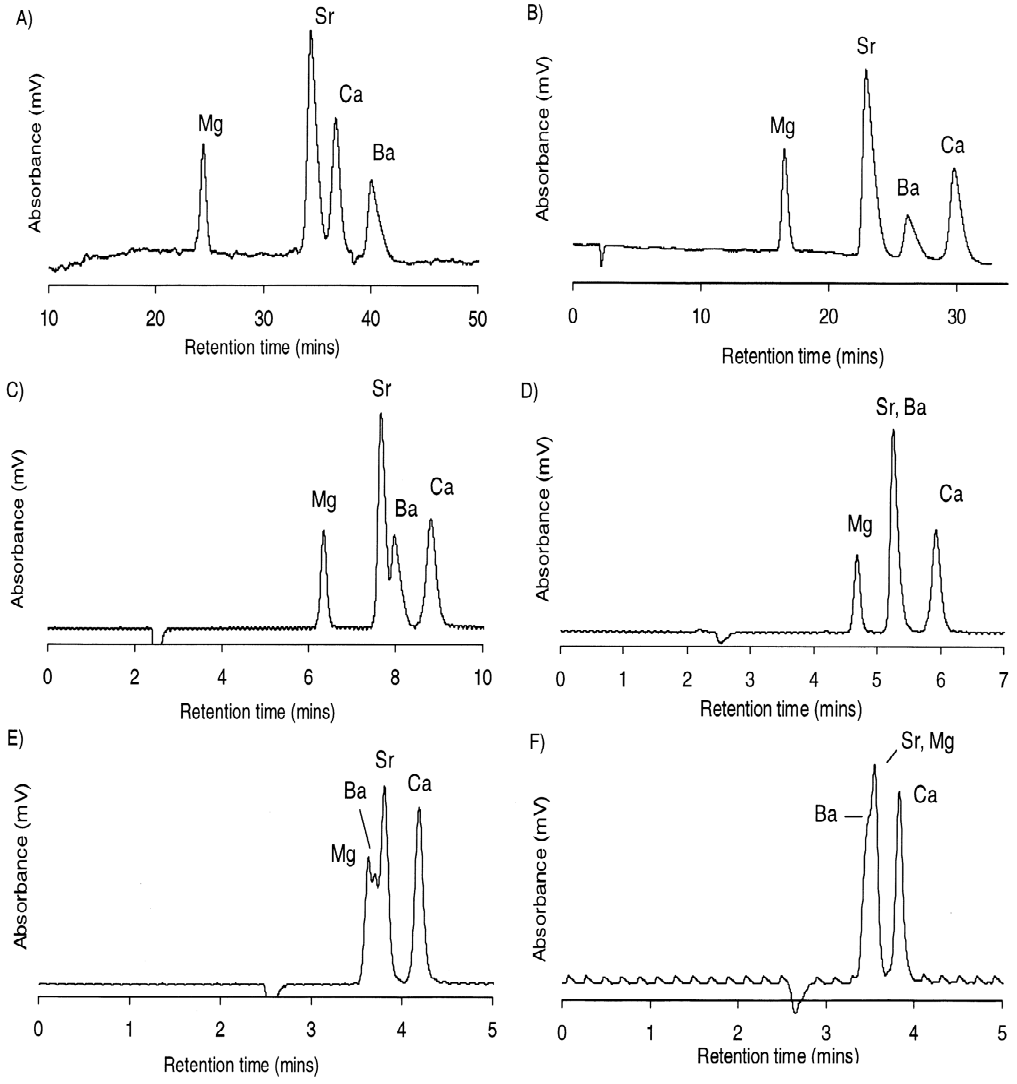

Figure 1.34: Separation of alkaline earth metals using an IDA bonded silica particulate column using (a) 0.1 *M* KNO_3, (b) 0.2 *M* KNO_3, (c) 0.3 *M* KNO_3, (d) 0.5 *M* KNO_3, (e) 1.0 *M* KNO_3 and (f) 1.5 *M* KNO_3 eluents. Reproduced from [130].

The changes in selectivity observed by Bashir *et al.* [130] were also observed by Sugrue *et al.* [125] using an IDA modified silica monolith. In this work, the authors investigated the selectivity of the alkaline earth metals using eluents varying in concentration from 0.1 *M* KNO_3 to 1.0 *M* KNO_3 and noted that retention of the alkaline earth metals using an IDA modified silica monolith was due to a combination of both ion exchange and chelation.

Following on from this work, Bashir *et al.* [132] studied the effect of the ionic strength of the eluent on the retention of transition and heavy metals using the same IDA bonded silica particulate column that was used for the alkaline earth metal analysis [130]. The authors studied the effect on the selectivity of transition and heavy metals using a 0.5 *M* or 1.0 *M* KNO_3, $NaNO_3$, KCl or NaCl eluents. In all cases the pH of the eluent was kept constant with HNO_3. No change in selectivity for Mn(II), Cd(II), Co(II), Zn(II) or Pb(II) was observed when KNO_3 or $NaNO_3$ was used as the eluent and the same trend was observed when the eluents were changed to KCl and NaCl. However, the authors did notice differences in selectivity between the nitrate eluent and the chloride eluent. Using the 0.5 *M* nitrate eluent, an elution order of Mn(II) < Cd(II) = Co(II) < Zn(II) was obtained and Pb(II) was heavily retained, however with the 0.5 *M* chloride eluent, the Cd(II) co-eluted with Mn(II) and the retention of Pb(II) was reduced. The change in selectivity of Cd(II) and Pb(II) observed between the nitrate eluent and the chloride eluent was due to the formation of stable chloro complexes between the chloride eluent and Pb(II) and Cd(II). Formation constants for Pb(II) with chloride is 0.9 and for Cd(II) is 1.35 as opposed to other metals, such as Mn(II), where the formation constant is 0.04 and Zn(II) is 0.11 (values at 0.5 – 1 *M* ionic strength and 25 ^{o}C). Unlike the alkaline earth metals shown previously [130], changes in selectivity were not observed when the ionic strength of the eluent was increased. This was also observed by Nesterenko *et al.* [133] using a single column method for the trace metal analysis in complex samples using an IDA bonded silica particulate column.

Shaw *et al.* [142] showed the retention of alkaline earth metals and transition metals using an IonPac CS12A pellicular column with attached carboxylic and phosphonic acid groups. The authors studied the effect of ionic strength in the eluent on the retention of various alkaline earth metals and transition metals. Increasing the potassium content of the KNO_3 eluent resulted in a decrease in the retention of all metals and through manipulation of the eluent pH, the authors successfully separated Mg(II), Sr(II), Ba(II), Mn(II), Co(II), Ni(II) and Zn(II) which was not possible through simple ion exchange alone. The authors also showed the effect of increasing the Cl^- ion concentration in the eluent, on retention. Similiar to that observed by Bashir *et al.* [132], the retention of Cd(II) and Pb(II) was greatly reduced, with Cd(II) eluting as the least retained metal.

1.7.5.3 Temperature effects

Increasing the column temperature has proven to be beneficial in HPCIC, as increases in temperature can result in improved column efficiency and changes in retention and selectivity [51]. However, the effect of temperature on the separation of metal cations in HPCIC and IC is not widely used, despite its ease of incorporation into a chromatographic system.

The effect of temperature on retention can be shown by the van't Hoff equation (Equation 1.3).

$$\ln k = - \Delta H/RT + \Delta S/R + \ln \varphi \qquad \text{Eqution 1.3}$$

where k is the retention factor, ΔH is the enthalpy change for the exchange reaction, R is the universal gas constant, T is the absolute temperature, ΔS is the entropy change and φ is the column phase ratio (which is constant for a given column). ΔS is assumed to be constant, therefore the equation becomes:

$$\ln k = - \Delta H/RT \qquad \text{Equation 1.4}$$

Plots of ln k versus 1/T should be linear and have a slope = - $\Delta H/R$ [123].

The changes in retention and selectivity due to increases in temperature are related to both thermodynamic properties and kinetic properties. Generally, in the case of separation due to ion exhange interactions, the adsorption process is exothermic (negative values of ΔH) and an increase in temperature results in a decrease in retention. In HPCIC, both exothermic and endothermic behaviour has been observed. Generally, for complexation of metals with IDA ligands, endothermic behaviour is exhibited and an increase in temperature generally results in an increase in retention [51]. In relation to kinetic properties, an increase in temperature can result in the formation of complexes with a higher denticity and therefore a slower dissociation rate, thus leading to an increase in retention with an increase in temperature [51].

In 2001, Hatsis *et al.* [143] studied the effect of temperature on the retention of alkali and alkaline earth metals using a Dionex CS12A analytical column, with attached surface carboxylic and phosphonate functionalities. Using a methanesulfonic acid eluent, separations of various alkali metals, alkaline earth metals and amines were carried out at temperatures ranging from 23 ^{o}C to 60 ^{o}C. In all cases, the authors noted a decrease in retention with an increase in temperature. In this case, retention was due to ion exchange interactions. The authors noted, that while no change in selectivity was observed within the same group of metals studied, a change in selectivity between each group of analytes was observed. Figure 1.35 (left) shows van't Hoff plots obtained for various alkali, alkaline earth metals and amines showing that changes in selectivity were obtained with an increase in temperature. Figure 1.35 (right-top trace) shows a chromatogram for the separations of Mg(II), Ca(II), butylamine (BuA) and Sr(II) carried out at 27 ^{o}C and the same separation carried out at 46 ^{o}C. Clearly a change in selectivity was obtained at the higher temperature and this demonstrates the improvement in the separation of the selected analytes through the implementation of temperature (bottom trace).

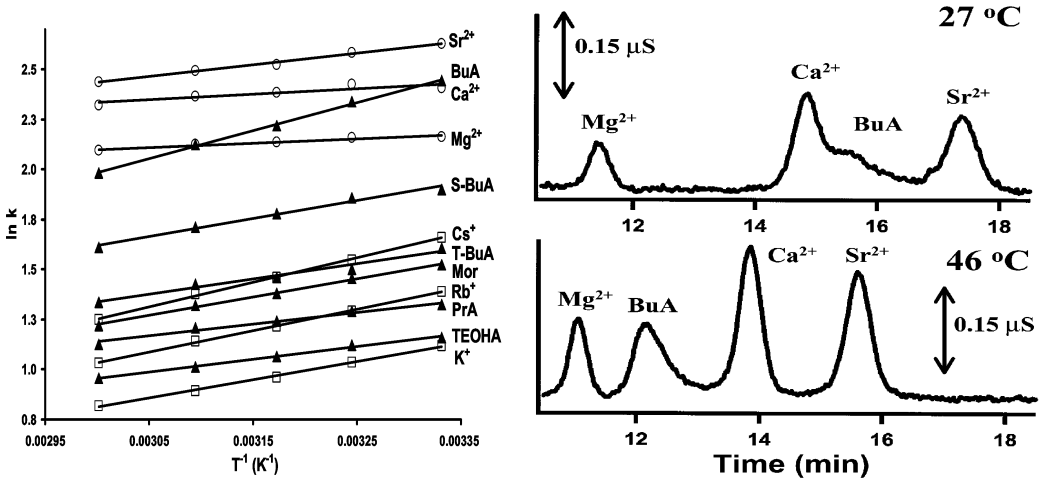

Figure 1.35: (left): Van't hoff plots of alkali metals, alkaline earth metals and amines showing changes in selectivity as the temperature is increased. (right): Separation of selected alkaline earth metals and BuA carried out at 27 ^{o}C (top) and 46 ^{o}C (bottom) demonstrating the benefits of the use of temperature to alter separation selectivity. Reproduced from [143].

Following on from this work in 2003, Shaw *et al.* [142] studied the effect of temperature on the retention of selected transition and heavy metals using the same CS12A analytical column as Hatsis *et al.* [143]. Using a 0.2 *M* KCl with 0.9 m*M* nitric acid eluent, Shaw *et al*. [142] observed an increase in retention with an increase in temperature for all transition and heavy metals studied (Figure 1.36). The temperature range studied was 25 ^{o}C to 55 ^{o}C. Changes in the retention of Sr(II) and Ba(II) were considered negligible over the range of temperatures studied due to the fact that complex formation between Sr(II) and Ba(II) and the phosphonic acid ligand on the stationary phase surface were the weakest of all the metals studied. This allowed for changes in selectivity with an increase in temperature which led to improvements in the separation of 8 alkaline earth and transition and heavy metals as shown in Figure 1.36 (right). At 25 ^{o}C, Ba(II) co-eluted with Zn(II), however at 50 ^{o}C, an increase in the retention of Zn(II) and with the change in retention due to increase in temperature proving negilible for Ba(II), allowed the separation of both metals with optimised temperature conditions. Also worth mentioning is the improvements in the separation of Mn(II) and Sr(II) which exhibited similiar *k* values at 25 ^{o}C but clear separation of both metals at 50 ^{o}C.

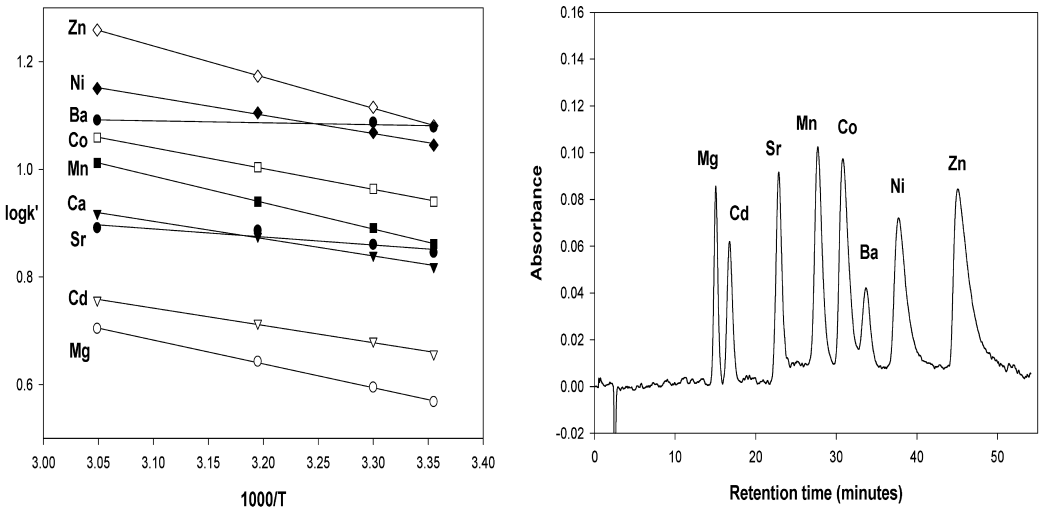

Figure 1.36: (left): Van't Hoff plots for alkaline earth metals, transition and heavy metals cations obtained by increasing the temperature from 25 ^{o}C to 55 ^{o}C. (right): Separation of selected alkaline earth metals, transition and heavy metals using optimised temperature conditions (50 ^{o}C). The eluent used was 0.2 *M* KCl and 0.9 m*M* nitric acid. Reproduced from [142].

A comprehensive study on the effects of temperature on the retention of metal cations using cation exchange and chelation chromatography was carried out by Paull and Bashir [131]. The effect of temperature on the retention of alkali, alkaline earth and transition metals was studied using four different stationary phases namely, a Dionex CS10 (sulfonated) column, a CS14 (carboxylated) column, a Hamilton PRP-X800 (itaconic acid – dicarboxylated) column and a silica based IDA analytical column. In the case of the alkali metals, an increase in temperature resulted in a decrease in Li^+, Na^+, NH_4^+, K^+ and Cs^+ on all four columns. Generally, in chromatographic systems where chelation in the dominant separation mechanism, heats of adsorption (ΔH) are higher than those observed for simple ion-exchange mechanisms and heats of absorption obtained for ion exchange separations do not exceed 3 kJ mol^{-1} [51]. Paull *et al.* [131] reported ΔH values for all columns, which were consistent with expected values when ion exchange was the mode of retention. The authors also studied the effect of temperature on the retention of alkaline earth metals using the four columns mentioned earlier. Unlike the alkali metals, the effect of temperature on the retention of the alkaline earth metals was more complicated. The authors found that using the CS10 column (sulphonated) and a HNO_3 eluent, an increase in retention was observed with an increase in temperature. However, using the CS14 (carboxylated) column, an increase in temperature resulted in a decrease in retention. Due to differences in the capacity of the two columns, a higher eluent concentration was required to elute the metals using the CS10 column and under these acidic conditions, the charge density of the CS10 column was higher than that of the CS14 column. As mentioned previously, an increase in temperature resulted in a decrease in retention of all alkaline earth metals studied using the CS14 column. However, when the ion exchange interactions were suppressed (through the addition of KCl to the eluent), the opposite trend was observed and an increase in temperature resulted in a increase in retention. Heats of adsorption, which were calculated to be between -3.34 to -6.25 using the nitric acid eluent, were 2.17 to 6.51 when ion exchange was suppressed and chelation became the dominant separation mechanism. The clear change in ΔH values supported the change in retention mechanism from ion exchange using the acidic eluent to chelation when high ionic strength eluents were used. Using acidic conditions the effect of temperature on the IDA bound silica and the itaconic acid columns was minimal, however using eluents with increasing ionic strength, the effect of temperature on both columns was more pronounced. Increasing the temperature

resulted in a clear increase in retention of all metals studied. As for the CS10 and the CS14 columns, ΔH values support the change from retention due to ion exchange under acidic conditions to chelation with the ionic strength of the eluent was increased. Finally, the authors studied the effect of temperature on the retention of transition metals using the four different stationary phases. In all cases, using eluents with increasing ionic strength, an increase in temperature resulted in an increase in retention of the transition metals studied. In conclusion the authors observed that for strong cation exchangers, such as the sulphonated column, under acidic conditions, an increase in temperature resulted in an increase in retention and for the weak cation exchanger (carboxylated) under acidic conditions, an increase in temperature resulted in a decrease in retention. For the functional groups capable of forming complexes with metal cations, using eluents with high ionic strength suppressed the ion exchange interactions and an increase in temperature resulted in an increase in retention. More recently, Barron *et al.* [52] demonstrated the effect of temperature on the retention of metals on a Dionex ProPac IMAC-10 analytical column (poly(IDA) functionalised polymer resin) and observed an increase in retention for all metals. Fe(II) and Mn(II) co-eluted at ambient temperatures, however resolution of Fe(II) from Mn(II) was obtained at higher temperatures, demonstrating the use of temperature to improve separation.

1.8 Conclusions

The use of capIC has grown in popularity over the last number of years due to improvements in instrumentation and stationary phase technology. The extensive analysis carried out using monolithic stationary phases over the years has ensured that the topic is well understood. Due to the lack of capIC instrumentation commercially available (until 2011), the use of C^4D detection has ensured that capIC is widely used for the separation of anions and cations. From reviewing the literature, it is clear that polymer monoliths are less efficient than their silica based counterparts for the separation of small ions. The work carried out in the following chapters of this thesis aim to further improve on the methods currently available for surface modification of polymer monoliths for the separation of small ions as well as aiming to fabricate the first capillary polymer monolith with immobilised chelating ligands for the separation of metal cations.

Chapter 2.0:

Experimental

2.0 Materials and Reagents

Glycidyl methacrylate (GMA), butyl methacrylate (BuMA), lauryl methacrylate (LMA), ethylene dimethacrylate (EDMA), propan-1-ol, butane-1,4-diol, decanol, 1-dodecanol, cyclohexanol, 2,2-dimethoxy-2-phenolacetophonone (DAP), boric acid, nitric acid, copper sulphate, 3-sulfopropyl methacrylate (SPM), 4-(2-pyridylazo) resorcinol (PAR), *o*-cresolphthalein complexone (*o*-CPC), acetone, sodium hydroxide, sodium benzoate, benzophenone, hydrochloric acid, methanol, [2(methacryloyloxy)ethyl] trimethylammonium chloride (META), iminodiacetic acid (IDA) and 3(trimethoxysilyl)-propyl methacrylate were all purchased from Sigma Aldrich (Gillingham, UK). Vinyl azlactone (VAL) was purchased from TCI Europe (Boerenveldseweg, Belgium).

Fluoride, chlorite, bromate, chloride and nitrite were purchased as their sodium or potassium salts from Sigma Aldrich (Gillingham, UK). The cations used for the chromatographic separations were magnesium, calcium and barium and were purchased as their chloride salts from Sigma Aldrich and prepared weakly to stock concentrations of 1000 mg/L. Dilutions of the stock standards were carried out to the required concentrations with deionised water and filtered prior to use. The metal standards used were copper nitrate, cobalt chloride (Sigma Aldrich), cadmium nitrate, nickel chloride, manganese, magnesium sulfate-hepta-hydrate, calcium chloride dihydrate, barium chloride dihydrate and strontium nitrate (VWR, Dublin, Ireland), zinc chloride (Merck, Darmstadt, Germany) and were prepared to stock concentrations of 1000 mg/L using 1 m*M* nitric acid. The PCR used was 0.4 m*M* PAR dissolved in 0.1 *M* ammonia, pH 10.6 and was prepared daily.

All eluents and standards were prepared using a Millipore water purification system (Bedford, MA, USA) and filtered through a 0.45 µm nylon membrane filter. UV transparent Teflon coated 100 µm internal diameter fused silica capillary (375 µm outer diameter) was purchased from CM Scientific Ltd. (Shipley, UK).

2.1 Instrumentation

2.1.1 Instrumentation for fabrication and surface modification of polymer monoliths

The pump used for the vinylisation of the fused silica capillary was a KDS-100-CE, KD Scientific syringe pump from Cole Parmer (Illinois, USA). Polymerisation of the polymer monoliths (using thermal polymerisation) was carried out using a water bath at 60 ^{o}C (GFL 1002, VWR International, Dublin, Ireland) and the polymer monoliths prepared using UV polymerisation was carried out using a Spectrolinker XL-1000 UV Crosslinker at 254 nm (Spectronics Corp. NY, USA).

For photo-grafting of the monolithic columns, a Spectrolinker XL-1000 UV Crosslinker at 254 nm (Spectronics Corp. NY, USA) was used. Surface modification of the polymer monoliths were carried out using a Knauer Smartline 100 high pressure analytical pump (Knauer, Bedforshire, UK). The polymer monoliths were connected to the pumping system using low dead volume capillary fittings from Upchurch Scientific (Oak Harbour, WA, USA). An Orion pH meter with a glass electrode was used for all pH measurements (Thermo Orion, Beverly, MA, USA).

2.1.2 Commercially available capillary ion chromatography system

The system used for the chromatographic separation of anions was a Dionex Ultimate 3000 capillary chromatography system, (Sunnyvale, CA, USA) with 50 nL partial loop injection volume, using a 1 µL injection loop. The eluent flow was introduced using a calibrated flow splitter (101:1) to deliver an accurate flow-rate of 1 µL/min. The polymer monolith was connected to the injector valve using 25 µm fused silica capillary (25 cm x 25 µm, internal volume of ~ 120 nL) using a low dead volume MicroTight union with a swept volume of 17 nL (Upchurch Scientific, Oak Harbour, WA, USA). Detection was carried out using on-column C^4D detection (Innovative Sensor technologies, GmbH, Innsbruck, Austria). The recording and processing of chromatograms was carried out electronically using Chromeleon software.
Chromatograms were processed using the following equations:

Asymmetry $$A = \frac{RW + LW}{2 \times LW_{5\%}}$$ Equation 2.1

where RW = width of right hand side of peak, LW = width of left hand side of peak measure at 5 % peak height.

Resolution $$R_s = \frac{2(t_{rb} - t_{ra})}{W_{b1/2} + W_{a1/2}}$$ Equation 2.2

where t_{rb} and t_{ra} are the retention time of solute b and a and W_b and W_a is the peak widths measured at 50 % peak height.

Efficiency $$N = \frac{5.5\ (t_r)^2}{(W_{1/2})^2}$$ Equation 2.3

where t_r is the retention time of the peak of interest and $W_{1/2}$ is the peak width as 50 % peak height.

2.1.3 In–house assembled capillary ion chromatography system (capIC) used for the separation of anions and cations.

An in-house constructed capillary ion chromatography (capIC) system was assembled, which consisted of a Knauer Smartline 100 high pressure analytical pump (Knauer, Bedforshire, UK) and a Cheminert fixed loop 20 nL injector valve (Global FIA, WA, USA). Detection was carried out using on-column C^4D detection for anions analysis and C^4D detection was replaced with a capillary UV detector with a 3 nL flow cell (Dionex Ultimate 3000, Sunnyvale, CA, USA) for cation analysis. The photo-grafted polymer monoliths were plumbed directly into the injector valve as shown in Figure 2.1.

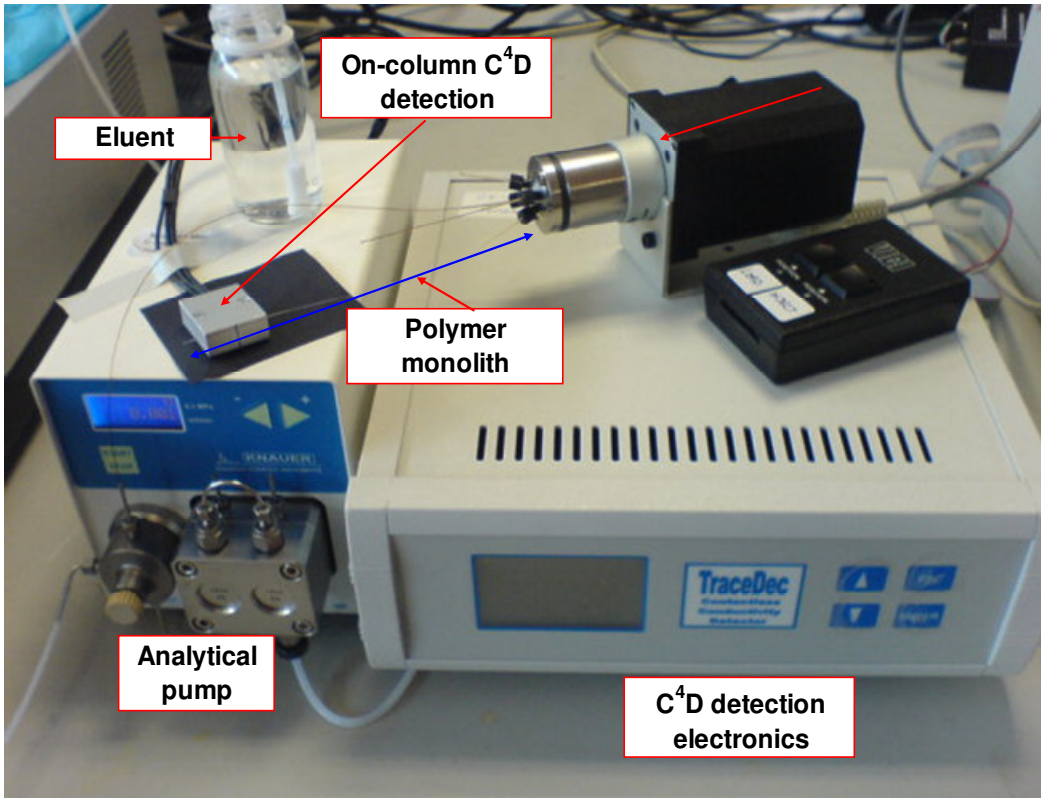

Figure 2.1: The in-house constructed capIC system incorporating a high pressure analytical pump, a 20 nL injector valve, the poly(META) functionalised anion exchange polymer monolith and on-column C^4D detection.

2.1.4 CapIC system used for the separation of metal cations.

The IDA functionalised polymer monolith was connected to the injector valve using 10 cm x 25 µm I.D. fused silica capillary and a second Knauer pump was used to introduce the post-column reagent. A T-connector (Upchurch, WA, USA) was used to connect the IDA monolith and the post-column reagent pump to the UV-visible detector equipped with a 3 nL flow-cell (Dionex, Sunnyvale, CA, USA). In this case, a post-column mixer was not incorporated into the system as the connective tubing (fused silica capillary) associated with the UV-Vis detector was long enough so as to allow mixing. The system also incorporated on-column C^4D detection (Innovative Sensor technologies, GmbH, Innsbruck, Austria). The minimum amount of 25 µm I.D. fused silica capillary (Composite Metal Services Ltd., Shipley, UK) was used to connect all the separate components of the system using zero dead volume MicroTight unions (Upchurch, WA, USA) to reduce the effects of band broadening.

Characterisation of the IDA modified polymer monoliths was also carried out using a Dionex Ultimate 3000 capillary chromatography system (Dionex, Sunnyvale, CA, USA) with a 100 nL injection volume. Similar to the set-up described above (Section 2.1.4), PCR was delivered using a second Dionex Ultimate 3000 analytical pump. The fluidic set-up can be seen in Figure 2.2. A PCR mixing device, which allowed mixing of the column eluate with the PCR, was prepared by coiling polyimide fused silica capillary (17 cm x 25 µm ID, internal volume = 87 nL) around a plastic tube (5 cm x 15 mm ID). Detection was carried out using on-column C^4D detection (Innovative Sensor Technologies GmbH, Innsbruck, Austria) and UV-Vis detection (Dionex, Sunnyvale, CA, USA) with a 3 nL flow-cell. Eluents of either 0.1 m*M* or 0.2 m*M* nitric acid were delivered at 1µL/min. The separation column was connected to the injector valve using 20 cm x 25 µm fused silica capillary (internal volume of 98 nL) via a zero dead volume union (MicroTight, Upchurch Scientific, Oak Harbour, WA, USA).

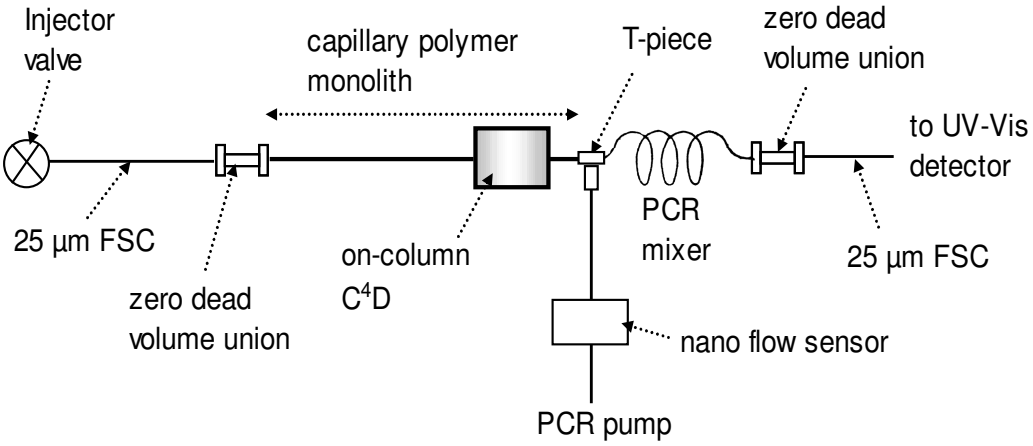

Figure 2.2: Fluidic set-up for dual detection HPCIC.

2.1.5 Temperature studies

2.1.5.1 Temperature heater used for alkaline earth metals using cation exchange separations.

The capillary column oven was constructed using a polyimide flexible heating tape, (dimensions 2.5 x 10 cm) (Kapton, Omega, UK). Figure 2.3 (a) shows the heating tape which was folded to form a cylinder. The cylindrical heating tape was wrapped with insulating tape and covered with aluminum foil as shown in Figure 2.3 (b). Using

two zero dead volume unions, the column was positioned within the column heater in such a way that the column was suspended down the central bore of the device and not touching the heated walls. The ends of the column heater were plugged and the temperature was controlled using a variable voltage power supply (Maplin, Dublin, Ireland). The temperature was monitored using a digital multimeter and a thermocouple wire (Maplin, Dublin, Ireland) placed inside the column heater.

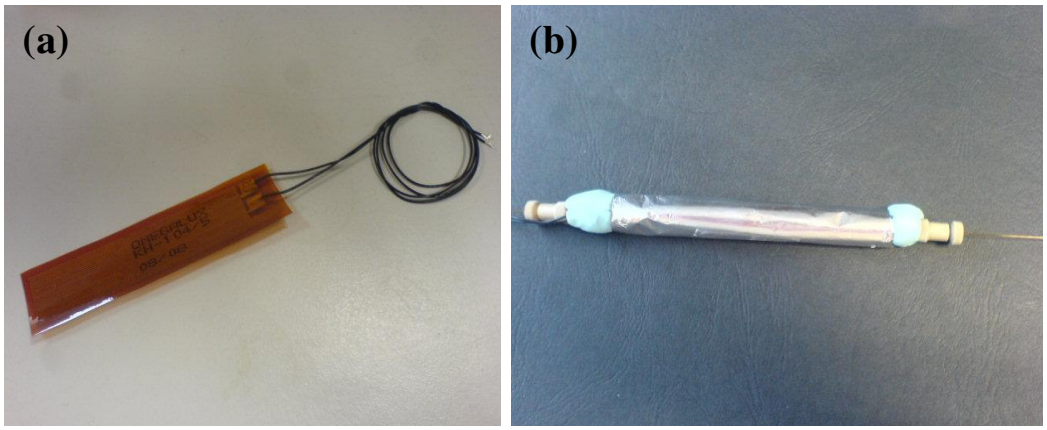

Figure 2.3 (a) Kapton flexible heating tape used in the manufacture of the capillary column heater (dimensions: 2.5 cm x 10 cm) and (b): Kapton heater wrapped in insulating tape and aluminum foil, encasing the cation exchange polymer monolith. The column was placed in the centre of the heater with 2 MicroTight unions positioned at each end.

2.1.5.2 Calibration of the capillary column heater.

Calibration of the capillary column heater was carried out using a multimeter with a temperature setting. Voltage was applied in 0.5 V increments and the temperature noted. Temperature was recorded using a thermocouple wire placed inside the heater.

2.1.5.3 Temperature heater used for metal cation separations using chelation ion chromatography.

Temperature studies were carried out using a capillary column heater, which was constructed using a flexible heating tape (Kapton, Omega, UK). The heating tape (30 cm x 2 cm) was gently folded into a cylindrical shape and pushed inside a stainless steel tube (30 cm x 1 cm I.D.) to form a column heater as shown in Figure 2.4 (a). A

thermocouple wire (Maplin, Dublin, Ireland) was used (via a small hole drilled mid-way down the tube) to monitor temperature as shown in Figure 2.4 (b). Voltage (0-35 V) was applied to heat the flexible tape using an EA-PS2316-050 triple power supply (Elektro Automatik, Germany).

Empty fused silica capillary (7 cm x 25 µm I.D.) was connected to the end of the column to facilitate off-column C^4D detection as shown in Figure 4.2 (b)

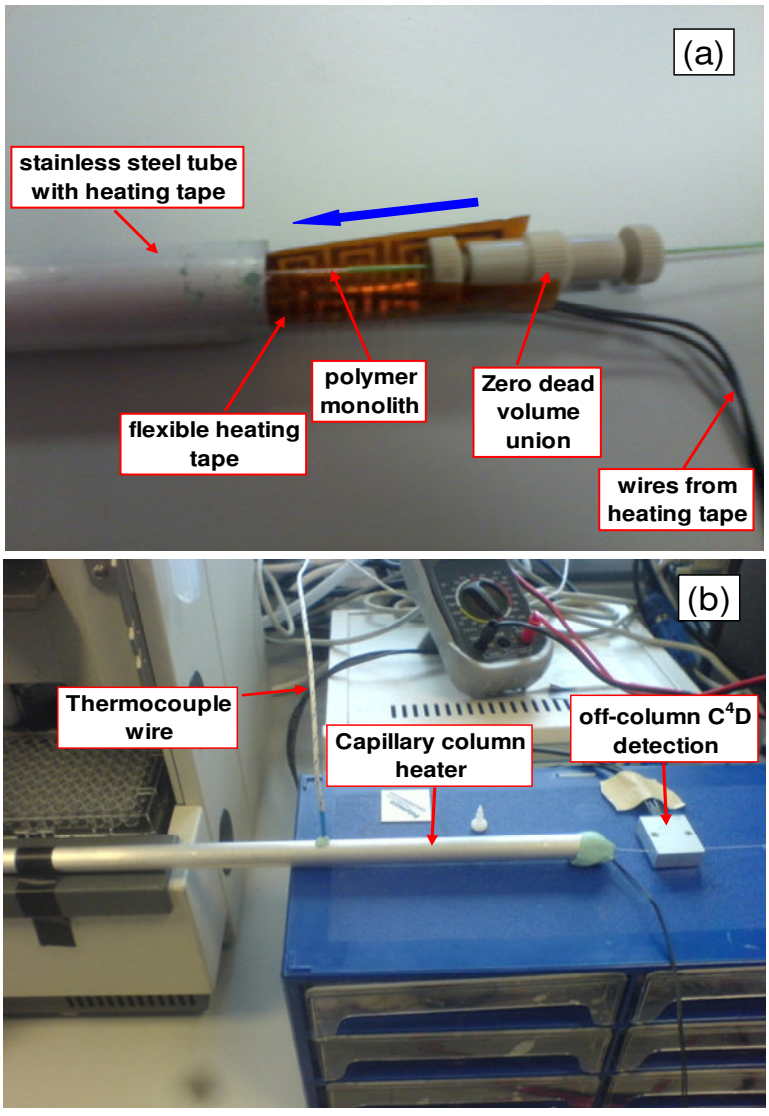

Figure 2.4: (a) Placement of the flexible heating tape inside a stainless steel tube and (b): In-house constructed capillary column heater demonstrating off-column C^4D detection. Temperature monitoring was carried out using a thermocouple wire.

2.2 Procedure

2.2.1 Vinylisation of fused silica capillary

To ensure attachment of the monolith to the walls of the capillary, pretreatment with 3-(trimethoxysilyl)propyl methacrylate was required. The walls of the fused silica capillary were first activated with 200 m*M* NaOH for 30 mins at a flow-rate of 2 µL/min followed by washing with water for 10 mins. Various solutions were subsequently pumped through the fused silica capillary in the following sequence: 200 m*M* solution of HCl at 2 µL/min for 30 mins, deionised water at 2 µL/min for 10 mins, acetone 2 µL/min for 10 mins, followed by purging with nitrogen for 10 mins and finally a 50 % solution of 3-(trimethoxysilyl)propyl methacrylate in acetone at 2 µL/min for 30 mins. The fused silica capillary was sealed with rubber septa and placed in a water bath at 60 ^{o}C for 20 hours. Following removal from the water bath, the fused silica was washed with acetone for 30 mins at a flow-rate of 2 µL/min followed by purging with nitrogen for 10 mins [116].

2.2.2 Fabrication of polymer monoliths

2.2.2.1 Fabrication of GMA-*co*-EDMA monolith

A GMA-*co*-EDMA monolith was prepared for the separation of anions according to the procedure described by Ueki *et al*. [49]. A polymerisation solution was prepared consisting of 30 wt % GMA and 10 wt % EDMA dissolved in a porogenic solution consisting of 35 wt % propan-1-ol, 20 wt % butane-1,4-diol and 5 wt % of water. The polymerisation mixture also contained 4 mg of AIBN (1 % weight with respect to the total monomer concentration). The mixture was de-oxygenated for 10 minutes with nitrogen and allowed to fill into previously vinylised Teflon coated fused silica capillary (100 mm x 100 µm I.D.) by capillary action. The filled capillary was sealed with rubber septa and placed into a water bath at 60 ^{o}C for 24 hours. The resulting monolith was subsequently washed with methanol to remove any unreacted monomers at 1 µL/min for one hour.

2.2.2.2 Fabrication of BuMA-*co*-EDMA polymer monolith

A polymerisation mixture was prepared consisting of 23 % v/v BuMA and 13 % v/v EDMA dissolved in 63 % v/v decanol containing 4 mg DAP (1 % weight with respect to total monomer concentration). The monomer mixture was vortexed to ensure the DAP was fully dissolved followed by de-oxygenating with nitrogen for 10 minutes. Fused silica capillary tubing (100 µm x 120 mm) was filled with the monomer mixture by capillary action and each end was sealed with a rubber septum. It was then placed in the UV oven where 1 J/cm^2 of UV energy at 254 nm was applied. Following irradiation, the monolith was washed with methanol at 1 µL/min for 1 hour to remove any excess porogen and unreacted monomer.

2.2.2.3 Fabrication of LMA-co-EDMA polymer monoliths

Monomer mixture consisting of 24 wt % LMA, 16 wt % EDMA, 45.5 wt % 1-propanol, 14.5 wt % 1,4-butanediol and 4 mg of DAP (1% weight with respect to the monomers) was prepared as described by Collins *et al.* [144]. The polymerisation mixture was de-oxygenated for ten minutes with nitrogen and filled into the previously vinylised UV transparent fused silica capillary (30 cm x 100 µm) by capillary action and sealed with rubber septa followed by irradiation with 2 J/cm^2 of UV energy at 254 nm.

2.2.3 Surface modification of polymer monoliths for ion exchange chromatography.

2.2.3.1 Immobilisation of free radical initiator benzophenone onto the polymer monolith

In all cases, benzophenone, a free radical initiator, was covalently attached to the surface of the polymer monoliths by flushing the monolith with a 50 mg/mL benzophenone in methanol solution, which had been de-oxygenated with nitrogen for 10 minutes. Following irradiation with 1 J/cm^2 of UV energy at 254 nm, the monolith was then washed with methanol at 3 µL/min for 1 hour.

2.2.3.2 Photo-grafting of poly(META) on the surface of the polymer monolith for anion exchange chromatography.

A 15 % w/v poly(META) solution was prepared in water and de-oxygenated for 10 minutes with nitrogen. The monolith was flushed with the META reagent at a flow-rate of 1 µL/min for 30 minutes. The monolith was end capped, irradiated with 0.252 J/cm^2 of UV energy at 254 nm [103] and washed with methanol at 1 µL/min for three hours. The column was then washed with water for 1 hour at 1 µL/min and equilibrated with a 2 m*M* sodium benzoate eluent for 12 hours.

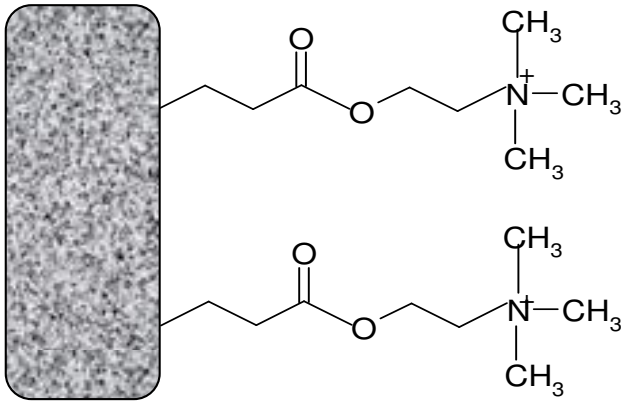

Figure 2.5: Photo-grafting of poly(META) on the surface of the polymer monolith.

2.2.3.4 Surface grafting of the polymer monolith with poly(SPM) for cation exchange chromatography

A 6 % w/v SPM solution was prepared in de-ionised water and de-oxygenated with nitrogen for 10 minutes. This mixture was pumped through the benzophenone modified monolith at a flow-rate of 0.2 µL/min for 1 hour. The monolith was irradiated with 0.25 J/cm^2 of UV energy at 254 nm. A preliminary wash with methanol was carried out at 1 µL/min for 10 minutes. The monolith was washed with water at 1 µL/min for 1 hour and left to equilibrate with a 1 m*M* copper sulfate eluent at 1 µL/min. This resulted in a polymer monolith with immobilised sulfonated groups as shown in Figure 2.6.

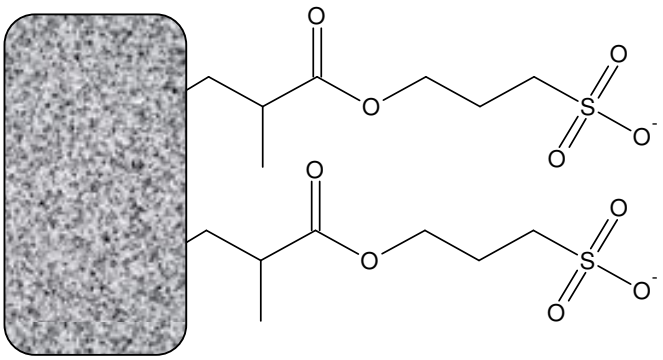

Figure 2.6: Photo-grafting of poly(SPM) on the surface of the polymer monolith.

2.2.4 Surface grafting of polymer monoliths for metal cation separations using chelation ion chromatography

2.2.4.1 Photo-grafting of poly(VAL) or poly(GMA) on the monolith surface

The monolith was flushed with a 5 % w/v solution of benzophenone in methanol, as described in Section 2.2.3.1. Following this, deoxygenated poly(VAL) solutions (15–30 % v/v) in methanol of poly(GMA) solutions (15–35 % v/v) were flushed through the polymer monolith at 1 µL/min for 1 hour and 1 J/cm^2 of UV energy at 254 nm was applied.

2.2.4.2 Fabrication of acetylimino-diacetic acid (AIDA) or poly(GMA) photo-grafted polymer monolith

A 1 mg/ml aqueous solution of IDA was flushed through the monolith at 1 µL/min for 5 hours, followed by a water flush at 1 µL/min for 3 hours. IDA covalently attached to VAL as shown in Figure 2.7. Figure 2.8 shows the covalent attachment of GMA and IDA.

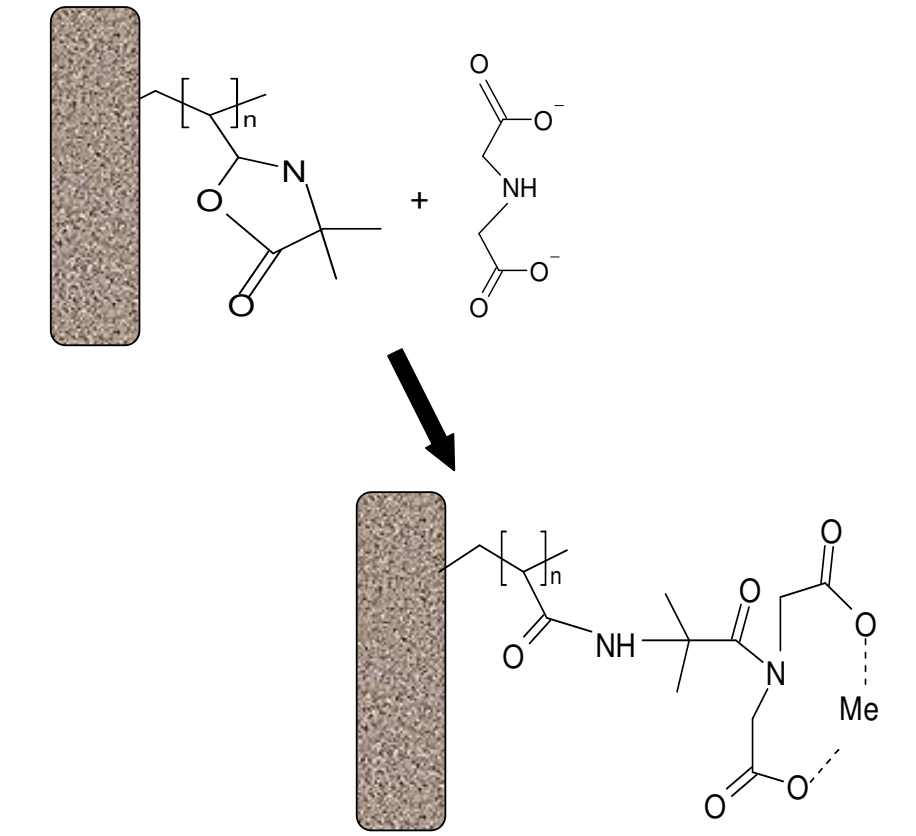

Figure 2.7: Immobilisation of IDA on the VAL grafted polymer monolith.

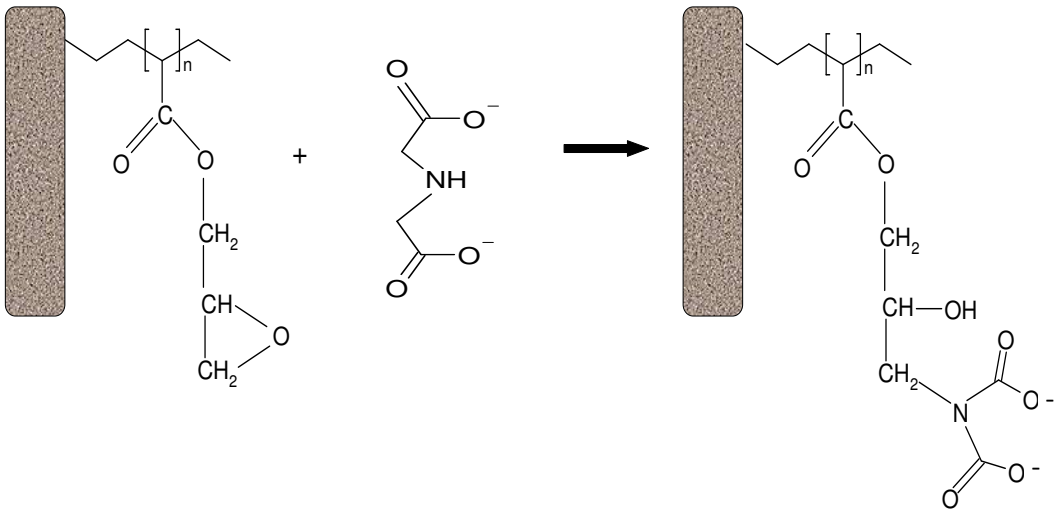

Figure 2.8: Immobilisation of AIDA on the poly(GMA) photo-grafted polymer monolith

A number of AIDA monoliths were used throughout this work and are denoted as in Table 2.1. The same naming system was used for all poly(GMA) IDA monoliths.

Table 2.1: Description of the monoliths used throughout this work.

Monolith name	*VAL (% v/v)*	*Effective column length (mm)*
VAL15a	15	280
VAL15b	15	280
VAL15c	15	100
VAL20	20	100
VAL25	25	100
VAL30	30	100

2.2.5 Separation of anions using the poly(META) modified polymer monolith

Six anion standards were prepared (fluoride, chlorite, bromate, chloride nitrite and bromide) to a stock concentration of 1000 mg/L. The stock solution were diluted with deionised water to yield a six anion standard mix containing 0.7 mg/L fluoride, 3 mg/L chlorite, 3 mg/L bromate, 0.7 mg/L chloride, 0.7 mg/L nitrite and 3 mg/L bromide. A number of other inorganic and organic anions were also prepared to stock concentrations of 1000 mg/L in deionised water and chromatographic performance data obtained. The eluent used for all separations was 2 m*M* sodium benzoate.

2.2.6 Separation of alkaline earth metals using poly(SPM) polymer monolith

The cation exchange polymer monolith with photo-grafted sulfonated groups was used for the separation of calcium, magnesium and barium with UV detection at 210 nm. Copper sulphate was chosen as the eluent as it has been shown to be suitable for the separation of cations [49].

2.2.7 Separation of metal cations using poly(VAL) and poly(GMA) modified polymer monoliths

Stock solutions of Mn(II), Co(II) and Ni(II), Zn(II), Cd(II) and Cu(II) were prepared daily and diluted accordingly with 1 m*M* nitric acid. The eluent used for the separation of metal cations ranged from 0.1 mM - 0.4 mM nitric acid.

2.2.8 Sample preparation for applications of fabricated poly(GMA) modified polymer monoliths

A simulated seawater sample consisting of 0.5 *M* (33,000 ppm) NaCl, 400 ppm Ca(II) and 1100 ppm Mg(II) was prepared with de-ionised water. A second simulated seawater sample was prepared as described which was spiked with 10 ppm Co(II), 10 ppm Cd(II) and 10 ppm Zn(II). Tap water samples spiked with 10 ppm Co(II), Cd(II) and Zn(II) were prepared and injected without further dilution. A bottled water sample was diluted accordingly using the appropriate eluent and filtered prior to use.

2.2.9 Characterisation of IDA modified monoliths by scanning C^4D

At selected stages during the monolith modification, scanning C^4D was used to measure the distribution of IDA functional groups along the column length as described by Connolly *et al*. [45]. Specifically, while continuously flushing the monolith with a 1 m*M* ethanolamine buffer (pH 9.8), the detector head was moved at 2 mm increments along the column and the conductive response recorded at each detector location.

Chapter 3.0:

Modification of capillary polymer monoliths using photo-grafted chains of [2(methacryloyloxy)ethyl] trimethylammonium chloride (META) for the separation of anions

3.1 Introduction

Polymer monoliths have been shown to be highly suited for the separation of large biomolecules, such as peptides and proteins, due to convection dominated mass transfer as opposed to diffusive mass transfer [145]. This is due to the eluent being forced to flow through the monolith bed, in comparison to particle packed columns, where separation depends on diffusion of the analytes in and out of the particle. However, the use of polymer monoliths for the separation of small ions has proven difficult, due to the lack of mesopores on the surface of the monolith, greatly reducing the surface area in comparison to its silica based counterparts [66]. To date, little focus has been placed on the separation of small ions using polymer based capillary monoliths.

Connolly *et al.* [103] recently reported the use of a GMA-*co*-EDMA (110 mm x 100 µm internal diameter) polymer monolith which was functionalised with [2(methacryloyloxy)ethyl] trimethylammonium chloride (META) to produce an anion exchange capillary polymer monolith with surface photo-grafted quaternary ammonium functional groups. Efficiencies of 15,000 N/m were reported for fluoride at 1 µL/min

The aim of this work was to fabricate a high capacity ion exchange polymer monolith for the separation of small anions. This was carried out by photo-grafting polymer chains of [2(methacryloyloxy)ethyl] trimethylammonium chloride (META) on a polymer monolith previously immobilised with benzophenone. The effect of the method of photo-grafting of poly(META) on the polymer monolith was investigated and compared to the method of surface modification carried out by Connolly *et al* [103]. Separations of anions were carried out on the poly(META) polymer monolith using a Dionex capillary LC system and an in-house assembled capillary ion chromatography system. Chromatographic performance data using both systems were compared. The selectivity of the poly(META) polymer monolith, for a wide range of selected inorganic and organic anions, was studied.

3.2 Results and Discussion

3.2.1 Monolith fabrication and functionalisation with poly(META)

Polymer monoliths exhibit lower surface areas in comparison to their silica based counterparts, due to the absence of mesopores on the monolith scaffold. The reduction in the surface area of the polymer monolith requires the incorporation of a large number of functional groups for the efficient separation of small ions. This work aimed to increase the ion exchange capacity using photo-grafting techniques. To increase the surface coverage of poly(META), benzophenone was immobilised on the surface of the monolith.

The ability of benzophenone to form free radicals on surfaces has been documented by Rånby *et al.* [101]. This was followed by Stachowiak *et al.* [146] who demonstrated the ability to form grafted polymer chains from the surface of the monolith in the presence of the free radical initiator benzophenone. Benzophenone abstracts hydrogen atoms exposed at the surface of the monolith and in this work, as the META solution was introduced and UV irradiation applied, graft polymerisation is initiated from the surface of the monolith due to the presence of a source of free radicals directly at the surface. This resulted in a strong anion exchange polymer monolith with quaternary ammonium functionalities. This method of functionalisation is known as a two step functionalisation procedure i.e. immobilisation of benzophenone was carried out in the first step followed by photo-grafting of poly(META) in a second step.

Conversely, Connolly and Paull [103] prepared a GMA-*co*-EDMA generic monolith with which they introduced benzophenone and META onto the surface in a single step process. Briefly, a 15% META solution was dissolved in a water/t-butanol mix (1:3) to which benzophenone was added (1 % relative to META). Following de-oxygenation with nitrogen, the solution was flushed through the monolith and 0.252 J/cm^2 of UV energy at 254 nm was applied. The poly(META) photo-grafted monolith was applied to the separations of common anions.

3.2.2 Effect of the method of functionalisation of the META polymer monolith on the separation of common anions.

The method of photo-grafting of poly(META) on the polymer monolith carried out here in this thesis was modified from that reported by Connolly *et al*. [103]; therefore it was important to investigate the effect of the method of photo-grafting on the chromatographic separation of anions. An identical standard anion mix to that reported by Connolly *et al.* [103] was prepared and the same chromatographic separation conditions used. The advantages of using a two-step photo-grafting method over a one step procedure have been documented by Stachowiak *et al.* [146], including a greater degree of control over the grafting process as the free radical initiator and monomer were grafted in separate steps. Free radicals are formed on the polymer surface which favours graft polymerisation and reduces the formation of non-grafted polymer gel in the solution, which are removed during a washing step. Figure 3.1 (a) shows an isocratic separation of 6 common anions (fluoride, chlorite, bromate, chloride, nitrite and bromide) using the Dionex capillary ion chromatography system. This separation was carried out using the poly(META) functionalised polymer monolith prepared using the two step procedure by the author of this thesis. Using a 2 m*M* benzoate eluent, separation of the 6 anions was obtained in 9 minutes. Retention factor precision was calculated for $n = 3$ injections and was ≤ 3.3 % for all six anions in the standard solution. Retention time precision for the first four anions was ≤ 0.45 % for $n = 3$ injections. Figure 3.1 (b) shows a separation of a mixture of the same anions obtained by Connolly *et al.* [103] on the poly(META) functionalised polymer monolith prepared using the one-step method of functionalisation. The authors calculated retention time precision for the first four anions to be < 1.2 % ($n = 5$ injections). Chromatographic performance data was compared for both methods of functionalisation i.e. the method reported by Connolly *et al.* [103] and the method reported in this thesis and can be seen in Table 3.1. In the work carried out in this thesis, the polymer monolith was connected to the injector valve of the Dionex LC system with 25 cm x 25 µm fused silica capillary, identical to that reported by Connolly *et al.* [103]. As all other chromatographic separation conditions were identical, any changes in chromatographic performance should have been due to differences within the polymer monolith.

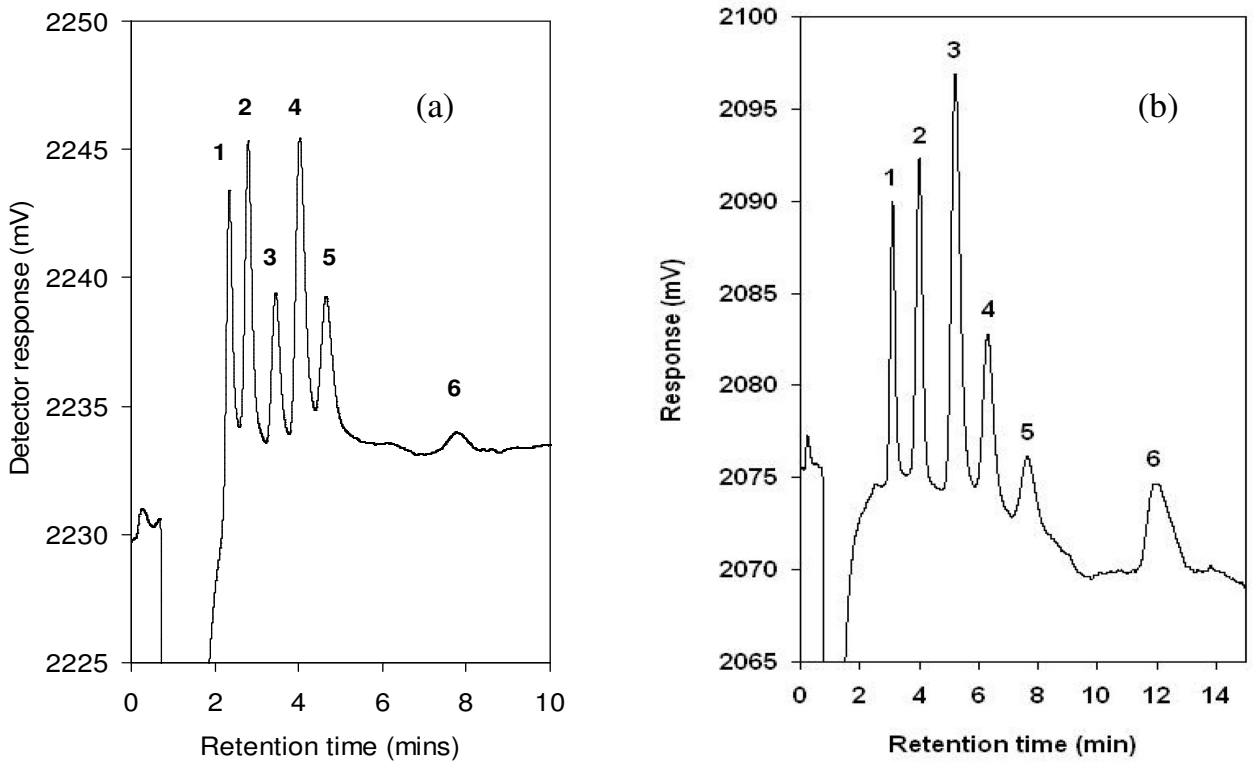

Figure 3.1: (a) Separation of 6 anions on poly(META) polymer monolith using the two-step functionalising procedure and (b) separation of the same anion mix using the poly(META) functionalised polymer monolith using the one step procedure. Figure 2.2 (b) reproduced from [103]. Chromatographic conditions: effective column length: 100 mm x 100 µm (a) and 110 mm x 100 µm (b), eluent: 2 m*M* sodium benzoate, injection volume: 50 nL, detection: on-column C^4D, flow-rate: 1 µL/min. Peak (1) 0.7 mg/L fluoride, (2) 3 mg/L chlorite, (3) 3 mg/L bromate, (4) 0.7 mg/L chloride, (5) 0.7 mg/L nitrite and (6) 3 mg/L bromide.

From Table 3.1, differences in the retention of the 6 anions were noted. A decrease in *k* of ~ 40 % was observed with the two-step photo-grafted monolith. The increased retention shown by the poly(META) polymer monolith using the one step process suggests that an increased ion exchange capacity was obtained using this monolith.

An increase in column efficiency was noted for chlorite, bromate, chloride and bromide using the poly(META) column prepared using the two-step process (polymer monolith prepared in this thesis). Mass transfer was enhanced using this polymer monolith resulting in improved efficiency.

Peak widths (measured at 50 % peak height) increased using the poly(META) monolith prepared with the one step process. For example, an increase in peak width of ~ 35 % was noted for bromate and bromide when the one step process was compared to the two step process. Increased column efficiency (8 %) was obtained for fluoride using the poly(META) column prepared by Connolly *et al.* [103] (i.e. poly(META) polymer monolith prepared using the one-step procedure). This was possible due to the close proximity of fluoride to the void peak using the poly(META) fabricated in this thesis. A slight decrease in efficiency (2.5 %) was also observed for nitrite using the poly(META) monolith prepared using the two step process.

Table 3.1: Chromatographic performance data obtained for the separation of the 5 anion mix on a one-step META functionalised polymer monolith and a two- step META functionalised monolith using a Dionex capillary ion chromatography system. This Table also contains performance data for the same separation of the anion standard mix using an in-house constructed capIC system. Chromatographic conditions: as in Figure 3.1.

	Monolith using one step functionalisation procedure. Data reproduced from [103]				*Monolith using two step functionalisation procedure.*				*Monolith using two step functionalisation procedure.*			
Instrument	Dionex capillary LC system				Dionex capillary IC system				capIC system			
Eluent	2m*M* sodium benzoate				2m*M* sodium benzoate				2m*M* sodium benzoate			
Anion	**N/m**	***k***	**Res.**	**Asy**	**N/m**	***k***	**Res.**	**Asy**	**N/m**	***k***	**Res.**	**Asy**
Fluoride	15,000	2.6	-	1.15	13,800	1.7	-	1.18	12,000	1.7	-	1.04
Chlorite	14,000	3.6	2.5	1.40	14,800	2.2	1.7	1.17	11,000	2.2	1.5	0.96
Bromate	13,000	5.0	2.5	1.26	16,000	3.0	2.0	1.14	11,100	3.1	1.8	0.91
Chloride	14,500	6.2	1.8	1.20	16,900	3.6	1.5	1.35	13,200	3.7	1.3	1.04
Nitrite	11,200	7.8	1.8	1.16	10,900	4.4	1.6	1.43	15,400	4.5	1.4	0.95
Bromide	6,300	10.76	2.8	2.55	10,700	8.2	3.36	2.70	-	-	-	-

Asy – asymmetry calculated at 5 % peak height.
Res – resolution
k – retention factor
N/m- peak efficiency /m

Baseline resolution of all anions using both monoliths was achieved, with the one-step monolith exhibiting slightly greater resolution for all anions, due to the increase in column capacity. Peak asymmetries using both poly(META) monoliths showed slight tailing with the more strongly retained bromide showing asymmetries > 2 using both monoliths. Improved peak asymmetries were obtained for chlorite and bromate using the poly(META) monolith prepared using the two step method of photo-grafting. Peak shape for chloride, nitrite and bromate obtained for the 6 anions were comparable for the poly(META) monoliths prepared using both methods of functionalisation.

Although the poly(META) functionalised polymer monolith fabricated using the two-step procedure showed improved efficiency and faster run times, the one-step procedure used in the preparation of the poly(META) monolith carried out by Connolly *et al.* [103] appeared to produced a column with a higher capacity (increased number of functional groups). This monolith was also faster to fabricate and functionalise, as the functionalisation was carried out in a single step.

The chromatographic data discussed thus far was carried out using a Dionex capillary LC system. Table 3.1 also contains chromatographic data for the same separation on the poly(META) monolith using an in-house assembled capillary ion chromatography (capIC) system which is described in Section 2.1.3 and will be discussed in greater detail in Section 3.2.4.

3.2.3 Effect of eluent concentration on efficiency, *k* and peak width.

In ion chromatography, the eluent concentration is one of the most important parameters effecting retention. Salts of aromatic carboxylic acid are commonly used as eluents in non-suppressed ion chromatography as dilute concentrations of these salts produce eluents with low background conductance, thus facilitating the use of on-column C^4D detection. In this work, a weak sodium benzoate eluent (2m*M*) was chosen. The effect of eluent concentration on the retention on the 5 anions was investigated using a series of benzoate eluents ranging in concentration from 0.6 m*M* to 2 m*M* and the resultant chromatograms can be seen in Figure 3.2.

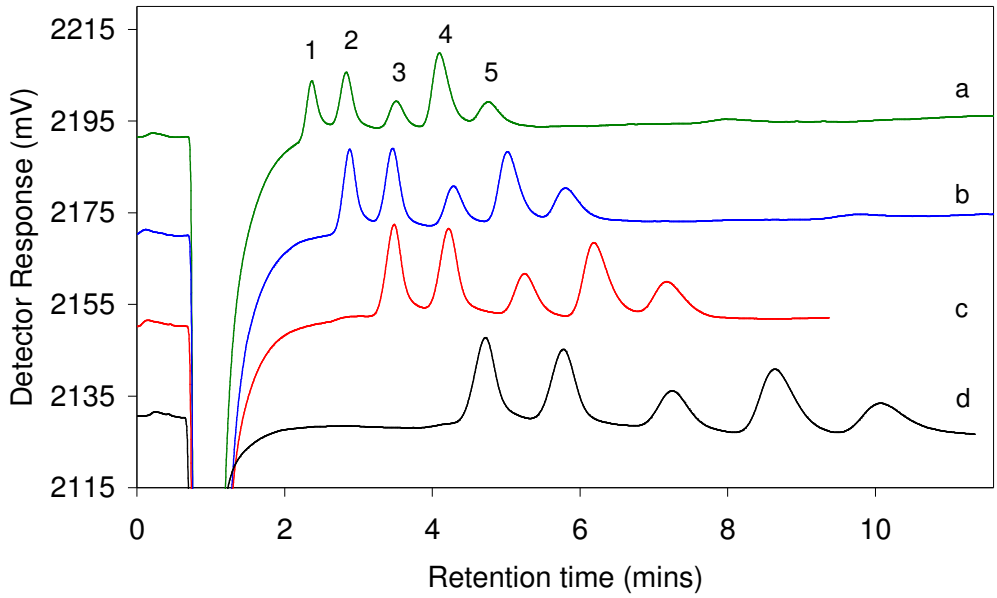

Figure 3.2: Overlaid chromatograms of separations of the 5 anions using the META functionalised polymer monolith obtained by varying the eluent concentration where (a) 2 mM sodium benzoate, (b) 1.4 mM sodium benzoate, (c) 1 mM sodium benzoate and (d) 0.6 mM sodium benzoate. Chromatographic conditions: as in Figure 3.1. Peaks: (1) 0.7 mg/L fluoride, (2) 3 mg/L chlorite, (3) 3 mg/L bromate, (4) 0.7 mg/L chloride, (5) 0.7 mg/L nitrite.

A decrease in eluent concentration resulted in an increase in the retention of all 5 anions (Figure 3.2), as is generally the case in ion chromatography. Using the 2 m*M* benzoate eluent, the 5 anions were separated in a retention window of < 6 minutes. The run time, when the eluent concentration was reduced to 1.4 m*M,* was 7 minutes.

Table 3.2 shows the chromatographic performance data obtained for the separation of the 5 anion mix by varying the concentration of the benzoate eluent from 1 m*M* to 2 m*M*. A comparison of the chromatographic data obtained using the 2 m*M* benzoate eluent and the 1.4 m*M* benzoate eluent showed that an increase in efficiency was obtained for all 5 anions when the eluent concentration was decreased from 2 m*M* to 1.4 m*M* without any significant difference in peak asymmetry. As expected, decreasing the eluent concentration resulted in an increase in peak width. The largest change in peak width was obtained for nitrate. Using a 2 m*M* benzoate eluent, the peak width was 0.28 minutes and was 0.61 minutes using the 0.6 m*M* benzoate eluent.

Table 3.2 (a): Effect of eluent concentration on efficiency, retention and peak width using the META functionalised polymer monolith using 2 m*M* and 1.4 m*M* benzoate eluents and (b) 1 m*M* and 0.6 m*M* benzoate eluents.

(a)	*2 mM benzoate*					*1.4 mM benzoate*				
Anion	N/m	*k*	Peak width	Asy	Res	N/m	*k*	Peak width	Asy	Res
F^-	13,000	1.7	0.16	1.2	-	13,400	2.2	0.19	1.2	-
ClO_2^-	15,000	2.2	0.17	1.2	1.7	15,240	2.9	0.21	1.2	1.7
BrO_3^-	15,500	3.0	0.21	1.2	2.1	15,700	3.8	0.25	1.2	2.1
Cl^-	16,500	3.6	0.24	1.2	1.5	17,100	4.6	0.29	1.3	1.6
NO_3^-	15,500	4.4	0.28	1.3	1.5	15,900	5.5	0.34	1.3	1.5

(b)	*1 mM benzoate*					*0.6 mM benzoate*				
Anion	N/m	*k*	Peak width	Asy	Res	N/m	*k*	Peak width	Asy	Res
F^-	13,200	3.0	0.23	1.1	-	12,700	4.7	0.31	1.1	-
ClO_2^-	15,200	3.8	0.26	1.1	1.8	14,800	5.9	0.35	1.1	1.9
BrO_3^-	15,850	5.0	0.31	1.2	2.1	14,700	7.7	0.45	1.2	2.2
Cl^-	16,750	6.0	0.36	1.3	1.7	16,000	9.4	0.51	1.3	1.7
NO_3^-	15,500	7.1	0.43	1.3	1.5	15,300	11	0.61	1.3	1.5

Asy. – asymmetry calculated at 5 % peak height.

Res. – resolution

Peak width – measured at 50 % peak height in minutes.

Slight changes in resolution were noted as the eluent concentration was decreased. An increase in resolution of ~ 10 % was observed between chlorite and fluoride and also between the bromate/chloride pair. Peak efficiencies were comparable using the 2 m*M*, 1.4 m*M* and 1 m*M* benzoate eluent. Using the 0.6 m*M* benzoate eluent, decreases in efficiency of < 6 % for all anions was obtained. From a comparison of all chromatographic data in Table 3.2, it appeared that the optimised eluent concentration was 1.4 m*M*.

A plot of log *k* versus log [benzoate] was prepared using retention data and can be seen in Figure 3.3. This plot showed linear correlation for all 5 anions with R^2 values > 0.99. Table 3.3 shows linearity data obtained from Figure 3.3 for the 5 separated anions. The values for the slopes obtained for all 5 anions are in broad agreement with the theoretical slope of - 1.0 for anion exchange elution of a singly charged anion using a single charged eluent ion [146]. One eluent ion displaces one analyte ion of the same charge. This demonstrates that the mode of separation was predominately ion exchange.

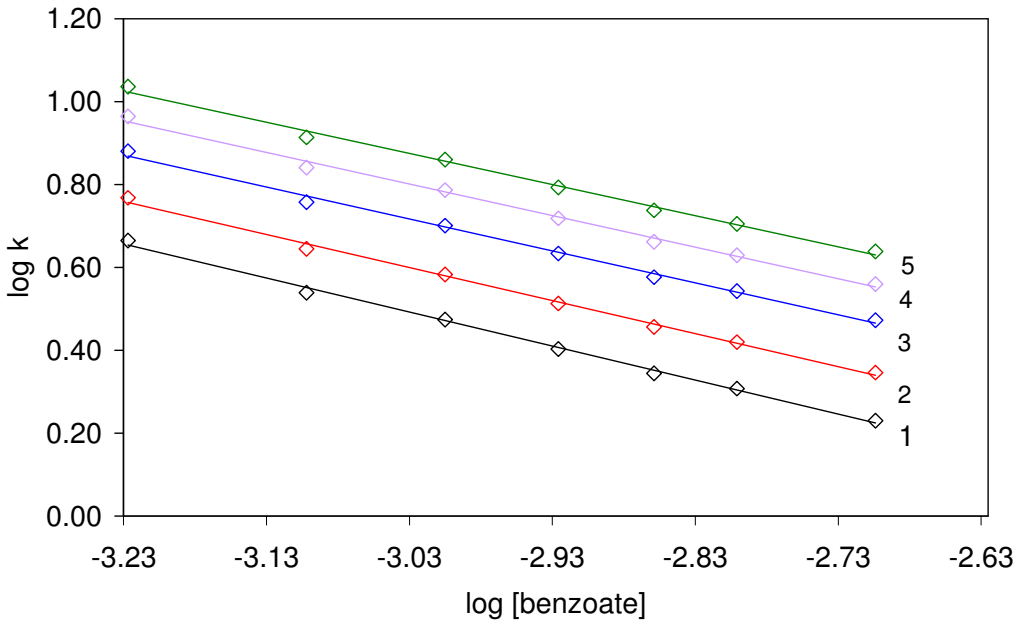

Figure 3.3: Plots of log *k* versus log[benzoate] demonstrating that the mode of separation was anion exchange using the META functionalised polymer monolith. (1) nitrite, (2) chloride, (3) bromate, (4) chlorite and (5) fluoride.

Table 3.3: Linearity regression data obtained on the META functionalised polymer monolith from a variation in the eluent concentration.

Anion	*Slope*	*Intercept*	R^2
Fluoride	-0.82	-1.99	0.99
Chlorite	-0.80	-1.81	0.99
Bromate	-0.77	-1.61	0.99
Chloride	-0.76	-1.51	0.99
Nitrite	-0.75	-1.40	0.99

3.2.4 Separation of inorganic anions on the poly(META) polymer monolith using the capIC system.

Trends in recent years have seen an increase in interest in the area of portable and field deployable analytical devices, such as the portable ion chromatography system reported by Kiplagat *et al.* [147] used for the separation of cations and transition metals using open tubular columns, and the portable CE system reported by Hutchinson *et al.* [148] which was applied to the separation of inorganic anions and cations in post blast explosive residues from homemade inorganic explosive devices. Both of the systems in [147] and [148] incorporated C^4D detection. Here in this thesis, separation of anions using the poly(META) surface modified polymer monolith were also carried out on an in-house assembled capIC system. This capIC system has the potential to be used as a field deployable, portable device.

Figure 3.4 shows a separation of the 5 anion standard mix, previously separated on the Dionex system, using the capIC system as described in Section 2.1.3. Separation of the 5 anions occurred in < 2.5 minutes. Using the capIC system, the poly(META) monolith was plumbed directly into the injector valve and on-column C^4D detection was employed at the mode of detection accounting for differences in the run-times observed with both systems. Table 3.1 shows the retention factors for the separations carried out on the capIC system and the Dionex capillary ion chromatography system. As can be seen from Table 3.1, the retention factors are extremely comparable, however, a difference in run time was observed due to the elimination of extra system

dead volume. The capIC system had a run time of < 2.5 mins (for the first five anions) and the same separation on the Dionex capillary ion chromatography system had a run time of < 6 mins, thus demonstrating a portable capIC system suitable for the fast ion chromatography separation of the selected anions.

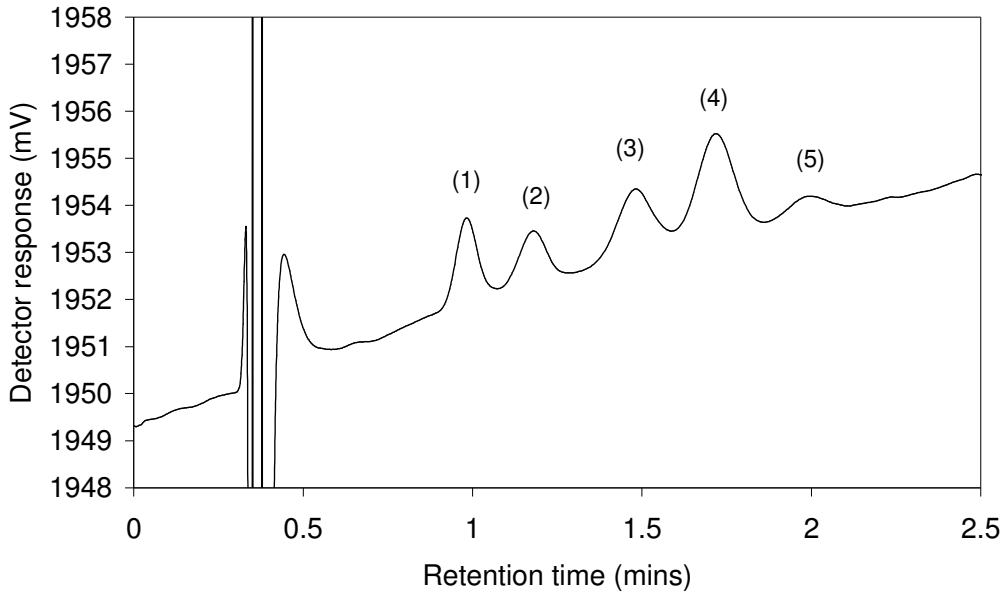

Figure 3.4: Separation of 5 anions using an in-house constructed capIC system. Chromatographic conditions: Column dimensions: 100 mm x 100 µm, eluent: 2 m*M* sodium benzoate, injection volume: 20 nL, flow rate: 1.3 µL/min and detection: on-column C^4D detection. Peak: (1) 0.7 mg/L fluoride, (2) 3 mg/L chlorite, (3) 3 mg/L bromate, (4) 0.7 mg/L chloride, (5) 0.7 mg/L nitrite.

Although faster analysis was obtained using the capIC system, a decrease in column efficiency was obtained for fluoride (13 %), chlorite (27 %), bromate (30 %) and chloride (22 %), when compared with the same separation using the Dionex LC system. A decrease in resolution was also observed particularly between bromate and chloride where a resolution of 1.3 was obtained. As mentioned above, the poly(META) monolith was plumbed directly into the injector valve, thus eliminating any excess connective tubing, which would have an effect on the run time. A second reason for the decrease in retention of the anions on the capIC system may lie in the pumping system used. The Dionex capillary ion chromatography system contained a calibrated flow splitter, therefore ensuring an accurate flow-rate, even at low µL/min levels. On the capIC system, a high pressure pump was used which did not contain a

flow splitter, thus anomalies in the flow-rate may have occurred. The flow-rate was monitored at 1 µL/min using a flow sensor (Upchurch Scientific, Oak Harbour, WA, USA) and it was discovered that the actual flow-rate was 1.3 µL/min. An increase in the flow-rate would account for the decrease in resolution and efficiency, particularly for chlorite, bromate and chloride, obtained on the capIC system. Connolly *et al.* [103] obtained an efficiency of 15,000 N/m for fluoride using a flow-rate of 1 µL/min and an efficiency of 29,500 N/m when the flow-rate was reduced to 100 nL/min.

An improvement in peak asymmetry was observed for the separation of the standard mix on the capIC system. Peak asymmetries close to 1 were obtained for fluoride, chlorite, bromate, chloride and nitrite, respectively. These values represent an ideal Gaussian peak shape. The asymmetry values, obtained for the separation of the standard mix using the Dionex LC system, showed some tailing of the analyte peaks, possibly due to the extra column volume associated with the set-up of this system.

Limits of detection were calculated for the Dionex system and the capIC system and can be seen in Table 3.4. This table also shows absolute limits which take the injection volume into account. Signal/noise ratios of 105 for the Dionex system and 10 for the capIC system were calculated (using chloride) showing that the Dionex system was a more sensitive than the capIC system. C^4D detection used in both cases was on-column and the difference in the signal/noise ratios was due to increase pump noise associated with the use of the analytical pump in the capIC system.

The LOD values obtained on the capIC system were comparable to those obtained by Kiplagat *et al.* [147], who reported concentration LOD's of 0.8 – 8 µmol/L which corresponded to 40 - 400 fmole injected cations using a portable, lightweight ion chromatography system, which employed C^4D as the mode of detection. Although the Dionex system exhibited a superior sensitivity over the capIC system, this capIC system showed the ability to separate the five selected anions within a short retention time window (run time < 2.5 minutes).

Table 3.4: Approximate detection limits calculated for the anions separated on the capIC system and for the same separation on the Dionex system. Chromatographic conditions: as in Figure 3.4.

	Dionex capLC system		*capIC system*	
Anion	mg/L	Absolute limits (pmole)	mg/L	Absolute limits (pmole)
Fluoride	0.03	0.08	0.2	0.20
Chlorite	0.1	0.07	1.5	0.45
Bromate	0.2	0.08	1.3	0.20
Chloride	0.02	0.03	0.2	0.11
Nitrite	0.2	0.20	1	0.43

3.2.5 Chromatographic performance data for 30 organic and inorganic anions using the capIC system.

Using the in-house constructed capIC system, retention data for 30 anions (organic and inorganic) was carried using the poly(META) monolith. Chromatographic performance data, including column efficiency, retention time data and peak width, were obtained and can be seen in Table 3.5. Table 3.5 also includes retention factor data obtained by Ó'Ríordáin *et al.* [149] using an Onyx C_{18} silica based monolithic column (150 mm x 0.1 mm) modified with DDMAU. In this work, Ó'Ríordáin *et al.* [149] used a system similar to that described in this work (capIC) and also plumbed the capillary column directly into the injector valve. Detection was carried out using on-column C^4D detection, therefore the effects of extra column band broadening were eliminated. Retention in ion chromatography depends on a number of factors, such as the charge of the analyte ion, the solvated size and the polarisability of the analyte ion and the type of eluent used [2]. In general, retention time increases with increased anion charge. As electroneutrality is maintained at all times, one monovalent eluent ion displaces one monovalent analyte ion. From Table 3.5, the retention of anions on the poly(META) monolith is in broad agreement (with some deviations) with this statement whereby most of the singly charged anions were less retained than the divalent anions.

Table 3.5: *k* values for organic and inorganic anions using the GMA-*co*-EDMA polymer monolith functionalised with META.

Anion #	*Anion*	*k*	*N/m*	*k [149]*	*Order of elution from [149]*
1	Methanesulfonate ($CH_3SO_3^-$)	0.52	8,430	-	-
2	Chloroacetate ($CH_2ClCO_2^-$)	0.73	9,900	1.23	8
3	Trifluoroacetate ($CF_3CO_2^-$)	0.75	6,700	-	-
4	Dichloroacetate ($CHCl_2CO_2^-$)	0.86	8,300	-	-
5	Carbonate (CO_3^{2-})	1.06	9,900	-	-
6	Acetate (CH_3COO^-)	1.30	11,000	-	-
7	Fluoride (F^-)	1.32	12,000	-	-
8	Iodate (IO_3^-)	1.38	7,100	0.71	3
9	Selenite (SeO_3^{2-})	1.48	6,700	0.49	2
10	Chlorite (ClO_2^-)	1.52	11,000	1.32	9
11	Formate ($HCOO^-$)	1.56	11,300	0.77	4
12	Bicarbonate (HCO_3^-)	1.69	9,000	0.30	1
13	Bromate (BrO_3^-)	2.16	11,600	1.00	5
14	Sulphite (SO_3^{2-})	2.36	10,900	7.09	13
15	Dithionate ($S_2O_4^{2-}$)	2.49	9,200	-	-
16	Chloride (Cl^-)	2.78	13,200	1.03	6
17	Nitrite (NO_2^-)	2.97	15,400	1.17	7
18	Chlorate (ClO_3^-)	4.50	9,200	2.25	12
19	Bromide (Br^-)	4.81	11,100	1.39	10
20	Nitrate (NO_3^-)	5.55	8,600	1.52	11
21	Persulphate ($S_2O_8^{2-}$)	7.40	2,800	-	--
22	Molybdate (MoO_4^{2-})	11.46	1,350	-	-
23	Oxalate ($C_2O_4^{2-}$)	15.34	1,510	-	-
24	Thiocyanate (SCN^-)	15.41	1,550	20.88	15
25	Dichromate ($Cr_2O_7^{2-}$)	16.97	2,300	-	-
26	Hydrogen phthalate $C_6H_4(CO_2)_2^{2-}$	18.37	5,500	-	-
27	Tungstate (WO_4^{2-})	19.66	4,500	-	-
28	Perchlorate (ClO_4^-)	21.61	1,700	23.40	16
29	Thiosulphate ($S_2O_3^{2-}$)	22.40	4,900	13.12	14
30	Chromate (CrO_4^{2-})	59.02	9,530	-	-

Note: Column number 5 in Table 3.5 are *k* values taking from [149] and column number 6 compares the elution order obtained from [149] with the elution order obtained for the same anions in this thesis.

Retention in ion chromatography also depends on the solvated size of the analyte ion. Smaller molecules, such as nitrite (NO_2^-) have a smaller solvated size than larger molecules such as nitrate (NO_3^-), holding water molecules more strongly. The water molecules shield the analytes ion charge from the charge on the ion exchange functional group which results in less retention in comparison to a less hydrated analyte ion. An increase in the hydrated ionic radii of the analyte ion results in a decrease in retention. Ionic radii increase on descending a group in the periodic table, therefore the retention order for the halogen anions should be $F^- < Cl^- < Br^- < I^-$. This order of elution was observed using the poly(META) polymer monolith.

From Table 3.5, an elution order of $IO_3^- < BrO_3^- < NO_2^- < Br^- < NO_3^-$ was obtained demonstrating the same selectivity for the poly(META) monolith to separations reported in the literature using both polymer and silica monoliths. For example, Zakaria *et al.* [104] prepared a BuMA-*co*-EDMA-*co*-AMPS polymer monolith (300 mm x 250 µm I.D.), which was modified with latex nano-particles bearing quaternary ammonium functionalities. Using contactless conductivity detection and a 1 m*M* KOH eluent, the authors obtained an elution order of $IO_3^- < BrO_3^- < NO_2^- < Br^- < NO_3^-$. This work was followed up by Hutchinson [105] who obtained an elution order of $IO_3^- < BrO_3^- < NO_2^- < Br^- < NO_3^- < I^-$ using a GMA-*co*-EDMA polymer monolith which was modified with the same latex nano-particles described by Zakaria *et al.* [104]. An elution orders of $IO_3^- < BrO_3^- < NO_2^- < Br^- < NO_3^-$ was obtained using silica monoliths modified with cetyltrimethylammonium chloride (CTAC) [110] and dilauryldimethylammonium bromide (DDAB) [111] surfactants, respectively.

As mentioned, Table 3.5 also contains *k* data obtained by Ó'Ríordáin *et al.* [149] using an Onyx C_{18} silica based monolithic column (150 mm x 100 µm I.D.) modified with DDMAU and changes in selectivity between the poly(META) polymer monolith and the DDMAU coated silica monolith were evident. The most weakly retained anion using the DDMAU coated silica monolith was bicarbonate (*k* of 0.30). With the poly(META) polymer monolith, a *k* value of 1.69 was obtained for bicarbonate, while

the retention for a range of anions, including fluoride, chlorite, formate and iodate were eluted prior to bicarbonate. Formate, bromate, chloride and nitrite showed the same order of elution on both columns. Figure 3.5 shows an overlay of chromatograms obtained for formate, bromate and chloride using the poly(META) polymer monolith demonstrating the possibility of the separation of the three anions using the separation conditions reported in this thesis. With the DDMAU coated silica monolith [149], *k* values of 0.80, 1.00 and 1.03 were obtained for formate, bromate and chloride demonstrating the inability to separate the three anions with the chromatographic conditions used by the authors.

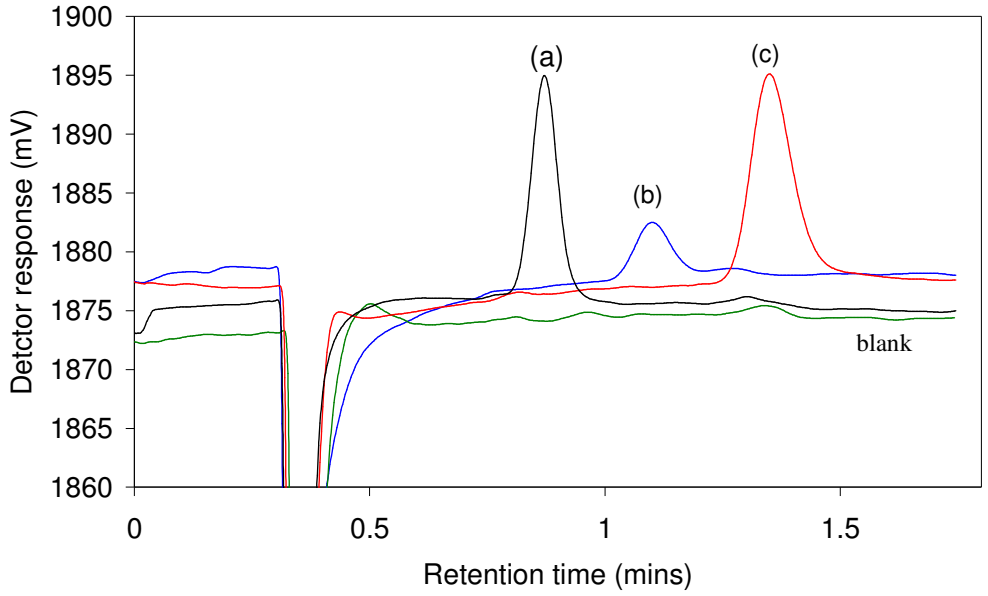

Figure 3.5: Overlay of chromatograms obtained using the poly(META) polymer monolith. Chromatographic conditions: as in Figure 2.5. Peaks: (a) 10 ppm formate, (b) 10 ppm bromate and (c) 10 ppm chloride. Also included in Figure 3.5 is the chromatogram obtained for a blank injection (green trace). Chromatographic conditions: as in Figure 3.4.

Chloroacetate (*k* of 1.23) showed a similar *k* value to nitrite (*k* of 1.17) using the DDMAU coated silica monolith, whereas a *k* value of 0.73 was obtained for chloroacetate and 2.97 for nitrite using the poly(META) modified polymer monolith described in this thesis. Sulfite was retained significantly longer than nitrate using the DDMAU coated silica monolith but was retained prior to nitrate using the poly(META) polymer monolith.

Figure 3.6 shows an overlay of chlorate, chloride and chlorite using the poly(META) polymer monolith. Ó'Ríordáin *et al.* [149] carried out a separation of chlorate, chloride and chlorite using a silica based monolithic column modified with DDMAU. The authors reported a run time of 4.5 minutes. In this work, the overlaid chromatograms of these three anions show the potential for their separation in a short retention window (2.5 minutes). The retention order was chlorite < chloride < chlorate, which demonstrated a change in selectivity to that reported by Ó'Ríordáin *et al.* [149] where a retention order of chloride < chlorite < chlorate was obtained using the DDMAU coated silica monolith.

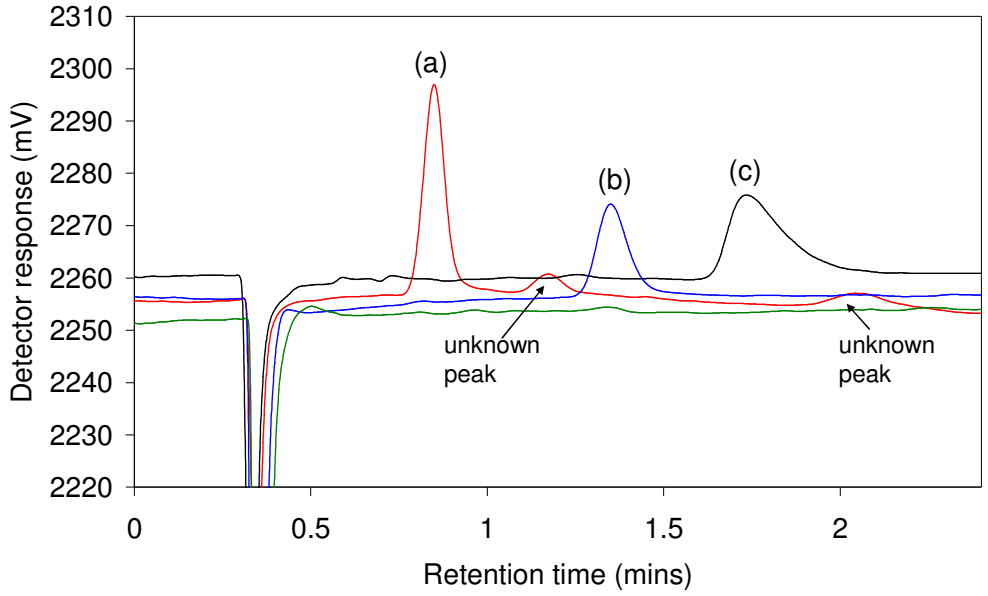

Figure 3.6: Overlay of chromatograms obtained using the META functionalised polymer monolith. Chromatographic conditions: as in Figure 2.6, peak (a) 100 ppm chlorite, (b) 10 ppm chloride and (c) 100 ppm chlorate. Also included in Figure 3.6 is the chromatogram obtained for a blank injection (green trace). Chromatographic conditions: as in Figure 3.4.

Traditionally, anions such as fluoride are difficult to retain due to their high hydrated ionic radii and their ability to attract water molecules. Previous work has reported the difficulty in the isocratic separation of these anions from the void peak. Glenn *et al.* [150] reported a k value of 0.49 for fluoride using a silica monolith coated with DDAB but failed to obtain retention for fluoride using a silica monolith with electrostatically bound latex nano-particles using a 4-hydroxybenzoic eluent. In this

work, a *k* value of 1.32 was obtained for fluoride demonstrating the strong anion exchange properties of the poly(META) monolith, while Connolly *et al.* [103] obtained a *k* value of 2.6 for fluoride using the poly(META) monolith described previously.

Small organic acid ions such as formate and acetate have proven difficult to separate isocratically due the small differences in their affinities [151]. Short retention times for these organic acids are generally reported and a large number of solute-sorbent interaction sites are required for their separation [152]. Figure 3.7 shows overlaid chromatograms of formate and acetate carried out on the META functionalised polymer monolith using the capIC system. *k* values of 1.30 and 1.56 were obtained for acetate and formate respectively, showing the potential for their separation under fully optimised chromatographic conditions.

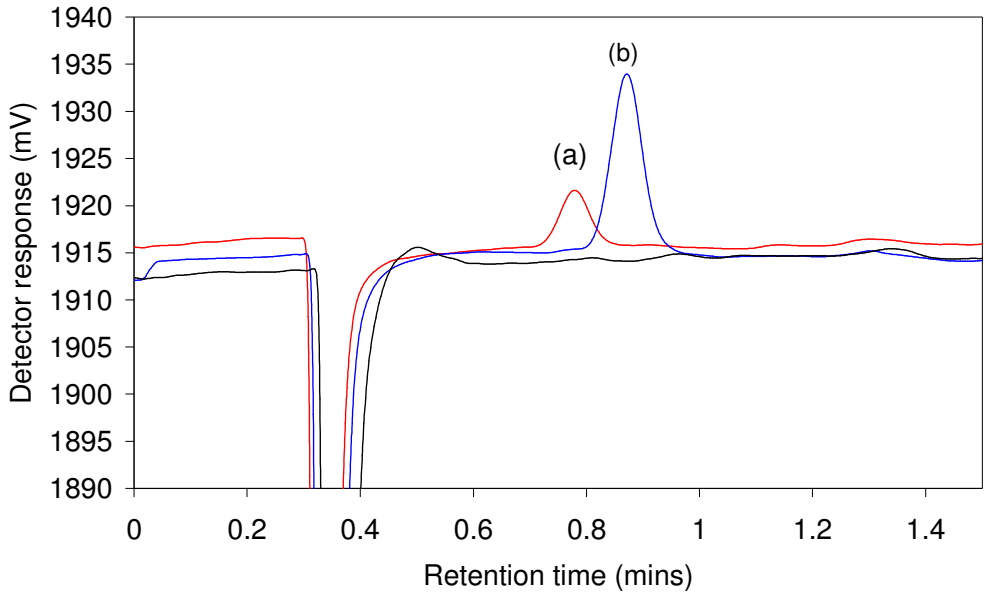

Figure 3.7: Overlay of chromatograms obtained using the META functionalised polymer monolith. Peak (a) = 10 ppm acetate and peak (b) = 10 ppm formate. Also included in Figure 3.7 is the chromatogram obtained for a blank injection (black trace). Chromatographic conditions: as in Figure 3.4.

As mentioned previously, the one of the aims of this research thesis was to try to improve the separation of small ions using polymer monoliths. Table 3.6 shows a comparison of column efficiencies obtained for the poly(META) polymer monolith

with other capillary columns with various ionogenic functionalities carried out by different research groups. Peak efficiencies obtained by the poly(META) polymer monolith in this thesis were slightly improved upon when compared to other capillary ion exchange columns.

Table 3.6: Comparison of peak efficiencies of other anions exchange capillary columns.

Column	*Column dimensions*	*Eluent*	*Detection*	*Efficiency (N/m)*	*Anions*	*Ref*
poly(META) photo-grafted polymer monolith (Dionex LC system)	100 mm x 100 µm I.D.	2 m*M* sodium benzoate	on-column C^4D detection	10,700 - 16,900 N/m	F^-, Cl^-, NO_2^-, Br^-, BrO_3^- and ClO_2^-	Present work
BuMA-co-EDMA-co-AMPS with attached AS18 particles	300 mm x 250 µm I.D.	1 m*M* KOH	suppressed conductivity	5400 N/m	IO_3^-	[9]
Particle packed AS11	500 mm x 180 µm I.D.	electrodialytic NaOH generator	Conductivity detection	21,018 - 27,300 N/m	Cl^- and SO_4^{2-}	[22]
GMA-co-EDMA functionalised by reaction of triethylamine	750 mm x 100 µm I.D.	10 m*M* NaClO4	UV detection at 210 nm	75,000 N/m (100 nL/min) 18,000 N/m (700 nL/min)	NO_2^-, BrO_3^-, NO_3^-	[23]
AS18 coated GMA-co-EDMA monolith sulfonated using method (ii)*	348 mm x 250 µm I.D.	10 m*M* NaClO4	UV detection	2,680 - 4,550 N/m	NO_2^-, BrO_3^-, NO_3^-, IO_3^-, Br^-, I^-, benzenesulfonate	[11]
AS18 coated GMA-co-EDMA monolith sulfonated using method (iii)*	143 mm x 250 µm I.D.	10 m*M* NaClO4	UV detection	7,980 - 11,200 N/m	NO_2^-, BrO_3^-, NO_3^-, IO_3^-, Br^-, I^- benzenesulfonate	[8]

*(ii) Ring opening of the epoxy groups through reaction with thiobenzoic acid in the presence of triethylamine in acetonitrile at 60 ^oC, followed by flushing with methanol. The generated thiol groups were oxidised using tert-butyl hydroperoxide before coating with the latex nano-particles.
*(iii) The GMA-co-EDMA monolith was sulfonated using a solution of sodium sulfate and coated with the latex nano-particles.

3.3 Conclusion

A GMA-*co*-EDMA polymer monolith was fabricated using thermally initiated polymerisation. The surface of the polymer monolith was subsequently grafted with polymer chains of poly(META) using UV irradiation, in a two step procedure, following photo-grafting of benzophenone. This poly(META) polymer monolith was compared to a similar poly(META) polymer monolith reported in the literature, whereby the benzophenone and poly(META) were photo-grafted in a single step. To the author's knowledge, the work reported by Connolly *et al.* [103] was the first reported instance of the functionalisation of a polymer monolith, for anion analysis, using photo-grafting techniques. Separation of the six anions was carried out and due to increased retention of all anions, the poly(META) polymer monolith prepared using the one step method of functionalisation (produced by Connolly *et al*. [103]) produce a higher ion exchanger than the two-step procedure (produced in this thesis). However, the poly(META) polymer monolith prepared using the two step process, yielded faster run times and higher peak efficiencies while still maintaining baseline resolution of all anions.

Characterisation of the poly(META) polymer monolith (using the two step procedure) was also carried out using an in-house assembled capIC system. The *k* values obtained for the Dionex LC system were comparable with those obtained using the capIC system demonstrating a novel, portable system suitable for the fast separation of the analytes of interest. The incorporation of grafted chains of poly(META) produced a suitable monolith for the retention of a wide range of organic and inorganic anions. Peak efficiencies obtained using the poly(META) polymer monolith were also comparable to other polymer monoliths with ion exchange functionalities.

Chapter 4.0:

Separation of cations using a capillary polymer monolith functionalised with 3-sulfopropyl methacrylate

4.1 Introduction

To date, limited research has been carried out on the fabrication of capillary polymer monoliths for the separations of small cations. In 2004, Ueki *et al.* [49] prepared a GMA-*co*-EDMA monolith in 250 µm I.D. fused silica capillary. Sulfonation of the surface of the monolith was carried out by flushing a solution of Na_2SO_2 through the monolith at 75 ^oC, allowing attachment of sulfonated groups through ring opening of the epoxy groups on the monolith surface. The authors found that increasing the reaction time, from 1 hour to 12 hours during the sulfonation procedure, allowed the fabrication of sulfonated capillary monolith exhibiting ion exchange capacities. The resultant monoliths were used for the separation of sodium, ammonium, potassium, magnesium and calcium using a copper sulphate eluent. Column efficiencies > 20,000 N/m were obtained for all cations studied in this work. Gillespie *et al.* [112] reported the use of a capillary monolithic column, albeit a silica monolith, for the separation of alkaline earth metals. The authors modified the monolith with the ionic surfactant DOSS, rendering it suitable for cation exchange chromatography. Column efficiencies > 40,000 N/m were obtained for all 4 alkaline earth metals, thus demonstrating the differences in column efficiencies when polymer monolith are compared to silica monoliths.

In the work in this thesis, a polymer monolith was functionalised with 3-sulfopropyl methacrylate (SPM) using photo-grafting techniques, following the formation of free radicals on the surface of the monolith using benzophenone. The resultant monolith was applied to the separation of alkaline earth metals using a copper sulphate eluent. Temperature analysis, using an in-house constructed capillary column heater is also presented.

4.2 Results and Discussion

4.2.1 Monolith fabrication and functionalisation with poly(SPM)

The functionalisation of the polymer monolith was carried out using a two step process, similar to the method described for the functionalisation of the poly(META) polymer monolith in Chapter 3.0. The first step involved immobilisation of

benzophenone onto the surface of the monolith by a process of hydrogen abstraction allowing the formation of free radicals, which favours the growth of polymer chains from the surface of the monolith [146]. This resulted in a polymer monolith with surface sulfonated groups.

4.2.2 Separation of alkaline earth metals using poly(SPM) polymer monolith

The cation exchange polymer monolith (90 mm x 100 µm I.D.) with photo-grafted sulfonated groups was used for the separation of calcium, magnesium and barium with UV detection at 210 nm. Copper sulphate was chosen as the eluent as it has been shown to be suitable for the separation of cations [49]. Under these chromatographic conditions, the elution order on the SPM functionalised BuMA-*co*-EDMA polymer monolith was Mg(II) < Ca(II) < Ba(II), as shown in Figure 4.1, which is the typical elution order when retention is due to ion exchange [49, 112]. Negative peaks were obtained as the peaks were detected using indirect UV detection.

Chromatographic performance data was obtained and can be seen in Table 4.1. Column efficiencies of 10,600 N/m were obtained for Mg(II), 10,900 N/m for Ca(II) and 7,600 N/m for Ba(II). Table 4.1 also includes peak width (measured at 50 % peak height) of 0.28 mins, 0.33 mins and 0.48 mins for Mg(II), Ca(II) and Ba(II). respectively. Mg(II) showed a peak asymmetry of 1.2 while Ca(II) and Ba(II) showed peak asymmetries of 0.7 and 0.8 suggesting clear fronting of both peaks. Resolution of 1.3 was obtained for the Mg(II)/Ca(II) pair showing that these cations were not baseline resolved however baseline resolution between Ca(II) and Ba(II) was achieved (resolution of 1.5). Ueki *et al.* [49] prepared a sulfonated GMA-*co*-EDMA polymer monolith and applied it to the separation of alkali and alkaline earth metals (Na^+, $NH4^+$, K^+, Mg^{2+} and Ca^{2+}). Theoretical plates > 20,000 N/m were obtained for all cations (figures for individual cations not given) using a 10 m*M* copper sulfate eluent, a flow-rate of 0.3 µL/min and indirect UV detection at 210 nm.

Comparing the monolith in this work (BuMA-*co*-EDMA) to that obtained by Ueki *et al.* [49], a clear difference in efficiency is evident. Using flow-rates of 3 µL/min, Ueki *et al.* [49] obtained *k* values of 2.25 and 5.25 were obtained for Mg(II) and Ca(II) respectively. In this present work, *k* values of 2.2 and 2.9 were obtained for Mg(II)

and Ca(II) using a flow-rate of 1 µL/min and an eluent of 1 m*M* copper sulphate. Although *k* values for Mg(II) were comparable, Ueki *et al.* [49] showed increased retention for Ca(II) clearly demonstrating the differences in capacity between the two monoliths.

The sulfonation of the polymer monolith by ring opening of the epoxy groups prepared by Ueki *et al*. [49] was restricted to the number of epoxy groups on the surface of the monolith. The method of sulfonation of the polymer monolith used by Ueki *et al*. [49] using Na_2SO_3 appeared to yield a higher capacity than the polymer monolith prepared in this work. The method of photo-grafting poly(SPM) onto the surface of the monolith requires further optimisation of the procedure to improve column capacity and in turn improve column efficiency and retention.

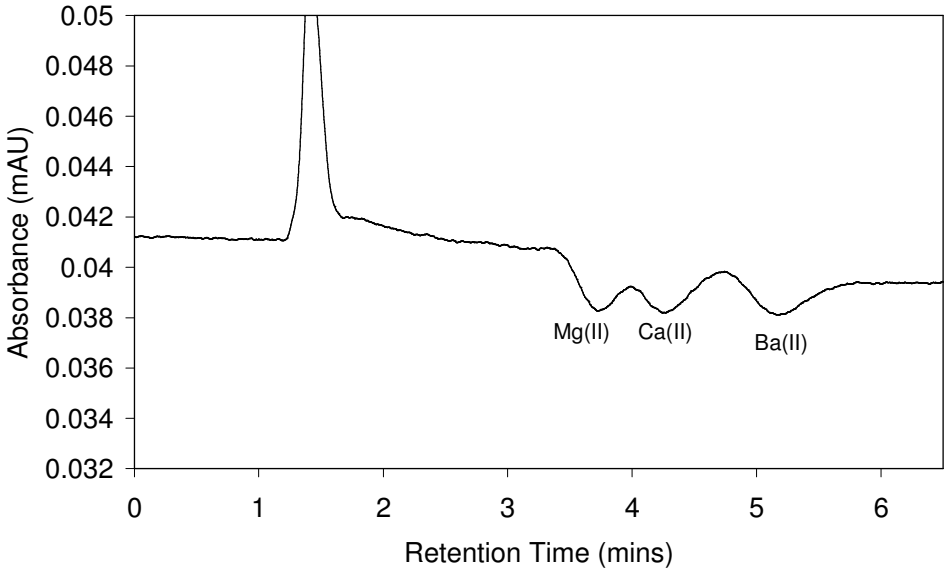

Figure 4.1: Separation of 100 ppm Mg(II), 100 ppm Ca(II) and 100 ppm Ba(II) using the in-house constructed capIC system. Chromatographic conditions: column: BuMA-*co*-EDMA functionalised with SPM (100 µm I.D x 90 mm), eluent: 1 m*M* copper sulpfate, flow-rate: 1 µL/min, injection volume: 20 nL, detection: indirect UV at 210 nm.

Table 4.1: Chromatographic performance data for the separations of Mg(II), Ca(II) and Ba(II). Chromatographic conditions: as in Figure 4.1.

Cation	*N/m*	*k*	*Peak width$^{1/2}$ (mins)*	*Asy.*	*Res.*
Mg(II)	10,600	1.8	0.28	1.2	-
Ca(II)	10,900	2.2	0.33	0.7	1.25
Ba(II)	7,600	2.9	0.48	0.8	1.53

4.2.3 Temperature studies.

Temperature effects are often omitted in chromatographic method development as the retention and selectivity of a chromatographic separation can be manipulated by varying the concentration of the eluent or changing the stationary phase. There are a number of advantages to using high temperatures in LC, such as lower solvent viscosity, resulting in lower back-pressure generated [153]. Lower solvent viscosity allows for use of higher flow rates of the eluent, which increases the speed of analysis. Increasing the temperature may also be a simple way of varying retention [154] or selectivity [143] and can be easily incorporated into a separation system.

4.2.3.1 Calibration of capillary column heater.

To investigate the effect of temperature on the retention and efficiency of the 3 selected cations, a column heater had to be incorporated into the in-house assembled capIC system. In order to determine if the flexible tape was suitable for use as a capillary heater, calibration was carried out using a multimeter with a temperature setting and a thermocouple wire placed inside the heater. Voltage was applied in 0.5 V increments and the temperature noted. Figure 4.2 shows a plot of temperature versus voltage applied (n=4), including error bars, between 25 – 80 ^{o}C. The temperature was reproducible for any given voltage applied with % RSD values < 0.8 %.

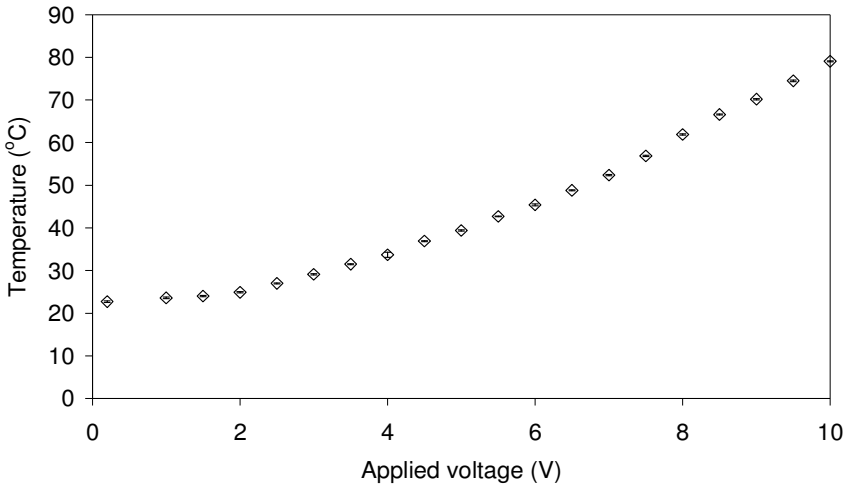

Figure 4.2: Plot of temperature versus voltage applied to the heating tape showed a linear correlation between 25 – 80 °C.

4.2.3.2 Effect of temperature on the separation of Ca(II), Mg(II) and Ba(II)

The effect of temperature on Ca(II), Mg(II) and Ba(II) was investigated using the sulfonated polymer monolith. Separations were carried out at temperatures ranging from 27 °C to 70 °C. The column was allowed to equilibrate for 30 minutes prior to use. An overlay of the separations carried out at 27 °C and 62 °C can be seen in Figure 4.3.

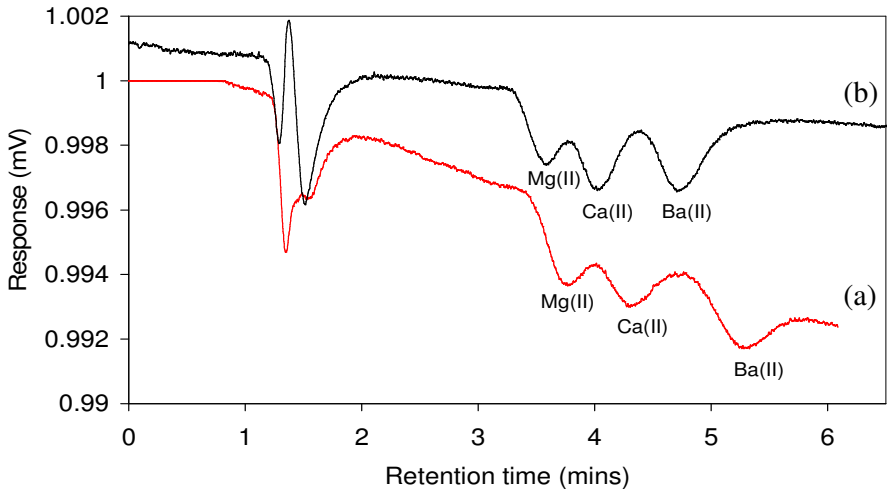

Figure 4.3: Separation of Ca(II), Mg(II) and Ba(II) at 27 °C (a) and 62 °C (b). All chromatographic conditions as in Figure 4.1.

As can be seen from Figure 4.3, an increase in temperature resulted in a decrease in retention of all three metals cations. Previous studies have also shown a decrease in retention of cations with an increase in temperature [143, 153]. From Table 4.2, an increase in efficiency for all three cation was observed with an increase in temperature up to 67 ^{o}C. Decrease in retention factors of 7 % for Mg(II), 11 % for Ca(II) and 15 % for Ba(II) were observed. An increase in efficiency of 80 % was observed for Mg(II), 70 % for Ca(II) and 50 % for Ba(II) when the temperature was increased from 27 ^{o}C to 62 ^{o}C. At ambient temperature, resolution of Mg(II)/Ca(II) was not achieved (resolution of 1.25) however resolution for Ca(II)/Ba(II) was achieved (resolution of 1.53). Although an increase in efficiency was achieved at higher temperatures, baseline resolution was further compromised.

Rey *et al.* [154] observed a significant increase in efficiency with an increase in temperature, while observing a decrease in retention of common cations including alkaline earth metals, using a CS12A (carboxylated and phosphonic functionalities) with a methanesulfonic acid eluent. The authors reported increases in column efficiency of 30 % for Mg(II), 34 % for Ca(II) and 35 % for Ba(II) when the temperature was increased to 50 ^{o}C from 25 ^{o}C . Decreases in retention factors of 13 % for Mg(II), 19 % for Ca(II) and 44 % for Ba(II) were reported. Increases in efficiency were also noted by Hatsis *et al.* [143] with an increase in temperature.

Here, in this present work, increases in efficiency of 20 % for Mg(II), 12 % for Ca(II) and 25 % for Sr(II) were obtained when the temperature was increased from 27 ^{o}C to 60 ^{o}C. Table 4.2 also contains peak width data, measured at 50 % peak height. The largest difference in peak width was observed for Ba(II), where a decrease from 0.48 mins at ambient temperature to 0.35 mins at 62 ^{o}C. Differences in peak width for Mg(II) and Ca(II), when the temperature was increased to 62 ^{o}C were minimal. To determine if temperature (above 62 ^{o}C) had a deleterious effect of the sulfonated groups on the polymer monolith, the temperature was allowed to return to ambient temperature. A separation of the three cation standard mix was carried out and no loss of retention or efficiency was observed.

Table 4.2: Chromatographic performance data obtained for the separation of the 3 cation standard mix using the SPM functionalised polymer monolith. Chromatographic conditions: as in Figure 3.3.

Temp. (^{o}C)	*N/m*	*k*	*Peak width*	*N/m*	*k*	*Res.*	*Peak width*	*N/m*	*k*	*Res.*	*Peak width*
	Mg(II)			Ca(II)				Ba(II)			
25	10,600	1.8	0.28	10,900	2.2	1.25	0.33	7,600	2.9	1.53	0.48
29	12,700	1.8	0.28	13,100	2.2	1.24	0.31	9,600	2.94	1.57	0.45
33	15,100	1.77	0.27	16,300	2.29	1.34	0.29	10,200	2.93	1.62	0.43
39	16,200	1.76	0.25	16,100	2.20	1.34	0.32	10,000	2.86	1.55	0.45
45	16,300	1.77	0.26	15,900	2.19	1.32	0.30	10,900	2.85	1.58	0.42
52	17,000	1.80	0.25	16,300	2.23	1.37	0.30	12,200	2.78	1.39	0.38
57	17,000	1.73	0.24	16,500	2.15	1.34	0.28	12,900	2.70	1.44	0.36
62	19,400	1.67	0.23	18,700	2.04	1.17	0.26	12,800	2.56	1.33	0.36
67	15,900	1.56	0.24	16,600	1.95	1.18	0.27	11,800	2.47	1.28	0.35

The relationship between column temperature and retention can be described by the van't Hoff equation (Equation 4.1).

$$\ln k = - \Delta H/RT + \Delta S/R + \ln \varphi \qquad \text{Equation 4.1}$$

where k is the retention factor, ΔH is the enthalpy change for the exchange reaction, R is the universal gas constant, T is the temperature, ΔS is the entropy change and φ is the column phase ratio (which is constant for a given column). ΔS is assumed to be constant, therefore the equation becomes:

$$\ln k = - \Delta H/RT \qquad \text{Equation 4.2}$$

Plots of ln k versus 1/T should be linear and have a slope = - $\Delta H/R$ [155]. Van't Hoff plots were constructed for Ca(II), Mg(II) and Ba(II). Positive slopes for the three metals were obtained indicating that the absorption process exhibited exothermic behaviour i.e. the retention of metals decreased with an increase in temperature [153]. From the linear regression data in Table 4.3, it is clear that increasing the temperature did not have the same effect on all three cations. The more strongly retained Ba(II) showed the largest van't Hoff slope in comparison to Ca(II) and Mg(II) showing that the effects of temperature on the retention of Ba(II) were more pronounced.

Table 4.3: Linear regression data from van't Hoff plots.

	Slope	*Intercept*	R^2
Mg(II)	56.53	0.07	0.97
Ca(II)	69.92	0.12	0.94
Ba(II)	149.28	- 0.02	0.96

Heats of adsorption generally do not exceed 3 kJ mol^{-1} when ion exchange is the dominant separation mechanism [51]. In this present work, heats of adsorption of - 0.45, - 0.58 and - 1.2 kJ mol^{-1} for Mg(II), Ca(II) and Ba(II), respectively were obtained (calculated from the linear regression data in Table 4.3), showing exothermic behaviour (a decrease in retention with an increase in temperature). Paull *et al.* [155] obtained ΔH values of -1.01 for Mg(II) and – 0.46 for Ca(II) using a dicarboxylated polymeric cation exchanger and a 2 m*M* nitric acid eluent. However, when a strong electrolyte was added to the eluent ΔH values significantly increased (17.32 for Mg(II) and 13.61 for Ca(II)) showing that the ion exchange interactions were suppressed and chelation became the dominant separation mechanism. Kolpachnikova *et al.* [129] obtained ΔH values of - 8.5, - 8.6 and -9.1 kJ mol^{-1} for Mg(II), Ca(II) and Ba(II), respectively using a lyseine-silica particulate column and - 1.1, - 1.1 and - 1.6 using a glutamic acid-silica particulate column. In both cases a weak perchloric acid eluent was used and under these eluent conditions the authors concluded that the dominant separation mechanism was ion exchange due to the low ΔH values (as mentioned earlier, ΔH values do not exceed 3 kJ mol^{-1} when ion exchange is the dominant separation mechanism [51].

4.2.3.3 Effect of temperature on backpressure

As the temperature increases, the viscosity of the eluent decreases, which in turn reduces the backpressure of the system. Figure 4.4 shows a plot of increased temperature versus back-pressure. The backpressure decreased from 53 bar at ambient temperature to 34 bar at 67 ^{o}C. An advantage of lowering the backpressure is the ability to use higher flow-rates which reduces analysis times. This was reported by Chong *et al*. [153] who showed that at 27 ^{o}C, run times of 8 minutes for nine alkali and alkaline earth metals were obtained using a flow-rate of 0.9 mL/min. However at a temperature of 60 ^{o}C, a decrease in backpressure was obtained, allowing an increased flow-rate of 1.3 mL/min to be used, this reducing the run time for the same nine cations to 5 minutes.

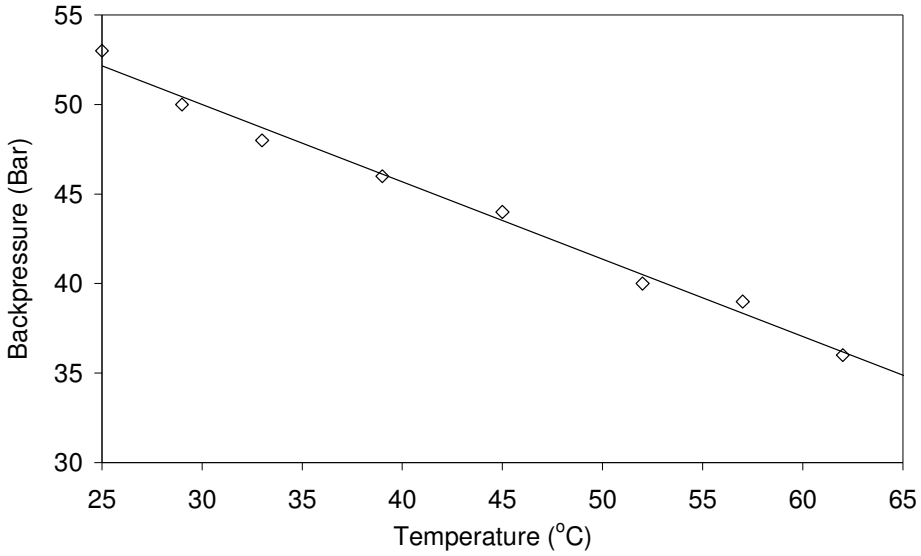

Figure 4.4: Plot of temperature versus backpressure showing linear correlation (R^2 = 0.99). Measurements obtained using the capIC system with the backpressure noted as the temperature of the column heater was increased.

4.3 Conclusion

In this present work, a BuMA-*co*-EDMA monolith was functionalised with 3-sulphopropyl methacrylate (SPM) and applied to the separation of alkaline earth metals (calcium, magnesium and barium) using indirect UV detection. Temperature studies were carried out using a novel, inexpensive capillary heater with calibration data showing reproducible temperatures at the particular applied voltage. Van't Hoff plots showed that the absorption process was exothermic (decrease in retention with an increase in temperature) and calculated heats of adsorption showed that ion exchange was the dominant separation mechanism. A decrease in back pressure was also observed using higher temperature which would allow for the use of longer columns or faster flow rates. This work demonstrates the use of an in-house constructed capIC system which incorporated an inexpensive capillary column heater.

Further work is required on the functionalisation procedure reported in this Chapter to produce polymer monoliths exhibiting higher capacities. Increasing the concentration of the SPM during the photo-grafting of the polymer monolith or increasing the

photo-grafting irradiation time are some of the conditions that should improve the surface coverage of poly(SPM).

Chapter 5.0:

Separation of selected transition metals by chelation ion chromatography using acetyl-iminodiacetic acid modified polymer monoliths

5.1 Introduction

Chelation ion chromatography (CIC) for the determination of metal cations in complex samples has received considerable attention over the last number of years. For the successful separation of metal cations using CIC, chelating stationary phases must exhibit high hydrolytic stability, the complexes formed should be kinetically labile and the chelating ligand should be chemically stable in order to withstand changes in eluent composition, pH and ionic strength [51, 160]. The most efficient separations of metals ions on chelating stationary phases are achieved when the chelating exchangers are negatively charged or have acidic functional groups, such as iminodiacetic acid (IDA).

Although the surface area of silica monoliths is greater than their polymer based counterparts, at low pH, the silylether bond is hydrolysed and as the eluents used in CIC are mainly acidic, this can lead to a loss of the bonded ligand. The aim of this work was to surface modify polymer monoliths with a chelating ligand to produce capillary chelation ion exchangers. The resultant monoliths were applied to the chromatographic separations of selected metal cations. Temperature studies were carried out using an in-house constructed capillary column heater. A novel combination of on-column C^4D detection and UV-Vis detection (following the reaction of the eluted metals with PAR) is also presented.

5.2 Results and discussion

5.2.1 Fabrication of acetylimino-diacetic acid (AIDA) modified monoliths.

The main requirement for the base monolith used in this work is that they contain abstractable hydrogen's, on the monolith surface, they exhibit sufficient UV transparency as the process of surface modification of the polymer monolith is carried out using UV processes and they exhibit suitable pore morphology for the separation of small molecules. LMA was chosen as the monomer in the monolith fabrication as work carried out by Collins *et al.* [144] demonstrated suitable pore morphology for the reversed phase separation of small molecules (toluene, ethylbenzene,

propylbenzene, butylbenzene, and pentylbenzene). Following the fabrication of the LMA-*co*-EDMA polymer monolith, benzophenone was immobilised onto the surface of the monolith by a process of hydrogen abstraction, which favours the growth of poly(VAL) chains from the surface of the monolith structure [102, 146]. The presence of the poly(VAL) grafts allowed for the covalent attachment of IDA. IDA immobilised via the amine groups of the poly(VAL) produced AIDA functional groups, a new method for the retention of metal ions using chelation in chromatography.

5.2.2 Retention of transition and heavy metals using the AIDA immobilised polymer monolith

The retention of selected transition and heavy metals was studied using VAL15a (see Table 5.1), where an elution order of Mn(II) = Co(II) = Ni(II) < Zn(II) < Cd(II) < Cu(II) was obtained using a 0.1 m*M* HNO_3 eluent. Retention factors of 3.8 were obtained for Mn(II), Co(II) and Ni(II), with Zn(II) exhibiting a *k* value of 4.1, Cd(II) of 6.4 and Cu(II) of 12.8. This was a same elution order obtained by Barron *et al.* [52] using a ProPac IMAC-10 analytical column (10 µm polymeric beads coated with a poly(acrylate) layer with covalently attached poly-IDA groups. Using a 0.25 m*M* nitric acid eluent, the authors obtained an elution order of Mn(II) < Fe(II) < Co(II) < Zn(II) < Cd(II), however Pb(II) and Cu(II) were retained > 3 hours at this eluent concentration. Interestingly, the selectivity exhibited by the AIDA monolith in this work and that reported by Barron *et al.* [52] was different to that exhibited by other IDA stationary phases. Sugrue *et al.* [126] reported an elution order of Mn(II) < Co(II) < Cd(II) << Zn(II) <<< Cu(II) using a silica monolithic column with immobilised IDA functionalities. The authors used an eluent comprising of 0.065 *M* KNO_3 and 0.035 *M* KCl. The order of elution showed a reversal in elution of Zn(II) and Cd(II) when compared to the AIDA polymer monolith in this work, which was due to the tendency of the chloride ions in the eluent, used by Sugrue *et al.* [126], to form chloro complexes with Cd(II) in comparison to Zn(II). Barron *et al.* [52] observed a selectivity change for Cd(II) and Zn(II) when the ionic strength of the eluent was increased (eluent comprising of 0.25 m*M* HNO_3 and 7.5 m*M* KCl). Using a column packed with 5 µm spherical IDA bonded silica particles (150 mm x 4 mm I.D.), Jones *et al.* [161] observed an elution order of Mn(II) < Co(II) < Cd(II) < Zn(II)

with an 8 m*M* nitric acid eluent, an elution order similar to that obtained by Sugrue *et al*. [126]. Due to the use on C^4D detection in the work in this thesis, the use of high ionic strength eluents was not possible.

In the work in this thesis, the change in the elution order of Cd(II) and Zn(II) and the weak retention of Ni(II) and Cu(II) may be connected with the contribution to retention of cation exchange under the dilute nitric acid eluent condition used. This change in selectivity may also be due to the presence of the carbonyl group next to the nitrogen atom in the attached AIDA ligand on the poly(VAL) graft. The carbonyl groups located in this position should decrease the electron density on the nitrogen and reduce its capabilities to coordinate transition metals, such as Ni(II), Zn(II) and Cu(II), which have a high selectivity for coordination with nitrogen.

5.2.3 Effect of eluent concentration on the selectivity and retention of various transition and heavy metals.

IDA immobilised on the surface of a substrate has the ability to form kinetically labile surface complexes with metal ions and retention depends on the stability of the complexes formed. As the stability constants for metals with IDA are not excessively high, strong eluents are generally not required for their separation [142]. Chromatographic performance data for a range of transition and heavy metals, using VAL15a was obtained. This analysis was performed on the capIC system described in Section 2.1.3 using on-column C^4D detection. Using weak nitric acid eluents, the effect of eluent concentration on the retention of 6 transition and heavy metals was investigated. The concentration of the nitric acid eluent was varied from 0.2 m*M* (pH 3.7) to 0.4 m*M* (pH 3.3). Increasing the concentration of the eluent resulted in a decrease in the pH. As the chelating ligand in this work (IDA) is a conjugate base of a weak acid, the chelating ligand will have a strong affinity for hydrogen ions therefore, changes in pH will affect the association/dissociation of the metals complexes formed on the stationary phase surface [142, 162]. Table 5.1 shows the chromatographic performance data obtained when the eluent concentration was increased from 0.2 m*M* to 0.4 m*M* nitric acid. From this data, an increase in the eluent concentration resulted in a decrease in retention of all metals studied. As the pH of the eluent affects the degree of dissociation of the immobilised chelating ligand, a

decrease in the eluent pH induces protonation of the functional groups available on the stationary phase surface [51, 162].

Table 5.1: Chromatographic performance data for transition and heavy metals obtained by varying eluent pH. Chromatographic conditions: Eluent: 0.2 m*M* – 0.4 m*M* nitric acid, column: VAL15a (250 mm x 100 µm I.D), injection volume: 20 nL, detection: on-column C^4D, flow-rate: 1 µL/min.

Eluent conc. (HNO_3 mM)	*Metal (conc., mg/L)*	*N/m*	*k*	*Asy.*	*Peak width*
0.2 (pH 3.70)	Mn(II) (0.5)	4,700	3.81	1.14	0.33
0.3 (pH 3.57)		3,700	2.11	1.10	0.23
0.4 (pH 3.31)		4,400	1.39	1.23	0.17
0.2	Ni(II) (5)	4,000	3.77	1.61	0.35
0.3		4,250	2.06	1.24	0.21
0.4		4,350	1.41	1.25	0.16
0.2	Zn(II) (5)	1,850	4.13	1.64	0.55
0.3		3,300	2.14	1.31	0.24
0.4		3,500	1.51	1.42	0.19
0.2	Co(II) (5)	5,150	3.81	1.09	0.32
0.3		4,400	1.99	1.24	0.20
0.4		4,200	1.34	1.35	0.16
0.2	Cd(II) (5)	3,900	6.39	1.12	0.56
0.3		3,450	3.08	1.19	0.30
0.4		3,200	2.08	1.32	0.24
0.2	Cu(II) (5)	3,200	12.84	1.19	1.12
0.3		2,350	5.74	1.27	0.60
0.4		2,300	3.81	1.32	0.44

A decrease in pH led to reductions in peak width for all metals studied. Decreases in peak width of > 47 % were obtained for all metals studied, with Cu(II) showing improvements in peak width of 65 % when 0.4 m*M* nitric acid was used as the eluent in comparison to 0.2 m*M*. A decrease in *k* of ~ 65 % was noted for all metals studied, with a decrease in pH

In all cases, narrower peaks were obtained for all metals with a decrease in eluent pH, however, increases in peak tailing were observed with the exception of Ni(II) and Zn(II), where decreases in peak tailing were noted. A decrease in eluent pH resulted

in a decrease in efficiency of Mn(II), Co(II), Cd(II) and Cu(II) which correlated with increases in peak tailing. Ni(II) and Zn(II) showed decreases in peak tailing of 22 % and 13 % respectively, with a decrease in eluent pH, as well as an increase in efficiency.

Plots of - log [HNO_3] versus log *k* were linear as shown in Figure 5.1 (R^2 values > 0.99) and changes in selectivity of the 6 metals were minimal over the range of eluent concentrations studied. Slopes ranging from 1.4 for Zn(II) and Ni(II) to 1.8 for Cu(II) were obtained. In theory, the slopes should be proportional to the number of protons replaced by each metal complex formed with the immobilised ligand [51, 163]. Divalent metal cations, such as the metals used in this work, form metal complexes with the chelating ligand IDA with the release of two protons. Slopes obtained for Cd(II) and Cu(II) were 1.7 and 1.8 respectively and were in broad agreement with a slope of two for the formation of surface metals complexes with IDA. Zn(II), Mn(II), Co(II) and Ni(II) showed slopes between 1.4 and 1.5.

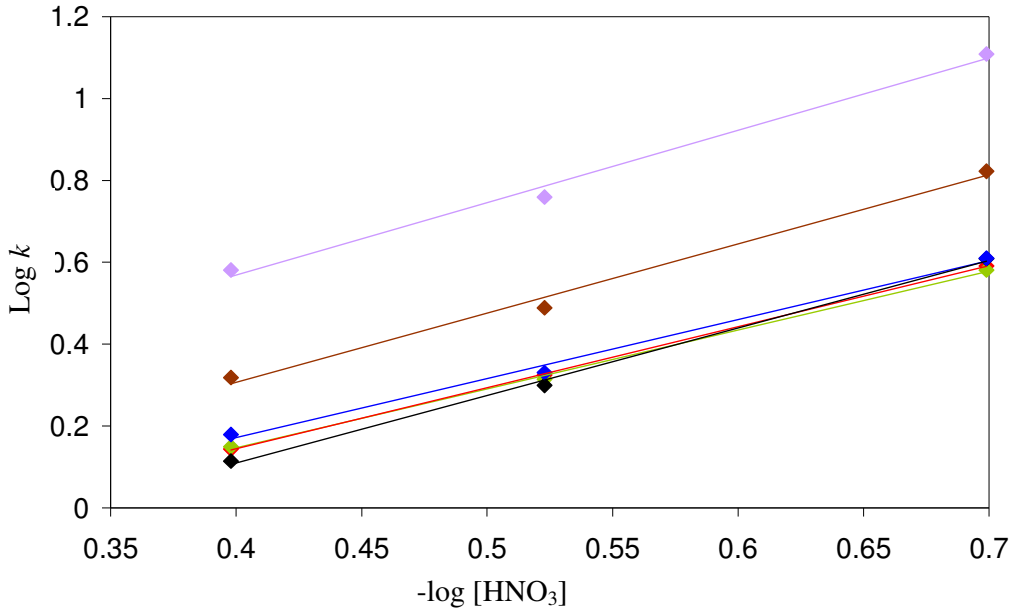

Figure 5.1: Plots of - log [HNO_3] versus log *k* for the 6 metals studied where ♦ = Co(II), ♦ = Mn(II), ♦ = Ni(II), ♦ = Zn(II), ♦ = Cd(II) and ♦ = Cu(II). Chromatographic conditions: Eluent: 0.2 – 0.4 m*M* nitric acid, all other conditions as in Table 5.1.

5.2.4 Separation of metal cations, using the capIC system, incorporating simultaneous on-column C^4D detection and UV-Vis detection

Improvements in sensitivity using HPCIC can be obtained with the use of PCR chemistry. PAR is one of the most widely used PCR reagents for transition and heavy metal analysis [130, 133]. The use of post-column mixing presents considerable difficulty when used at capillary scale as the incorporation of a PCR mixer increases the system dead volume resulting in band broadening and subsequently a loss in efficiency.

From the retention data in Table 5.2, a difference in the *k* factors of Mn(II), Cd(II) and Cu(II) should allow their separation using the AIDA polymer monolith, therefore a standard mix containing Mn(II), Cd(II) and Cu(II) was prepared. The chromatographic separation of the metal mixture was performed on the capIC system described in Section 2.1.3. This system set-up allowed for a separation of metals using simultaneous conductivity and UV-Vis detection.

Figure 5.2 shows a separation of Mn(II), Cd(II) and Cu(II) using simultaneous on-column C^4D detection (a) and UV-Vis detection (b). Chromatographic performance data was obtained and can be seen in Table 5.2. An increase in retention was observed using UV-Vis detection, which was due to the incorporation of the post-column mixer as well as the increase in effective column length (using on-column C^4D detection the effective column length was 250 mm, which increased to 280 mm using UV detection) A decrease in efficiency was observed with UV-Vis detection, due to an increase in peak width caused by extra column broadening associated with the post-column reaction mixing device as well as the MicroTight unions (swept volume of 17 nL) required in the system set-up. An increase in extra column volume (from the end of the column to the UV detector flow-cell) of 134 nL was calculated.

Table 5.2: Chromatographic performance data showing the direct comparison of on-column C^4D detection with UV-Vis detection for the separation of 5 ppm Mn(II), 10 ppm Cd(II) and 10 ppm Cu(II). Chromatographic conditions: Eluent: 0.2 m*M* HNO_3, all other chromatographic conditions as in Table 5.1.

Metal	*Detection*	*N/m*	*Retention time (mins)*	*Asy.*	*k*	*Res.*	*Peak width*
Mn(II)	C^4D	3,900	3.60	1.57	4.01	-	0.28
	UV-Vis	2,100	6.03	1.78	-*	-	0.59
Cd(II)	C^4D	3,600	5.83	1.14	6.74	3.45	0.48
	UV-Vis	2,400	9.25	1.45	-*	2.65	0.84
Cu(II)	C^4D	2,650	10.28	1.15	12.84	3.64	0.97
	UV-Vis	2,700	14.98	0.97	-*	3.19	1.27

-* *k value not obtained due to the absence of a void peak.*

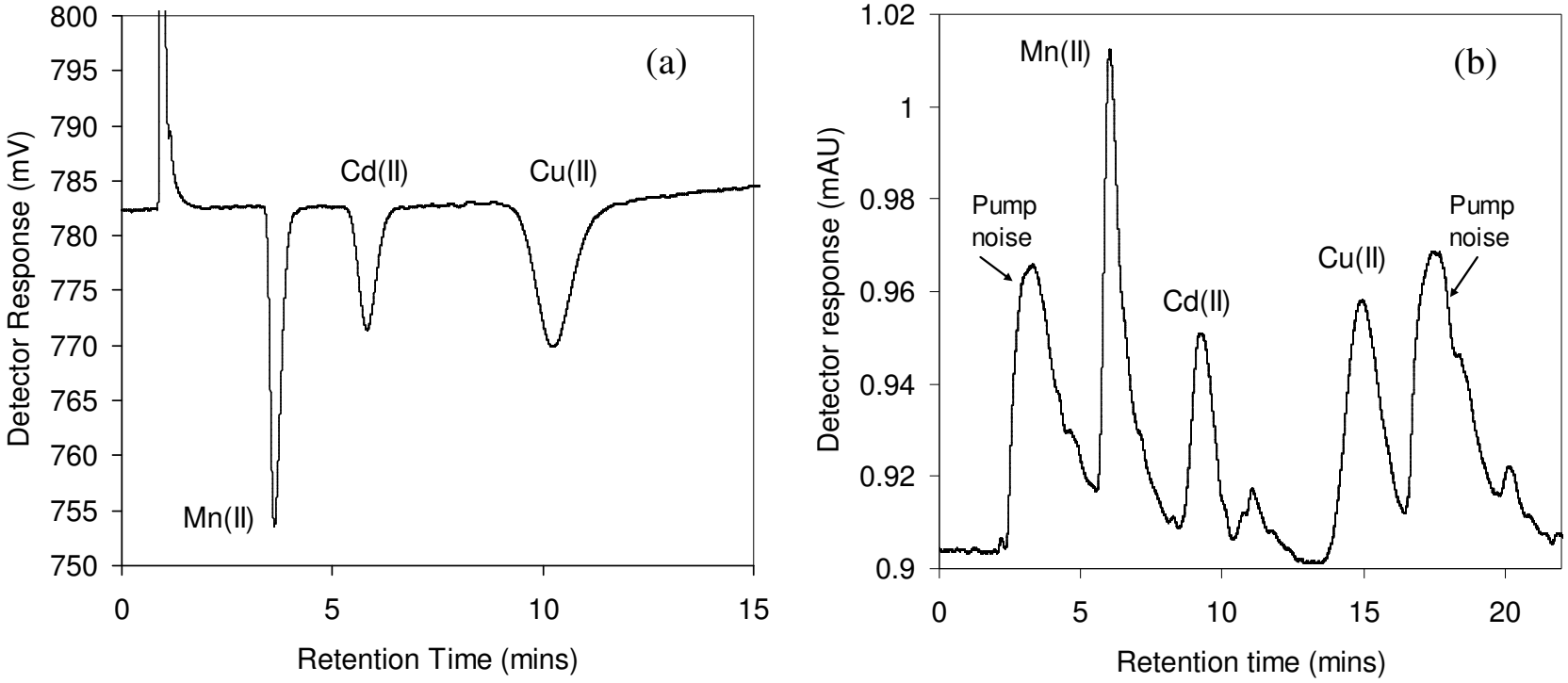

Figure 5.2: (a) Separation of 5 ppm Mn(II), 10 ppm Cd(II) and 10 ppm Cu(II) using C^4D detection. Chromatographic conditions: Column: VAL15a, eluent: 0.2 m*M* nitric acid, flow-rate: 1 µL/min, column length: 250 mm x 100 µm I.D., injection volume: 20 nL. (b): Same separation using simultaneous post column reaction and UV-Vis detection. Chromatographic conditions: Eluent: 0.2 m*M* nitric acid, PCR: 0.15 m*M* PAR in 0.5 *M* ammonia, pH = 10.4, PCR flow-rate: 1µL/min, all other conditions as in Table 5.1.

The extra column tubing associated with the post-column mixer had an impact on the peak width (increase of ~ 50 % in the case of Mn(II) and Cu(II)). Increased peak tailing was noted, using UV-Vis detection in comparison to C^4D (except in the case of Cu(II), however this result may have suffered from interferences from the pump noise). As seen from Table 5.2, an increase in the peak tailing and peak width, using PCR and UV-Vis detection, led to a decrease in the resolution of the three peaks. From Table 5.2, it appeared that C^4D detection was a superior detection device in comparison to UV-Vis detection. Faster elution times and improved peak shape were observed. However, chromatographic performance using UV-Vis detection may have been improved using fully optimised PCR conditions. As can be seen from Figure 5.2(b), a significant amount of pump noise was present. According to the manufacturers, these pumps are suitable for use at flow-rates > 100 µL/min and a flow-rate of 1 µL/minute were outside the recommended working range. One major advantage of using on-column C^4D is the simplicity of the overall system set-up. Extra hardware, such as post-column mixers and extra pumps for delivering the PCR reagent were not required. As the two high pressure eluent pumps used in the capIC system were not suitable for use in this work, all future work where C^4D and UV-Vis were employed as the detection modes were carried out using the Dionex Ultimate 3000 capillary ion chromatography system which incorporated a second Dionex capillary pump for delivery of the PCR reagent.

5.2.5 Repeatability of functionalisation procedure.

The repeatability of the functionalisation procedure for attachment of the chelating ligand onto the surface of the monolith was investigated. Two LMA-*co*-EDMA monoliths (denoted monoliths VAL15b and VAL15c) were fabricated and functionalised using the procedure described in Section 2.2.2.3. Separations of the three metals previously shown in Figure 5.2, were again carried out using VAL15b and VAL15c and performance data compared (Table 5.3). Clearly, differences in *k* can be seen from the separation of Mn(II), Cd(II) and Cu(II) shown in Figure 5.2(a) (denoted VAL15a) and the same separation using VAL15b and VAL15c (Figure 5.3). VAL15a had an effective column length of 250 mm and VAL15b and VAL15c had effective column lengths of 280 mm. A *k* value of 4.01, 6.74 and 12.84 were obtained for Mn(II), Cd(II) and Cu(II) using VAL15a. Table 5.3 shows the *k* data obtained for

VAL15b and VAL15c. During the fabrication of the AIDA polymer monoliths, the following observation was noted; the backpressure exhibited by VAL15a using the 0.2 m*M* HNO_3 eluent was 140 bar at 1 µL/min whereas the backpressures for VAL15b and VAL15c using the same conditions were 76 bar and 79 bar, respectively. The higher backpressure observed for VAL15a indicated that during the polymerisation of the polymer monolith, smaller flow-through pores were formed in the monolith structure in comparison to VAL15b and VAL15c, therefore resulting in an increased surface area of VAL15a. This increased surface area would result in increased sites available for the photo-grafting of benzophenone, which in turn would result in an increase in the overall complexation capacity of VAL15a, following the covalent attachment of IDA. The increase in complexation capacity would result in an increase in the retention of all metals, which was observed when compared to VAL15b and VAL15c. As all other columns prepared during the completion of this study exhibited similar *k* data to VAL15b and VAL5c, it can be concluded that an error may have occurred during the fabrication of VAL15a. This may have been incorrect monomer/porogen ratios during the preparation of the polymerisation mixture or an increase in the UV grafting time during the polymerisation of the monolith.

Table 5.3: Chromatographic performance data obtained from the separations of 5 ppm Mn(II), 10 ppm Cd(II) and 10ppm Cu(II). Chromatographic conditions: Eluent: 0.2 m*M* nitric acid, all other conditions as in Table 5.1.

Monolith	*Metal*	*k*	*Asy.*	*N/m*	*Res.*	*peak width*
VAL15a	Mn(II)	4.01	1.57	3,900	8.14	0.28
	Cd(II)	6.74	1.14	3,600	3.45	0.48
	Cu(II)	12.84	1.15	2,700	3.64	0.97
VAL15b	Mn(II)	0.86	1.17	4,900	6.25	0.21
	Cd(II)	1.4	1.08	4,700	2.35	0.28
	Cu(II)	2.6	1.12	2,900	3.12	0.54
VAL15c	Mn(II)	0.89	1.28	5,000	6.47	0.21
	Cd(II)	1.46	1.13	4,300	2.32	0.30
	Cu(II)	2.73	1.16	2,700	3.06	0.57

Figure 5.3 shows an overlay of separations of Mn(II), Cd(II) and Cu(II) using VAL15b and VAL15c. Differences in k of < 4 % were observed between VAL15b and VAL15c for Mn(II) and Cd(II), with the later eluting Cu(II) exhibiting the largest difference in k (5 %). VAL15b showed an improved efficiency over VAL15c for Cd(II) and Cu(II) which correlates with improvements in peak asymmetry whereas a difference in efficiency of 2 % was observed for Mn(II). All other chromatographic data was comparable.

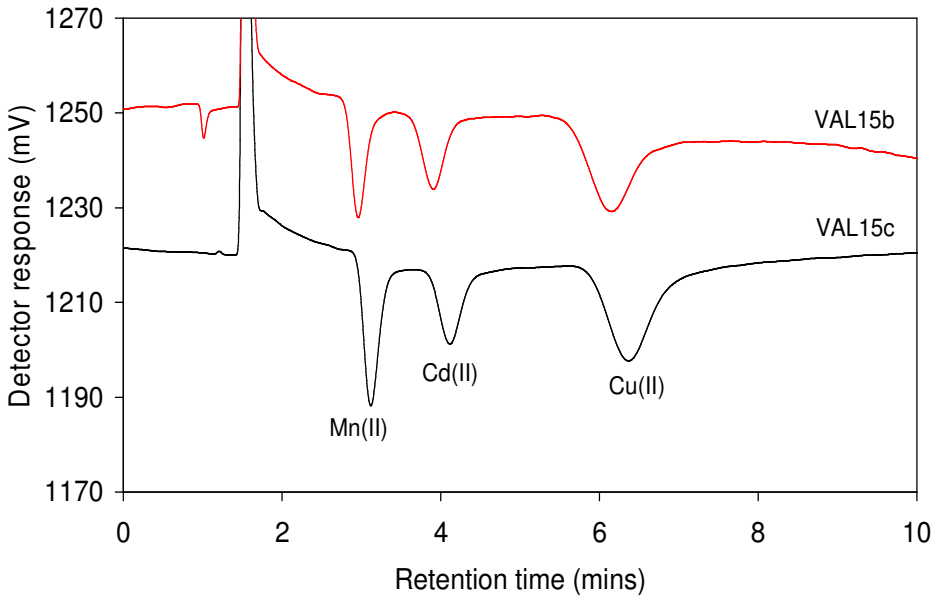

Figure 5.3: Overlay of chromatograms obtained for the separation of 5 ppm Mn(II), 10ppm Cd(II) and 10ppm Cu(II) using VAL15b and VAL15c. Chromatographic conditions: Eluent: 0.2 mM HNO_3, all other conditions as in Table 5.1.

5.2.6 Temperature studies

5.2.6.1 Development and calibration of capillary column heater

A capillary column heater was constructed as described in Section 2.1.5.3 using a flexible heating tape which emits heat when voltage is applied. The column heater was calibrated by applying increased voltage and recording the temperature increase. Figure 5.4 shows a calibration plot, including error bars, showing that for an applied voltage the temperature increase was reproducible (n = 4), with % RSD values < 0.8

% for all voltages tested. The separation column was placed inside the column heater and the use of zero dead volume unions on either end of the separation column ensured that the column was not in physical contact with any part of the heating tape, therefore avoiding any associated local temperature gradients. The ends of the column heater were plugged to minimise heat loss. The resultant capillary column heater was inexpensive to prepare and was easily incorporated into the chromatography system.

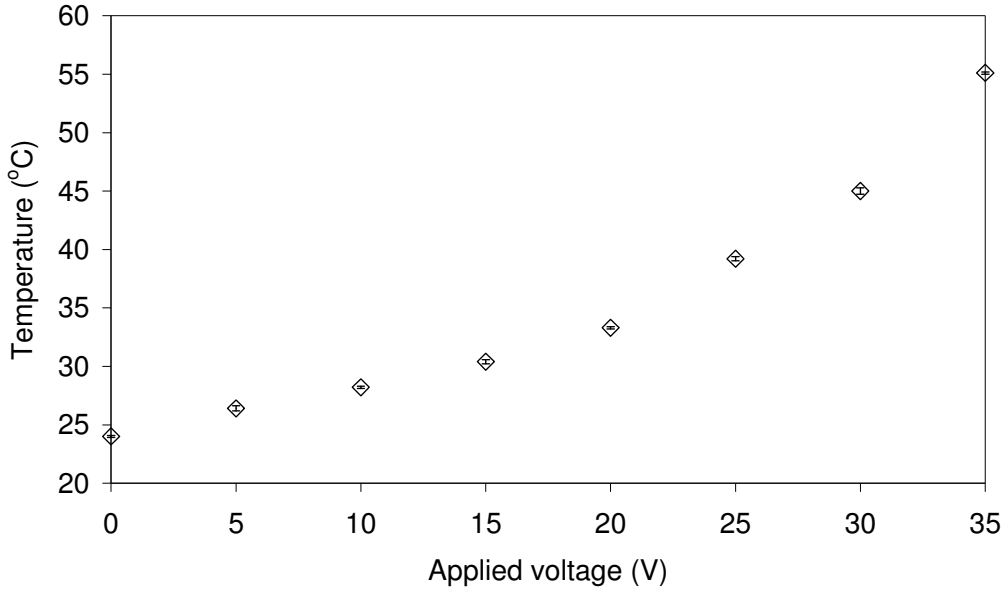

Figure 5.4: Calibration plot of applied voltage (V) versus temperature (^{o}C) for the capillary column heater.

5.2.6.2 Effect of temperature on separation performance.

It has been shown previously that an increase in retention is observed with an increase in temperature when chelation is the dominant separation mechanism [52, 130, 142, 155]. Using a Dionex Ultimate 3000 capillary chromatography system, the effect of column temperature on retention of Mn(II), Cd(II) and Cu(II) was investigated. The AIDA polymer monolith was placed inside the capillary column heater. In this case, off-column C^4D was used as the AIDA polymer monolith was housed inside the capillary heater. Figure 5.5 shows the chromatograms obtained for the separations of the metals carried out at 24, 34, 43 and 53 ^{o}C. Temperature analysis was carried out using VAL15b.

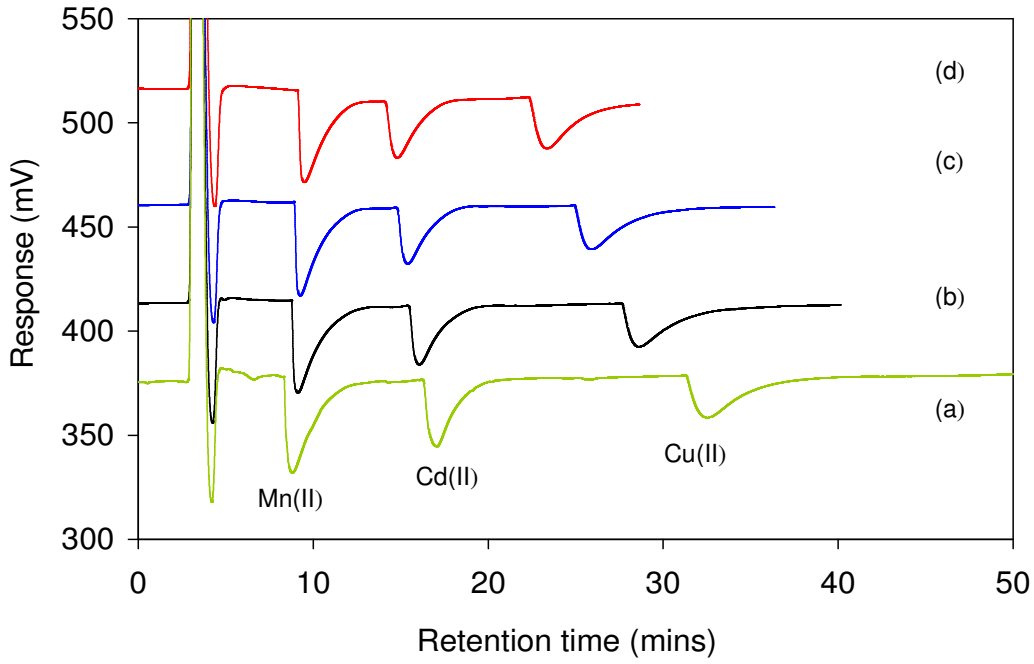

Figure 5.5: Overlay of chromatograms showing the effect of temperature on retention where (a) = 54 ^{o}C, (b) = 43 ^{o}C, (c) = 34 ^{o}C and (d) = 24 ^{o}C. Chromatographic conditions: column length: 230 mm x 100 µm I.D., eluent: 0.1 m*M* nitric acid, all other conditions as in Table 5.1.

Table 5.4 shows the chromatographic performance data obtained for the separations of Mn(II), Cd(II) and Cu(II) at the four selected temperatures. Cd(II) and Cu(II) exhibited endothermic behaviour (an increase in retention with an increase in temperature), indicating the chelation was the dominant separation mechanism. A decrease in retention with an increase in temperature was observed for Mn(II) which was indicative of ion-exchange being the dominant separation mechanism. A decrease in *k* of 8 % was observed for Mn(II) while an increase in *k* of 22 % and 50 % was obtained for Cd(II) and Cu(II) respectively when the temperature was increased from 24 ^{o}C to 53 ^{o}C. This clearly shows that increasing the temperature did not have the same effect on all three metals.

In all cases, peak asymmetries > 4.0 were observed for Mn(II), showing significant tailing. Peak tailing was also observed for Cd(II) and Cu(II), although to a lesser extent than Mn(II) (peak asymmetries > 2.0 in all cases). The increase in peak width and peak asymmetry (in comparison to the results shown in Table 5.3) was due to the

use of a 0.1 m*M* nitric acid eluent. An increase in the eluent pH resulted in an increase in the dissociation of the carboxylic acid groups on the IDA structure, producing an increase in the conditional stability constants of the surface metal complexes. An increase in the conditional stability constants results in an increase in retention, which in this case, led to an increase in peak width and asymmetry when compared to the chromatographic performance data obtained for the separations of Mn(II), Cd(II) and Cu(II) using a 0.2 m*M* nitric acid eluent, shown in Table 5.3 above.

Table 5.4: Chromatographic performance obtained for the separation of Mn(II), Cd(II) and Cu(II) with increasing column temperature. Chromatographic conditions: Column: VAL15b, eluent: 0.1 mM HNO_3, effective column length: 230 mm x 100 µm I.D., all other conditions as in Table 5.1.

Column temp (^oC)	*Metal*	*k*	*N/m*	*Asy.*	*Res.*	*peak width*
23	Mn(II)	1.90	1,350	4.4	3.6	1.27
	Cd(II)	3.53	2,750	2.2	2.4	1.37
	Cu(II)	6.14	3,350	2.0	3.0	1.98
34	Mn(II)	1.83	1,300	4.9	3.6	1.26
	Cd(II)	3.74	3,100	2.5	2.8	1.35
	Cu(II)	6.98	4,350	2.0	3.8	1.94
43	Mn(II)	1.81	1,150	4.9	3.4	1.32
	Cd(II)	3.96	3,400	2.8	3.0	1.39
	Cu(II)	7.82	4,000	2.7	4.1	2.24
54	Mn(II)	1.75	800	4.3	3.0	1.52
	Cd(II)	4.32	3,150	2.4	3.2	1.50
	Cu(II)	9.17	3,750	2.6	4.4	2.59

From Table 5.4, a decrease in efficiency of 30 % for Mn(II) was observed with an increase in temperature, whereas Cd(II) showed increases in column efficiency of 19 % when the temperature was increased from 24 ^oC to 43 ^oC, followed by a decrease of 7 % when the temperature was further increased to 54 ^oC. A column efficiency of 4,350 N/m was reported for Cu(II) at 34 ^oC, an increase of 23 % when compared to analysis carried out at 23 ^oC. At temperatures above 34 ^oC, Cu(II) showed a decrease

in column efficiency of 14 %. A 25 % increase in resolution between Mn(II) and Cd(II) was observed with an increase in temperature while a 32 % increase in resolution was observed for Cd(II) and Zn(II). While the use of temperature improved column efficiency for Cd(II) and Cu(II), increases in analysis runtime were observed.

Van't Hoff plots which relate changes in retention to changes in column temperature were plotted and can be seen in Figure 5.6. As mentioned previously, increasing the temperature did not have the same effect on all three metals which is evident from the slopes of each metal obtained from the van't Hoff plots (Table 5.5). Negative slopes of -571 and -272 were obtained for Cu(II) and Cd(II) respectively demonstrating that the sorption process was endothermic. A positive slope of +131 was obtained for Mn(II), demonstrating that the sorption process in this case was exothermic. Cu(II) exhibited the largest slope value, showing that the effect of temperature on Cu(II) was more pronounced than Cd(II) and Mn(II). A similar trend was also observed by Bashir *et al.* [130]. Using an IDA-silica packed analytical column (240 x 4 mm I.D), the authors noted that Zn(II) and Co(II), the more strongly retained metal ions exhibited more rapid responses to increases in temperature in comparison to the more weakly retained metals such as Mn(II). The effects of temperature on the retention of Cd(II) were less pronounced than Zn(II) and Co(II) and the authors concluded that the effects of temperature on Cd(II) may have been more significant if a non-chloride eluent was used. Bashir *et al.* [130] did observe an increase in the retention of Mn(II) with an increase in temperature. In this work the opposite was observed.

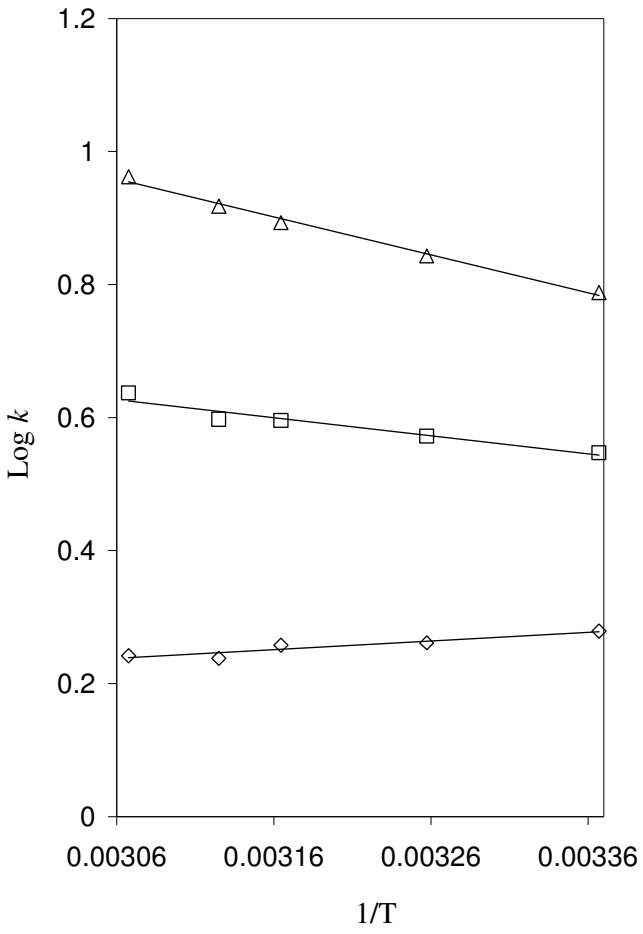

Figure 5.6: Van't Hoff plots constructed for Mn(II) (◊), Cd(II) (□) and Cu(II) (Δ) demonstrating that for Cu(II) and Cd(II), the sorption process exhibited exothermic behaviour and for Mn(II) the sorption process exhibited endothermic behaviour.

Table 5.5: Linear regression data from van't Hoff plots.

	Slope	*Intercept*	R^2
Mn(II)	131	-0.16	0.89
Cd(II)	-272	1.46	0.93
Cu(II)	-571	2.71	0.99

Heats of adsorption (ΔH) were calculated and can be seen in Table 5.6. Generally, in chromatographic systems where chelation in the dominant separation mechanism, heats of adsorption (ΔH) are higher than those observed for simple ion-exchange mechanisms and heats of absorption obtained for ion exchange separations do not exceed 3 kJ mol^{-1} [51]. In Chapter 4.0, temperature studies were carried out using a sulfonated functionalised polymer monolith which was used for the ion exchange separation of the alkaline earth metals Ca(II), Mg(II) and Ba(II). Heats of absorption (ΔH) were calculated to be -0.45, -0.58 and -1.2 for Mg(II), Ca(II) and Ba(II) respectively. An increase in temperature resulted in a decrease in retention for all alkaline earth metals studied using the sulfonated polymer monolith. In this work, heats of adsorption were 4.75 kJ mol^{-1}, 2.26 kJ mol^{-1} and -1.87 kJ mol^{-1} for Cu(II), Cd(II) and Mn(II) respectively. As mentioned earlier, Mn(II) exhibited exothermic behaviour and ΔH was lower than that obtained for Cd(II) and Cu(II).

Table 5.6 also shows ΔH values obtained using separation columns with various ionogenic functional groups. In the case of [52] and [131], KCl was added to the eluent to suppress ion exchange interactions and allow chelation to be the dominant separation mechanism. Paull *et al*. [131] obtained ΔH values of 0.84 for Cd(II) using a silica based IDA column and ΔH values of 3.78 using the sulfonated polymeric resin (CS10) column. Barron *et al.* [52] obtained ΔH value of 2.5 for Cd(II) using an polymer based IDA resin while Eleftorov *et al.* [162] obtained ΔH values for Cd(II) of 3.95, using a glutamic acid-bonded column. Glutamic acid is an aminodicarboxylic acid which can form complexes with metal cations through the nitrogen and oxygen atoms. $NaClO_4$ was used as the eluent to suppress ion exchange and allow chelation to become the dominant separation mechanism. Although the heats of adsorption obtained for Cd(II) are comparable to those obtained by Paull *et al.* [131], Barron *et al.* [52] and Eleftorov *et al.* [162], in this present work a decrease in retention was observed for Mn(II) with an increase in temperature. The dicarboxylate polymeric resin (PRP-X800) exhibited higher ΔH values in comparison to the carboxylated resin (CS14) due to an increase in the number of available carboxylic groups available for the formation of surface metal complexes.

Table 5.6: Comparison of heats of adsorption (ΔH) on various analytical columns

Column	*IDA-polymer monolith LMA-co-EDMA (Current study)*	*ProPac-IMAC [52] (poly-IDA functionalised polymer 10 µm resin)*	*CS10 [131] (Sulphonated polymeric cation exchange)*	*CS14 [131] (Carboxylated polymeric cation exchange)*	*PRP-X800 [131] (Polymeric dicarboxylate cation exchange)*	*Silica-IDA [131]*	*Glutamic acid-bonded silica [162] (5 µm particle size)*
Column dimensions	230 mm x 100 µm I.D.	50 x 2 mm	250 x 4 mm	250 x 4 mm	150 x 4 mm	250 x 4 mm	100 x 4.6 mm
Eluent	0.1 m*M* HNO_3	0.25 m*M* HNO_3 – 10 m*M* KCl	100 m*M* HNO_3 – 100 m*M* KCl	1.5 m*M* HNO_3 – 20 m*M* KCl	0.3 m*M* HNO_3 – 20 m*M* KCl	10 m*M* HNO_3 – 20 m*M* KCl	0.2 *M* $NaClO_4$ (pH 4.0)
Mn(II)	-1.87	8.3	6.95	4.02	10.59	0.73	3.01
Cd(II)	2.26	2.5	3.78	5.07	12.19	0.84	3.95
Cu(II)	4.75	-	-	-	-	-	-

5.2.7 Increasing complexation capacity of immobilised chelating ligand.

The advantages of the method of functionalisation carried out in this work, i.e. post-polymerisation, have been highlighted in a review by Nordborg and Hilder [12]. The separation of the monolith fabrication procedures and the surface functionalisation methods allows each of the processes to be optimised independently, allowing for changes to be made to the overall complexation capacity of the AIDA monolith, without re-optimisation of the entire monolith fabrication procedure. An increase in the photo-grafted density of poly(VAL) should lead to an increase in the density of the chelating ligand on the surface of the monolith. To investigate this, 4 monoliths were prepared according to Table 2.1 with increased photo-grafted density of VAL (denoted VAL15c, VAL20, VAL25 and VAL30). In each case, the concentrations of benzophenone and IDA were kept constant.

5.2.7.1 Scanning C^4D

Sugrue *et al.* [125, 126] modified a commercially available silica monolith with IDA. The authors evaluated the surface coverage of the immobilised ligand along the entire length of the monolith using atomic absorption spectroscopy (AAS). Individual sections of the silica monolith were saturated with $CuSO_4$ followed by washing with deionised water. The copper was desorbed using nitric acid (10 m*M*) and the concentration of copper was determined using AAS. This method was only possible by destruction of the monolith and could only be carried out at the end of the study. Since its inception as a detection device in capillary electrophoresis in 1998 [36], C^4D has grown in popularity, expanding into the fields of liquid chromatography (LC). More recently, the ability to place the detector cell at various positions along the analytical column led researchers to investigate the information to be gained by scanning the entire length of the column. The applications of scanning C^4D within capillary chromatography have been highlighted in a recent review by Connolly *et al.* [45].

In this present work, scanning C^4D was employed as a non-destructive method to visualise axial homogeneity of the IDA ligand density along the entire length of the column. By scanning the monolith before (i.e. the un-functionalised monolith) and after immobilisation of IDA using an ethanolamine buffer (pH 9.8), a clear change in the conductive response indicated the successful immobilisation of IDA onto the surface of each of the 4 monoliths.

Figure 5.7(a) depicts a typical scanning C^4D profile (VAL20) showing the increase in conductive response following the modification of the polymer monolith with AIDA. Figure 5.7(b) shows an overlay of corrected scanning C^4D profiles obtained for VAL15c, VAL20, VAL25 and VAL30 (i.e. the profiles were obtained by subtracting the conductive response obtained after modification of IDA from the subsequent base monolith scan carried out prior to surface modification). Increases in conductive response indicated that an increase in the poly(VAL) concentration during photo-grafting, resulted in an increase in the number of sites available for the covalent attachment of IDA. Gillespie *et al.* [100] also used scanning C^4D to show an increase in conductivity using polymer monoliths photo-grafted with increasing concentrations of 2-acrylamido-2-methyl-1-propanesulfonic acid (AMPS).

Finally, the scanning C^4D profiles also demonstrated an axial homogeneous distribution of the chelating ligand for each monolith with % RSD (calculated from the conductive response obtained at each 2 mm increment) of ≤ 3 % all monoliths scanned. An anomaly in conductivity was observed at the head of the column (between 3 and 4 cm) with VAL25. The average conductivity of the first 4 points was 774 mV, a decrease in conductivity of 11 % when compared with the average conductivity obtained between 5 cm and 9 cm. The use of scanning C^4D techniques in this work ensured that the monoliths could be profiled prior to any chromatographic applications as destruction of the monolith was not required.

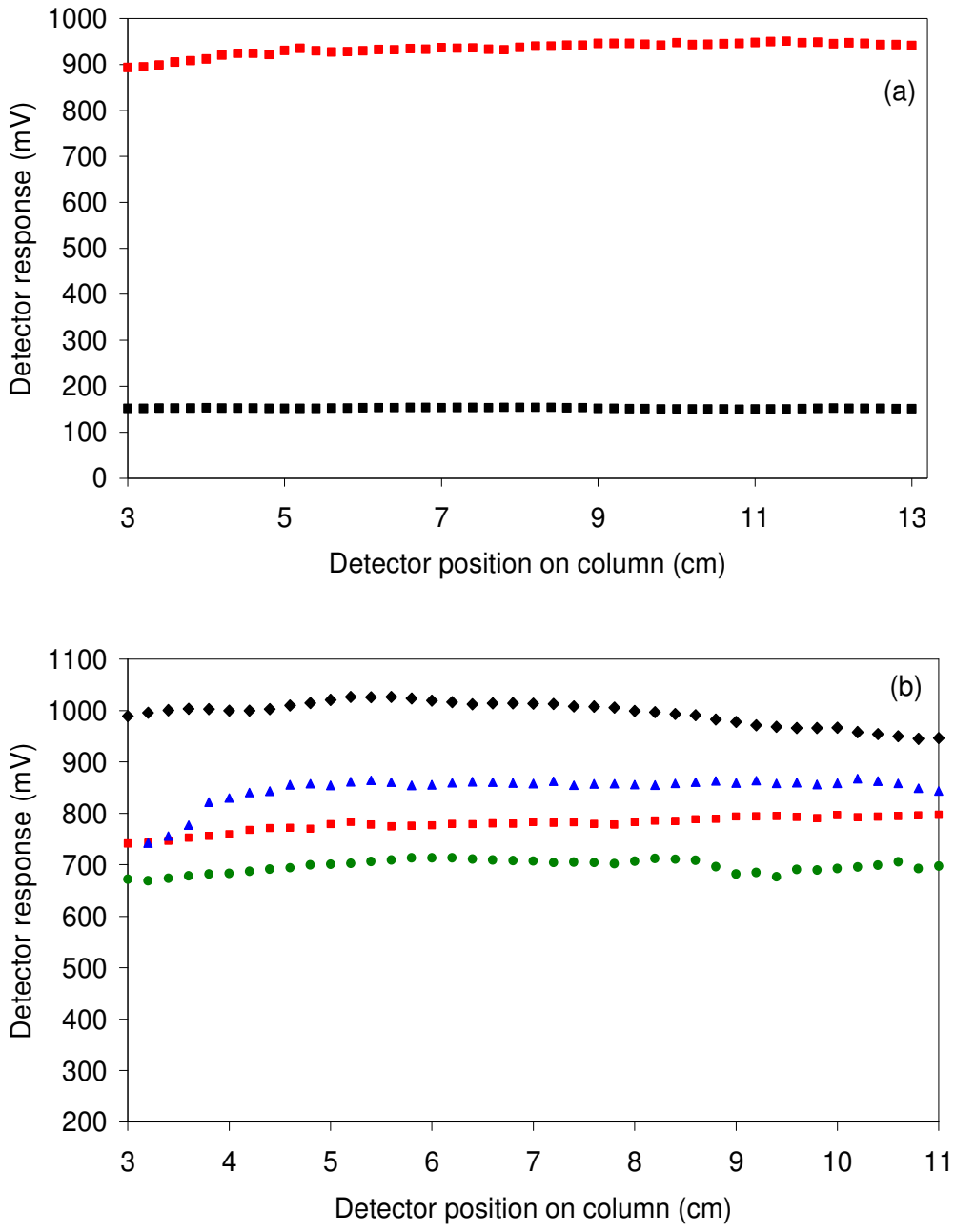

Figure 5.7: (a) Scanning C^4D profiles obtained using a 1 m*M* ethanolamine buffer pH = 9.8 for VAL20 where (■) is the scan of the un-modified polymer monolith and (■) is the scan following modification with IDA. (b): Scanning C^4D profiles where (●) VAL15, (■) VAL20, (▲) VAL25 and (♦) VAL30.

5.2.7.2 Effect of increasing the chelation capacity on the retention of selected metals.

The effect of increasing the complexation capacity on the retention time of various metals was investigated using the modified polymer monoliths with on-column C^4D detection. Using a 0.1 m*M* nitric acid eluent, increases in *k* were obtained for all metals when the complexation capacity was increased. Table 5.7 shows the chromatographic performance data for the AIDA polymer monoliths with increased complexation capacity. With VAL15c, retention of Mn(II), Co(II), Ni(II) and Zn(II) was not achieved. VAL20 exhibited similar *k* values for Mn(II), Cd(II), Co(II) and Zn(II). However, Mn(II) was retained using VAL20 and resolved from Cd(II) which was not achieved using VAL15c.

All polymer monoliths showed poor peak shape for Zn(II), with peak asymmetries > 4 in all cases. Co(II) exhibited a decrease in column efficiency of 13 % from VAL15c to VAL30, while an increase in efficiency of 25 % was noted for Cu(II). Although Cu(II) showed an improvement in column efficiency using VAL30, increases in peak width (80 %) were obtained using a 0.1 m*M* nitric acid eluent due to the increase in the chelation capacity of the column. Due to the increased capacity exhibited by VAL30, a stronger eluent (0.2 m*M* HNO_3) was required for the elution of the metal cations.

Table 5.7: Chromatographic performance data for 6 metals using IDA modified polymer monoliths with increasing complexation capacity. Chromatographic conditions: eluent: 0.1 m*M* nitric acid, metal concentrations: 1 mg/L, all other conditions as in Table 5.1.

Monolith	*Metal*	*k*	*N/m*	*Asy*	*Peak width*
VAL15c	Mn(II)	-	-	-	-
	Co(II)	-	-	-	-
	Ni(II)	-	-	-	-
	Zn(II)	-	-	-	-
	Cd(II)	0.85	3,300	0.79	0.26
	Cu(II)	6.89	3,480	0.77	1.45
VAL20	Mn(II)	2.8	1,650	2.46	0.8
	Co(II)	2.9	1,740	4.11	0.82
	Ni(II)	2.96	1,510	1.65	0.88
	Zn(II)	3.36	956	4.33	1.22
	Cd(II)	5.63	3,245	1.61	0.97
	Cu(II)	11.76	2,990	1.65	1.97
VAL25	Mn(II)	3.44	580	1.5	3.13
	Co(II)	5.01	460	1.15	2.07
	Ni(II)	3.79	540	1.13	3.77
	Zn(II)	5.23	1,500	0.97	2.96
	Cd(II)	9.93	2,920	1.4	3.5
	Cu(II)	23.5	3,780	1.29	6.85
VAL30	Mn(II)	8.26	1,088	6.08	2.77
	Co(II)	11.02	1,254	7.86	4.28
	Ni(II)	11.07	2,270	8.6	3.03
	Zn(II)	12.43	555	4.37	5.04
	Cd(II)	21.14	2,875	5.85	4.66
	Cu(II)	45.22	4,640	5.25	7.25

- not retained

5.2.8 Separations of selected metals using simultaneous on-column C^4D and UV-Vis detection.

An open tubular post-column mixer was prepared using fused silica capillary (25 µm x 17 cm, internal volume 89 nL). Figure 5.8 shows the system set-up used for the separation of Mn(II), Cd(II) and Cu(II) incorporating on-column C^4D detection and UV-Vis detection following reaction of the column eluate with PAR. A T-piece was used to allow mixing of the eluted metals with the PCR.

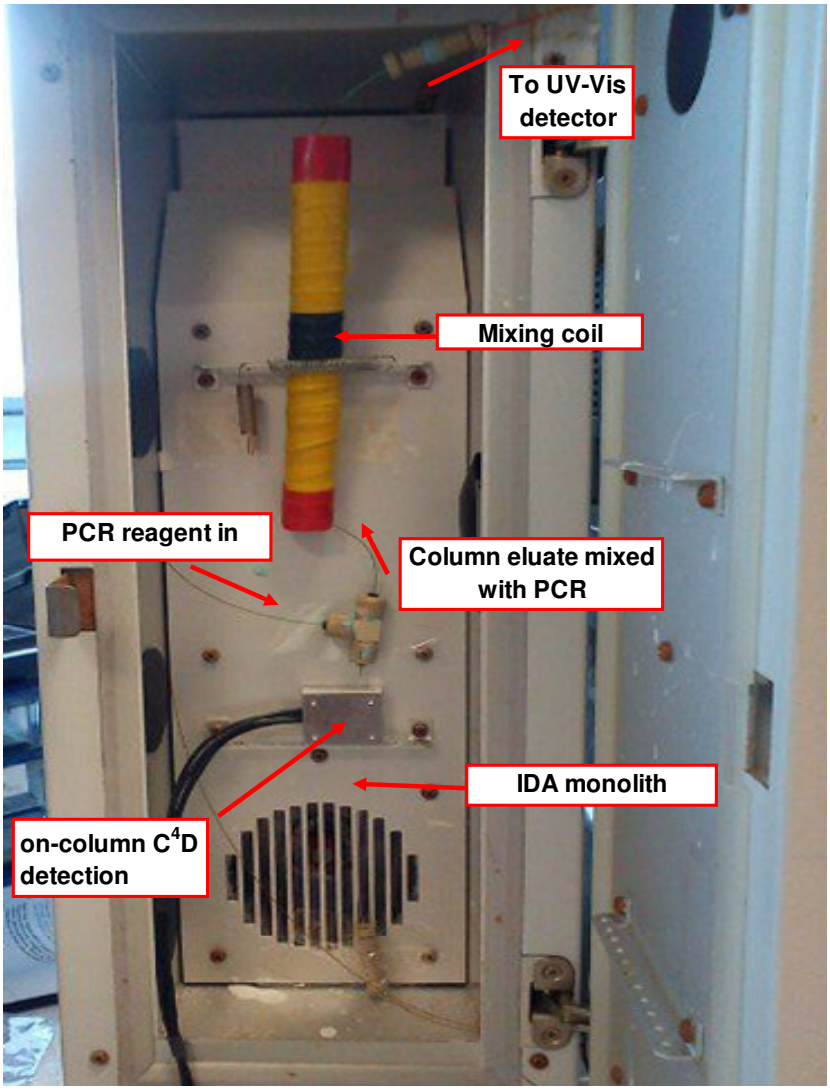

Figure 5.8: Chelation ion chromatography system set-up incorporating on-column C^4D and UV-Vis detection.

The AIDA polymer monolith was used for the analysis of the common transition and heavy metals Cu(II), Cd(II) and Mn(II) utilising a low pH nitric acid eluent (0.2 m*M*) and PAR as a PCR. Separations of transition and heavy metals were achieved using the novel combination of simultaneous on-column C^4D detection (Figure 5.9(a)) and UV-Vis detection (Figure 5.9(b)) using VAL25 and VAL30. An increase in the retention of the three metals was obtained when the complexation capacity was increased. Table 5.8 shows the chromatographic performance data obtained for the separation of Mn(II), Cd(II) and Cu(II) using simultaneous C^4D and UV-Vis detection. From the separation of the standard mixture using VAL25, baseline separation of Mn(II) and Cd(II) was not achieved. A resolution of 1.1 for C^4D and 1.2 for UV-Vis was obtained, however when the complexation capacity was increased (VAL30), baseline resolution between these two metals improved (1.6 for C^4D and 2.3 for UV-Vis), when the same eluent was employed.

An increase in efficiency (between VAL25 and VAL30) was observed for Cd(II) using C^4D detection, with Mn(II) and Cu(II) showing similar efficiencies. When both forms of detection are compared, superior column efficiencies was obtained for all peaks using PCR and UV-Vis detection, except for Cd(II) and Cu(II) using VAL25. The peak widths (measured at 50 % peak height) obtained for VAL25 were comparable for Mn(II) and Cd(II), however for the later eluting peak Cu(II), a significant increase in peak width was observed due to the increase in the complexation capacity exhibited by VAL30. This trend in peak widths was also observed using UV-Vis detection. The peak width values obtained using UV-Vis detection for Mn(II), Cd(II) and Cu(II) increased in all cases when compared to C^4D detection, with the Cu(II) exhibiting the largest increase in peak width. This was due to the increase in the column length due to the system set-up (C^4D was on-column, therefore reducing the effective column length in comparison to UV-Vis detection) and the increased flow path due to the PCR mixer and plumbing associated with the UV-Vis detector. As mentioned previously, an increase in extra-column tubing in capillary chromatography can have a deleterious effect on band broadening.

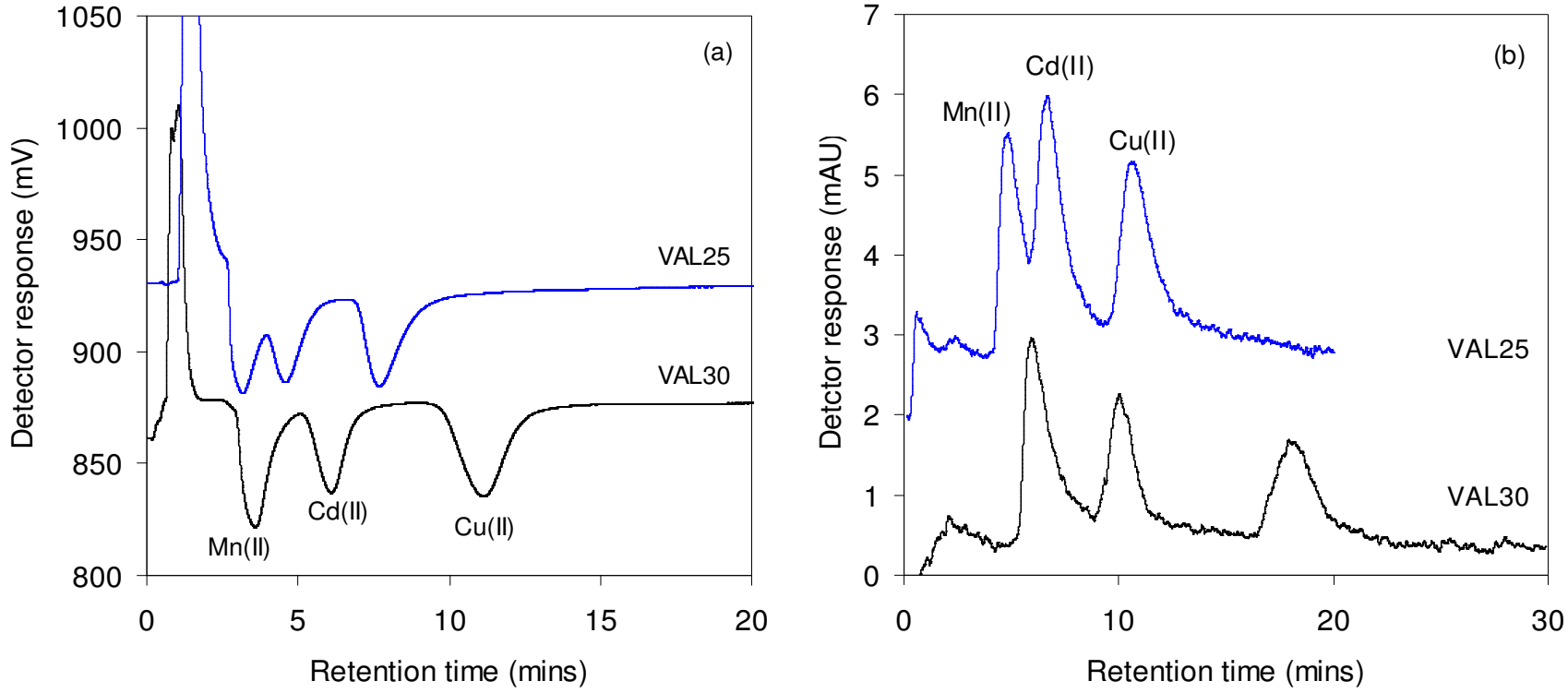

Figure 5.9: Separation of transition/heavy metals utilising simultaneous on-column C^4D detection (a) and UV-Vis detection at 500 nm following reaction of the eluted metals with PAR (b). Chromatographic conditions: Eluent: 0.2 mM nitric acid, Eluent flow-rate: 1 µL/min, PCR flow-rate: 1 µL/min, PCR: 0.4 mM PAR in 0.1 M ammonia, pH 10.7. Peak (1) 0.5 ppm Mn(II), (2) 1 ppm Cd(II) and (3) = 1ppm Cu(II). A 10 pt moving average was applied to the chromatograms (using Microsoft excel) obtained using UV-Vis detection.

Table 5.8: Chromatographic performance data for the comparison of IDA polymer monoliths with varying degrees of complexation capacity using on-column C^4D and UV-Vis detection.

		C^4D					*UV-Vis*			
Metal	Monolith	N/m	*k*	Asy.	Peak width	Res.	N/m	Asy.	Peak width	Res.
Mn(II)	VAL25	900	1.00	1.6	0.8	-	1,200	1.1	0.9	-
	VAL30	900	2.46	1.3	0.9	-	1,300	1.8	1.0	-
Cd(II)	VAL25	1,800	2.02	1.3	0.8	1.1	1,700	1.6	1.1	1.2
	VAL30	2,700	4.94	1.1	0.9	1.6	3,300	1.1	1.1	2.3
Cu(II)	VAL25	3,100	4.03	1.6	1.1	1.9	2,500	1.3	1.4	2.0
	VAL30	3,100	9.94	1.1	1.6	2.4	3,600	1.1	1.9	3.2

5.2.9 Effect of varying the effective column length on retention.

As mentioned previously, Connolly *et al.* [45] recently documented the applications of scanning C^4D within the field of capillary chromatography. A further application of C^4D includes the ability to place the detector cell at any position along the capillary column, thus changing the effective column length, without the need to cut the polymer monolith. Figure 5.10 shows an overlay of chromatograms obtained for the separations of Mn(II), Cd(II) and Cu(II) by varying the effective column length using VAL30. By decreasing the effective column length from 9 cm (Figure 5.10(a)) to 7 cm (Figure 5.10(e)), the run time for the separation was reduced. At an effective column length of 9 cm, resolution of Mn(II) and Cd(II) was 1.80 which decreased to 1.58 at an effective column length of 7 cm, however resolution was maintained. This demonstrates the ability to separate the three selected metals using a 100 µm x 70 mm IDA immobilised polymer monolith.

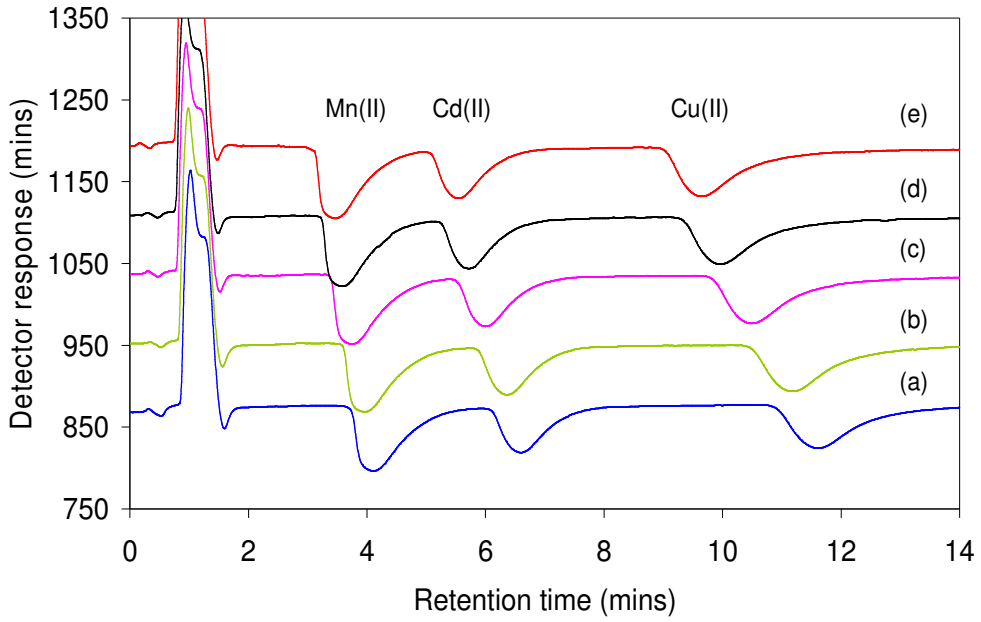

Figure 5.10: Overlay of chromatograms obtained for the separations of 0.5 ppm Mn(II), 1 ppm Cd(II) and 1 ppm Cu(II) by varying the effective column length where (a) = 9 cm, (b) = 8.5 cm, (c) = 8 cm, (d) = 7.5 and (e) = 7 cm. Chromatographic conditions: Column: VAL30, eluent: 0.2 m*M* nitric acid, all other conditions as in Table 5.1.

5.3 Conclusions

A number of AIDA modified polymer monolith have been fabricated and applied to the direct separation of metal cations. This work exploited the use of photo-grafting techniques, allowing the ability to increase in the surface coverage of AIDA without the requirement of re-optimisation the polymerisation conditions used during the fabrication of the LMA-*co*-EDMA polymer monolith. An increase in the complexation capacity was investigated and resulted in an increase in the retention of all metal cations studied. The increase in the complexation capacity of the immobilised ligand was achieved and verified through the use of scanning C^4D techniques with results showing that the surface coverage of the AIDA ligand was homogeneous along the entire length of the column. Separations of Mn(II), Cd(II) and Cu(II) were achieved using a novel combination of on-column C^4D and UV-Vis detection following reaction with PAR. Mixing of the PCR with the column eluate was carried out using a capillary post-column mixing device. Temperature studies

were also carried out using an in-house constructed capillary column heater with results showing that the temperature was reproducible for any given voltage. Increases in column temperature did not have the same effect on the retention of Mn(II), Cd(II) and Cu(II). While the adsorption process for Mn(II) was exothermic (showing that ion exchange was the dominant separation mechanism for Mn(II)), Cd(II) and Cu(II) exhibited endothermic, suggesting that the dominant separation mechanism for both metals were due to the formation of surface complexes.

This work demonstrates a novel capillary chelating ion exchanger for the direct separation of metal cations. In the following Chapter, LMA-*co*-EDMA polymer monoliths were fabricated and attachment of IDA was possible following the photo-grafting of poly(glycidyl methacrylate) on the monolith surface. Both IDA chelating polymer monoliths, prepared using poly(VAL) and poly(GMA) were compared and contrasted.

Chapter 6.0:

Modification of capillary polymer monoliths with iminodiacetic acid using poly(glycidyl methacrylate) for the separation of metal cations by high performance chelation ion chromatography

6.1 Introduction

One method to increase the overall surface area of the polymer monoliths prior to the attachment of the functional group is through the use of photo-grafting techniques [88, 102, 103]. Photo-grafting allows the formation of branch like structures emanating from one reactive surface site on the polymer monolith, thus increasing the surface density of the functional group, as opposed to direct modification of the polymer monolith with ionogenic functionalities (one functional group attached to one reactive site on the monolith scaffold) which would result in a reduced surface coverage. The use of polymer monoliths for the analysis of small ions, including the various methods of surface modification rendering a monolith suitable for ion chromatography have recently been reviewed by Connolly and Paull [103].

To date, no reports have appeared in the literature using GMA as a linker for the attachment of IDA onto the surface of a polymer monolith for the separations of metal cations. The aim of this work was to modify LMA-*co*-EDMA polymer monoliths (in 100 µm internal diameter formats) with IDA functionalities. This was carried out using photo-grafting techniques to introduce branched poly(GMA) on a monolith previously modified with benzophenone which was then reacted with IDA. Scanning C^4D techniques were used to characterise the distribution of the chelating ligand along the length of the column, prior to the application of the IDA-modified polymer monolith to the separations of metals cations. The fabricated chelating ion exchanger was applied to the determination of Mg(II) and Ca(II) in bottled water samples as well as selected transition metals in spiked seawater and tap water samples. The IDA polymer monoliths prepared in this work were also compared to the AIDA polymer monoliths prepared in Chapter 5.0.

6.2 Results and discussion

6.2.1 Fabrication of poly(GMA) IDA modified monoliths

In Chapter 5.0, a LMA-*co*-EDMA chelating polymer monolith was prepared by surface modification of the LMA structure with vinyl azlactone (VAL), following the

immobilisation of benzophenone. IDA functionalities were covalently attached to the immobilised poly(VAL) grafts, allowing the separation of metal cations. In this work, LMA-*co*-EDMA polymer monoliths were prepared using a protocol set out by Collins *et al.* [144]. The advantages of using GMA as an IDA linker include the greater flexibility of the linker group, reducing steric hinderance which could affect metal ion complexation as well as the elimination of the amide (seen in the previous Chapter) and hence greater stability and coordination capability of the IDA ligand.

6.2.2 Characterisation of IDA-modified polymer monoliths using scanning C^4D

As in Chapter 5.0, characterisation of the IDA modified polymer monoliths was carried out using C^4D techniques according to Connolly *et al.* [45]. For each polymer monolith, a C^4D scan was performed following the fabrication of the polymer monolith (i.e. the un-modified polymer monolith) and after modification with IDA.

During the scanning process, differences in the backpressure exhibited before and after the modification of the grafted monolith with IDA were noted. Monolith GMA30 for example, showed a backpressure of 23 bar during the C^4D scan of the un-modified polymer monolith with the 1 m*M* ethanolamine buffer. Following the modification with GMA and IDA, the backpressure exhibited during the second C^4D scan was ~ 90 bar, demonstrating a clear difference in backpressure following the attachment of IDA.

Figure 6.1(a) shows an overlay of the scanning C^4D profiles obtained for GMA15, GMA20, GMA25, GMA30 and GMA35. The data shown in this plot was obtained by subtracting the conductivity obtained from the scan of the un-modified polymer monolith from the conductivity obtained from the corresponding monolith following modification with IDA. Figure 6.1(b) shows a typical scanning C^4D profile obtained for monolith GMA30 where the bottom trace was obtained by scanning the un-modified polymer monolith and the top trace obtained following the modification with IDA. As expected, the scan of the un-modified yielded a low conductivity due to the absence of charged groups on the un-modified polymer monolith surface. A clear difference in conductive response indicated the successful modification of the monolith surface with IDA. As mentioned previously, an ethanolamine buffer at pH

9.8, ensured that both carboxylic groups on the IDA structure were deprotonated, ensuring the maximum stationary phase charge during the scanning of the monolith.

As seen previously with the poly(VAL) IDA-modified polymer monoliths, an increase in the conductive response was noted with an increase in the concentration of GMA during photo-grafting which led to a correspondingly higher IDA ligand density during the surface modification process. One of the main advantages of using scanning C^4D techniques is the ability to measure axial homogeneity of the immobilised IDA along the entire length of the column. Following each scan, % RSD values were calculated with results obtained as follows: GMA20 was 0.24 %, GMA25 was 0.6 %, GMA30 was 0.8 % and GMA35 was 0.3 %. The longitudinal homogeneity obtained in this present work represents an improvement in the longitudinal homogeneity obtained during the scans of the AIDA polymers prepared in Chapter 5.0.

The % RSD value (calculated from the conductive response measured at each detector position) obtained for monolith GMA15 was 8 %. As can be seen from Figure 6.1(a), an increase in the conductive response was noted between 13 and 15 cm during the scan of the IDA-modified GMA15 polymer monolith. The baseline disturbance was not observed in the scan of the polymer monolith prior to modification, therefore suggesting that the anomaly occurred during the modification process.

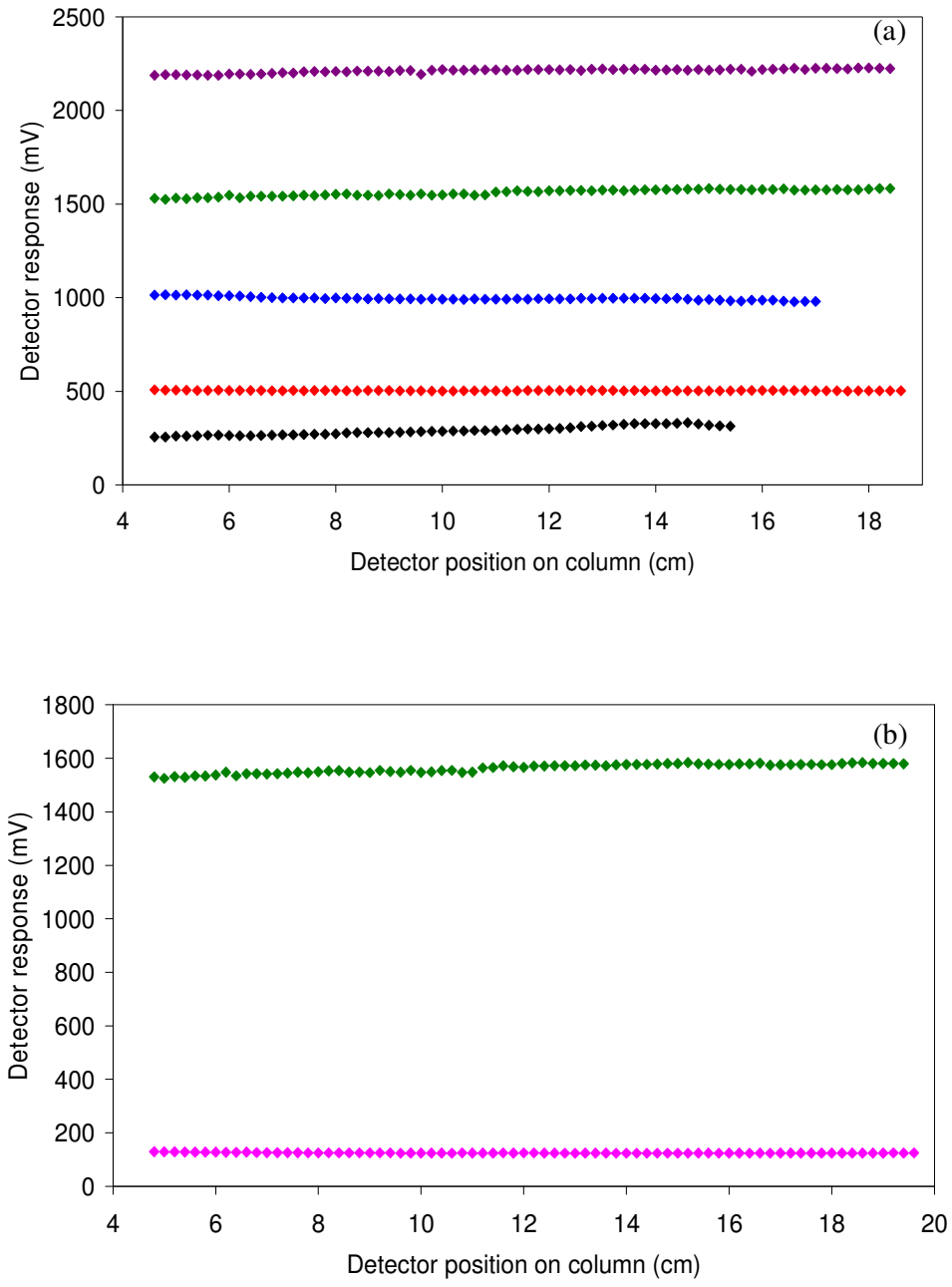

Figure 6.1: (a) Overlay of scanning C^4D profiles obtained for GMA15 (♦), GMA20 (♦), GMA25 (♦), GMA30 (♦) and GMA35 (♦). (b): Scanning C^4D profile obtained for GMA30 where (♦) is the profile of the un-modified polymer monolith and (♦) is the profile obtained after modification with IDA. All scans were carried out using a 1 m*M* ethanolamine buffer (pH 9.8) at a flow-rate of 1 µL/min.

The measurement of axial homogeneity by calculating % RSD values from the data obtained for each scan in this work represents an improvement in axial homogeneity obtained during the scanning C^4D profiles carried out for the poly(VAL) IDA-modified polymer monoliths in Chapter 5.0. For the poly(VAL) IDA-modified polymer monoliths, % RSD values of between 1.5 and 2.2 % were obtained for each polymer monolith.

Figure 6.2 shows a comparison of the conductive responses obtained during the scans of all poly(GMA) IDA-modified polymer monoliths and poly(VAL) IDA-modified polymer monoliths. This data was obtained by calculating the average conductivity obtained following the C^4D scans of each monolith, i.e. the data point for GMA15 was determined by subtracting the conductivity obtained at each 2 mm increment during the C^4D scan of the polymer monolith after IDA from its conductivity obtained during the scan of the un-modified monolith and an average of the corrected conductivity values calculated. The same detector conditions and ethanolamine buffer were used during the C^4D scans of the poly(GMA) IDA-modified polymer monoliths and poly(VAL) IDA-modified polymer monoliths allowing for a direct comparison of the both methods used for the modification with IDA. VAL15 and VAL20 showed an increased conductive response in comparison to GMA15 and GMA20. A difference in conductive response of 59 % and 35 % were noted. GMA25 showed a slight increase in conductivity of 15 % when compared to VAL25 whereas GMA30 and GMA35 showed larger increases in conductivity of 36 % and 40 % respectively when compared to VAL30 and VAL35. A larger increase in detector response was noted between GMA15 and GMA35 (increase in detector response of 1930 mV) as opposed to VAL15 and VAL35 where an increase in conductive response of 615 mV was noted.

From Figure 6.2, it appears that the attachment of IDA using poly(GMA) results in increased IDA ligand density, when used at higher concentrations i.e. GMA30 and GMA35. The effect of this increase in the density of the chelating ligand on the retention of selected metal cations will be discussed in more detail in Section 6.2.4. Significant information was gained from the use of scanning C^4D, which could be obtained prior to the chromatographic application of the polymer monoliths, as this method of characterisation does not require destruction of the polymer monoliths.

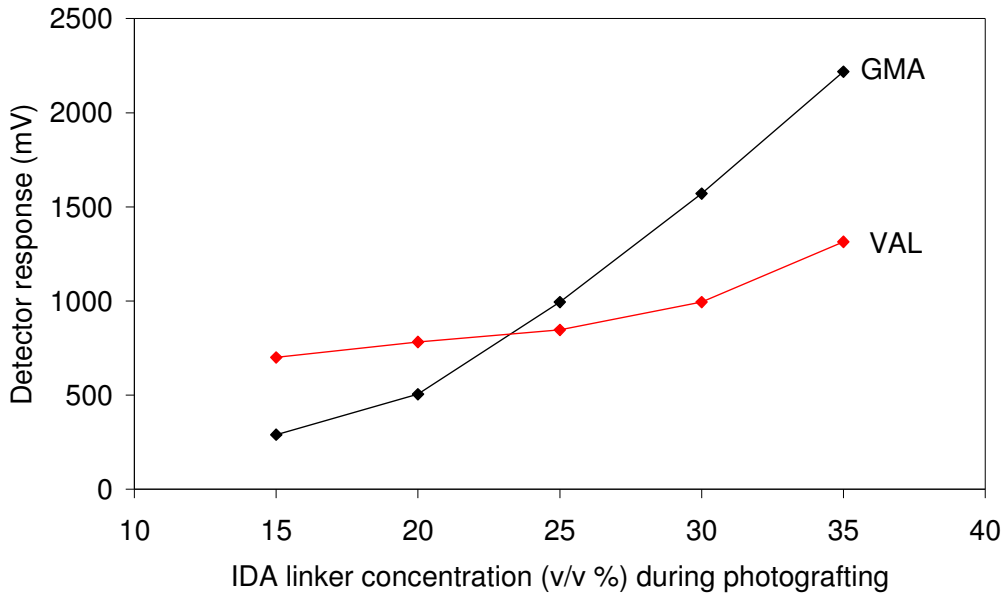

Figure 6.2: Differences in corrected conductive response obtained during the C^4D scanning of the poly(VAL) IDA-modified polymer monoliths and GMA-IDA polymer monoliths.

6.2.3 Retention studies of transition and heavy metals using IDA-modified poly(GMA) grafted monoliths

Using the IDA-modified poly(GMA) grafted monoliths polymer monoliths, retention data for a range of transition and heavy metals were obtained. This data can be seen in Table 6.1. The eluent used for GMA15, GMA20 and GMA25 was 0.1 m*M* nitric acid. Previously, using poly(VAL) IDA-modified polymer monoliths, an increase in the complexation capacity of each monolith resulted in an increase in the retention times of the metal cations studied. Using GMA15, retention of Mn(II) was not possible and no peak for Cu(II) was observed after 45 minutes while Co(II) and Cd(II) showed similar *k* values. Retention of Mn(II) was achieved using GMA20. As with GMA15, Co(II) and Cd(II) exhibited similar *k* values using GMA20. GMA25 also showed similar *k* values for Cd(II) and Co(II), while Cu(II) was retained > 120 minutes when an eluent of 0.1 m*M* HNO_3 was used. Using a 0.2 m*M* HNO_3 eluent, the Cu(II) peak was observed with a *k* value of 0.8 (data not displayed in Table 6.1). Due to the broad peak shape exhibited by Zn(II) using GMA25 with a 0.1 m*M* HNO_3 eluent (peak width, at 50 % peak height, was 3.71 minutes) as well as the increased

retention, an eluent comprising of 0.2 m*M* nitric acid eluent was used for retention studies of metal cations using GMA30 and GMA35. Interestingly, the GMA30 and GMA35 resulted in significant differences in the *k* values for Co(II) and Cd(II) allowing for the possibility of the separation of these two metals, which did not appear to be possible using GMA25. Cu(II) was retained > 60 minutes using GMA30 and GMA35.

Table 6.1: Retention factor values for transition and heavy metals using poly(GMA) IDA-modified polymer monoliths with increasing complexation capacity. Chromatographic conditions: effective column length: 140 mm, detection: on-column C^4D and flow-rate: 1 µL/min.

Monolith	*GMA15*	*GMA20*	*GMA25*	*GMA30*	*GMA35*
Eluent	0.1 m*M* nitric acid			0.2 m*M* nitric acid	
		k		*k*	
Mn(II)	-*	0.82	1.53	1.61	2.21
Co(II)	0.72	2.19	6.77	5.85	10.02
Cd(II)	0.72	2.21	6.61	8.18	13.18
Zn(II)	1.32	4.45	13.29	11.04	19.88
Cu(II)	-	-	-	-	-

-* unretained - not eluted

6.2.4 Comparison of metal cation retention and elution order using poly(VAL) IDA-modified polymer monoliths and poly(GMA) IDA-modified polymer monoliths.

Table 6.2 shows a comparison of *k* values obtained for poly(GMA) IDA-modified polymer monoliths and poly(VAL) IDA-modified polymer monoliths. The eluent used for the retention of the metal cations using VAL30 and GMA30 was 0.2 m*M* nitric acid. For all other monoliths, the eluent used was 0.1 m*M* nitric acid. Using VAL15, the retention of Mn(II), Co(II) and Zn(II) was not possible. Retention factors of 0.85 and 6.89 were obtained for Cd(II) and Cu(II) respectively. Retention of Mn(II) was also not possible using GMA15. Although retention of Co(II) and Zn(II) was achieved using GMA15, it is worth noting that the effective column length of all the poly(VAL) IDA-modified polymer monoliths was 100 mm, while the effective column length of poly(GMA) IDA-modified polymer monoliths was 140 mm.

Table 6.2: Comparison of *k* values for metal cations studied using poly(GMA) IDA-modified polymer monoliths and poly(VAL) IDA-modified polymer monoliths. Eluents used: VAL15, VAL 20 and VAL25: 0.1 m*M* HNO_3 and VAL30: 0.2 m*M* HNO_3

	VAL15	GMA15
	k	
Mn(II)	-	-
Co(II)	-	0.72
Zn(II)	-	1.32
Cd(II)	0.85	0.72
Cu(II)	6.89	-*
	VAL20	GMA20
	k	
Mn(II)	2.8	0.82
Co(II)	2.9	2.19
Zn(II)	3.36	4.45
Cd(II)	5.63	2.21
Cu(II)	11.76	-*
	VAL25	GMA25
	k	
Mn(II)	3.44	1.53
Co(II)	5.01	6.77
Zn(II)	5.23	13.29
Cd(II)	9.93	6.61
Cu(II)	23.5	-*
	VAL30	GMA30
	k	
Mn(II)	2.46	1.61
Co(II)	-▲	5.85
Zn(II)	-▲	11.04
Cd(II)	4.94	8.18
Cu(II)	9.94	-*

- not retained, - retained > 60 minutes, -▲Data not available*

A number of observations were noted when the retention of the metal cations using VAL20 were compared to GMA20. The elution order obtained for VAL20 was Mn(II) = Co(II) < Zn(II) < Cd(II) (although Zn(II) only showed a slight increase in retention in comparison to Co(II)). The elution order for the retention of the metal cations using GMA20 was Mn(II) < Co(II) = Cd(II) < Zn(II) demonstrating a change

in selectivity between the polymer monoliths as shown in Figure 6.3. Zn(II) eluted before Cd(II) using VAL20 and eluted after Cd(II) using GMA20.

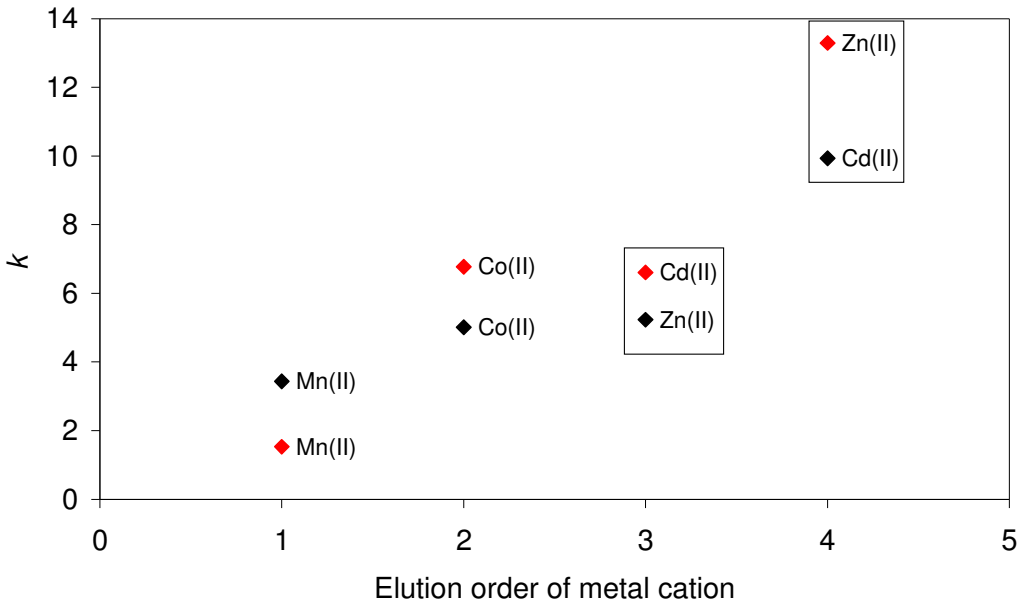

Figure 6.3: Order of elution of the four metal cations using monolith VAL25 (♦) and GMA25 (♦) showing the changes in selectivity.

Also worth noting is the similar *k* values observed for Mn(II) and Co(II) (*k* values of 2.8 and 2.9) which are well separated from Cd(II), which had a *k* value of 5.63 using VAL20 whereas using GMA20, Co(II) showed similar *k* values to Cd(II) (*k* values of 2.19 and 2.21) which were separated from Mn(II) which had a *k* value of 0.82. Increasing the chelation capacity resulted in improvements in the retention of Mn(II) from Co(II) using VAL25. Zn(II) exhibited a similar *k* value to Co(II) which were both well resolved from Cd(II) and as with GMA20, the elution order was Mn(II) < Co(II) < Cd(II) < Zn(II). The data for VAL30 published in Table 6.2 was obtained using an eluent comprising of 0.2 m*M* nitric acid. However, data was only obtained for Mn(II), Cd(II) and Cu(II). Using a 0.1 m*M* nitric acid eluent, the following *k* values were obtained: Mn(II) 8.26, Co(II) 11.02, Zn(II) 12.43, Cd(II) 21.14 and Cu(II) 45.22. Using a 0.2 m*M* nitric acid eluent, Mn(II) had a *k* value of 2.46, Cd(II) was 4.94 and Cu(II) was 9.94. As the order of elution for all poly(VAL) IDA-modified polymer monoliths did not change with an increase in eluent concentration, this would suggest that *k* values for Co(II) and Zn(II) using VAL30 with a 0.2 m*M* nitric acid

eluent would be between 2.5 and 4.94 and it would appear that the separation of Mn(II), Cd(II), Co(II) and Zn(II) would not be possible.

As mentioned above, increasing the concentration of the poly(GMA) from 25 % to 30 %, during the modification of the polymer monolith surface with IDA, resulted in clear differences in *k* values for Co(II) and Cd(II) which co-eluted using GMA25 and the ability to separated 4 metal cations using GMA30 and a 0.2 m*M* nitric acid eluent was possible. Finally, increased retention for Mn(II) was obtained for VAL20, VAL25 and VAL30 in comparison to their equivalent poly(GMA) IDA-modified polymer monoliths showing an increased affinity of the poly(VAL) IDA-modified polymer monoliths for Mn(II). With the poly(VAL) IDA-modified polymer monoliths, it was also possible to elute Cu(II) in the same run as Mn(II) and Cd(II). Cu(II) forms the most stable surface complexes with IDA of all the metals studied in this work, according to known stability constants of metals with IDA published in the literature [16]. Cu(II) was retained > 60 minutes in all cases using poly(GMA) IDA-modified polymer monoliths and it was not possible to detect Cu(II) in the same run as Mn(II), Co(II), Cd(II) and Zn(II) isocratically.

6.2.5 Comparison of elution order of metal cations using poly(VAL) IDA-modified polymer monoliths and poly(GMA) IDA-modified polymer monoliths with other IDA functionalised columns

As seen in Chapter 5.0, an elution order of Mn(II) < Co(II) < Zn(II) < Cd(II) < Cu(II) using a VAL30 polymer monolith was achieved (using a 0.1 m*M* nitric acid eluent). This was a similar elution order obtained by Barron *et al.* [52] using a ProPac IMAC-10 analytical column (10 μm polymeric beads coated with a poly(acrylate) layer with covalently attached poly-IDA groups). The authors obtained an elution order of Mn(II) < Co(II) < Zn(II) < Cd(II) while Pb(II) and Cu(II) were retained > 3 hours using a 0.2 m*M* nitric acid eluent. Using the GMA30 polymer monolith, an elution order of Mn(II) < Co(II) < Cd(II) < Zn(II) <<< Cu(II) was obtained demonstrating a change in the selectivity between the poly(VAL) IDA-modified polymer monolith and the poly(GMA) IDA-modified polymer monolith.

The elution order exhibited by the GMA30 monolith was similar to that obtained by Sugrue *et al.* [126] and Jones *et al.* [161]. Sugrue *et al*. [126] used a silica monolith, surface modified with IDA functionalities and obtained an elution order of Mn(II) < Co(II) < Cd(II) < Zn(II) <<< Cu(II) using an eluent comprising of 0.065 *M* KNO_3 and 0.035 *M* KCl. Jones *et al*. [161] observed an elution order of Mn(II) < Co(II) < Cd(II) < Zn(II) with an 8 m*M* nitric acid eluent, a column packed with 5 µm silica particles with bonded IDA (150 mm x 4 mm I.D.).

Table 6.3 shows a comparison of the column efficiency obtained for GMA30, VAL30 and other IDA functionalised polymer monoliths in the literature namely, a ProPac IMAC-10 column consisting of 10 µm diameter particles with attached IDA and a commercially available silica monolith, surface modified with IDA Clearly, there exists a large difference in column efficiency exhibited by the IDA modified silica monolith when compared to GMA30, VAL30 and the ProPac IMAC-10. Using the IDA modified silica monolith, Co(II) exhibited the highest peak efficiency, similar to that observed by GMA30. The data shown in Table 6.3 for the ProPac IMAC-10 column were obtained using optimised eluent conditions. Calculated efficiencies of 2,720 N/m and 3,900 N/m were obtained for Mn(II) and Cd(II) respectively using an eluent consisting of 0.25 m*M* nitric acid, similar to the eluent used with the GMA30 monolith. This demonstrated similarities in the efficiencies obtained for Mn(II) using the ProPac IMAC-10 column and GMA30, while Cd(II) showed improved efficiency with the GMA30.

Peak efficiencies obtained for GMA30 were superior to those obtained using VAL30 when C^4D was used as the mode of detection. However, an improvement in peak efficiency was obtained for VAL30 using UV-Vis detection at 500 nm following reaction of the eluted metals with PAR when compared to the peak efficiencies obtained using on-column C^4D detection. It is worth pointing out that the effective column length of VAL30 using on-column C^4D detection was 100 mm while the effective column length using UV-Vis detection was 140 mm. The increase in the effective column length of VAL30 using UV-Vis detection was due to the placement of a post column reactor at the end of the column, thus increasing the column length. This may have accounted for the increase in efficiency noted for the metal cations detected using UV-Vis detection.

Table 6.3: Comparison of efficiency of poly(GMA) IDA-modified polymer monoliths and poly(VAL) IDA-modified polymer monoliths with other IDA functionalised columns.

	GMA30 *(140 mm x 100 µm I.D* [a]	*VAL30* *(100 mm x 100 µm I.D)*		*ProPac IMAC-10* *(50 mm x 2 mm I.D)*[c] *[17]*	*Silica monolith (100 mm x 4.6 mm I.D)*[d] *[18]*
Detection	*C^4D*	*C^4D*	*UV-Vis*	*UV-Vis*	*UV-Vis*
	N/m	N/m	N/m	N/m	N/m
Mn(II)	2,310	930	1,300	3,470	16,300
Co(II)	7,480	1,250[b]	-	4,500	27,530
Cd(II)	5,900	2,700	3,300	10,060	9,400
Zn(II)	4,579	3,100	3,600	10,420	16,450

Eluents: *a = 0.2 mM HNO_3,*

b = 0.1 mM HNO_3,

c = 0.25 mM HNO_3–10 mM KCl,

d = 0.2 M KCl

6.2.6 Separation of metal cations using poly(GMA) IDA-modified polymer monoliths

Separations of metal standard samples were carried out on all five polymer monoliths and the chromatographic performance compared, which can be seen in Table 6.4. Figure 6.4(a) shows an overlay of separations of Mn(II), Cd(II) and Zn(II) using GMA15 and GMA20. Both separations were carried out using a 0.1 m*M* HNO_3 eluent. Mn(II) was not retained using GMA15, Cd(II) co-eluted with the void peak and baseline resolution between Cd(II) and Zn(II) was 1.4. Clearly, an increase in the chelating capacity (from GMA15 monolith to GMA20) resulted in the retention of Mn(II) and the ability to separate three metal cations, therefore resulting in improved separation capability. Baseline resolution of Mn(II) and Cd(II) was achieved (resolution of 1.6), however a resolution for Cd(II) and Zn(II) was only 1.2, therefore baseline resolution was not achieved between these two metals. Peak asymmetry improved for all metals using GMA20 with Zn(II) showing a peak asymmetry of 2.8

for GMA15 and 1.5 for GMA20. Although peak shape was improved using GMA20, large increases in peak width (calculated at 50 % peak height) were observed. Peak width for Zn(II) using GMA15 was 0.34 minutes and for GMA20 was 1.95 minutes, an increased peak width of 82.

Baseline resolution of all three metals was achieved, with Mn(II) well resolved from the void. As seen previously, an increased chelation capacity resulted in improvements in peak shape with Zn(II) exhibiting a peak asymmetry of 1.1 and Mn(II) of 1.3. Peak shape for Cd(II) remained unchanged at 1.2 when compared to GMA20. A peak width of 3.5 minutes was observed for Zn(II) using GMA25. Figure 6.4(b) also shows a chromatogram obtained for the retention of Co(II). A k value of 6.77 was obtained for Co(II) which was similar to the k value of 6.78 obtained for Cd(II). Using GMA25, it was only possible to separate Mn(II), Cd(II) and Zn(II). Increasing the complexation capacity resulted in a decrease in column efficiency. A decrease in column efficiency of ~ 50 % was observed for Zn(II) and 35 % for Cd(II) when GMA15 was compared to GMA25. In this case, increasing the complexation capacity resulted in slower association/dissociation kinetics, which had a deleterious effect on peak efficiency and peak width.

Table 6.4: Chromatographic performance data obtained for the separation of Mn(II), Cd(II) and Zn(II) using GMA15, GMA20 and GMA25 and separations of Mn(II), Co(II), Cd(II) and Zn(II) using GMA30 and GMA35.

Monolith	*Metal*	*k*	*N/m*	*Asy.*	*Resolution*
GMA15	Mn(II)	-	-	-	-
	Cd(II)	0.69	1,650	1.6	-
	Zn(II)	1.32	2,600	2.8	1.4
GMA20	Mn(II)	0.81	1,020	1.5	1.9
	Cd(II)	2.20	800	1.2	1.6
	Zn(II)	4.40	525	1.5	1.2
GMA25	Mn(II)	1.61	1,100	1.3	3.0
	Cd(II)	6.78	1,060	1.2	3.1
	Zn(II)	14.72	1,230	1.1	2.2
GMA30	Mn(II)	1.39	2,310	4.2	3.3
	Co(II)	5.51	7,480	2.1	6.2
	Cd(II)	6.89	5,900	3.2	1.5
	Zn(II)	10.88	4,570	3.7	2.7
GMA35	Mn(II)	2.31	1,790	2.5	4.0
	Co(II)	10.05	4,680	1.6	7.3
	Cd(II)	12.71	4,045	2.7	1.5
	Zn(II)	19.09	4,080	2.0	3.3

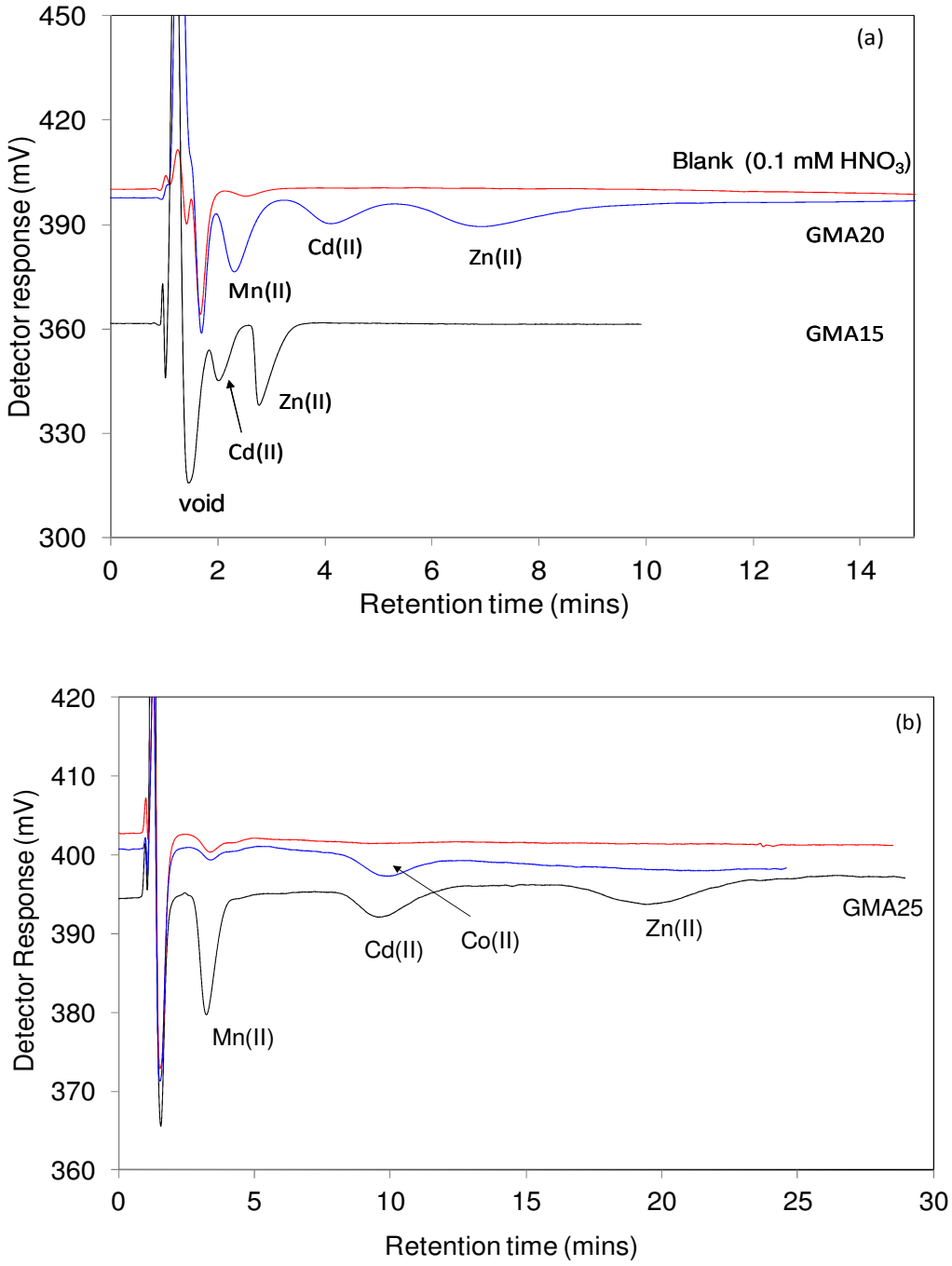

Figure 6.4: (a) Overlay of a separation of 5 ppm Mn(II), 10 ppm Cd(II) and 10ppm Zn(II) using GMA15 and GMA20. (b) Separation of 5 ppm Mn(II), 10ppm Cd(II) and 10ppm Zn(II) using GMA25 overlaid with a 10 ppm Co(II) standard. Chromatographic conditions: Eluent: 0.1 m*M* HNO_3, flow-rate: 1 µL/min, injection volume: 100 nL, detection: on-column C^4D, effective column length: 14 cm

Figure 6.5(a) shows an overlay of separations of Mn(II), Co(II), Cd(II) and Zn(II) using GMA30 and GMA35. The chromatographic performance data can be seen in Table 6.4. Due to the increased capacity of GMA30 and GMA35**,** the eluent used was 0.2 m*M* HNO_3. Figure 6.4(b) above shows an overlay of Co(II) with a separation of Mn(II), Cd(II) and Zn(II) using GMA25 demonstrating that the separation of these four metals was not possible. Using GMA30, an increase in the number of chelating moieties resulted in the ability of obtain baseline resolution of Co(II) and Cd(II). Significant increases in column efficiency were also observed using GMA30 when compared to GMA25**.** An increase in efficiency of 52 % was observed for Mn(II), 87 % for Co(II), 82 % for Cd(II) and 73 % for Zn(II).

A further increase in the complexation capacity (GMA35) resulted in a decrease in efficiency when compared to GMA30. A decrease in efficiency of 23 % was observed for Mn(II), 37 % and 31 % for Co(II) and Cd(II) respectively and 10 % for Zn(II). Although a decrease in efficiency was observed between GMA30 and GMA35, improvements in peak shape were noted, particularly for Mn(II) and Zn(II). A peak asymmetry of 4.2 and 3.7 was noted for Mn(II) and Zn(II) using GMA30 whereas a peak asymmetry of 2.5 and 2.0 was obtained for Mn(II) and Zn(II) using GMA35. Significant increases in peak width were also obtained when GMA30 was compared to GMA35**,** with Zn(II) showing an increase in peak width of 40 %.

Cu(II) was retained > 60 minutes using GMA30 and GMA35 with a 0.2 m*M* HNO_3 eluent and it was not possible to separate Cu(II) in the same run as Mn(II), Co(II), Cd(II) and Zn(II).

Figure 6.5(b) shows an overlay of $n = 5$ separations of Mn(II), Co(II), Cd(II) and Zn(II) using GMA30 and an eluent consisting of 0.2 m*M* HNO_3. Retention time precision was calculated to be < 1.5 % for Mn(II), Co(II) and Cd(II) and < 1.9 % for Zn(II). Retention time precision was also calculated for GMA35 and was < 2 % for Co(II), Cd(II) and Zn(II) and < 2.6 % for Mn(II).

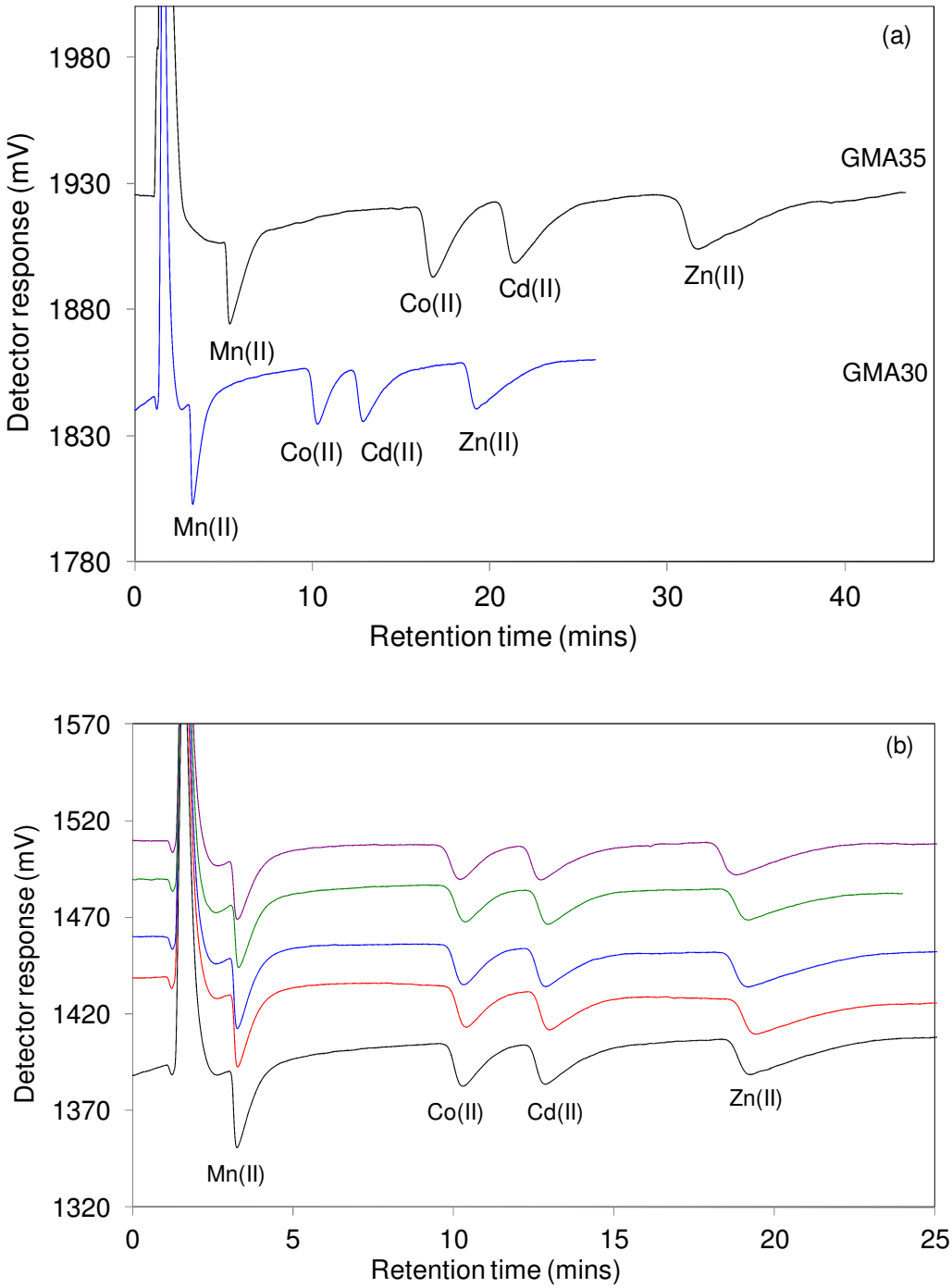

Figure 6.5: (a) Overlay of separations of 5 ppm Mn(II), 10 ppm Co(II), 10 ppm Cd(II) and 10 ppm Zn(II) using GMA30 and GMA35. (b) Overlay of separations of the metals standards carried out using GMA30. Chromatographic conditions: Eluent: 0.2 m*M* nitric acid. All chromatographic conditions as in Figure 6.4.

6.2.7 Column to column reproducibility

To investigate the reproducibility of the monolith fabrication and functionalisation procedure, 4 GMA30 monoliths and 4 GMA35 monoliths were prepared. Separations of Mn(II), Co(II), Cd(II) and Zn(II) were carried out on all monoliths and the chromatograms obtained using the 4 GMA30 monoliths can be seen in Figure 6.6. Retention time precision was calculated to be < 12 % for Co(II) and Zn(II) and < 14 % for Mn(II) and Cd(II) whereas the retention time precision using the 4 GMA35 monoliths was 13 % for Cd(II), 16 % for Co(II) and Zn(II) and 19 % for Mn(II).

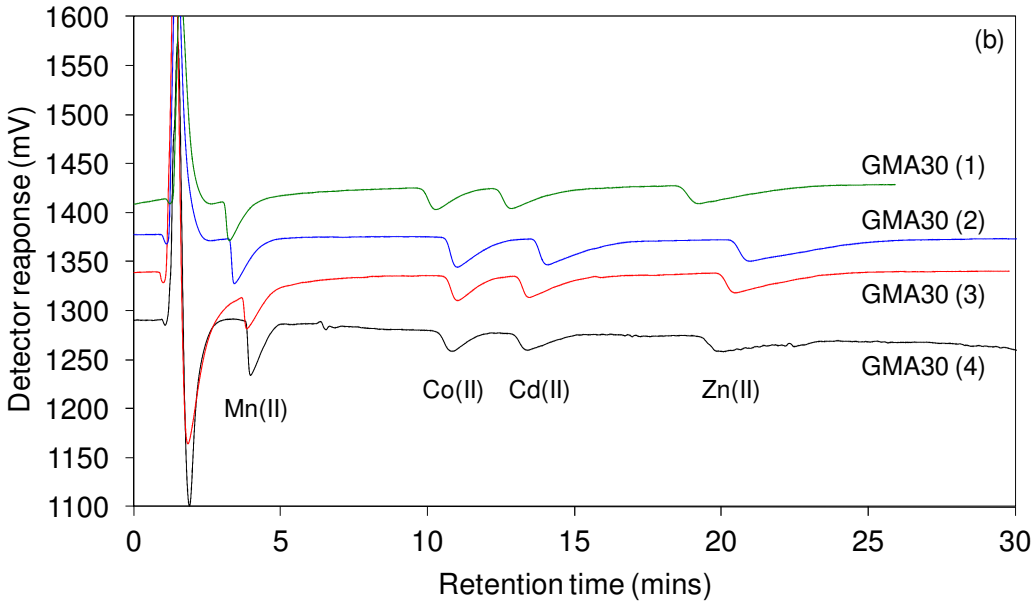

Figure 6.6: Overlay of separations of 5 ppm Mn(II), 10 ppm Co(II), 10 ppm Cd(II) and Zn(II) using 4 GMA30 monoliths. Chromatographic conditions: As in Figure 6.4.

6.2.8 Alkaline earth metals

The retention of alkaline earth metals using GMA25, GMA30 and GMA35 was studied. The effective column length for the separations of transition and heavy metals shown previously was 140 mm to allow direct comparison of each monolith. An advantage of using on-column C^4D is the ability to place the detector cell at various locations along the column, thus demonstrating a non-destructive method of varying the effective column length. For the retention of alkaline earth metals, the detector

cell was placed as close to the end of the column outlet as possible. Table 6.5 shows the chromatographic performance data obtained for Mg(II), Ca(II), Sr(II) and Ba(II) using GMA25, GMA30 and GMA35.

Table 6.5: Chromatographic performance data for alkaline earth metals using various GMA-IDA monoliths. Chromatographic conditions: Eluent: as specified in table, metals standard concentration: 5 ppm. All other condition as in Figure 6.4.

Monolith	*Metal*	*k*	*N/m*	*Column dimensions*	*Eluent (HNO_3)*
GMA25	Mg(II)	0.43	1,040	190 mm x 100 µm	0.1 m*M*
	Ca(II)	0.53	1,170		
	Sr(II)	0.55	1,110		
	Ba(II)	0.60	1,190		
GMA30	Mg(II)	1.48	3,300	250 mm x 100 µm	0.2 m*M*
	Ca(II)	1.79	2,400		
	Sr(II)	-	-		
	Ba(II)	1.80	2,350		
GMA35	Mg(II)	2.29	1,290	190 mm x 100 µm	0.2 m*M*
	Ca(II)	3.06	1,890		
	Sr(II)	3.24	3,620		
	Ba(II)	3.76	4,460		

- not injected

From Table 6.5, *k* values obtained for GMA25 were similar for all four alkaline earth metals studied. Peaks widths (calculated at 50 % peak height) were ~ 0.3 minutes for each metal cation and separation was not possible. As the eluent was 0.1 m*M* $HN0_3$, it would be difficult to accurately reduce the concentration of the eluent to a lower concentration to try and improve resolution. Also, the column would have to be significantly longer, so as to allow separation of the alkaline earth metals. Using GMA30, differences in the *k* values of the alkaline earth metals were obtained,

allowing the separation of Mg(II) and Ca(II), which can be seen in Figure 6.7. Ba(II) and Ca(II) had similar *k* values and separation was not possible. The retention of alkaline earth metals was also studied using GMA35. Using a 0.2 m*M* nitric acid eluent baseline separations of Mg(II) and Ca(II) were achieved (resolution of 1.63). An elution order of Mg(II) < Ca(II) < Sr(II) < Ba(II) was obtained and this shows that ion exchange appeared to be the dominant separation mechanism and retention was due to the formation of electrostatic interactions between the chelating ligand and the metal cations. Mg(II) showed significant peak tailing at 5 ppm (asymmetry of 5.90) but was greatly improved when the concentration was reduced to 0.5 ppm, where a peak asymmetry of 1.62 was obtained. Figure 6.7 also shows a separation of 0.5 ppm Mg(II), 1 ppm Ca(II) and 5 ppm Ba(II) and as can be seen from this plot, baseline resolution between Ca(II) and Ba(II) was not achieved (resolution of 0.86 was obtained). Sr(II) co-eluted with Ca(II) and baseline separation was not possible.

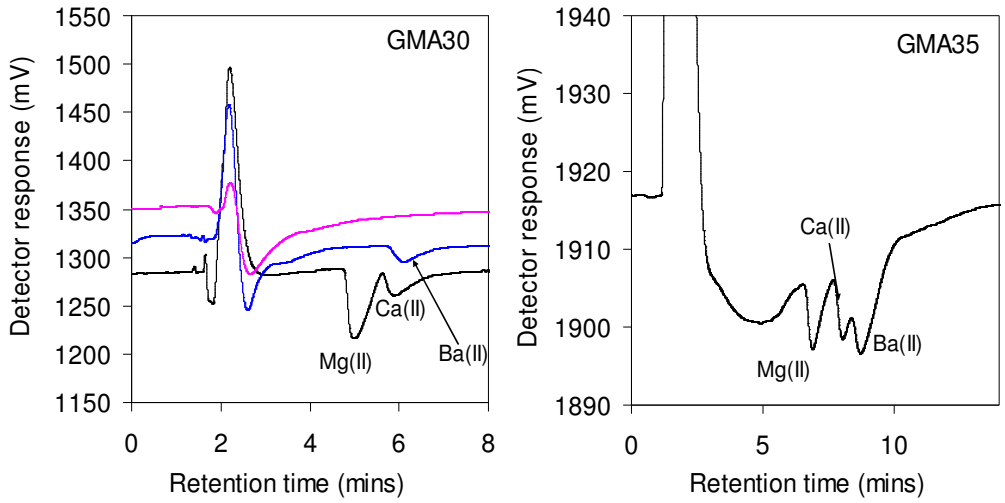

Figure 6.7: (left) Separation of 1 ppm Mg(II) and 5 ppm Ca(II) overlaid with 5 ppm Ba(II) using GMA30. (right) Separation of 0.5 ppm Mg(II), 1 ppm Ca(II) and 5 ppm Ba(II). Chromatographic conditions: Eluent: 0.2 m*M* HNO_3, effective column length: 250 mm (GMA30) and 190 mm (GMA35). All other conditions as in Figure 6.4.

6.2.9 Application of poly(GMA) IDA-modified polymer monoliths

6.2.9.1 Determination of Mg(II) and Ca(II) in a bottled water sample

Due to the ability of GMA35 to separate Mg(II) and Ca(II), the GMA35 monolith was applied to the determination of Mg(II) and Ca(II) in a bottled water sample. Linearity plots were constructed for Mg(II) and Ca(II) and can be seen in Figure 6.8. R^2 values of > 0.999 were obtained for both calibration curves.

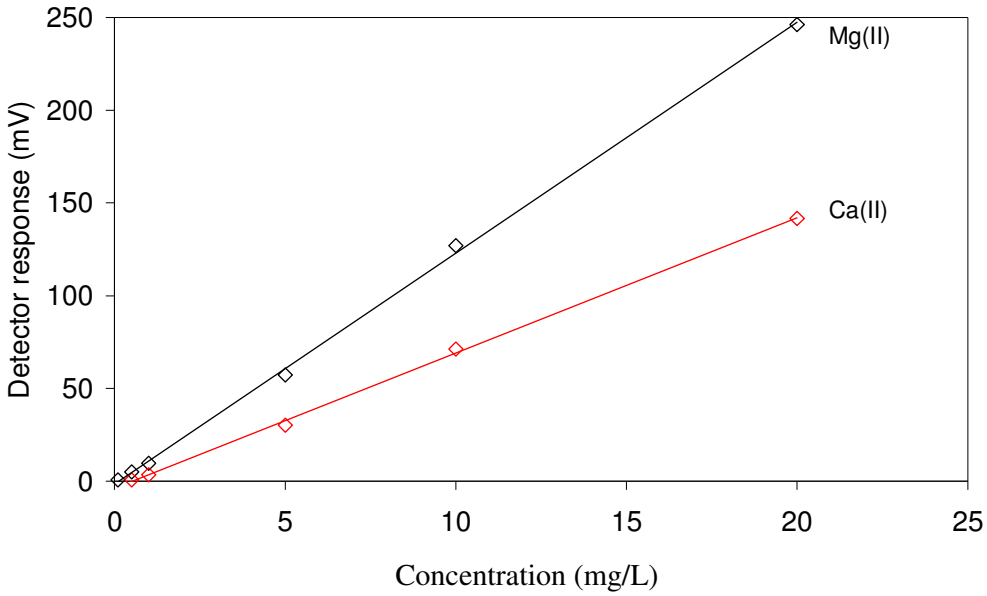

Figure 6.8: Linearity plots for Mg(II) and Ca(II) using GMA35 of concentration (mg/L) of Mg(II) and Ca(II) versus detector response (mV)

Figure 6.9 shows the chromatogram obtained for the determination of Mg(II) and Ca(II) in a bottled water sample (100 fold dilution) overlaid with the same concentration of a Mg(II) and Ca(II) standard (0.8 ppm Ca(II) and 0.25 ppm Mg(II)). A 100 fold dilution of the bottle water sample was required to obtain baseline resolution between Mg(II) and Ca(II). Using the peak areas obtained for the 100 fold dilution of the bottled water sample, the concentration of Ca(II) and Mg(II) were calculated using the equation of the line obtained from the linearity graph in Figure 6.8. The concentration of Ca(II) was calculated to be 77 ppm and the concentration of Mg(II) was calculated to be 28 ppm. According to the manufacturer's claims from the

label on the bottled water sample, the concentration of Ca(II) was 80 ppm and the concentration of Mg(II) was 26 ppm.

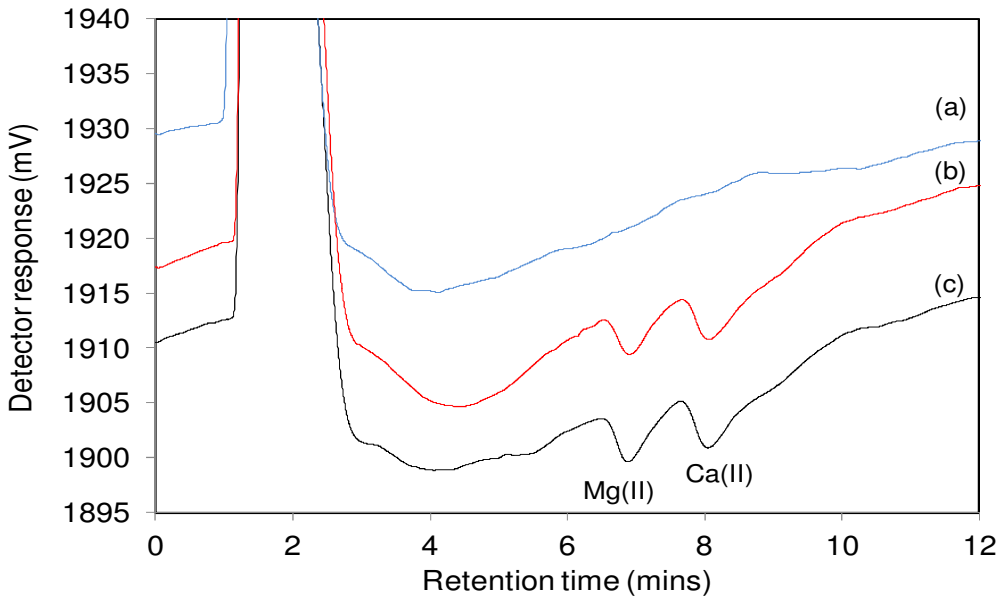

Figure 6.9: Overlay of chromatograms obtained for (a) blank sample (0.2 m*M* nitric acid), (b) 0.8 ppm Ca(II) and 0.25 ppm Mg(II) standard and (c) 100 fold dilution of the bottled water sample. Chromatographic conditions: Eluent: 0.2 m*M* nitric acid. All other conditions as in Figure 6.4.

6.2.9.2 Simulated seawater analysis

The determination of metals in seawater samples using conventional ion exchangers has the disadvantage in that the high concentration of salt ions present in the seawater sample would swamp the ion exchange sites available on the stationary phase matrix [135]. The use of chelating ion exchange can overcome this problem due to the reduced affinity of the chelating ligand for the alkali metals. Alkali metals form weak coordinate bonds with the chelating ligand. As the retention of metal cations is based on the formation of stability constants between the metal cation and the chelating ligand, the high ionic strength of seawater samples should have little effect on retention of the metal cations.

Figure 6.10 shows a separation of a standard solution containing Mg(II), Mn(II), Co(II), Cd(II) and Zn(II) using GMA30 with an effective column length of 250 mm. The elongation of the effective column length, to facilitate the resolution of Mn(II) from Mg(II) and Ca(II), resulted in an increase in the run–times for the separation of Co(II), Cd(II) and Zn(II). A total run-time of 40 minutes was observed when the effective column length was 250 mm as opposed to a run-time of 25 minutes when the effective column length was 140 mm. Due to the inability to resolve Mn(II) from Ca(II) and Mg(II), the effective column length was reduced to 100 mm and the effect of ionic strength on the retention of Co(II), Cd(II) and Zn(II) was studied.

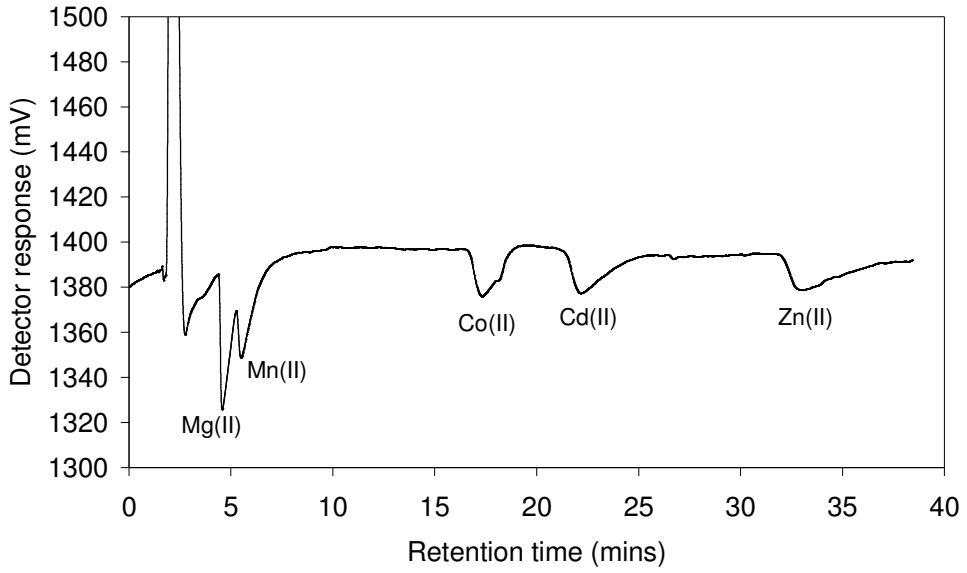

Figure 6.10: Separation of 5 ppm Mg(II), 5 ppm Mn(II), 10 ppm Co(II), Cd(II) and Zn(II) using GMA30. Chromatographic conditions: Eluent: 0.2 mM nitric acid, effective column length: 250 mm. All other conditions as in Figure 6.4.

A simulated seawater sample was prepared to investigate the effect of ionic strength on the retention of the metal cations. Figure 6.11 shows a separation of a 10 fold dilution of the simulated seawater sample spiked with 10ppm Co(II), Cd(II) and Zn(II) (a) overlaid with a standard solution containing only the metals (b). The plot also shows a 10 fold dilution of the un-spiked simulated seawater sample. From this plot, the effect of ionic strength (10 fold dilution, therefore concentration of Na^+ is ≈ 3,300 ppm) on the retention time of the metals appears to be minimal. Retention times of 7.4, 8.5 and 12.6 minutes were obtained for Co(II), Cd(II) and Zn(II) standards

respectively while retention times of the metals in the spiked simulated seawater samples were 7.3, 8.6 and 12.4 minutes for Co(II), Cd(II) and Zn(II) representing a difference of < 1.6 % in retention times. Retention factor values were not calculated due to the inability to accurately integrate the void peak in the high ionic strength samples as the conductivity reached a maximum of 2500 mV (Figure 6.12). The spiked simulated seawater sample also contained 110 ppm Mg(II) and 40 ppm Ca(II) which were unretained (or very slightly retained).

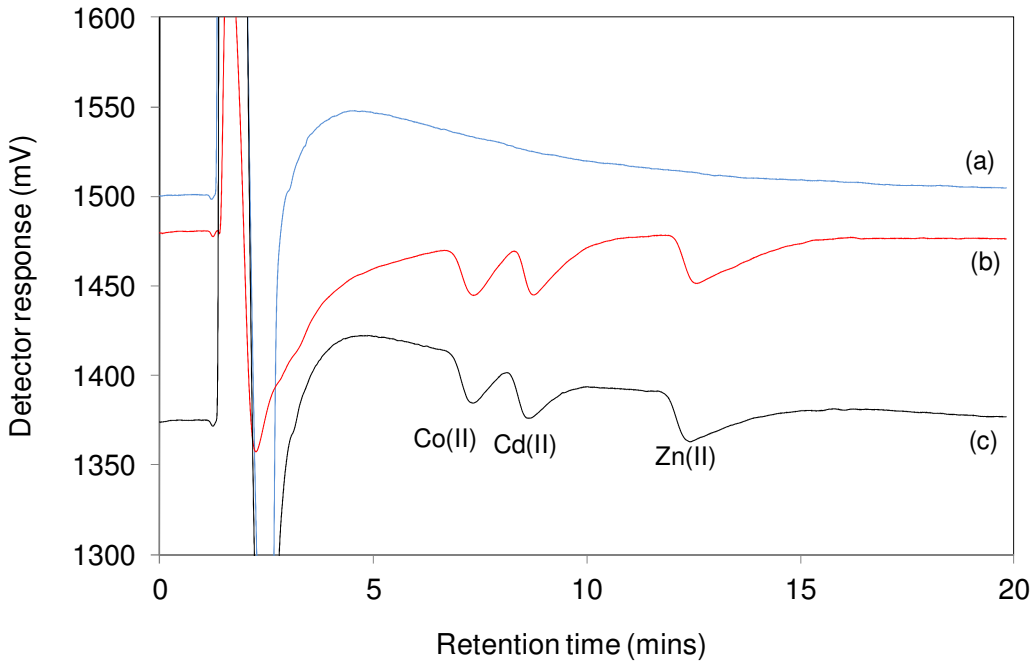

Figure 6.11: Overlay of 10 fold dilution of spiked pseudo seawater sample (a), 10 ppm Co(II), Cd(II) and Zn(II) standard solution (b) and un-spiked pseudo seawater (c). Chromatographic conditions: Column: GMA30, effective column length: 100 mm, eluent: 0.2 m*M* HNO_3. All other conditions as in Figure 6.4.

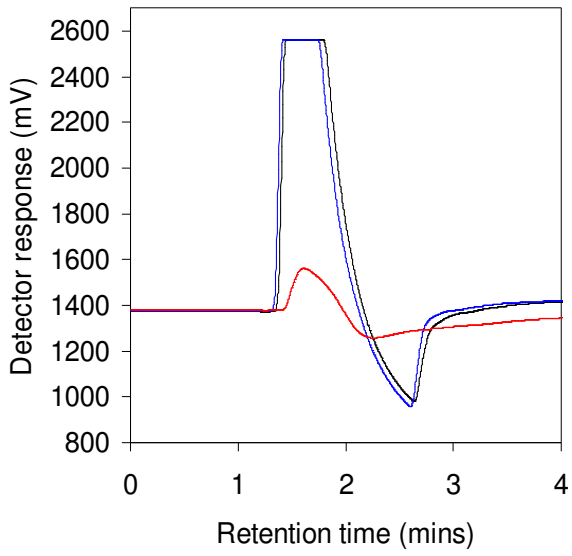

Figure 6.12: Void peaks for injections of spiked pseudo seawater (black), un-spiked pseudo seawater (blue) and 10 ppm Co(II), Cd(II) and Zn(II) (red). The high ionic strength of the samples resulted in a maximum conductivity at 2500 mV. The void peaks contained high concentrations of Mg(II) and Ca(II) which were unretained.

6.2.9.3 Separation of transition metals in seawater samples

The retention of transition and heavy metals was investigated using real seawater samples. The seawater samples were obtained from Quays beach in Co. Clare (seawater sample 1) and Ringsend, Co Dublin (seawater sample 2). Figure 6.13 shows a 10 fold dilution of a seawater sample spiked with 10 ppm Co(II), Cd(II) and Zn(II).

As mentioned previously, *k* values could not be determined due to the high ionic strength of the seawater sample reaching a maximum conductivity at 2500 mV in the void peak (see Figure 6.12), therefore retention times were compared. It is also worth pointing out the error associated with the comparison of retention times and not *k* values. For seawater sample 1, differences in retention times of 2.2 % for Co(II), 1.4 % for Cd(II) and 4.5 % for Zn(II) were observed when the retention times of the spiked seawater sample were compared to the retention times obtained for the metal cation standard mixture. For seawater sample 2, differences in retention times of 3.7 % for Co(II), 2.7 % for Cd(II) and 5.5 % for Zn(II) were obtained.

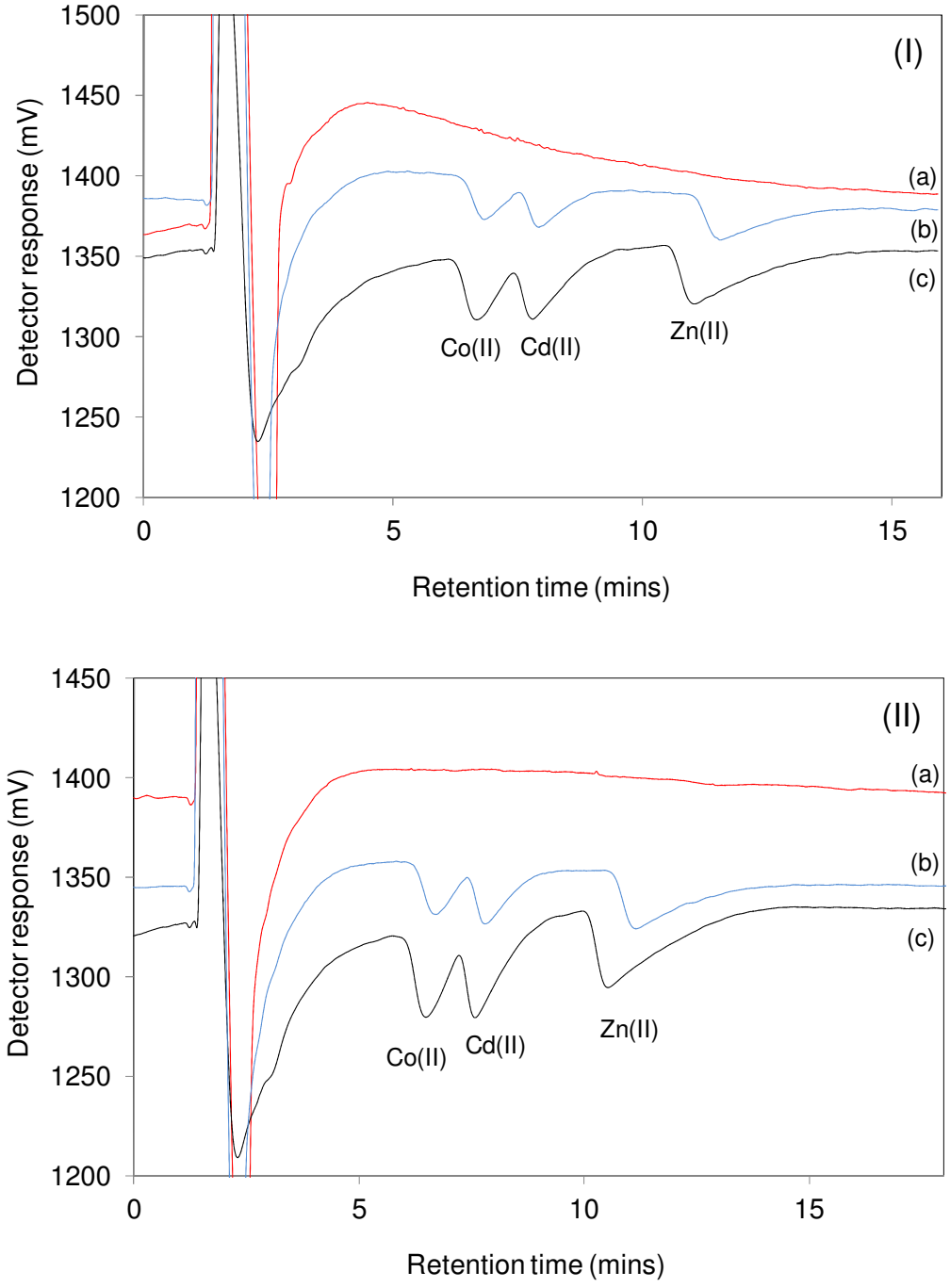

Figure 6.13: Metal analysis of seawater samples from (I) Quays beach, Co. Clare and (II) Ringsend, Co. Dublin where (a) is unspiked seawater sample, (b) 10 ppm Co(II), Cd(II) and Zn(II) standards (b) and spiked seawater (c). Chromatographic conditions: Eluent: 0.2 m*M* HNO_3, column: GMA30, effective column length: 100 mm. All other conditions as in Figure 6.4.

Figure 6.13 demonstrates the ability of the chelating polymer monolith to separate Co(II), Cd(II) and Zn(II) in the presence of 3,300 ppm NaCl as well as in the presence of 40 ppm Ca(II) and 110 ppm Mg(II). The separation of metal cations in seawater samples shown above could only be carried out by spiking the seawater with the metal cations. As transition and heavy metals are available in trace levels, a pre-concentration step is required. Rahmi *et al.* [139] recently reported the use of GMA-*co*-EDMA monoliths, fabricated in commercially available syringe filter tips, for the solid phase micro-extraction of 29 transition/heavy metals and rare earth elements prior to their determination by ICP-MS.

6.2.9.4 Separation of transition metals in a tap water sample

A tap water sample was taken from within the research laboratory and spiked with 10 ppm Co(II), Cd(II) and Zn(II). The sample was filtered prior to use and no dilution of the tap water sample was required. Figure 6.14 shows a separation of Co(II), Cd(II) and Zn(II) in a spiked tap water sample (black trace) overlaid with a standard mixture containing Co(II), Cd(II) and Zn(II) (blue trace). Figure 6.14 also shows the chromatogram obtained for the un-spiked tap water (red trace). Retention factors of 3.49, 4.45 and 6.81 were obtained for Co(II), Cd(II) and Zn(II) respectively in the metal standard mixture while k values of 3.48, 4.31 and 6.58 were obtained for Co(II), Cd(II) and Zn(II) in the spiked tap water sample. Differences in k of 0.29 % were observed for Co(II), 3.14 % for Cd(II) and 3.4 % for Zn(II).

No metal peaks were observed in the un-spiked tap water sample, therefore future work would include a pre-concentration step prior to the determination of metals in tap water samples.

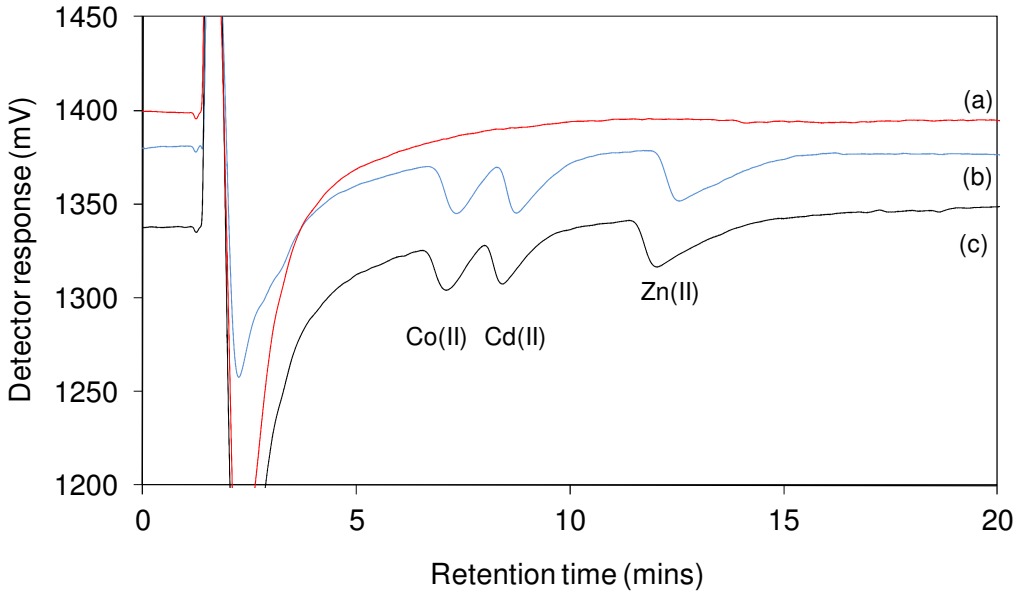

Figure 6.14: Un-spiked tap water (a), 10 ppm Co(II), Cd(II) and Zn(II) standards (b) and tap water sample spiked with 10 ppm Co(II), Cd(II) and Zn(II) (c). Chromatographic conditions as in Figure 6.4.

6.2.10 Column stability

Throughout this work, it was noticed that the stability of the column deteriorated over time (i.e. a loss of retention of the metal cations), therefore stability of GMA30 was closely monitored. The column volume was calculated to be 1.2 µL, (calculated taking the porosity into account). Throughout the life-time of GMA30, it was calculated that 7,980 µL of the eluent (0.2 m*M* nitric acid) had passed through the column before a complete loss of retention was observed, which translated into 6,650 column volumes. The number of column volumes that passed through the column when a change in retention was observed was 5,450.

Figure 6.15 shows an overlay of chromatograms obtained for the separations of Co(II), Cd(II) and Zn(II) over a 12 hour period (when a loss of retention was first observed). Within this time frame, a decrease in *k* of 26 % was observed for Co(II), 30 % for Cd(II) and 31 % for Zn(II)

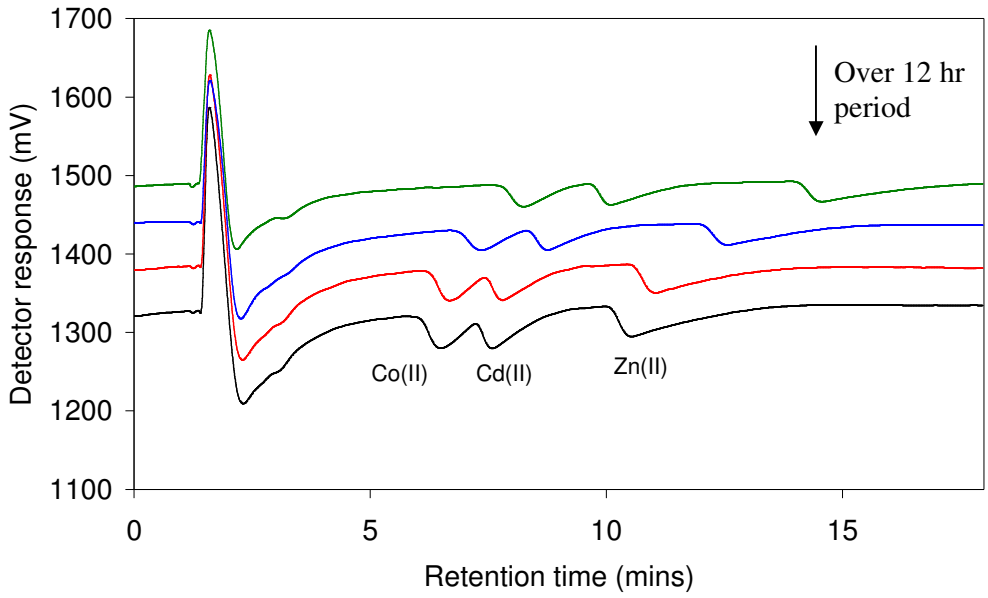

Figure 6.15: Overlay of chromatograms of Co(II), Cd(II) and Zn(II) obtained over a 12 hour period. Chromatograms offset for clarity. All other chromatographic conditions as in Figure 6.4.

6.3 Conclusions

LMA-*co*-EDMA polymer monoliths were fabricated and surface modified with IDA using photo-grafting techniques. Attachment of the IDA was possible through the ring opening of the epoxide group on the GMA structure, which was used to attach the IDA. Scanning C^4D techniques were used to characterise the chelating stationary phase with results showing that an increase in the complexation capacity resulted in an increase in the conductive response during scanning of each monolith. Results also showed that the axial distribution of the IDA groups were homogeneous along the length of the column with % RSD values < 1 %. Increasing the GMA concentration from 20 % to 35 % during the grafting step resulted in a linear increase in the conductive response during the C^4D scanning of each monolith. As the same detector settings and ethanolamine buffer were used for the C^4D scanning the poly(GMA) IDA-modified polymer monoliths were also used during the C^4D scanning of the poly(VAL) IDA-modified polymer monoliths in Chapter 5.0, it was possible to compare the C^4D scans obtained in both sections of work. Results showed that the use of higher concentrations of GMA (30 and 35 %) during the modification of the

monolith surface with IDA, resulted in an increased conductive response during scanning C^4D profiling when compared to VAL30 and VAL35, suggesting that an increased surface coverage of IDA was achieved using poly(GMA) as the IDA linker. The use of scanning C^4D profiling used throughout this work demonstrated the vast amount of information to be gained during the fabrication of new stationary phases

The poly(GMA) IDA-modified polymer monoliths were used for retention of selected metal cations. The elution order obtained for the retention of Mn(II), Co(II), Cd(II) and Zn(II) was different that obtained using the poly(VAL) IDA-modified polymer monoliths. A reversal in selectivity of Cd(II) and Zn(II) was obtained using GMA-IDA when compared to poly(VAL) IDA-modified polymer monoliths demonstrating that the linker used in the attachment of the IDA functionalities has an overall effect on the selectivity of the metal cations during chromatographic applications.

Overall, the use of poly(GMA) for the attachment of IDA, as opposed to poly(VAL), produced a more efficient stationary phase when chromatographic performance data was compared. From the analysis carried out in this work, it seemed that the most efficient results were obtained using a polymer monolith with an increased chelating ligand density used in conjugation with a higher concentration of eluent (i.e. GMA30 used with a 0.2 m*M* HNO_3 eluent resulted in a more efficient column in comparison to GMA25 used with an eluent comprising of 0.1 mM HNO_3)

Chapter 7.0:

Final conclusions and summations

To date, little work has focused on the incorporation of ion exchange functionalities on polymer monolith substrates for the separation of small ions using photo-grafting techniques. In this work, polymer monoliths were fabricated and subsequently functionalised producing ion exchange polymer monoliths. Anion exchange monoliths were prepared by photo-grafting chains of poly(META). The poly(META) polymer monolith was applied to the separation of a six standard mix. Peak efficiencies were comparable to other work carried out using other polymer monoliths. Retention time precision was < 3 % for all six anions studied. Absolute LOD limits between 0.1 and 0.4 pmole were obtained which were comparable to other portable chromatography systems in the literature. The fabrication of the poly(META) polymer monolith worked well and showed the ability to retain a large number of organic and inorganic anions.

Alkaline earth metals were separated using a cation exchange polymer monolith, again prepared using photo-grafting techniques. Separation efficiency and resolution was poor demonstrating the low capacity exhibited by these monoliths. Increase in the ion exchange capacity could have been increased using an increased concentration of poly(SPM) during the functionalisation procedure. Temperature studies were carried out using an inexpensive capillary column heater, which was constructed using a flexible heating tape. The fabrication of the column heaters were easily incorporated into the system.

Ion exchange polymer monoliths with attached chelating ligands were prepared and used for the separation of metal cations. In this work, two methods of IDA attachment were investigated. The first method involved the covalent attachment of IDA to poly(VAL) photo-grafted on the monolith surface and the second method involved the attachment of IDA on a poly(GMA) polymer monolith through ring opening of the epoxy groups. The use of photo-grafting techniques allows the ability to increase the surface coverage of the attached chelating ligand by increasing the concentration of the VAL or GMA during the photo-grafting step.

C^4D has been used for a number of years as a detection device in capillary chromatography and more recently it has become clear that valuable information can be gained from scanning the entire length of the column and measuring the conductive

response at pre-defined intervals. As well as measuring the axial distribution of IDA along the column length, scanning C^4D plots also showed an increase in conductive response with an increase in the poly(VAL) or poly(GMA) concentrations used during photo-grafting. In the work in this thesis, a wealth of knowledge was obtained from constructed scanning C^4D profiles. Characterisation of the IDA modified polymer monoliths was possible without destruction of the monolith and any anomalies associated with the stationary phase could be detected prior to chromatographic applications. While the longitudinal homogeneity obtained during the scanning of the IDA monoliths prepared using poly(VAL) showed an even distribution of the IDA groups (% RSD of 3 %), this was further improved upon when IDA was immobilised through the use of poly(GMA). Excellent longitudinal homogeneity was obtained (% RSD of < 1 %). This improvement suggests a more quantitative conversion (to bonded IDA groups) of available attachment sites with grafted poly(GMA) than achieved with the previous poly(VAL) grafted monoliths.

The IDA modified polymer monoliths (prepared using poly(GMA) were applied to the determination of Ca(II) and Mg(II) in a bottled water sample. The results obtained were comparable to the manufacturer's claims. A simple dilution step was required prior to the separation of the alkaline earth metals. The poly(GMA) monoliths were also used for the separation of transition metals in high ionic strength samples.

The use of the chelating polymer monoliths demonstrated in this work were useful for the separation of metal cations. The work presented in this thesis on the use of polymer monoliths with attached chelating ligands for the separation of metal cations, resulted in the first publication on the topic. In the future, the use of capillary chelating polymer monoliths may replace other method of metal determination, such as atomic absorption spectroscopy.

Chapter 8.0:

References

[1] H. Small, T. Stevens, W. Bauman, *Analytical Chemistry*, 47 (1975)1801-1809.

[2] P. R. Haddad, P. E. Jackson, *Ion Chromatography: Principles and Applications,* (1990), Elsevier, Amsterdam.

[3] A. Krata, V. Kontozova-Deutsch, L. Bencs, F. Deutsch, R. Van Grieken, *Talanta,* 79 (2009) 16-21.

[4] R. Kadnar, *Journal of Chromatography A*, 804 (1998) 217-221.

[5] H. Small, *Journal of Chemical Education*, 81 (2004) 1277-1284.

[6] J. Fritz, *Journal of Chromatography A*, 1039 (2004) 3-12.

[7] C. Sarzanini, *Journal of Chromatography A,* 956 (2002) 3-13.

[8] P. R. Haddad, P. N. Nesterenko, W. Buchberger, *Journal of Chromatography A,* 1184 (2008) 456-473.

[9] C. A. Lucy, *Journal of Chromatography A,* 739 (1996) 3-13.

[10] B. Paull, P. N. Nesterenko, *Analyst,* 130 (2005) 134-146.

[11] B. Paull, P. N. Nesterenko, *Trends in Analytical Chemistry*, 24 (2005) 295-303.

[12] A. Nordborg, E. F. Hilder, *Analytical and Bioanalytical Cheimstry*, 394 (2009) 71-84.

[13] S. D. Chambers, K. M. Glenn. C. A. Lucy, *Journal of Separation Science*, 30 (2007) 1628-1645.

[14] C. A. Pohl, J. R. Stillian, P. E. Jackson, Journal of Chromatography A, 789 (1997) 29-41

[15] R. Michalski, *Critical Reviews in Analytical Chemistry*, 39 (2009) 230-250.

[16] C. Sarzanini, M. C. Bruzzoniti, *Analytica Chimica Acta*, 540 (2005) 45-53.

[17] B. Lopez-Ruiz, *Journal of Chromatography A*, 881 (2000) 607-627.

[18] J. S. Fritz, D. Gjerde, *Ion chromatography*, Wiley, New York, 1999

[19] H.Small, *Ion Chromatography*, Plenum Publishing Corp., New York, 1989.

[20] P. Kuban, P. K. Dasgupta, *Journal of Separation Science*, 27 (2004) 1441-1457.

[21] X. Dong, R. Wu, J. Dong, Y. Zhu, H. Zou, *Electrophoresis*, 30 (2009) 141-154

[22] http://www.dionex.com/en-us/products/ion-chromatography/ic-rfic-solutions/capillary-ic/columns/lp-88588.html. Accessed on 21/02/12.

[23] http://www.dionex.com/en-us/products/ion-chromatography/ic-rfic-solutions/capillary-ic/lp-88602.html. Accessed on 21/02/12.

[24] A. Sjogren, C. B. Bradley, P. K. Dasgupta, *Analytical Chemistry*, 69 (1997) 1385-1391.

[25] C. B. Boring, P. K. Dasgupta, A. Sjogren, *Journal of Chromatography A*, 804 (1998) 45-54.

[26] E. Gillespie, D. Connolly, M. Macka, P. Hauser, B. Paull, *Analyst*, 133 (2008) 1104-1110.

[27] P. Haddad, M. Shaw, G. Dicinoski, *Journal of Chromatography A,* 956 (2002) 59-64.

[28] Y. Michigami, M. Morooka, K. Ueda, *Journal of Chromatography A,* 732 (1996) 403-407.

[29] H. Meng, T. Wang, B. Guo, Y. Hashi, C. Guo, J. Lin, *Talanta,* 76 (2008) 241-245.

[30] L. Barron, P. N. Nesterenko, B. Paull, *Journal of Chromatography A,* 1072 (2005) 207-215

[31] www.dionex.com/en-us/webdocs/4696-tn12.pdf. Accessed on 18/0212.

[32] N. Gros, B. Gorenc, *Journal of Chromatography A*, 770 (1997) 119-124.

[33] D. Thomas, M. Rey, P. E. Jackson, *Journal of Chromatography A,* 956 (2002) 181-186.

[34] P. R. Haddad, P. E. Jackson, M. J. Shaw, *Journal of Chromatography A*, 1000 (2003) 725-742.

[35] http://www.dionex.com/en-us/products/accessories/suppressors/ces-300/lp-85432.html. Accessed on 18/02/12.

[36] A. Zemann, E. Schnell, D. Volgger and G. Bonn, *Analytical Chemistry*, 70 (1998) 563-567.

[37] C. Ó Ríordáin, E. Gillespie, D. Connolly, P. N. Nesterenko, B. Paull, *Journal of Chromatography A,* 1142 (2007) 185-193.

[38] J. Wang, M. Pumera, *Analytical Chemistry*, 74 (2002) 5919-5923.

[39] P. Kuban, P. C. Hauser, *Electrophoresis*, 30 (2009) 176-188.

[40] P. Kuban, P. C. Hauser, *Analytica Chimica Acta*, 607 (2008) 15-29.

[41] P. Kuban, P. C. Hauser, *Electrophoresis*, 32 (2011) 30-42.

[42] P. Kubán, P. C. Hauser, *Electroanalysis* 24 (2004) 2009-2021.

[43] P. Kubán, M. A. Muri, P. C. Hauser, *Analyst,* 129 (2004) 82-86.

[44] P. Kuban, B. Karlberg, P. Kuban, V. Kuban, *Journal of Chromatography A,* 964 (2002) 227-241

[45] D. Connolly, P. Floris, P. N. Nesterenko, B. Paull, *Trends in Analytical Chemistry,* 29 (2010) 870-884.

[46] R. J. Williams, Analytical Chemistry, 55 (1983) 851-854

[47] C. Ó Ríordáin, P. N. Nesterenko, B. Paull, *Journal of Chromatography A*, 1070 (2005) 71-75

[48] J. Li, Y, Zhu, Y, Guo, *Journal of Chromatography A*, 1118 (2006) 46-50

[49] Y. Ueki, T. Umemura, J. Li, T. Odake, K. Tsunoda, *Analytical Chemistry*, 76 (2004) 7007-7012.

[50] S. Echiog, R. Minear, H. Yamada, P. Jackson, *Journal of Chromatography A,* 920 (2001) 205-211.

[51] P. N. Nesterenko, P. Jones, B. Paull, *High Performance Chelation Ion Chromatography*, RSC Publishing, Cambridge, UK, 2011.

[52] L. Barron, M. O'Toole, D. Diamond, P. Nesterenko, B. Paull, *Journal of Chromatography A*, 1213 (2008) 31-36.

[53] N. Cardellichio, S. Cavalli, P. Ragore, J Rivello, *Journal of Chromatography A,* 847 (1999) 251-259.

[54] L. Barron, P. N. Nesterenko, D. Diamond, M. O'Toole, K.T. Lau, B. Paull, *Analytica Chimica Acta*, 577 (2006) 32-37.

[55] W. Bashir, B. Paull, *Journal of Chromatography A,* 910 (2001) 301-309.

[56] T. Takeuchi, R. Zein, E. Munaf, T. Miwa, *Journal of Chromatography A*, 755 (1996) 37-42.

[57] R. Zein, E. Munaf, T. Takeuchi, T. Miwa, *Analytica Chimica Acta*, 335 (1996) 261-266.

[58] T. Takeuchi, Safni, T. Miwa, Y. Hashimoto, H. Moriyama, *Chromatographia,* 50 (1999) 70-74.

[59] https://phenomenex.blob.core.windows.net/documents/0b443e75-6169-4b6a-b1a3-14d0bf63d914.pdf. Product brochure accessed on 21/02/12

[60] https://phenomenex.blob.core.windows.net/documents/7cad4475-d5f3-4037-a06f-0e262cdc2e07.pdf. Product brochure accessed on 21/02/12

[61] K. Kaczmorski, J. Kostka, W. Zapcla, G. Guiochon, *Journal of Chromatography A*, 1216 (2009) 6560-6574.

[62] http://www.dionex.com/en-us/products/columns/ic-rfic/hydroxide-selective-packed/ionpac-as18/lp-73261.html. Product brochure accessed on 21/02/12

[63] http://www.dionex.com/en-us/products/columns/ic-rfic/hydroxide-selective-packed/ionpac-as19/lp-73262.html. Product brochure accessed on 21/02/12

[64] http://www.dionex.com/en-us/products/columns/ic-rfic/cation-packed/ionpac-cs16/lp-73228.html. Product brochure accessed on 21/02/12

[65] http://www.dionex.com/en-us/products/columns/ic-rfic/cation-packed/ionpac-cs12a/lp-73224.html. Product brochure accessed on 21/02/12

[66] D. Schaller, E. F. Hilder and P. R. Haddad, *Journal of Separation Science*, 29, (2006) 1705-1719.

[67] D. T. T. Nguyen, D. Guillarme, S. Rudaz, J. L. Veuthey, *Journal of Separation Science,* 29 (2006) 1836-1848.

[68] A. M. Siouffi, *Journal of Chromatography A,* 1126 (2006) 86-94

[69] K. K. Unger, R. Skudas, M. Schulte, *Journal of Chromatography A*, 1184 (2008) 393-415.

[70] F. Svec, *Journal of Chromatography A*, 1217 (2010) 902-924.

[71] E.G. Vladh, T.B. Tennikova, *Journal of Chromatography A*, 1216 (2009)2637-2650.

[72] G. Guiochon, *Journal of Chromatography A*, 1168 (2007) 101-168.

[73] A. Nordborg, E. F. Hilder, *Analytical and Bioanalytical Chemistry*. 394 (2009) 71-84.

[74] F. Svec, *Journal of Separation Science*, 32 (2004) 3-9.

[75] B. Paull, P. N. Nesterenko, *Trends in Analytical Chemstry,* 24 (2003) 295-303.

[76] A. Nordborg, E. F. Hilder, *Annual Review of Analytical Chemistry*, 4 (2011) 197-226.

[77] D. Sykora, F. Svec, J. M. J. Frechet, *Journal of Chromatography A*, 852 (1999) 297-304.

[78] J. R. Thayer, K. J. Flook, A. Woodruff, S. Rao, C. A. Pohl, *Journal of Chromatography B*, 878 (2010) 933-941.

[79] C. P. Bisjak, R. Bakry, C. W. Huck, G. K. Bonn, *Chromatographia,* 62 (2005) 531-536.

[80] Q. Luo, H. Zou, X. Xiao, Z. Guo, L. Kong, X. Wao, *Journal of Chromatography A*, 926 (2001) 255-264.

[81] B. Gu, Y. Li, M. L. Lee, *Analytical Chemistry*, 79 (2007) 5848-5855.

[82] M. Y. Ding, R. Zhang, H. Peng, *Chinese Journal of Analytical Chemistry*, 37 (2009) 395-398.

[83] E. F. Hilder, F. Svec, J. M. J. Frechet, *Journal of Chromatography A,* 1053 (2004) 101-106.

[84] F. Svec, *Journal of Separation Science*, 27 (2004) 1419-1430.

[85] E. Vlakh, T. Tennikova, *Journal of Separation Science*, 30 (2007) 2801-2813.

[86] R. Wu, L. Hu, F. Wang, M. Ye, H. Zou, *Journal of Chromatography A*, 1184 (2008) 369-392.

[87] S. Chambers, K. Glenn, C. Lucy, *Journal of Separation Science*, 30 (2007) 1628-1645.

[88] S. Eeltink, E. F. Hilder, L, Geisler, F. Svec, J. M. J. Fréchet, G. Rozing, P. J. Schoenmakers, W. Kok, *Journal of Separation Science*, 30 (2007) 407-413.

[89] C. Viklund, F. Svec, J.M.J. Fréchet, *Chemical Materials,* 8 (1996) 744-750.

[90] D. Lee, F. Svec, J. M. J. Frechet, *Journal of Chromatography A*, 1051 (2004)

[91] A. Sáfrány, B. Beiler, K. Laszló, F. Svec, *Polymer*, 46 (2005) 2862-2871. 53-60.

[92] A. Bruchet, V. Dugas, C. Mariet, F. Gouteland, J. Randon, *Journal of Separation Science*, 34, (2011) 2079-2087.

[93] X. Jiang and W. Tu. *Journal of Applied Polymer Science*, 115 (2010) 963-968.

[94] J. H. Mohr, R. Swart, C. G. Huber, *Analytical and Bioanalytical Chemistry*, 400 (2011) 2391-2402.

[95] I. Nischang, I. Teasdale, O. Bruggemann, *Journal of Chromatography A*, 1217 (2010) 7514-7522.

[96] J. Urban, F. Svec, J. M. J. Frechet, *Analytical Chemistry,* 82 (2010) 1621-1623.

[97] B. Gu, Z. Chen, C. D. Thulin, M. L. Lee, *Analytical Chemistry*, 78 (2006) 3509-3518.

[98] Y. Li, B. Gu, H. D. Tolley, M. L. Lee, *Journal of Chromatography A*, 1216 (2009) 5525-5532.

[99] A. Y. Kanatyeva, E. N. Viktorova, A. A. Korolev and A. A. Kurganov, *Journal of Separation Science,* 30 (2007) 2836-2842.

[100] E. Gillespie, D. Connolly, B. Paull, *Analyst,* 134 (2009) 1314-1321.

[101] B. Rånby, *International Journal of Adhesion and Adhesives*, 19 (1999) 337-343.

[102] T. Rohr, E. F. Hider, J. J. Donovan, F. Svec, J. M. J. Frechet, *Macromolecules,* 36 (2003) 1677-1684.

[103] D. Connolly, B. Paull, *Journal of Separation Science*, 32 (2009) 2653-2658.

[104] P. Zakaria, J. P. Hutchinson, N, Advalovic, Y. Liu, P. R. Haddad, *Analytical Chemistry*, 77 (2005) 417-423.

[105] J. P. Hutchinson, E. F. Hilder, R. A. Shellie, J. A. Smith, P. R. Haddad, *Analyst,* 131 (2006) 215-221.

[106] F. Svec, T. B. Tennikova, Z. Deyl, *Monolithic materials: preparation, properties and applications,* Elsevier, Amsterdam 2003.

[107] E. Sugrue, P. N. Nesterenko, B. Paull, *Journal of Chromatography A*, 1075 (2005) 167-175.

[108] P. Hatsis, C. A. Lucy, *Analyst*, 127 (2002) 451-454.

[109] S. Pelletier, C. A. Lucy, *Journal of Chromatography A*, 1118 (2006) 12-18.

[110] A. Suzuki, L. W. Lim, T. Hiroi, T. Takeuchi, *Talanta*, 70 (2006) 190-193.

[111] A. Suzuki, L. W. Lim, T. Takeuchi, *Analytical Sciences*, 23 (2007) 1081-1084.

[112] E. Gillespie, D. Connolly, B. Paull, *Analyst*, 132, (2007) 1238-1245.

[113] J. Urban, P. Jandera, *Journal of Separation Science*, 31 (2008) 2521-2540.

[114] F. Svec, J. M. J. Frechet, *Chemistry of Materials*, 7 (1995) 707-712.

[115] J. Urban, S. Eeltink, P. Jandera , P. J. Schoenmakers, *Journal of Chromatography A*, 1182 (2008) 161-168.

[116] D. Connolly, V. O'Shea, P. Clark, B. O'Connor, B. Paull, *Journal of Separation Science*, 30 (2007) 3060-3068.

[117] L. A. Colón, T. D. Maloney, A. M. Fermier, *Journal of Chromatography A*, 887 (2000) 43-53.

[118] D. Connolly, L. P. Barron, E. Gillespie, B. Paull, *Chromatographia,* 70 (2009) 915-920.

[119] K. M. Glenn, C. A. Lucy, *Analyst,* 133 (2008) 1581-1586.

[120] S. Pelletier, C. A. Lucy, *Journal of Chromatography A,* 1118 (2006) 12-18.

[121] E. Gillespie, D. Connolly, B. Paull, *Analyst,* 131 (2006) 886-888.

[122] Q. Xu, K. Tanaka, M. Mari, M. I. Helaleh, H. Toada, W. Hu, K. Hasebe, *Chromatographia*, 57 (2003) 19-22

[123] D. Connolly, D. Victory, B. Paull, *Journal of Separation Science*, 27 (2004) 10-11.

[124] E. Sugrue, P. N. Nesterenko, B. Paull, *Analytica Chimica Acta*, 553 (2005) 27-35.

[125] E. Sugrue, P. N. Nesterenko, B. Paull, *Analyst*, 128 (2003) 417-420.

[126] E. Sugrue, P. N. Nesterenko, B. Paull, *Journal of Separation Science*, 27 (2004) 921-930.

[127] P. N. Nesterenko, M. Shaw, S. J. Hill, P. Jones, *Microchemical Journal*, 62 (1999) 58-69.

[128] A. I. Elefterov, P. N. Nesterenko, O. A. Shpigun, *Journal of Analytical Chemistry,* 51 (1996) 887.

[129] M. G. Kolpachnikova, N. A. Penner, P. N. Nesterenko, *Journal of Chromatography A*, 826 (1998) 15.

[130] W. Bashir, B. Paull, *Journal of Chromatography A*, 907 (2001) 191-200.

[131] B. Paull, W. Bashir, *Analyst*, 128 (2003) 335-344.

[132] W. Bashir, B. Paull, *Journal of Chromatography A*, 942 (2002) 73-82.

[133] P. N. Nesterenko, P. Jones, *Journal of Chomatography* A, 770 (1997) 129-135.

[134] J. R. Jezorek, H. Freiser, *Analytical Chemistry*, 51 (1979) 366-373.

[135] P. Jones, O. J. Challenger, S. J. Hill, *Analyst*, 117 (1992) 1447-1450.

[136] B. Paull, M. Foulkes, P. Jones, *Analyst,* 119 (1994) 937-941.

[137] B. Paull, P. R. Haddad, *Analytical Communications*, 35 (1998) 13-16.

[138] S-C Chuang, C-Y Chang, C-Y, Liu. *Journal of Chromatography A*, 1044 (2004) 229-236.

[139] D. Rahmi, Y. Takasaki, Y. Zhu, H. Kobayashi, S. Konagaya, H. Haraguchi, T. Umemura, *Talanta,* 81 (2010) 1438-1445.

[140] P. N. Nesterenko, P. Jones, *Journal of Separation Science*, 30 (2007) 1773-1793.

[141] W. Bashir, E. Tyrell, O. Feeney, B. Paull, *Journal of Chromatography A*, 964 (2002) 113-122.

[142] M. J. Shaw, P. N. Nesterenko, G. W. Dicinoski, P. R. Haddad, *Journal of Chromatography A*, 997 (2003) 3-11.

[143] P. Hatsis, C. A. Lucy, *Analyst*, 126 (2001) 2113-2118.

[144] D. Collins, E. Nesterenko, D. Connolly, M. Vasquez, M. Macka, D. Brabazon, B. Paull, *Analytical Chemistry*, 83 (2011) 4307-4313.

[145] J. Krenkova, A. Gargano, N. A. Lacher, J. M. Schnelderheinge, F. Svec. *Journal of Chromatography A,* 1216 (2009) 6824-6830.

[146] T. B. Stachowiak, F. Svec, J. M. J. Frechet, *Chemistry of Materials,* 18 (2006) 5950-5957.

[147] I. K. Kiplagat, P. Kuban, P. Pelcova, V. Kuban, *Journal of Chromatography A*, 1217 (2010) 5116-5123

[148] J. P. Hutchinson, C. Johns, M. C. Breadmore, E. F. Hilder, R. M. Guijt, C. Lennard, G. Dicinoski, P. R. Haddad. *Electrophoresis*, 29 (2008) 4593-4602.

[149] C. Ó'Ríordáin, E. Gillespie, D. Connolly, P. N. Nesterenko, B. Paull. *Journal of Chromatography A,* 1142 (2007) 185-193.

[150] K. M. Glenn, C. A. Lucy, P. R. Haddad. *Journal of Chromatography A,* 1155 (2007) 8-14.

[151] V. Kontozova-Deutsch, A. Krata, F. Deutsch, L. Bencs, R. Van Greiken. *Talanta*, 75 (2008) 418-423.

[152] E. G. Vlakh, T. B. Tennikova. *Journal of Chromatography A,* 1216 (2009) 2637-2650.

[153] J. Chong, P. Hatsis, C. A. Lucy, *Journal of Chromatography A,* 997 (2003) 161-169.

[154] M. Rey, C. Pohl. *Journal of Chromatography A,* 739 (1996) 87-97.

[155] B. Paull, W. Bashir, *Analyst,* 128 (2003) 335-344.

[156] A. Beisler, E. Sahlin, K. E. Schaefer, S. G. Weber, *Analytical Chemistry,* 76 (2004) 639-645.

[157] H. Xu, S. Weber, *Journal of Chromatography A*, 1113 (2006) 116-122.

[158] T. Rohr, C. Yu, M. H. Davey, F. Svec, J. M. J. Frechet*, Electrophoresis*, 22 (2001) 3959-3967.

[159] D. A. Mair, T. R. Schwei, T. S. Dinio, F. Svec and J. M .J. Frechet, *Lab on a chip,* 9 (2009) 877-883.

[160] P. N. Nesterenko, O. A. Shpigun, *Russian Journal of Coordination Chemistry,* 28 (2002) 726-735.

[161] P. Jones, P. N. Nesterenko, *Journal of Chromatography A*, 1213 (2008) 45-49.

[162] A. I. Elefterov, M. G. Kolpachnikova, P. N. Nesterenko, O. A. Shpigun, *Journal of Chromatography A,* 769 (1997) 179-188.

[163] D. Muraviev, A. Gonzalo, M. Valiente, *Analytical Chemistry*, 67 (1995) 3028-3035.

Appendix 1.0

Use of capillary polymer monoliths in fused silica capillary formats as post-column mixing devices.

A1.1 Introduction

Post column reaction involves the reaction of the column eluate with a suitable reagent and measuring the reaction product often using UV-visible detection. The use of post-column mixing presents considerable difficulty when used at capillary scale, as any extra-column band broadening in the system leads to a substantial loss in efficiency [156]. The internal diameter of the post-column mixer is an important variable to consider, as this controls the mixer's contribution to band broadening [157]. The internal diameter and volume should be kept as low as possible, while still ensuring sufficient mixing. Rohr *et al*. [158] demonstrated the use of monoliths, as post-column mixers, prepared by direct polymerisation of the monolith within micro-fluidic channels. One advantage of direct polymerisation was the ability to place the monolith in specific regions in the micro-fluidic channels by masking off other areas. In this work, the authors demonstrated the effect of pore size and pore volume on the ability to mix two fluorescence dyes and found that the inclusion of the monolith in the channels of the micro-fluidic device did improve mixing when compared to mixing in an open channel mixer (i.e. no monolith), and that the best mixing was obtained with the monoliths with large irregular flow through pores. More recently, Mair *et al.* [159] demonstrated the ability to place 100 µm segments of monolith along the channel of a micro-fluidic device. In this work, the author mixed lysine with fluorescamine and measured the fluorescent intensity across an open channel, a 1 cm continuous monolith and a channel containing the segments of monolith. Mair found that while the continuous monolith increased mixing slightly, the mixing performance of the segmented monolith was found to be 22 % better than the open channel and the continuous monolith and this was due to the gaps between the segments of monoliths.

In this present work, the fabrication of polymer monolith for their potential use as post-column mixers was investigated. The use of post-column chemistry has been shown to improve sensitivity in the analysis of alkaline earth metals [54]. Post-column mixers must allow mixing of the eluted metals with a selected dye without significant increases in band broadening. Polymer monoliths in 100 µm Teflon coated fused silica capillary with varying pore size distribution were prepared and analysed for their suitablility as post-column mixers using a flow injection analysis system. The

monolith mixers were compared to a commercially available micro-fluidic nano-mixer and the equivalent amount of open tubular fused silica capillary.

A1.2 Instrumentation

A1.2.1 Flow injection analysis system to determine the suitability of polymer monoliths in capillary formats as post-column mixers

The flow injection system used in this analysis consisted of a Knauer Smartline 100 high pressure analytical pump (Knauer, Bedfordshire, UK), a nano-flow sensor (Upchurch, WA, USA) and a Chemiert 20 nL injector valve (Global FIA, WA, USA). A second Knauer pump was used to introduce the PCR and detection was carried out using a Dionex Ultimate 3000 capillary UV detector with a 3 nL flow cell (Sunnyvale, CA, USA). The monolith mixers were compared to a commercially available micro-fluidic nano-mixer purchased from Upchurch Scientific (Oak Harbor, WA, USA). The minimum amount of 25 µm fused silica capillary was used to connect all the separate components to reduce the effects of band broadening. A Dionex Ultimate 3000 capillary chromatography system (Dionex, Sunnyvale, CA, USA) was used for backpressure measurements. The PCR mixers were also compared to a low dead volume T-piece, where one arm of the T-piece was connected to the eluent pump, the second arm connected to the PCR pump and the outlet port of the T-piece connected to the UV-Vis detector. The pump used for the vinylisation of the fused silica capillary was a syringe pump from Cole Parmer (Illinois, USA). The water bath used was a GFL 1002 (VWR International, Dublin, Ireland). The monolithic columns were polymerised and photo-grafted using a Spectrolinker XL-1000 UV Crosslinker at 254 nm. (Spectronics Corp., NY, USA).

A1.3 Procedure

A1.3.1 Fabrication of polymer monoliths with increased pore size for use as monolith mixers

Six polymer monoliths with increasing pore size distribution were prepared according to the concentrations set out in Table A1.1 [158]. Each polymerisation mixture was

de-oxygenated for 10 minutes with nitrogen and allowed to fill into 7 cm segments of previously vinylised Teflon coated fused silica capillary by capillary action. The fused silica capillary was sealed and 1 J/cm^2 of UV energy at 254 nm was applied. The monoliths were subsequently washed with methanol at 1 µL/min for one hour.

Table A1.1: % composition of monomer, cross-linker, porogen and initiator used in the preparation of the six polymer monolith mixers.

Monolith #	**1**	**2**	**3**	**4**	**5**	**6**
	% concentrations					
HEMA	24	18	12	9	6	3
EDMA	16	12	8	6	4	2
1-dodecanol	42	36.3	38.7	41.1	43.5	45.9
Cyclohexanol	18	38.7	41.3	43.9	46.5	49.1
DAP (%)	1	1	1	1	1	1

A1.3.2 Measurement of back-pressure of the monolith mixers.

The backpressures of each of the monolith mixers prepared in Table A1.1 were measured using a Dionex capillary ion chromatography system. The measurements were taken using methanol as the eluent and varying the flow rate from 0.5 – 8 µL/min in 1 µL/min increments.

A1.3.3 FIA using polymer monolith mixers as post-column mixers

Using the FIA system described in Section A1.2.1, injections of Mg(II) were carried out using each of the monolith mixers in turn. The post-column reagent consisted of 4 m*M* *o*-CPC, 10 m*M* boric acid and pH adjusted to 9.8 with 250 m*M* NaOH and detected using UV-Vis detection (originally set to 575 nm and following optimisation of the wavelength was changed to 570 nm). The monolith mixers were also compared to a micro-fluidic nano-mixer and the equivalent amount of open tubular fused silica capillary. Peak heights and peak areas were noted for each mixer time and compared.

A1.4 Results and Discussion

A1.4.1 Backpressure measurements

To demonstrate the effect of monomer/porogen concentrations of the formation on pore formation, backpressure measurements were obtained for each monolith. The backpressure profiles obtained can be seen in Figure A1.1. Backpressure measurements were not carried out on the polymer monolith prepared using a polymerisation mixture consisting of 5 % monomer as it was observed that the monolith was breaking away from the walls of the fused silica capillary during the washing procedure. The monolith was not structurally stable which had the potential to block the flow cell of the UV detector if used and as a result, the 5 % monolith was omitted from any further analysis.

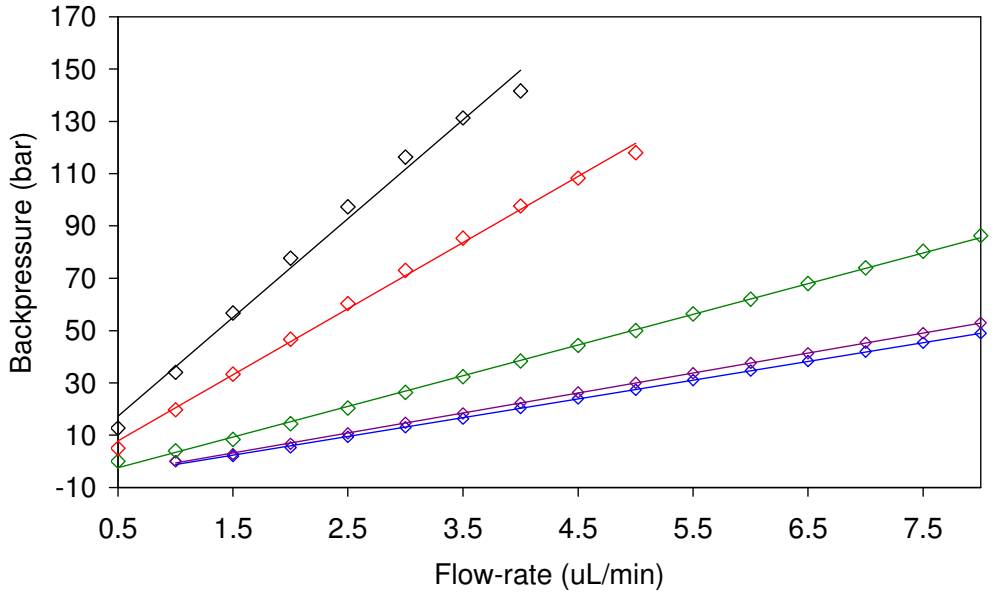

Figure A1.1: Backpressure profile obtained for HEMA-co-EDMA polymer monoliths with 40 % monomer (◊), 30 % monomer (◊), 20 % monomer (◊), 15 % monomer (◊) and 10 % monomer (◊). Measurements carried out using methanol and flow-rate increased from 0.5 – 8 µL/min.

The linear response for the backpressure measurements obtained for all other polymer monoliths showed that the monoliths were stable and covalently bound to the walls of the fused silica capillary. As can be seen from Figure A1.1, backpressures obtained for each monolith were as expected, with the monolith prepared using 10 % monomer and therefore containing the largest pores in comparison to the other monoliths, exhibited the lowest backpressure. The backpressure increased with an increase in monomer concentration. The 40 % monomer monolith was disregarded at this point due to the high backpressure exhibited.

A1.4.2 Scanning electron microscope imaging

Backpressure measurements obtained in Figure A1.1 showed that by increasing the porogen concentration, increased pore size was achieved, leading to decrease backpressure. Scanning electron microscope (SEM) imaging allowed the ability to visualise the pore morphology within the monolith structure. Figure A1.2(a) and (b) shows the polymer monoliths prepared using 5 % and 10 % monomer respectively. From these SEM images, it can be seen that the monolith only formed near the walls of the fused silica capillary. Figure A1.2(c) and (d) show the polymer monolith prepared using a monomer concentration of 15 %. The monolith obtained exhibited large, irregular pores. Figure A1.2(e) shows the SEM image obtained for the polymer monolith containing 20 % monomer and (f) shows the SEM image for the 30 % monomer monolith. These monoliths showed that a reduction in the diameter of the pores was obtained with an increase in monomer concentration. Figure 1.2 (g) and (h) shows the SEM image obtained using a 40 % monomer concentration, which exhibited the highest backpressure. As can be seen for the SEM images, a highly dense porous polymer monolith was obtained, which was evident in the backpressure measurements obtained for this monolith in Figure A1.1.

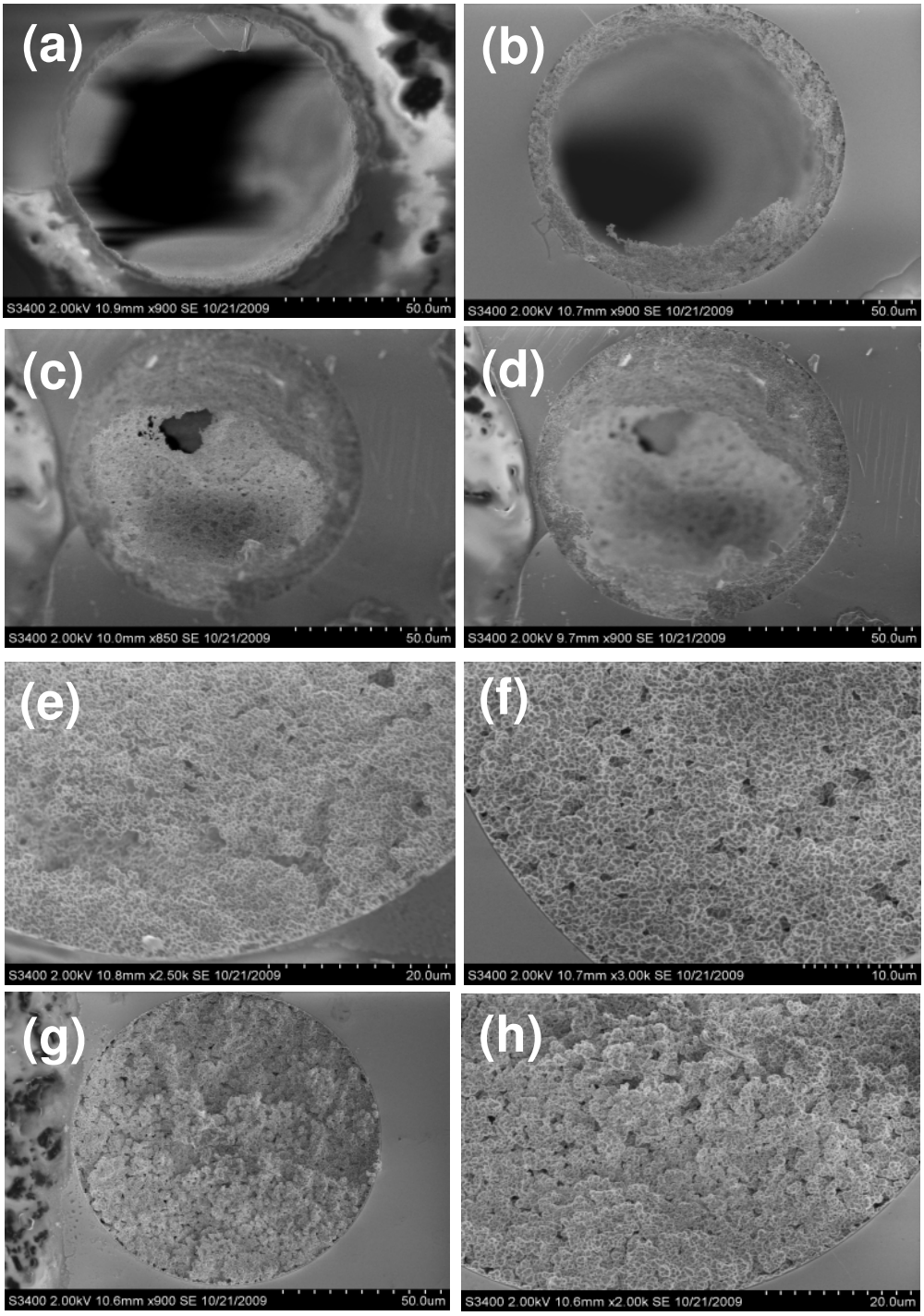

Figure A1.2: SEM images obtained for monolith mixers: (a) 5 % monomer, (b) 10 % monomer, (c,d) 15 % monomer, (e) 20 % monomer, (f) 30 % monomer and (g,h) 40 % monomer.

A1.4.3 Comparison of polymer monoliths in capillary formats as post-column mixers to a commercially available nano-mixer

A1.4.3.1 Orientation of chip in the nano-mixer

A commercially available nano-mixer consisted of a silica chip secured inside a plastic protective holding device. The micro-fluidic nano-mixer had 2 configurations, depending on which way the chip was placed in the chip holder. According to the manufacturers, the 'low' configuration had a flow path volume of 30 nL and mixes with low back pressure and the 'high' configuration had a flow path volume of 60 nL and gives superior mixing with a higher backpressure. Figure A1.3 shows a picture of the microchip, which sits inside a protective holder. The microchip was tested in the 'high' and 'low' configurations and as there was no appreciable difference in the backpressures exhibited, all investigative analysis using the micro-fluidic nano-mixer was carried out in the 'high' configuration.

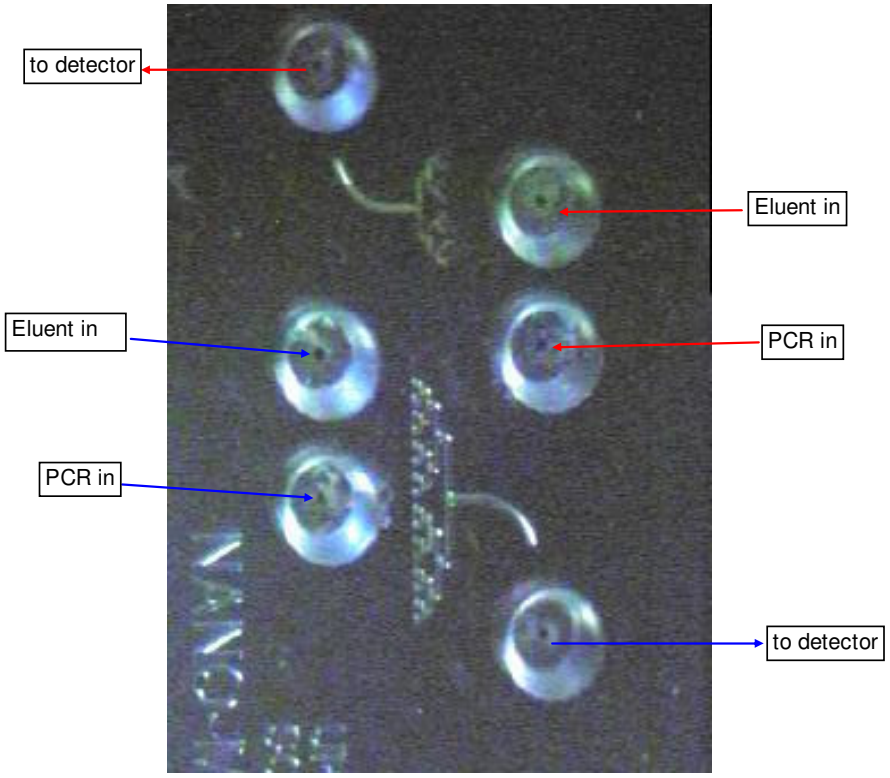

Figure A1.3: Micro-fluidic nano-mixer chip showing the low (red) and high (blue) configuration.

A1.4.3.2 Optimisation of detection wavelength.

Previous work on the analysis of alkaline earth metals using *o*-CPC as a post-column reagent has shown that the optimum detection wavelength was 575 nm [54]. However, it was important to determine the optimum wavelength using the conditions described in this work. Using the nano-mixer incorporated into the FIA system, injections of Mg(II) were carried out, varying the wavelength from 500 nm to 610 nm. Figure A1.4 shows a plot of wavelength (nm) versus peak area (V.s) and it can be seen from this plot that the optimum wavelength was between 565 nm and 570 nm, therefore all further work was carried using a detection wavelength of 570 nm.

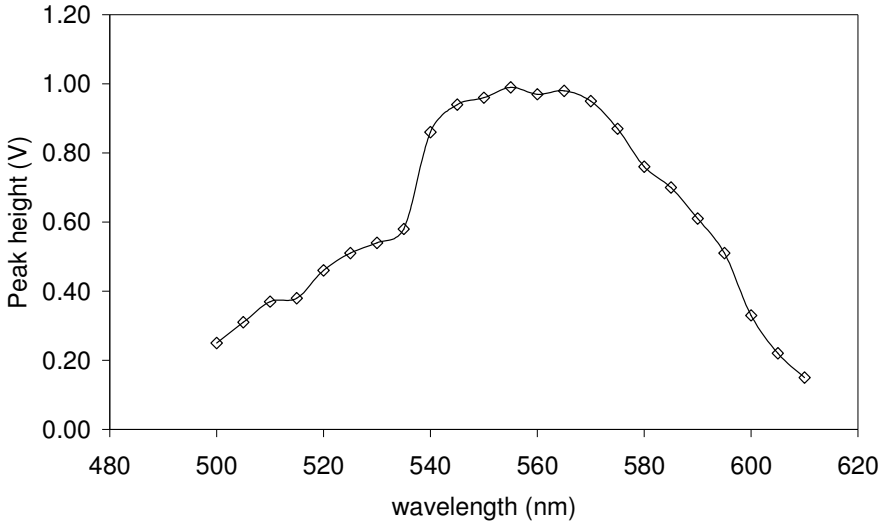

Figure A1.4: Plot of wavelength (nm) versus peak height (V) showing that the optimum wavelength was between 565 nm and 570 nm. Separation conditions: Injection volume: 20 nL, Eluent: 5 m*M* nitric acid, PCR: 4 m*M* o-CPC, 10 m*M* boric acid pH adjusted to 9.8 with 250 m*M* NaOH, flow-rate: 1 µL/min (eluent and PCR).

A1.4.3.3 Effect of polymer monolith post-column mixer length on peak shape

The FIA system was set up using a high pressure pump, a nano-flow sensor and a 20 nL injector valve. The least amount of 25 µm fused silica capillary was used to plumb the injector valve into the correct port of the nano-mixer. A second pump was used to introduce the post-column reagent which was connected to another port of the micro-fluidic mixer. The eluent mixed with the post-column reagent as it passed through the

channels of the nano-mixer and exited through the third port of the nano-mixer, which was connected to the UV-Vis detector.

Monolith mixers of various lengths were used (5 cm, 4 cm and 3.5 cm) and the effect of mixer length on peak height, area and width was investigated. Monolith mixers shorter than 3.5 cm could not be incorporated into the FIA system due to plumbing restrictions. The monolith mixers were also compared to the equivalent length of open tubular fused silica capillary (i.e. fused silica capillary containing no monolith). Table A1.2 shows the chromatographic performance data demonstrating the differences in peak width (measured at 50 % peak height), peak area and peak height, using monoliths mixers of varying flow-through pores, open tubular FSC and a commercially available nano-mixer. The peak area (V.s) indicated the degree of mixing while the peak height (V) indicated the band broadening.

Table A1.2: Chromatographic performance data comparing mixing efficiency of monoliths of varying monomer concentration and varying lengths with a commercially available micro-fluidic nano-mixer.

PCR mixer	*Mixer length (cm)*	*Peak width*	*Peak Area (V.s)*	*Peak Height (V)*
15% monomer	5	0.18	2.92	0.26
	4	0.15	3.16	0.31
	3.5	0.15	3.17	0.32
20% monomer	5	0.11	2.63	0.33
	4	0.18	2.56	0.20
	3.5	0.10	2.94	0.39
30% monomer	5	0.10	2.24	0.31
	4	0.11	2.33	0.30
	3.5	0.18	2.51	0.31
Empty fused silica capillary	5	0.09	2.64	0.43
	4	0.09	2.60	0.46
	3.5	0.08	2.64	0.47
nano-fluidic mixer	-	0.07	3.24	0.66

The effect of mixer length and therefore mixer volume was investigated. From Table A1.2, the length of the monolithic mixer had an effect on mixing capacity. Each of the monolith mixers reported an increase in peak area (10 – 12 %) and an increase in peak height when the lengths of the monolith mixers were reduced (from 5 cm to 3.5 cm), due to a decrease in the monolith mixer volume. The 15 % monomer monolith (3.5 cm) exhibited the largest peak area (3.17 V.s) when compared to the 20 % monomer monolith (3.5 cm) which showed a peak area of 2.94 V.s and for the 30 % monomer, a peak area of 2.51 V.s was obtained. As mentioned previously, a comparison of peak heights indicates the level of band broadening introduced by the monolith mixers. Peak heights of 0.32 V, 0.39 V and 0.31 V were obtained for 15 %, 20 % and 30 % monolith mixers respectively. However, when the peak heights from the monolith mixers are compared to the peak heights obtained from the equivalent length of open tubular fused silica capillary (0.47 V), it becomes evident that the introduction of the monolith into the fused silica capillary had an effect on the band broadening (~ 30 % increase in band broadening when compared to the 15 % monomer monolith, 3.5 cm in length). During this analysis, it appeared that the structural integrity of the 10 % monomer monolith was not sufficiently stable and in some cases, the porous polymer washed out of the end of the fused silica, therefore this monolith was ruled out as a potential monolith mixer. Although an increase in band broadening was observed when the monolith mixers (15 and 20 % monomer concentration) were incorporated in the flow injection system, in comparison with the same length of empty fused silica capillary, a closer inspection of peak areas indicated an increase in mixing efficiency of ~ 20 % when the monolith mixer was used. Comparing the 15 % monomer monolith (Figure 1.5(b) to the commercially available nano-mixer (Figure A1.6(b)) showed that the peak area's obtained were comparable (3.17 V.s for 15 % monolith mixer and 3.24 V.s for nano- mixer), however, when the peak height's are compared, it is clear that the 15 % monolith mixer contributes significantly to band broadening (~ 50 % decrease in peak height when the 15 % monolith mixer is used). Figure A1.5(c) shows FIA chromatograms obtained for injections of Mg(II) using the polymer monoliths prepared from a monomer concentration of 20 % and Figure 1.5(d) was obtained using empty fused silica capillary. All chromatograms shown in Figure 3.12 are to scale and it is evident that the introduction of the monolith within the fused silica resulted in band broadening.

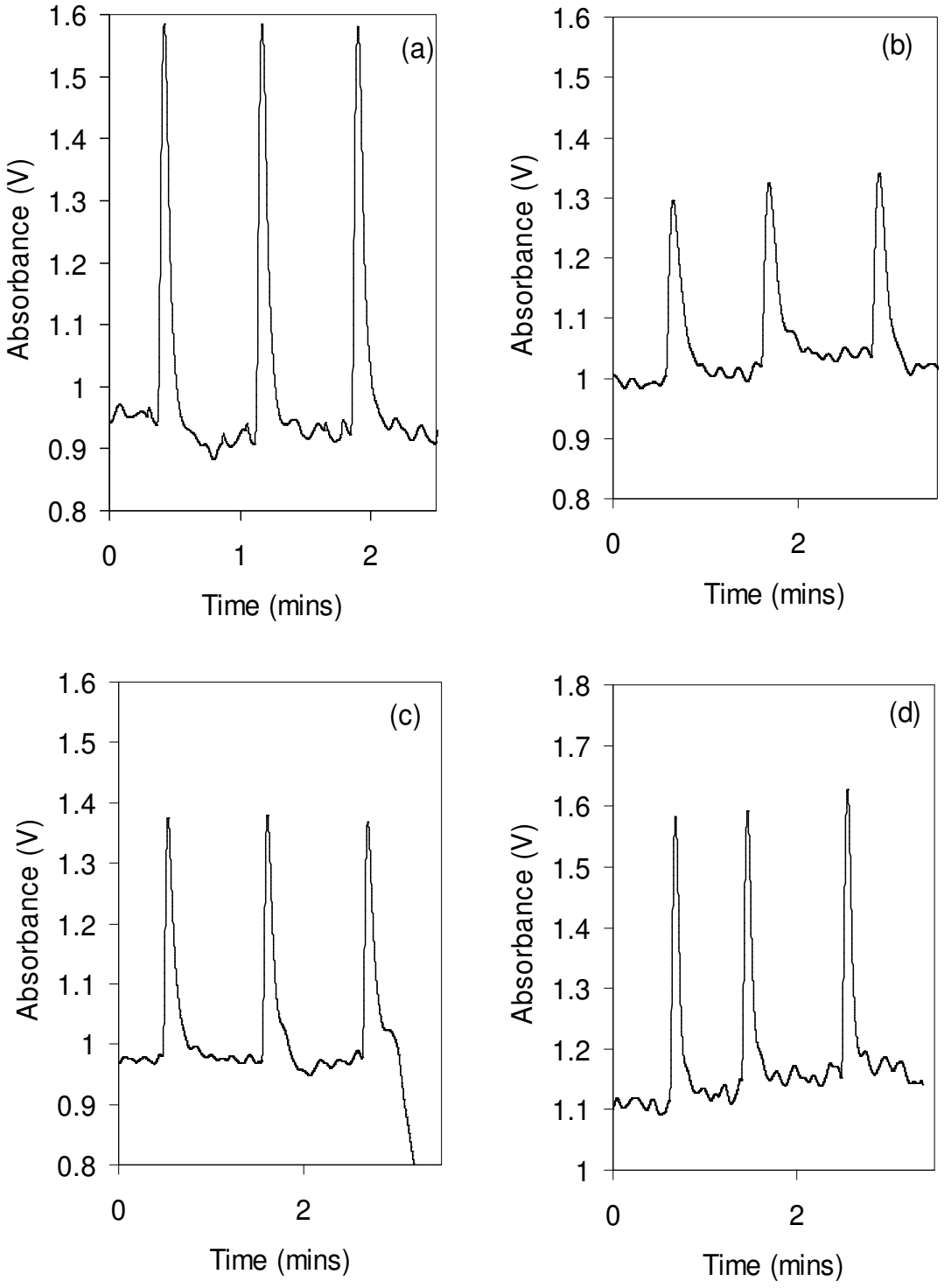

Figure A1.5: Mg(II) peaks obtained on the FIA system using (a) the nano-mixer, (b) 15 % monomer monolith, 3.5 cm in length, (c) 20 % monolith mixer, 3.5 cm in length and (d) 3.5 cm of empty FSC.

A1.3.3.4 Optimisation of post-column regent conditions

To show the full extent of the mixing efficiency of the monolith mixers, the PCR conditions were optimised. The *o*-CPC concentration was varied from 0.5 m*M* to 8 m*M*. The boric acid concentration was kept constant at 10 m*M* and the pH of each post-column reagent was adjusted to 9.8 with 250 m*M* NaOH. Injections of Mg(II) were carried out and it was found that the optimum concentration which exhibited the largest peak area and peak height was 1 m*M* *o*-CPC. This was repeated to find the optimum boric acid concentration where, the *o*-CPC concentration was kept constant at 1 m*M* and the boric acid concentration was varied between 2 m*M* and 20 m*M*. The optimum concentration was found to be 15 m*M* boric acid. Finally, using 1 m*M* o-CPC and 15 m*M* boric acid, the pH was adjusted from 8.5 to 11.5 and the optimum pH was found to be 9.8

A1.4.3.5 Comparison of commercially available nano-mixer and monolith mixers using the optimized PCR conditions conditions.

Using the optimised conditions, the commercially available micro-fluidic nano-mixer and the 15 % monolith mixer were compared. Figure A1.6(a) shows the Mg(II) peaks obtained using the nano-mixer, while Figure A1.6(b) shows Mg(II) peaks using the polymer monolith prepared using a 15 % monomer concentration (3.5 cm) incorporated into the flow injection system. The mixers were also compared to a 3.5 cm piece of open tubular FSC Figure A1.6(c). As all the chromatograms in Figure A1.6 are to scale, the effects of the incorporation of the monolith into the fused silica capillary become clear. Reductions in peak height were clearly visible as well as increase in peak width when the 15 % monomer mixer (b) is compared to (a). The PCR mixers, mentioned previously, were replaced with a low dead volume T-piece. Figure A1.7 shows Mg(II) peaks using the optimised conditions on the flow injection analysis system with a T-piece replacing the PCR mixer.

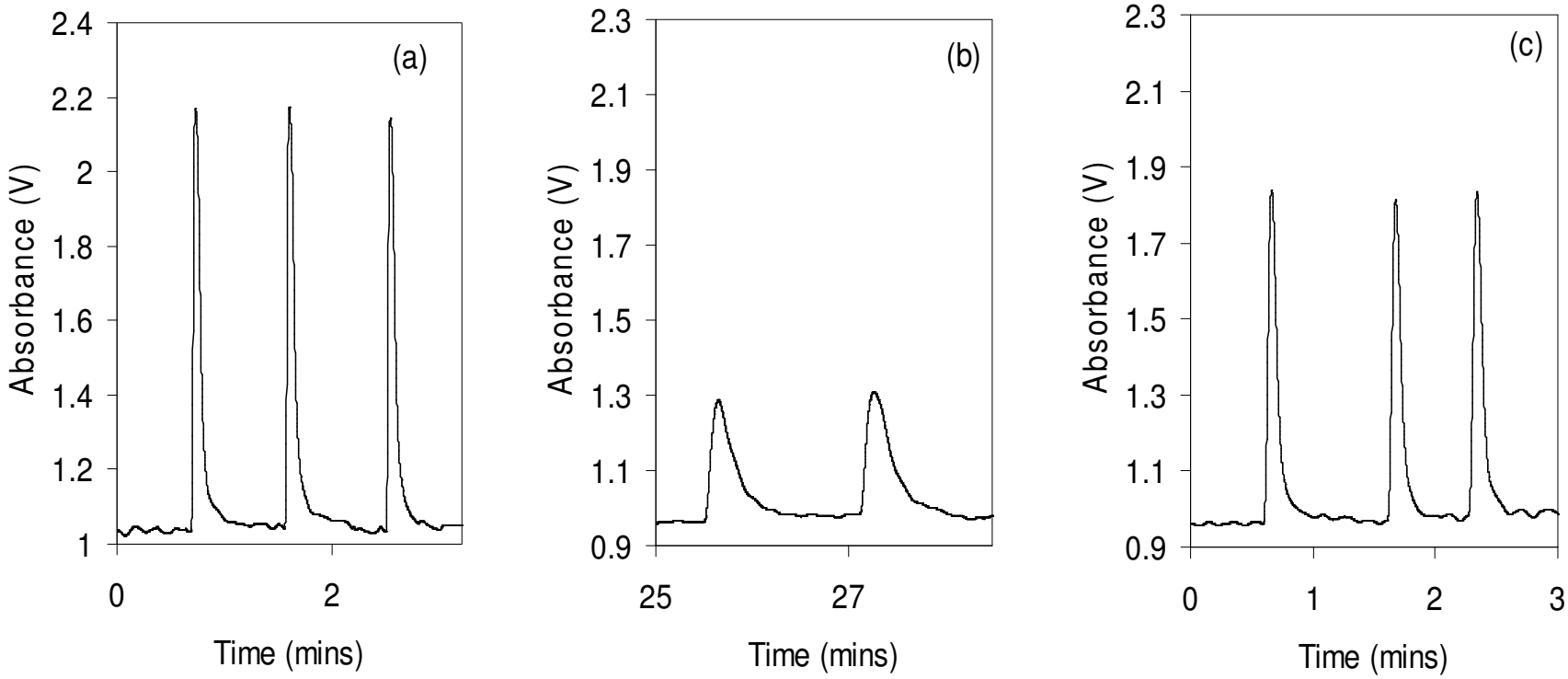

Figure A1.6: Mg(II) peaks obtained using the FIA system with (a) the micro-fluidic nano-mixer, (b) the 15 % monolith mixer, 3.5 cm in length and (c) open tubular FSC, 3.5 cm in length. Injection volume: 20 nL, Eluent: 5 m*M* nitric acid, PCR: 4 m*M* o-CPC, 10 m*M* boric acid pH adjusted to 9.8 with 250 m*M* NaOH., flow-rate: 1 µL/min (eluent and PCR).

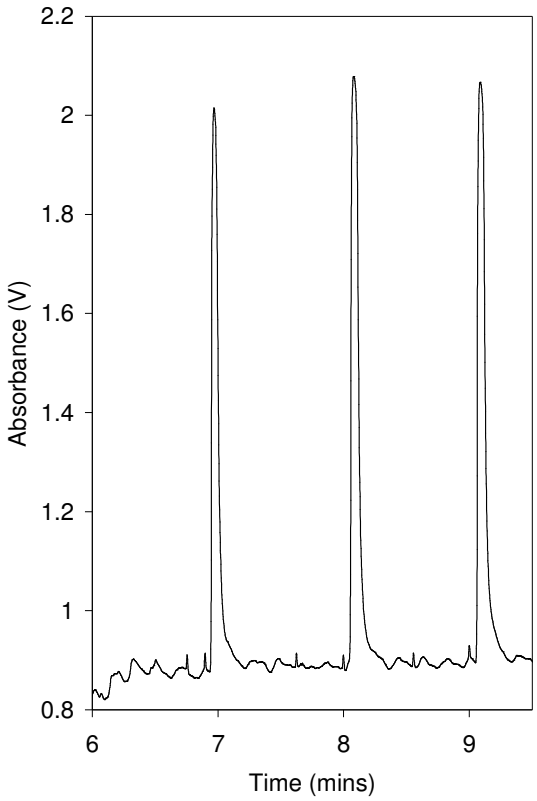

Figure A1.7: Injections of 500 ppm Mg(II) on the flow injection system using the optimised conditions. Chromatographic conditions: PCR mixer: Low dead volume T-piece, all other conditions as in Figure A1.6.

Table A1.3: Peak areas (V.s) (n=6 injections) using the micro-fluidic nano-mixer, 15 % monolith mixer, open tubular fused silica capillary and low dead volume T-piece.

Mixer	*Peak width*	*Peak Area (V.s)*	*Peak height (V)*
15 % monomer mixer (3.5 cm)	0.24	5.63	0.33
Micro-fluidic nano-mixer	0.07	5.62	1.11
Open tubular FSC (3.5 cm)	0.08	4.75	0.84
T piece	0.06	5.36	1.18

As can be seen from Table A1.3, the peak areas obtained from the nano-mixer and the 15 % monolith mixer are comparable. As mentioned previously, a comparison of the peak heights suggests that the monolith mixer introduced significant band broadening which is evident when peak heights are compared (peak height for monolith mixer was 0.33 V and 1.11 V for the nano-mixer). The equivalent amount of open tubular fused silica capillary resulted in a reduction in the mixing efficiency showing that the incorporation of the monolith within the fused silica capillary resulted in a higher degree of mixing, however, when the peak heights are compared (0.33 V for 15 % monolith mixer and 0.84 V for open tubular fused silica capillary), the monolith did increase band broadening.

The use of the T-piece with the 17 nL swept volume gave an interesting result. The fused silica from the UV detector was connected directly into the T-piece and it seemed that the length of fused silica from the detector connected to the flow-cell of the UV detector was long enough to ensure efficient mixing, when compared to the micro-fluidic mixer. A reduction in band broadening was also noted when the T-piece was compared to the monolith mixer. The results obtained for the T-piece were comparable to those obtained from the commercially available nano-mixer.

A1.5 Conclusion

The use of polymer monolith as post-column mixers is presented. Polymer monoliths were prepared with decreasing porogen concentrations resulting in monolith with various flow-through pore diameters. The differences in the flow-through pores were confirmed by obtaining back-pressure measurements and SEM images. Each monolith mixer was incorporated into a flow injection analysis system. Results showed that decreasing the length of the monolith mixer from 5 cm to 3.5 cm reduced the effects of band broadening due to decreases in the internal volume of the monolith mixer. The monolith mixer was also compared with an equivalent amount of open tubular fused silica capillary, which showed that the incorporation of the polymer monolith within the fused silica capillary did improve mixing, however an increase in band broadening was noted. The monolith mixer and open tubular fused silica capillary were also compared to a commercially available micro-fluidic nano-mixer. While peak areas of the monolith mixer and the micro-fluidic nano-mixer were comparable,

a increase in peak height of ~ 70 % was observed when the micro-fluidic nano-mixer was used demonstrating the significant effect on band broadening when the monolith mixer was used. Finally, all post-column mixers were replaced with a T piece with a low swept volume with results showing that the mixing capabilities were similar to those exhibited by the micro-fluidic nano-mixer.

Although the results obtained in this work showed that the use of a monolith as a mixer had a deleterious effect on band broadening, it is possible that that this problem may be overcome with the use of segmented monoliths similar to those reported by Mair *et al.* [159].